The role of FOXK transcription factors in Wnt signal transduction

Lisa Heinke

MRC Laboratory of Molecular Biology

Magdalene College, University of Cambridge

This dissertation is submitted for the degree of *Doctor of Philosophy*

May 2020

1st supervisor: Dr Mariann Bienz

2nd supervisor: Dr Katja Röper

University supervisor: Dr Sarah Bray

Declaration of Originality

This dissertation is the result of my own work and includes nothing which is the outcome of work done in collaboration except where specifically declared in the text. It is not substantially the same as any that I have submitted, or, is being concurrently submitted for a degree or diploma or other qualification at the University of Cambridge or any other University or similar institution. This dissertation does not exceed the word limit set by the Degree Committee for the Faculty of Biology.

_____

Lisa Heinke

21st of May, 2020

The role of FOXK transcription factors in Wnt signal transduction

Lisa Heinke

Wnt signalling is a highly conserved signal transduction pathway with key functions in developmental processes including patterning during embryogenesis and stem cell homeostasis in the adult organism. Wnt signals are received at the cell membrane and transduced through cytoplasmic and nuclear multiprotein complexes; the degradasome, signalosome and enhanceosome. The latter is tethered to enhancers by T-cell transcription factors (TCF), and core components include the chromatin reader Pygopus as well as the transcriptional repressor Groucho/TLE3. While much is known about the basic interactions within the enhanceosome, it remains elusive how the enhanceosome accesses native chromatin and is established during development. Furthermore, it is controversial how transcriptional inhibition is re-installed after active signalling ceases and whether Groucho/TLE3 remains attached to the enhanceosome throughout signalling.

In order to elucidate novel binding partners, as well as assess potential restructuring of the enhanceosome during different stages of signalling, I employed a proteomics approach based on proximity labelling (BioID) using TLE3 and Pygopus as bait proteins. This revealed little changes of the core enhanceosome subunits between active or inactive signalling but indicated the Forkheadbox transcription factors FOXK1/2 as potential members of the Wnt enhanceosome. FOXK proteins are interesting candidates as they are thought to function as pioneer factors that bind to closed chromatin resulting in its opening and increased accessibility for transcription factors.

Use of a minimal Ubx enhancer system corroborates the function of FOX proteins in general during Wg signalling in the fly. I found that a previously published FoxK fly mutant does not carry a FoxK null allele and consequently generated new knockout alleles using CRISPR/Cas9. Phenotypic analysis identified a function for

FoxK during early embryogenesis whereby null mutants derived from germ line clones arrest in early development and strikingly show lack of Wg as well as segmentation and gastrulation defects. I identified a specific requirement of FoxK for patterning of the wing blade. I further assessed a putative interaction of FOXK1/2 with DVL, a key player of the signalosome. Contrary to published results, I was able to show that FOXK1/2 do not function to recruit DVL into the nucleus and do not drive expression of a TCF reporter.

This work expands our knowledge on FOXK transcription factors during fly development and in mammalian cells and establishes a function for FOX proteins during processes known to be regulated by Wg.

Acknowledgements

I am thankful to the Bienz Lab for their experimental support during my PhD: Mariann Bienz, Juliusz Mieszczanek, Marc Fiedler, Melissa Gammons, Miha Renko, Moore van Tienen, Josh Flack, Janic Le Pen, Elsa Franco Eschevarria and Gonzalo Beitia. You have made the atmosphere in the lab quite special! Most importantly I want to thank Juliusz for teaching me everything he knows about fly pushing and many Wg reporter assays in *Drosophila*. As predicted, I already miss our fly flipping sessions and cannot imagine the amount of whining the lab will have to endure now that you're doing it by yourself again! Many thanks also to Melissa Gammons and Marc Fiedler for collaborating on experiments during my PhD and always being open to discuss ideas and experiments.

I also want to thank my second supervisor Katja Röper, who has always been supportive. Thank you to the entire fly community of the LMB and Cambridge itself. I am very grateful to have learned fly pushing in such a historic environment where the biggest names of *Drosophila* research are all around you and everyone is always keen to help with stocks and knowledge. I am especially grateful to Simon Bullock for his support throughout my PhD extending far beyond his help with my CRISPR experiments.

The LMB has created a fantastic and inspiring atmosphere, without which I would not have learned half as much as I did. Thanks to all the core facilities, most importantly mass spectrometry (Mark Skehel) and microscopy (Nick Barry and Jon Howe), for always being helpful and approachable.

Most importantly, thank you to the best friends I could have hoped for during this time, both in Cambridge and back home, for every coffee and Gin Tonic, every emergency meeting in confocal rooms when science or scientists were a pain, for countless LMB/tuck shop dinners, for every night out and every trip around Europe.

In no particular order special thanks to Antje, Aydan, Flo, Eva, Louise, Dina, Shirley, Edo, Daniele, Silvia, Zeynep, Chris, Laura, Charlotte, Lisa, Gonzalo…
Thank you also of course to my family, especially my mum for all the love and support (and the German Kehrpakete!).

Abbreviations and key terms

aa	Amino acid(s)
ABC	Active β-catenin
APC	Adenomatous polyposis coli protein
ATP	Adenosine triphosphate
BAF	BRG1-associated factors
BCL9	B-cell lymphoma 9
BCL9L/B9L	B-cell lymphoma 9-like
β-gal	β-galactosidase
BirA*	BirA-R118G
BioID	Proximity labelling of protein interactors
BSA	Bovine serum albumin
CBP	CREB-binding protein
cDNA	copy-Deoxyribonucleic acid
ChiLS	Chip/LDB1-SSDP
ChIP-Seq	Chromatin Immunoprecipitation Sequencing
CM	Control medium
CoIP	Co-immunoprecipitation
COS-7	CV-1 in origin, SV40 cell line 7
CRISPR	Clustered regularly interspaced short palindromic repeats
DAPI	Diamidino phenylindole
DEP	Domain of Dishevelled/Egl-10/Pleckstrin
DIX	Domain of Dishevelled/Axin
FoxK	*Drosophila* Forkhead Box Protein K
FOXK1/2	Mammalian Forkhead Box proteins K1 & K2
DMEM	Dulbecco's modified eagle's medium
DNA	Deoxyribonucleic acid
Dsh	Dishevelled (*Drosophila*)

DTT	Dithiothreitol
DVL	Dishevelled (mammalian)
EDTA	Ethylenediaminetetraacetic acid
EMT	Epithelial to mesenchymal transition
FBS	Fetal bovine serum
Fz	Frizzled
GFP	Green fluorescent protein
glc	Germ line clone
GO	Gene ontology
Gro	Groucho
GSK3-β	Glycogen synthase kinase-3β
HAT	Histone acetyltransferase
HD	Homology domain
HDAC	Histone deacetylase
HEK293T	Human embryonic kidney cells 293, carrying a mutant version of SV40 antigen T
HS	Heat shock
HSQC	1H-15N heteronuclear single-quantum correlation spectra
IF	Immunofluorescence
IP	Immunoprecipitation
kDa	Kilodalton
KO	Knockout
LC-MS/MS	Liquid chromatography tandem-mass spectrometry
LDB1	LIM domain binding-1
LEF1	Lymphoid enhancer factor-1
LiCl	Lithium chloride
LRP	Low-density lipoprotein receptor-related protein

miniTurbo	Biotin ligase developed by Branon et al., 2018
NHEJ	Nonhomologous end joining
NLS	Nuclear localisation signal
NMR	Nuclear magnetic resonance
PAGE	Polyacrylamide gel electrophoresis
PAM	Protospacer adjacent motif
PBS	Phosphate buffered saline
PCP	Planar cell polarity
PCR	Polymerase chain reaction
PDZ	Domain in PSD95, Discs-large 1, ZO-1
PFA	Paraformaldehyde
PHD	Plant homology domain
RNA	Ribonucleic acid
RT-qPCR	reverse-transcriptase quantitative polymerase chain reaction
SDS	Sodium dodecyl sulphate
SEM	Standard error of the mean
sgRNA	Single guide RNA
siRNA	small interfering RNA
RNAi	RNA interference
RUNX	Runt-related transcription factor
SNP	Single nucleotide polymorphism
SSBP/SSDP	Single stranded DNA-binding protein
SW480	Colorectal cancer cell line
SWI/SNF	Switch/sucrose non-fermentable
TCF	T cell factor
TF	Transcription factor
TGF-β	Transforming growth factor β

TLE	Transducin-like enhancer of split
TSC	Total spectral counts
TSS	Transcription start site
TurboID	Biotin ligase developed by Branon et al., 2018
Vg	Vestigial
WCM	Wnt3a-conditioned media
Wg/Wnt	Wingless in *Drosophila*/Vertebrates
WRE	Wnt-responsive element
WT	Wild type

Table of Contents

List of Figures

1. Introduction

Wnt, or Wingless (Wg), signalling is a signal transduction pathway that is highly conserved in species as simple as sponges or cnidarians as well as more complex organisms ranging from invertebrates to mammals (reviewed in Bejsovec, 2006; Loh et al., 2016). Its key function is to regulate developmental processes including patterning during embryogenesis and stem cell homeostasis in the adult organism.

The *Wnt1* gene was originally discovered in 1982 by Nusse and Varmus as a gene activated by integration of the mouse mammary tumour virus within chromosome 15, and termed Int-1 (Nusse et al., 1984). At this time, the *Drosophila* homologue *wingless* had already been described as a segment polarity gene by Nüsslein-Volhard and Wieschaus in their Nobel prize-winning work (Nüsslein-Volhard and Wieschaus, 1980), but it was only in 1987 that the two genes were found to be related (Rijsewijk et al., 1987) and the amalgam of Wg and Int-1 as Wnt was coined.

Much of the early Wnt research was done in *Drosophila* and *Xenopus* as many proteins of the Wnt pathway are conserved between invertebrates and vertebrates including mammals. However, it was the discovery that mutations in β-catenin or Adenomatous Polyposis Coli protein (APC; E-APC in *Drosophila*) are responsible for constitutive transcriptional activation of T cell factor (TCF) target genes in colon cancer (Korinek et al., 1997; Morin et al., 1997) that catapulted Wnt signalling into the focus of cancer research.

In the next paragraphs I will outline the Wnt pathway, with a particular focus on the aspects that are most relevant for this thesis. The introductions to the individual results chapters also contain detailed information that is pertinent to the specific proteins studied and experiments conducted.

1.1. Wnt signalling in human development and disease

Wnt signalling functions at several steps during mammalian development, ranging from events in early embryogenesis to stem cell homeostasis in adult tissues. Key events during patterning include the establishment of the anterior-posterior axis, gastrulation and the formation of the primitive streak, all of which require Wnt signalling (reviewed in Wang et al., 2012).

The pathway becomes reactivated in adult tissues, where it is crucial for the maintenance of stem cell niches, famously in the intestinal epithelium. Here, Wnt signalling controls the stem cell population in the crypts that divide to replace cells shed from the villi of the gut (reviewed in Reya and Clevers, 2005), Figure 1.1). In synergy with other signalling pathways such as Notch, TGFβ and Hedgehog, Wnt signalling is thus a vital player during development and, unsurprisingly, associated with a number of human diseases including cancer.

Since the discovery of APC as the main factor in familial adenomatous polyposis (FAP) and spontaneous colorectal cancers, a plethora of studies have described mutations in the Wnt pathway in other cancer types, including gastric (reviewed in Doucas et al., 2005), skin (Rubinfeld et al., 1997), ovarian (Arend et al., 2013) or hepatocellular (Miyoshi et al., 1998) carcinoma.

Wnt signalling is not only implicated in the initial formation of tumours but also in their progression to malignancy based on the dual role of several Wnt pathway components in cell adhesion and transcriptional regulation (see below, reviewed in Valenta et al., 2012). The most common mutations found in Wnt-related cancers affect APC (80% of colorectal cancers carry APC truncations (reviewed in Giles et al., 2003)) or β-catenin, the core effector of canonical Wnt signalling (Figure 1.2) and cause inappropriate activation of the pathway. Animal models such as the APC^{min} mouse, first described by the Dove lab (Moser et al., 1990), and cell lines isolated

from cancer patients have been invaluable in studying effects of Wnt pathway mutations *in vivo*.

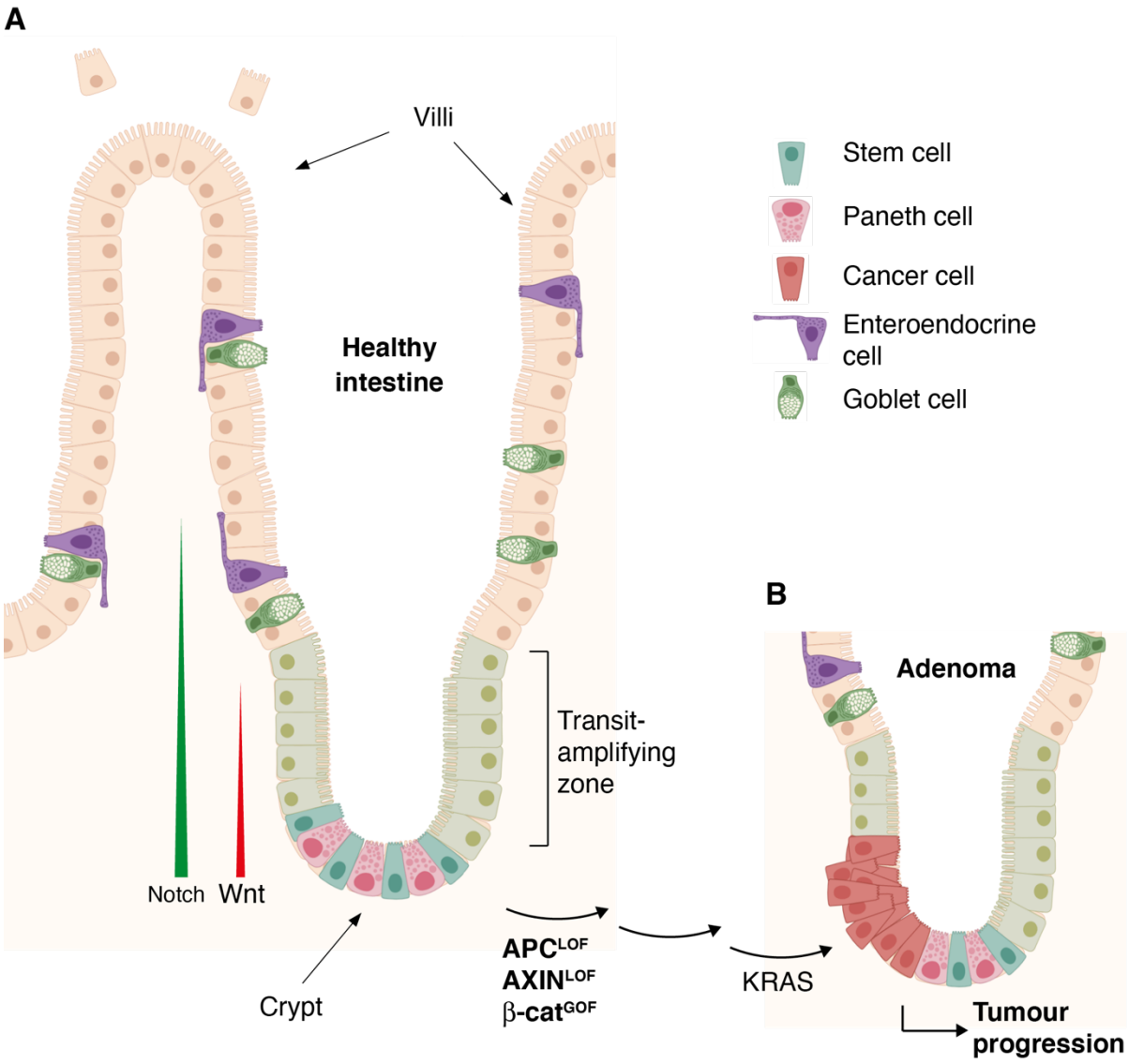

Figure 1.1. Wnt signalling in normal intestinal epithelium and Wnt mutations leading to cancer.
A) Stem cells in the crypts of the normal intestinal epithelium function to replenish cells of the intestine. Stem cell proliferation occurs close to the Wnt source and is tightly controlled by restricting Wnt activation to cells in the bottom of the crypts.
B) Initiating mutations in APC, Axin or β-catenin lead to formation of benign polyps that eventually accumulate further genomic mutations, e.g. in KRAS, resulting in genomic instability and tumour progression.
LOF = loss of function; GOF = gain of function. Figure adapted from Sancho et al. (2004).

To this day, colorectal cancers represent the third most common cancer type in the world with a high mortality rate (WHO, https://gco.iarc.fr/today/home). Research on Wnt signalling thus remains important to identify novel drug targets and develop therapeutic strategies.

1.2. Canonical Wnt signalling

Several divergent Wnt-based signalling cascades have been characterised, of which the Wnt/β-catenin pathway has been studied in the most detail due to its role in cancer. Signal transduction through β-catenin (Armadillo in *Drosophila*) is also known as canonical Wnt signalling and results in transcriptional control of Wnt target genes.

The two main non-canonical pathways are the planar cell polarity (PCP) pathway, which directs cell orientation (Yang and Mlodzik, 2015), and Wnt/Ca^{2+} signalling, which is involved in developmental processes including convergent extension (reviewed in De, 2011). The pathways diverge at the level of Dishevelled (DVL in vertebrates, Dsh in *Drosophila*), which constitutes a switch between the different Wnt pathways.

Wnt signalling is also tightly linked to cell adhesion: β-catenin is a component of adherens junctions through its binding to E-cadherin (Bienz, 2005) and accordingly functions in two distinct processes, cell adhesion and signalling, making it a dual function protein. Similarly, the function of APC is two-fold, and this provides an intriguing explanation for the link between aberrant signalling and cancer progression as these mutations increase metastasis by facilitating the epidermal-to-mesenchymal transition process (EMT) (Vincan and Barker, 2008).

A fundamental mechanism during Wnt signalling is the dynamic formation of oligomeric assemblies that act as interaction platforms to provide a high local

concentration of binding partners: the degradasome and signalosome complexes, both of which control Wnt signal transduction in the cytoplasm.

1.3. The Wnt degradasome and signalosome complexes

The initial step of the Wnt signalling cascade is the secretion of lipid-modified Wnt (Wg in *Drosophila*) ligands, of which 19 are described in the human genome. Although Wnts are typically listed as morphogens, they are thought to act as close-range signals and through direct cell contacts, whereas long-ranging signals are rare – the wing imaginal disc in *Drosophila* is one such instance and will be described below.

In the absence of a Wnt ligand, signal transduction to the nucleus is prevented by the Axin degradasome consisting of Axin as a scaffold, APC and the two kinases glycogen synthase kinase 3 (GSK3, Shaggy/Zeste-white 3 in *Drosophila*) and casein kinase 1α (CK1, discs overgrown/dco in *Drosophila*). This complex sequesters cytoplasmic β-catenin through binding of its characteristic Armadillo repeat domains (ARDs) by Axin (Ikeda et al., 1998). This process earmarks β-catenin for degradation, where CK1 acts as a priming kinase by phosphorylating β-catenin residue Ser45 resulting in subsequent phosphorylation of Ser33, Ser37 and Thr41 by GSK3 (Liu et al., 2002). Phosphorylated β-catenin thus becomes a substrate for the $SCF^{\beta\text{-}TRCP}$ E3 ubiquitin ligase (slmb in *Drosophila*) leading to its ubiquitylation and subsequent proteasomal degradation (Orford et al., 1997; Winston et al., 1999) (Figure 1.2, left panel).

Wnt ligands are bound by a heterodimeric complex consisting of a seven-transmembrane receptor called Frizzled (FZD1-10 in mammals) and its co-receptor low-density lipoprotein receptor-related protein 5/6 (LRP5/6, Arrow in *Drosophila*). Upon binding, the formation of a second multiprotein complex, the signalosome, is

triggered by DVL polymerisation (see Chapter 4) leading to recruitment of the Axin degradasome to the plasma membrane (Fiedler et al., 2011).

GSK3 and CK1 then sequentially phosphorylate the PPPSPxS motifs in LRP5/6 (Zeng et al., 2005), which strongly increases Axin binding and leads to inhibition of the active site of GSK3 ((Stamos et al., 2014), Figure 1.2, right panel). β-catenin is no longer a target of phosphorylation through the destruction complex and can translocate into the nucleus, where it is captured by the adaptor protein B-cell lymphoma 9 (BCL9/B9L, collectively referred to as BCL9 unless otherwise stated, Legless in *Drosophila*) and tethered to the Wnt enhanceosome.

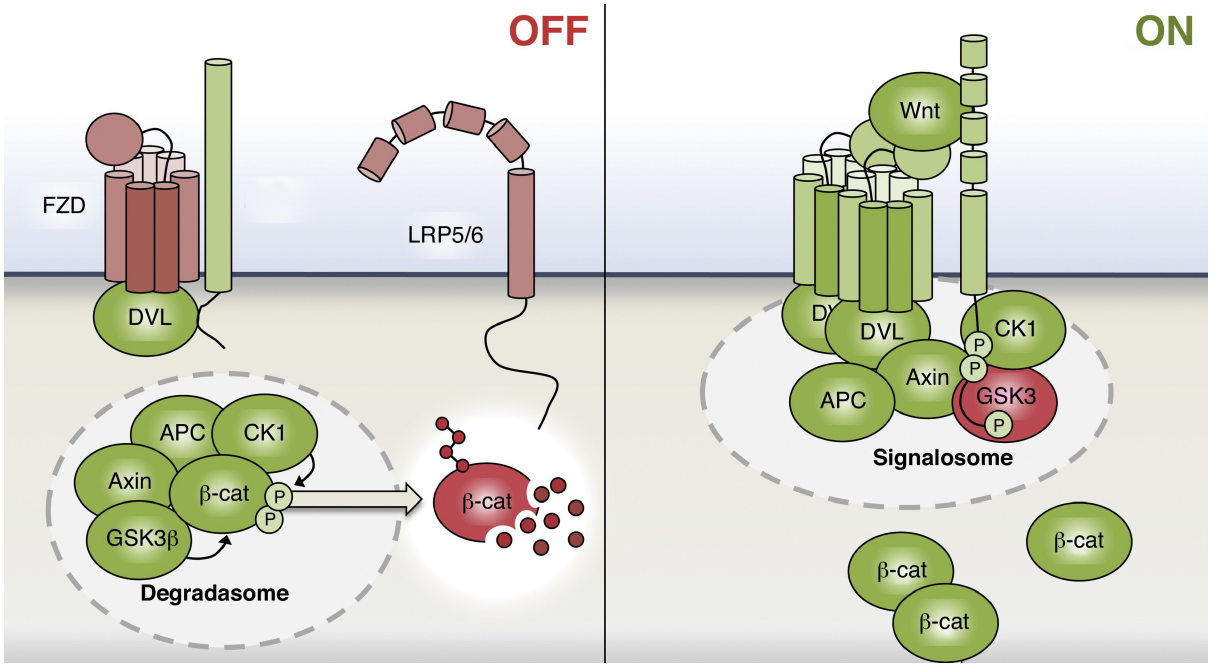

Figure 1.2. Wnt signalling is governed in the cytoplasm by multi-protein complexes termed the degradasome and the signalosome.
In the absence of a Wnt ligand, the Axin degradasome containing Axin, APC and the kinases GSK3 and CK1 leads to phosphorylation and subsequent proteasomal degradation of β-catenin, effectively blocking Wnt target gene transcription (left panel). Upon binding of Wnt to its receptor Frizzled and co-receptor LRP5/6, polymerisation of DVL is triggered and a signalosome is formed (right panel). This results in inhibitory phosphorylation of GSK3, which allows β-catenin to translocate into the nucleus. Figure from Gammons and Bienz (2018).

1.4. The Wnt enhanceosome

This type of multiprotein complex at enhancers allows for efficient signal integration and switching between ON and OFF stages through rapid exchange of bound factors. The term enhanceosome was initially coined by Panne et al. (2007) to describe the transcription factors, coactivators and nucleosome remodellers assembled at the interferon-β enhancer. The Wnt enhanceosome was first described at Wnt response elements (WREs) after the discovery that the ChiLS complex (see below) acts as a scaffold to connect proteins known to control Wnt target gene transcription (Fiedler et al., 2015).

Central to the Wnt enhanceosome are DNA-binding proteins of the T cell factor/lymphoid enhancer-binding factor family (TCF/LEF, dTCF/Pangolin in *Drosophila*). These proteins bind WREs via their consensus sequence 5'CTTTGAT (Molenaar et al., 1996; Riese et al., 1997) regardless of Wnt signalling directly through their HMG domain (Sierra et al., 2006). In the absence of Wnt stimulation, WREs are kept inactive by TCF binding to the repressor proteins TLE/Groucho which were first described for their role in Wnt/Wg signalling in the late 1990s (Cavallo et al., 1998; Levanon et al., 1998). TLE binding to TCF results in recruitment of histone deacetylases (HDAC) leading to chromatin compaction and transcriptional repression (Chen et al., 1999; Sekiya and Zaret, 2007). Binding of β-catenin overcomes this repression and different models exist to explain how TLE3-mediated silencing is inhibited during active Wnt signalling (see 2.1.2).

Unphosphorylated (active) β-catenin is captured by the PYGO-BCL9 module of the enhanceosome: chromatin-bound PYGO (PYGO1/2 in humans, Pygopus in *Drosophila*) binds to BCL9, which in turn directly interacts with β-catenin leading to nuclear retention of both proteins (Townsley et al., 2004). β-catenin subsequently binds to TCF, switching the enhanceosome from a repressive to an active state by

recruiting transcriptional coactivators and chromatin remodellers through its C-terminal transactivation domain. These include the histone acetyltransferase (HAT) CREB-binding protein (CBP/p300) (Hecht et al., 2000; Waltzer and Bienz, 1998) and methyltransferase SET1 (Sierra et al., 2006) among other factors – all of which function together to orchestrate the ON switch of transcription (see also Mosimann et al., 2009 for review).

The ternary complex between PYGO, BCL9 and β-catenin is instrumental in facilitating interaction of β-catenin with TCF, and PYGO has an additional function as a chromatin reader by interacting with histone modifications through its PHD finger (from plant homology domain; Fiedler et al., 2008). PYGO also contains an asparagine-proline-phenylalanine (NPF) motif (Städeli and Basler, 2005) which binds to the scaffold module ChiLS, consisting of two subunits of LIM-domain binding protein (LDB1, Chip in *Drosophila*) and four single-stranded DNA-binding protein subunits (SSDP1/2, also known as SSBP3/4) (Fiedler et al., 2015; Renko et al., 2019).

ChiLS fulfils an important role as a scaffold within the complex and connects a variety of enhanceosome components, thereby allowing for integration of lineage specific input (Fiedler et al., 2015). Importantly, ChiLS also mediates interaction with the Brg-1/Brahma-associated factor (BAF) complex through the ARID1 subunit of BAF (Osa in *Drosophila*; Fiedler et al., 2015). ARID1 antagonises β-catenin-mediated transcription (Collins and Treisman, 2000) and likely plays a role in re-silencing the enhanceosome once Wnt signalling ceases (van Tienen et al., 2017). The importance of this chromatin remodeller is further underscored by direct binding of β-catenin to its subunit Brg-1 (also known as SMARC4A, Brahma in *Drosophila*; (Barker et al., 2001)). The ChiLS complex is thus a core component of the enhanceosome and offers an interaction platform for integration of additional, context- or lineage-specific factors (Waterman and Jones, 1990).

Figure 1.3 summarises the current model of the enhanceosome as well as mapped protein-protein and protein-DNA interactions within the complex. It is unknown how the multitude of factors are initially assembled at Wnt target loci and whether a preceding priming event is required to set up the enhanceosome during development. It is conceivable that so-called pioneer factors play a role in this process.

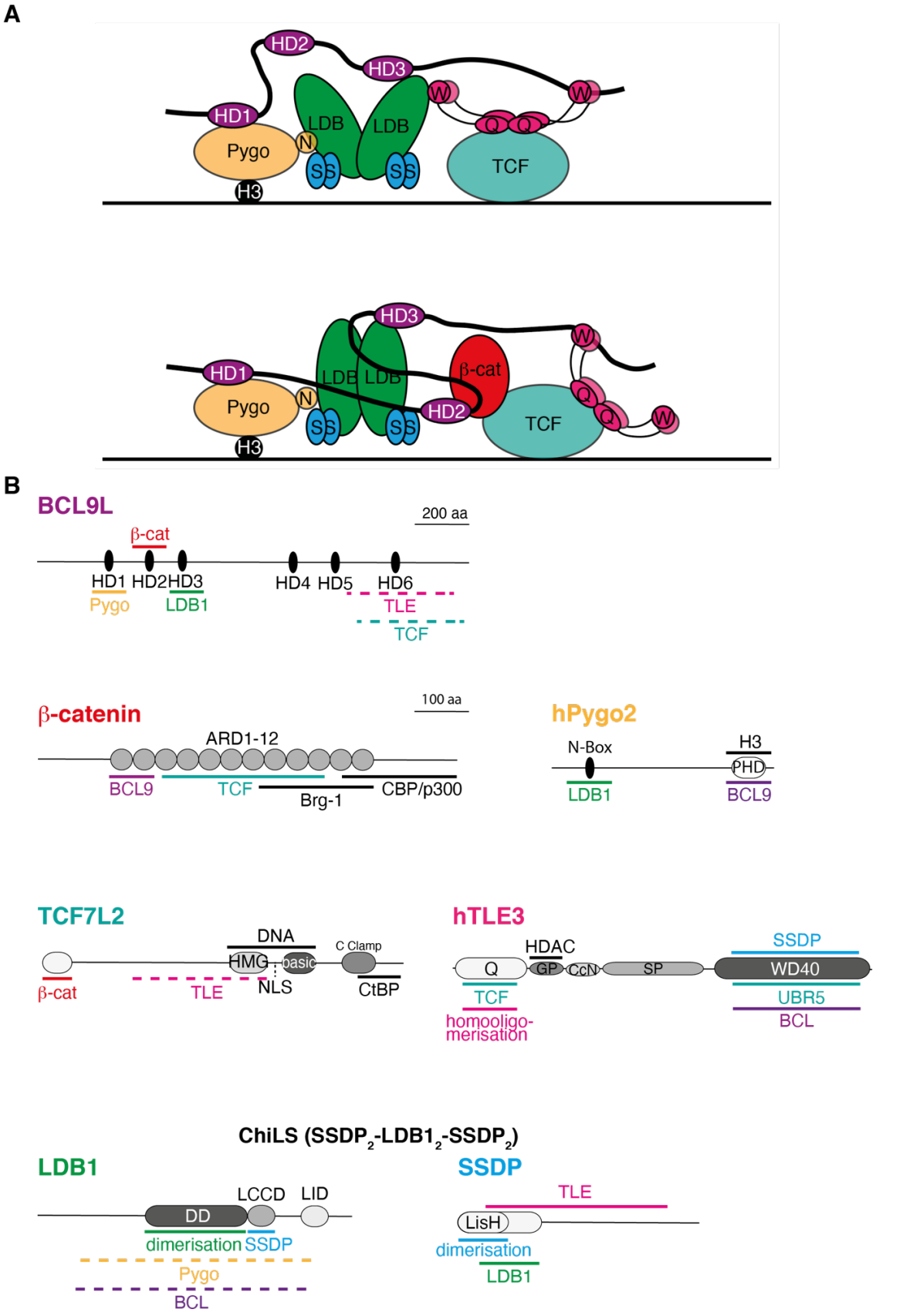

Figure 1.3. Schematic overview of the Wnt enhanceosome as outlined in van Tienen et al. (2017) and mapped interactions of core enhanceosome components.

A) In the nucleus, transcription of Wnt target genes is strictly controlled by a multiprotein complex centred around the scaffold complex ChiLS, consisting of 2 subunits LDB1 (green) and 4 subunits SSDP1/2 (blue). The ChiLS core module mediates interaction with several components including the corepressor TLE3 (pink) and the chromatin reader PYGO (yellow). The latter binds to the adaptor BCL9 (purple), which functions to capture β-catenin (red) facilitating formation of a β-catenin-TCF (turquoise) complex to activate transcription. In order to respond to changes in signalling, the enhanceosome needs to remodel and exchange repressive for activating factors. Figure adjusted based on van Tienen et al. (2017).
B) Interactions between proteins within the enhanceosome are depicted underneath the respective domain or, if the exact interacting domain is unknown displayed with a dotted line. See text (1.4) and section 2.1.1 & 2.1.2 for details. Scale bar = 100 amino acids (aa) for β-catenin, PYGO, TCF, TLE, LDB and SSDP; = 200 aa for BCL.

1.5. Pioneer factors prime silenced loci for gene expression

The existence of factors that engage with compact chromatin to facilitate accessibility for transcription factors has been hypothesised since the late 1990s, and this was underscored by the discovery that the Forkhead box factor FOXA (previously known as HNF3) is able to bind to inaccessible chromatin by Kenneth Zaret's lab in 2002 (Cirillo et al., 2002).

The Zaret lab has since assayed a range of pioneer factors in different developmental and disease contexts and has confirmed that FOXA binding results in opening of chromatin, thereby making it more accessible for downstream transcription factors. While FOX proteins and the FOXA subclass in particular have attracted a considerable amount of attention in the field, other pioneer factors have been described, including the pluripotency factor OCT4 (King and Klose, 2017), the GATA family (Wu et al., 2014, Theodorou et al., 2013) as well as RUNX proteins (Lee et al., 2019).

Pioneer factors are crucial for development, such as during differentiation of pluripotent embryonic cells, and are thought to initiate developmental lineages which are then further maintained by specialised transcription factors. In human and *Drosophila* development, the pioneer factors Oct4/Sox2 and Zelda, respectively,

play a central role in switching on zygotic gene expression (Schulz et al., 2015). Functionally, these proteins can either prime a locus actively by opening up chromatin structure through diverse interactions, or passively by reducing the number of subsequent binding events required for activation. This allows a rapid response later in development when the correct tissue- or context-dependent signals are present (Figure 1.4).

An active, but ATP-independent mechanism through histone binding and nucleosome positioning has been proposed for a number of FOX proteins, including FOXA (Cirillo et al., 2002, Iwafuchi-Doi et al., 2016), FOXE (Cuesta et al., 2007) and FOXO (Hatta and Cirillo, 2007). Conversely, OCT4 requires the chromatin remodelling protein BRG-1 to make chromatin accessible (King and Klose, 2017). GATA2 has been shown to form and maintain chromatin loops to put enhancer and promoter sequences in proximity (Wu et al., 2014). FOXA has also been identified as a binding partner of Groucho/TLE3 and, interestingly, this interaction results in silencing rather than activation (Sekiya and Zaret, 2007). The authors speculate that this might be a failsafe mechanism to prevent inappropriate gene expression following priming of the locus (Zaret and Carroll, 2011).

Overall, while pioneer proteins have been the focus of a significant amount of research in the past decade, mechanistic details are often lacking and, despite their considerable involvement in cancer development, therapeutic approaches are still under investigation.

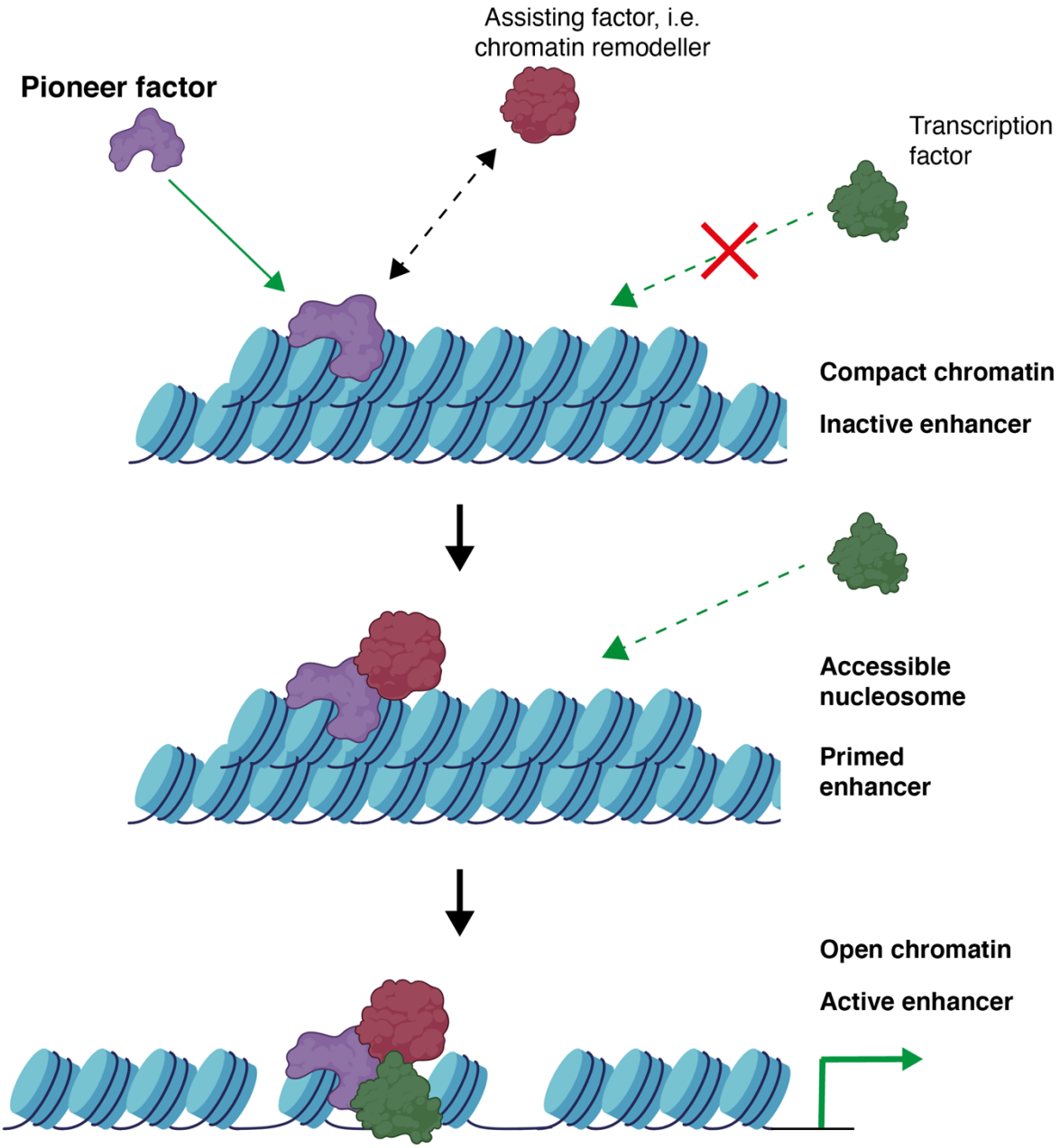

Figure 1.4. Pioneer factors access compact chromatin to prime it for binding by other transcription factors.
In contrast to most transcription factors (green), pioneer factors (purple) can access closed chromatin and make it more accessible by actively affecting nucleosome positioning or by recruiting remodellers (red) such as BRG-1.

1.6. Wingless signalling in *Drosophila* development

Given that much of this thesis, in particular Chapter 3, uses *Drosophila* as a model organism, I will briefly introduce the function of Wg during patterning and midgut development of the fly embryo as well as during larval development.

In the early fly embryo, a cascade of genes is switched on to provide the initial axis and broad body plan: maternal effect genes, gap genes, pair-rule genes, and segment polarity genes, each specifying smaller and smaller domains of the developing embryo. *Wg* is a classic example for a segment polarity gene and its expression is activated by Even-skipped (Eve) and Fushi-tarazu (Ftz) and restricted to the posterior boundary of parasegments during stage 9-10 of embryogenesis (Ingham et al., 1988).

Interactions between Wg, Hedgehog (Hh) and Engrailed (En) define and uphold the parasegment boundaries, and Wg and En govern the patterning of the cuticle through downstream factors such as Serrate, Rhomboid and Shaven baby (Alexandre et al., 1999; Payre et al., 1999) as well as Naked (Zeng et al., 2000): *en*-expressing cells specify 8 characteristic denticle belts on the ventral cuticle with Wg-specified naked cuticle separating them (Bejsovec and Wieschaus, 1993) (Figure 1.5, for review see Swarup and Verheyen, 2012).

Aberrant Wg signalling therefore affects the formation of these denticles, leading to a "denticle lawn" if underactive (e.g. through inactivation of *wg* itself) or an excess of naked cuticle when overactivated (e.g. following loss of *Axin* or *APC*). Differentiation of the embryonic cuticle is one of the earliest visible signs of mutations in the Wg pathway and is often used as a sensitive assay to determine function of putative Wg pathway components (Mieszczanek et al., 2008; Peifer et al., 1994).

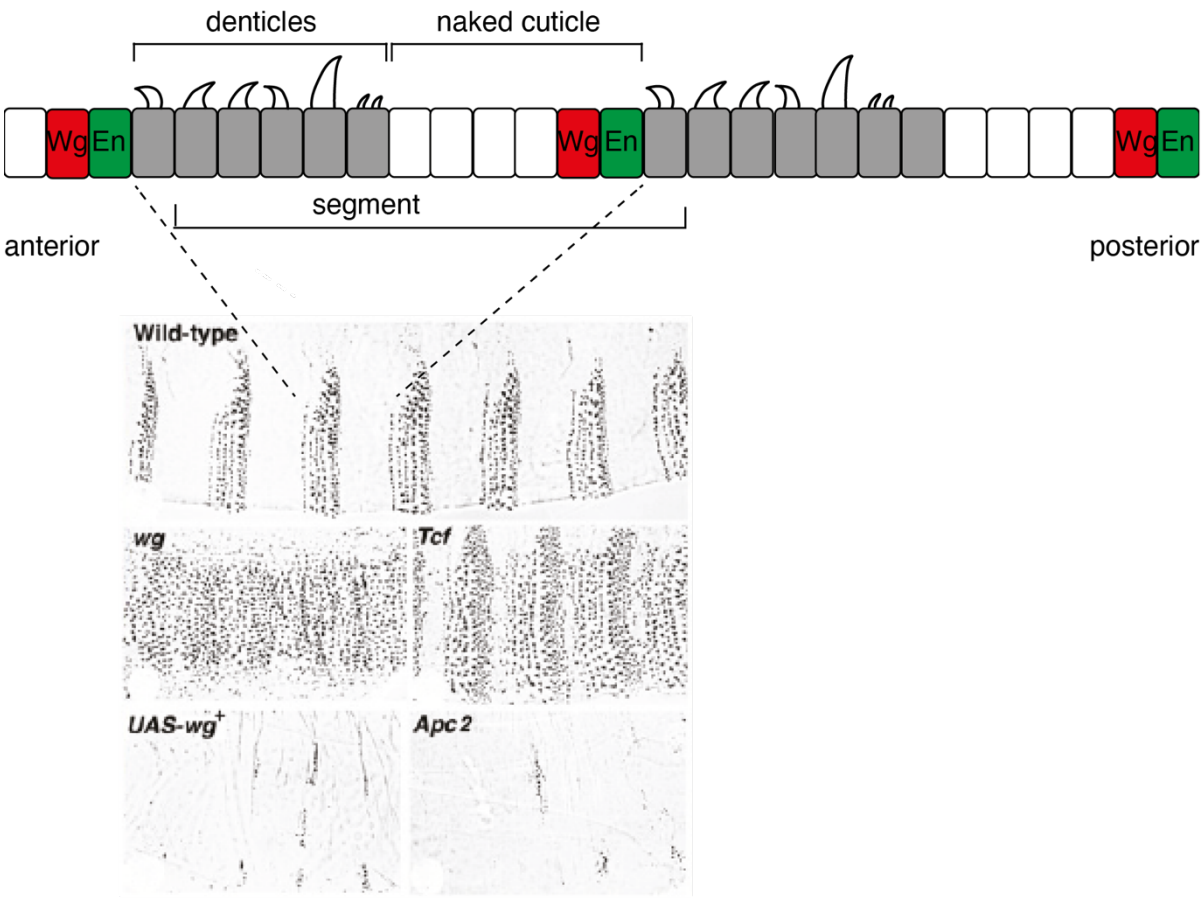

Figure 1.5. Wingless signalling is required for correct patterning of the cuticle during *Drosophila* embryogenesis.
Interaction of Wg, En and Hh define the parasegment boundary leading to specification of naked cuticle and denticle belts (upper panel). Loss of *wg* or *Tcf* results in loss of naked cuticle and embryos exhibit a characteristic denticle lawn (middle panel), whereas loss of negative regulators of Wg signalling such as *APC* or overexpression of *wg* results in excessive naked cuticle (lower panel).
Cartoon adjusted from Swarup and Verheyen, 2012; cuticle images taken from Bejsovec, 2006.

Later in embryogenesis, Wg signalling plays an important role during patterning of the midgut (reviewed in Bienz, 1994): *wg* is expressed in parasegment 8 of the visceral mesoderm and controls expression of two homeotic genes, *Ultrabithorax* (*Ubx*) and *labial* (*lab*) by acting at different thresholds (Hoppler and Bienz, 1995). Low levels of Wg lead to induction of *Ubx* and *lab* in their respective tissues, whereas high levels of Wg are required to activate *Teashirt*, which encodes a transcriptional

repressor that interacts with Armadillo to silence target genes in cells receiving a high amount of Wg (Waltzer et al., 2001).

Ubx is thus maintained in parasegment 7 by low Wg levels and itself induces Decapentaplegic (Dpp, of the TGFβ family of growth factors) (Sun et al., 1995; Yu et al., 1996). *Labial* expression is controlled by both Dpp and Wg in the subjacent endoderm where it directs differentiation of copper cells in the larval midgut (Hoppler and Bienz, 1994). Ubx is required for the formation of the middle midgut constriction (Bienz and Tremml, 1988) (Figure 1.6A) and loss-of-function of the Wg pathway results in defects in this process. Thus, *Ubx* expression in the midgut is a very sensitive assay to analyse activity of the Wg pathway *in vivo* (Thuringer et al., 1993).

Wg signalling is also crucial in larval stages, notably for the intricate patterning of the imaginal discs, the epithelial sacs of cells that give rise to ectodermal structures such as the body appendages. The most prominent example for Wg-mediated regulation in larval development is the wing disc, and weak mutations in *wg* itself give rise to wingless flies (Sharma and Chopra, 1976). Other well documented functions include the differentiation of the eye and leg discs.

In the wing disc, *wg* is initially expressed broadly across the entire disc in 2nd and early 3rd instar larvae before becoming more restricted: in wing discs of 3rd instar, "climbing" larvae, *wg* is expressed in two circles surrounding the presumptive blade tissue to specify the hinge region as well as along the presumptive wing margin at the dorso-ventral boundary (Baker, 1988). This expression pattern is the result of collaboration of several pathways, most importantly Notch signalling (Couso and Arias, 1994), which induces Vestigial (Kim et al., 1996) at the dorso-ventral boundary resulting in localised *wg* expression.

Here, Wg induces expression of *senseless* in cells directly adjacent to the Wg source (Parker et al., 2002) and acts in a morphogen-like fashion to induce genes requiring lower levels of Wg further away from the source, such as *Distalless* (Neumann and Cohen, 1997) (Figure 1.6B). The dorso-ventral boundary thus acts as an organising centre during wing patterning. This view was challenged by findings that membrane-tethered Wg leads to largely normal development and expression of target genes, although a mild decrease in wing size indicated a requirement of secreted Wnt for sustained proliferation (Alexandre et al., 2014). Newer studies showed that secreted Wg reaches cells up to 11 cells away from the margin (Chaudhary et al., 2019), reinforcing the definition of Wg as a morphogen.

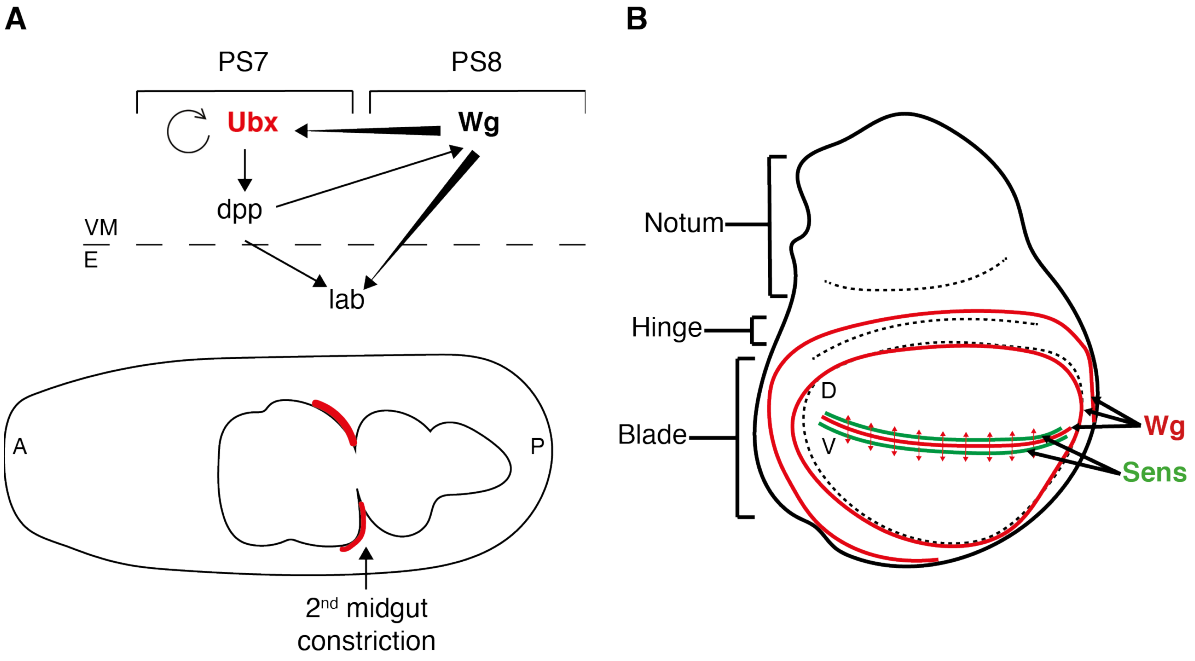

Figure 1.6. Wingless signalling during *Drosophila* development.
A) *Wg, Ubx* and *Dpp* form a regulatory circuit in the visceral mesoderm, whereby expression of *wg* in parasegment 8 (PS8) of the visceral mesoderm is required to maintain *Ubx* expression in PS7. Both Wg and Ubx (through *dpp*) are required for *labial* expression in the subjacent endoderm to drive cell differentiation. Ubx is further necessary for the formation of the 2nd midgut constriction.
B) Patterning of the 3rd instar wing imaginal disc requires Wg signalling at the presumptive wing margin as well as in two rings surrounding the blade. *Senseless* is a direct Wg target gene and is induced in two stripes flanking the dorso-ventral boundary.
VM = visceral mesoderm, E = endoderm, A = anterior, P = posterior, PS = parasegment, D = dorsal, V = ventral, Ubx = Ultrabithorax, dpp = decapentaplegic, lab = labial, Sens = Senseless.

1.7. Outstanding questions in the Wnt field

While the main steps of Wnt/Wg signalling during development and disease as presented here are generally accepted in the field, questions prevail concerning mechanistic details of several steps. One of the key issues that needs to be resolved is the mechanism of Wnt target gene regulation in the nucleus, and this will be the main focus of this thesis. Specifically, while we know that transcription is tightly regulated by an enhanceosome complex, open questions concerning its composition remain:

(1) In addition to the core components of the enhanceosome, what other factors, e.g. lineage-specific effectors, bind to and regulate enhanceosome activity?

(2) How is the composition of the enhanceosome adapted to different stages during development or disease as well as in different cell lineages?

(3) Are repressive and activating factors bound throughout the signalling cycle and become activated or inhibited as appropriate or is the enhanceosome a more dynamic structure, with factors coming and going as the signalling status changes?

(4) And, maybe most intriguingly, how is this multiprotein complex correctly assembled at its target loci? Does this process require pioneering factors?

In this work, I tackle some of these open questions using a proteomics approach based on BioID (Chapter 2) to assess enhanceosome remodelling during signalling as well as to uncover novel interactors of the core components PYGO and TLE3. I find the Forkheadbox factors FOXK1/2 associated with the enhanceosome and examine their potential role during Wnt/Wg signalling in *Drosophila* (Chapter 3) and mammalian cells (Chapter 4). Chapter 5 will discuss these novel findings and how they add to our knowledge of enhanceosome-based gene regulation. I will also highlight future strategies for the field in each chapter discussion as well as in Chapter 5.

2. Interactions within the Wnt Enhanceosome

2.1. Introduction

Many of the known components of the Wnt enhanceosome outlined in section 1.4 have been discovered using proteomic approaches. For example, the fundamental role of ChiLS as a scaffold became evident following tandem-affinity purification studies searching for novel ligands of PYGO-NPF (Fiedler et al., 2015). More recently, proximity labelling based on promiscuous biotin ligases (BioID) has helped elucidate remodelling of the enhanceosome as it switches from ON to OFF (van Tienen et al., 2017).

We decided to expand our model of the enhanceosome and address the open questions listed in Chapter 1 by using BioID with TLE3 and PYGO2 as bait proteins. The ensuing sections will introduce both bait proteins in more detail and will explain the advantages and limitations of the BioID system.

2.1.1. Role of PYGO in the Wnt enhanceosome

Pygopus/PYGO was discovered as a downstream effector of Wnt/Wg signalling in several independent genetic screens in *Drosophila* in the early 2000s (Kramps et al., 2002; Parker et al., 2002; Thompson et al., 2002). There are two *PYGO* paralogues in mammalian genomes (PYGO1/2), of which PYGO2 appears to be the more physiologically relevant protein based on its broader expression domain (Li et al., 2004).

Experiments using *Drosophila* revealed a strict requirement for PYGO function only in the presence of transcriptional repressors such as TLE3/Groucho, and *groucho pygo* double mutants show rescue of the *wg*-like phenotypes of *pygo* single mutant (Mieszczanek et al., 2008). PYGO thus has an important anti-repressor function that

predisposes the enhanceosome for rapid activation of transcription once β-catenin/Armadillo has docked to the complex (Figure 2.1).

PYGO is constitutively associated with Wnt target loci in a Wnt-independent, TCF-dependent manner (de la Roche and Bienz, 2007), which is in part mediated by binding of its NPF motif (also known as N-Box) to the ChiLS module of the enhanceosome (Fiedler et al., 2015). An important role of PYGO is to "read" the histone code by specific interaction between the PYGO-PHD finger and differentially methylated histones. Structural and biophysical analyses have shown that PYGO-PHD preferentially binds to H3K4me2, a sign of active transcription, but is less sensitive to methylation on H3K2, a marker of transcriptional repression (Fiedler et al., 2008).

Histone binding by PYGO is affected by simultaneous binding to the homology domain 1 (HD1) of BCL9: both interactions are mediated by opposite surfaces of the PHD finger, and binding of BCL9 allosterically increases affinity for histone binding (Miller et al., 2010), i.e. BCL9 acts as a modulator of PYGO histone decoding. Human and fly Pygo proteins differ in a crucial amino acid within the PHD finger resulting in slight differences in their histone binding properties. This appears to affect the activity of PYGO in Notch signalling – fly Pygo is exclusive to Wg signalling, but mutation of the fly amino acid to the residue found at this position in the human ortholog changes the property of Pygo, which becomes active in Notch signalling, leading to derepression of Notch targets (Miller et al., 2013).

It is currently not known whether the PYGO NPF motif or PHD finger have additional interaction partners that are required for its anti-repressor function.

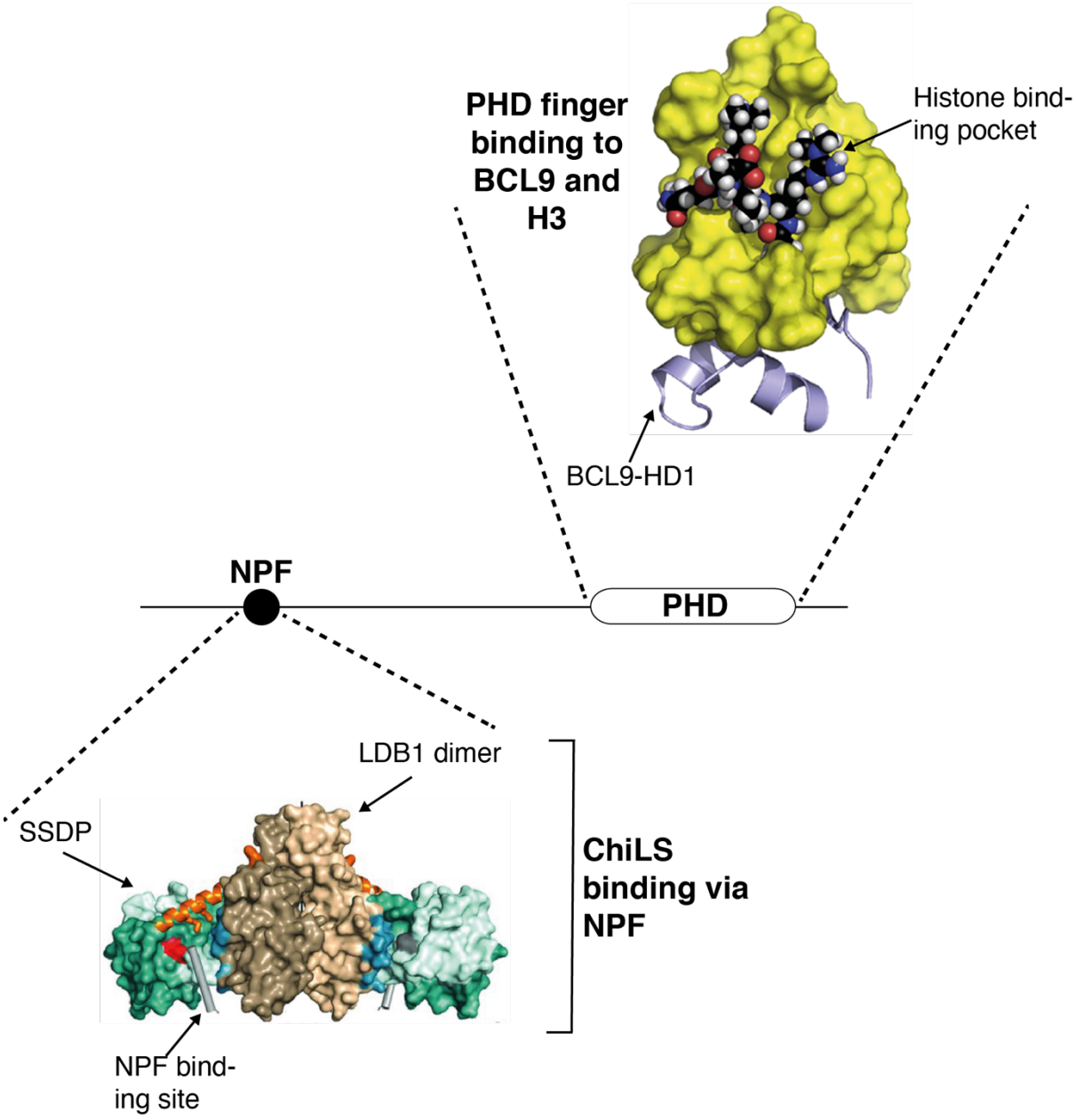

Figure 2.1. PYGO binds to methylated histones and BCL9 through its PHD finger and is tethered to the Wnt enhanceosome through binding to the ChiLS complex.
PYGO comprises a C-terminal chromatin-binding PHD finger (Parker et al., 2002) and an NPF motif in its N-terminus (Parker et al., 2002; Städeli and Basler, 2005). Biophysical studies revealed that binding of BCL9 results in allosteric changes within the PHD finger, increasing the affinity towards K4me2-methylated histone H3. The NPF motif is thought to bind to a pocket created by the SSDP2-LDB1-SSDP2 structure of the ChiLS complex.
ChiLS structure from Renko et al. (2019) (LDB1-DD (wheat), LDB1-LCCD (orange), SSDP dimers (cyan)). Ternary complex consisting of BCL9-PYGO-H3 from Miller et al. (2013), BCL9-HD1 shown as blue ribbon, PYGO-PHD as molecular surface representation in yellow with dually methylated histone (H3R2me2aK4me2) bound to the histone binding pocket.

2.1.2. Role of TLE3 in the Wnt enhanceosome

Given the constitutive association of WREs with TCF and PYGO, cells require a means to repress transcription in the absence of Wnt signalling. This mechanism relies heavily on binding of the corepressor protein transducin-like enhancer of split (TLE1-4, Groucho in *Drosophila*) to TCF via the TLE Q domain (Cavallo et al., 1998; Chodaparambil et al., 2014).

TLE proteins are broadly expressed and important for diverse developmental processes including segmentation, neurogenesis and haematopoiesis (reviewed in Agarwal et al., 2015). Apart from their role in Wnt signalling, TLE proteins are also crucial corepressors for Notch target genes (Barolo et al., 2002). Experiments in *Drosophila* found that Groucho-mediated repression of Wg target genes is limited to tissues that normally respond to Wg, such that loss of *groucho* does not lead to derepression of Wg targets in tissues that do not receive a Wg signal (Mieszczanek et al., 2008).

TLE3 is a large protein with several domains that mediate interaction with other proteins as well as oligomerisation (Figure 2.2). The N-terminal Q domain is required for transcriptional repression as well as tetramerisation (Pinto and Lobe, 1996; Song et al., 2004), which increases the number of interaction sites through which TLE can bind to different binding partners simultaneously. The Q domain is followed by a region rich for glycine and proline residues (GP domain), which mediates interaction with histone deacetylases that TLE recruits to silence loci (Brantjes et al., 2001; Chen et al., 1999). Further downstream are a CcN motif, which contains casein kinase II and cdc2 kinase phosphorylation sites and a nuclear localisation sequence, and a serine and proline rich region (SP domain). The C-terminal WD40 domain is highly conserved between different TLE proteins and is made up of several repeats of 40 amino acids separated by tryptophan-aspartic acid (WD) dipeptide sequences (Neer

et al., 1994). Structural analysis has shown that the repeats are arranged in a β-propeller structure with blades consisting of antiparallel β-sheets (Chen and Courey, 2000).

The WD40 domain mediates binding to crucial interactors including the Notch pathway regulator Hairy (Fisher et al., 1996), Runt factors (Aronson et al., 1997) and the Wnt proteins ChiLS and BCL9 (Fiedler et al., 2015; van Tienen et al., 2017). The same domain also binds UBR5, an agonist of Wnt-mediated transcription and negative regulator of TLE3 (Flack et al., 2017, see below). Since TLE proteins do not bind to DNA directly, these interactions are also necessary to recruit TLE to its respective loci as in the case of TLE recruitment to Notch targets by Hairy-related/HES proteins (Fisher et al., 1996).

While earlier evidence suggested that activation of Wnt signalling and associated nuclear translocation of β-catenin leads to displacement of TLE from TCF (Daniels and Weis, 2005; Hikasa and Sokol, 2011), newer studies have shown that β-catenin and TLE can bind to TCF simultaneously (Chodaparambil et al., 2014), and that recruitment of coactivators and/or inhibition of TLE3 ultimately allow target gene expression.

Recent evidence for TLE3 inhibition during Wnt signalling by Flack et al. (2017) describes the HECT3 ubiquitin ligase Hyd/UBR5 as instrumental for the inhibition of TLE3. Together with the AAA ATPase valosin-containing protein (VCP/p97) this results in extraction of TLE3 from the chromatin, thereby releasing repression and allowing the transcriptional switch to proceed. Other authors have proposed a model by which the E3 ubiquitin ligase XIAP mediates ubiquitination of the TLE3 Q domain, thereby disrupting the interaction with TCF and allowing transcription to be activated (Hanson et al., 2012).

It remains unknown whether these mechanisms act in parallel or sequentially, or whether additional mechanisms are required to facilitate the transcriptional switch of the Wnt enhanceosome.

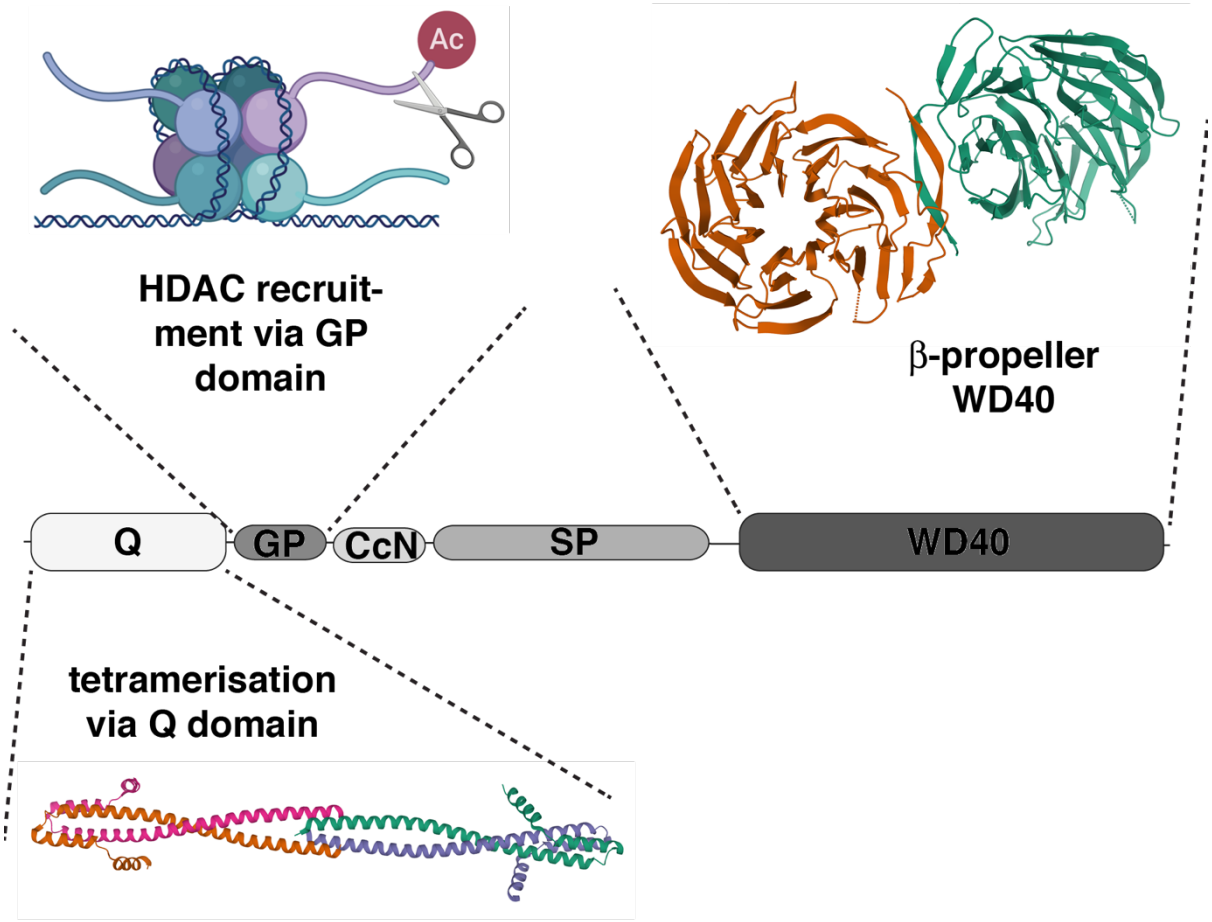

Figure 2.2. TLE3 oligomerisation is mediated through the N-terminal Q domain, while the GP and WD40 domains recruit additional interactors.
Tetramerisation of TLE via the Q domain is required for its repressive actions, which are mediated mostly by recruitment of histone deacetylases (HDACs) by the GP domain resulting in chromatin compaction. The 7-8 WD40 repeats per TLE protein form a β-propeller, allowing interaction with SSDP for tethering to the Wnt enhanceosome as well as with negative interactors such as UBR5.
Structure of Q domain: PDB 4OM2 (Chodaparambil et al., 2014); histone cartoon from biorender.com; structure of WD40 domain: PDB 1GXR (Pickles et al., 2002).

2.1.3. Proximity labelling of the enhanceosome interactome

In contrast to classic protein interaction assays, proximity-based approaches rely on labelling with a small molecule such as biotin, which allows identification of proteins

within up to 30 nm of the protein of interest (bait) and makes capture of indirect and transient interactors, in addition to direct binding partners, possible. The two main methods based on biotin labelling are APEX (established by the Ting lab; Rhee et al., 2013) and BioID, which was developed by Roux et al. (2012).

BioID employs engineered biotin ligases (BirA*) fused to bait proteins to assess interactomes of any protein of interest. This has been used to analyse the composition of the Wnt enhanceosome previously with PYGO and BCL9 as bait proteins (van Tienen et al., 2017). These experiments have confirmed its strength in detecting both novel and transient interactions as well as revealing subtle rearrangements upon ON switch of transcription: using BioID, the authors were able to show a re-organisation pertaining to the linker protein BCL9 which changes its orientation upon β-catenin binding, abutting its C-terminus with TCF (previously proposed by Sampietro et al., 2006). The same study also revealed a constitutive association of the BAF complex with the Wnt enhanceosome and identified an interesting link to nuclear co-receptor proteins.

The workflow for BioID experiments is described in the Materials and Methods chapter (section 6.9.) and summarised in Figure 2.3. The output is a list of peptides of putative interactors and the number of total spectral counts (TSC) is often taken as the basis for comparison (Liu et al., 2004). This list includes direct binding partners and proteins that bind these factors (i.e. indirect partners of the bait protein) as well as unrelated proteins within the same cellular compartment. To minimise the risk of taking forward hits that are not part of the bait interactome, the data needs to be carefully normalised to a suitable control (see below).

A caveat of BioID is that it relies on available and accessible lysine residues for biotinylation and the spectral counts for each protein hit are therefore dependent on the number of suitable lysines as well as abundance of the interacting protein leading to a risk of over- or underestimation of certain interactors. Candidate interactors

identified in BioID experiments need to be validated by coimmunoprecipitation (CoIP) and other methods, such as functional disruption, to verify the interaction and determine how this interaction affects cellular processes.

Early BioID experiments were subject to limitations based on use of the original set of BirA* enzymes from *E. coli* (BioID1) (Roux et al., 2012) or *A. aeolicus* (BioID2) (Kim et al., 2016). These enzymes are not very efficient and require high amounts of biotin as well as long labelling times (12-16 h) and a high amount of starting material (usually four confluent T175 cell culture flasks) to acquire a representative list of interactors. While the latter issue can be resolved by scaling the experiment as needed, the long labelling times pose a problem in capturing the temporal resolution of subtle adaptations within the Wnt enhanceosome upon β-catenin binding.

Fortunately, in later stages of this work a range of novel engineered BirA* enzymes became available for use in BioID essays. TurboID and MiniID have reported labelling times of as little as 1 min (Branon et al., 2018) and do not require high amounts of biotin, which is also of advantage for BioID studies in living organisms like *Drosophila*. While my initial BioID studies with PYGO2 as a bait relied on use of the original BioID1 enzyme (described in section 2.2.), I was able to employ the new TurboID enzyme for a time course experiment with TLE3 as the bait protein (see 2.3.).

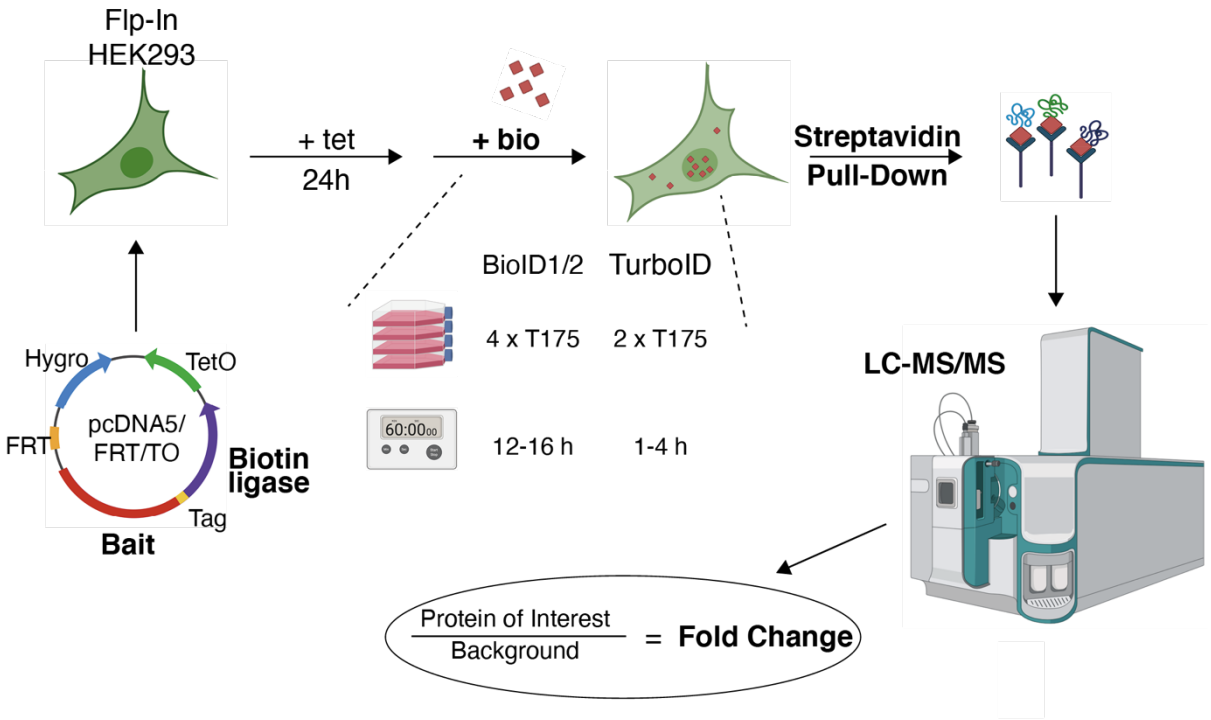

Figure 2.3. Workflow for proximity-based labelling of the interactome of different enhanceosome components.
The bait proteins (here TLE3 or PYGO2, including PYGO2 mutants) are fused to a BirA* enzyme and cloned into an FRT plasmid which is stably inserted into Flp-In HEK293 cells. Expression of bait-BirA* fusion proteins is controlled by tetracycline (tet). Duration of biotin (bio) as well as amount of cells required depend on the biotin ligase in use; BioID1/2 require a higher volume and longer labelling times than TurboID. Interactors labelled with biotin are pulled down using a streptavidin matrix, separated on a protein gel and measured using LC-MS/MS. Data analysis is done by comparing fold change of proteins associated with the bait of interest vs. proteins associated with a background or wildtype (WT) control.

As with other proteomic experiments, dealing with a large data set is another challenge of proximity labelling methods. Several aspects need to be considered: 1) abundance of each protein hit, i.e. how often are peptides from this protein found in the sample, 2) reproducibility of hits and 3) normalisation, i.e. how specific is association of this protein with a bait vs. a control construct.

Several methods exist to assign a score to each protein hit. The most straightforward method is to calculate the fold change of each protein identified in each condition in comparison with its respective control, as done in this work. This approach is most

suitable for experiments based on wildtype (WT) vs. mutant proteins, where background subtraction is easiest.

Similar to other proteomic approaches it is important to control for variability, since results can be inconsistent and vary dramatically in between independent experiments. The impact of variation can be minimised by generating several replicates and integrating sample data using the Comparative Proteomic Analysis Software Suite (CompPASS, http://besra.hms.harvard.edu/ipmsmsdbs/cgi-bin/tutorial.cgi) developed by the Harper lab. This approach identifies high-confidence candidate interacting proteins (HCIPs) based on reproducibility, which helps avoid bias in comparison of sample data (Sowa et al., 2009).

This suite also factors in metrics such as abundance and uniqueness by assigning a higher score to proteins that are exclusive to one sample even if they are identified with a low TSC. This scoring system thus prevents loss of potential specific interactors that are not very abundant. For example, a protein with a TSC of 1 is often disregarded because its fold change over the control is not high enough to meet exclusion criteria, but if this protein is only found in a specific bait sample it could be an important interactor for that bait protein.

Due to time limitations, I was unable to produce replicates of either of my BioID experiments and therefore the CompPASS suite was not applicable to my data set. I thus used fold change analysis to compare total spectral counts of my proteins.

2.2. Results I: BioID with PYGO2

I decided to extend the PYGO BioID data set published in van Tienen et al. (2017) by analysing deletion mutants of each PYGO2 domain (PYGO2$^{\Delta N\text{-}Box}$ and PYGO2$^{\Delta PHD}$, Figure 2.4A) and measuring changes in interacting partners. Constructs were designed to contain a C-terminal fusion to BioID1 (separated by GS linker sequences and an HA-Tag) and a nuclear localisation signal to ensure correct localisation of the fusion protein. These constructs were stably introduced into Flp-In HEK293 cells and independent cell lines selected for low background expression and biotinylation as well as strong inducibility using immunofluorescence (IF) and biotinylation assays (Figure 2.4B & C, see 6.9).

BioID experiments were conducted by inducing expression of fusion proteins with tetracycline for 12 hrs prior to adding biotin (1 mM) for another 12 hrs before harvest. I used four confluent T175 cell culture flasks (~93x10^6 cells) per bait protein for experiments with BioID1. Note that based on the constitutive association of PYGO with the Wnt enhanceosome and previous studies that showed little reorganisation upon Wnt activation (van Tienen et al., 2017) this experiment was conducted in the absence of Wnt signalling.

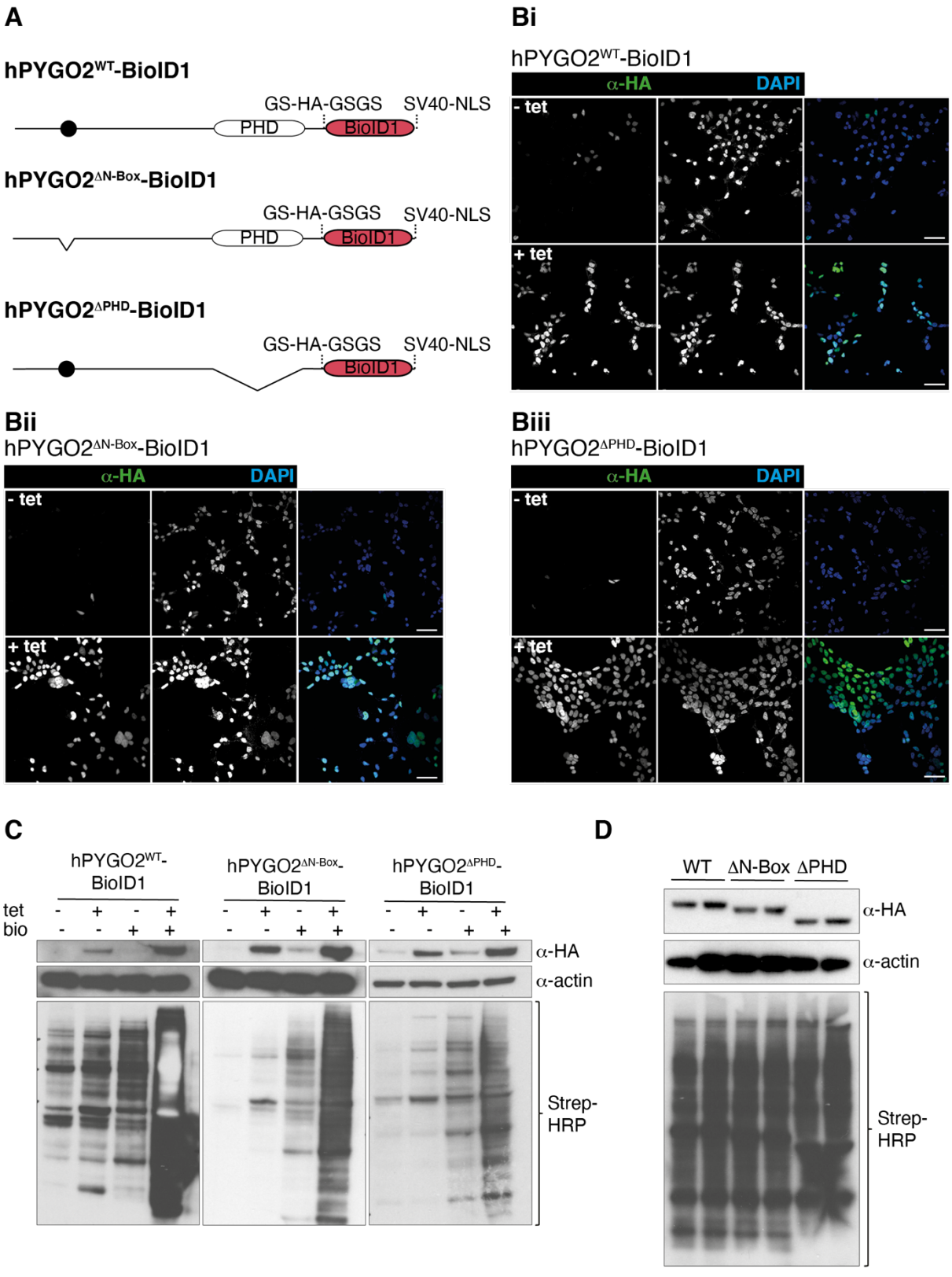

Figure 2.4. Construction and testing of lines for BioID experiments with PYGO2-WT and PYGO2 mutants PYGO2$^{\Delta N\text{-}Box}$ and PYGO2$^{\Delta PHD}$.

A) Cartoon of fusion constructs used in these experiments. Constructs were designed to include GS linkers as well as an internal HA tag for detection and a nuclear localisation signal from SV40.
Bi-iii) IF assays of HEK293 Flp-In lines expressing BioID1 fusion proteins, with or without tetracycline-mediated induction. Leaky expression is limited to few cells, whereas induction leads to expression of fusion constructs in ≥95% of cells. Bi) PYGO2-BioID1, Bii) PYGO2$^{\Delta N\text{-}Box}$-BioID1, Biii) PYGO2$^{\Delta PHD}$-BioID1. Scale bars = 50 μm.
C) Western blots of the same lines indicating inducible expression of fusion proteins upon tetracycline induction as well as biotinylation profiles. Background levels of expression as well as biotinylation prior to biotin supply are low in all lines.
D) BioID1 fusion lines found to be inducible and with low background expression were used in BioID experiments with 12h of biotin. Biotinylation smear resulting from these samples as sent for mass spectrometry.

2.2.1. PYGO2 interactome

The list of putative interactors for WT and the two PYGO2 mutants largely yielded similar results to the previously published data sets (van Tienen et al., 2017). BioID hits shown in Table 2.1 include the top hits (≥ 10 total spectral counts) and are pre-selected for nuclear proteins and those relevant to Wnt signalling, whereas unrelated, cytoplasmic proteins such as naturally biotinylated and highly abundant carboxylases are pre-filtered. A colour key was applied to sort proteins into groups (Wnt enhanceosome related (green), BAF complex components (blue), nuclear co-receptor components (orange) and histone modifiers (yellow)) for easier recognition. Raw data of this PYGO2 BioID experiment is listed in the appendix (8.7) with a cut-off at TSC ≥ 3 but without pre-selection of relevant interactors.

As expected, many Wnt components including TLE3, BCL9 and TCF7L2 (TCF4) showed high TSC in my PYGO2 BioID as do most components of the BAF complex (ARID1A/B, ARID2, ARID3B, SMARCA2/4/5 etc.). Additionally, my BioID results confirmed the strong connection between the Wnt enhanceosome and nuclear co-receptor components with NCOR1 as well as NCOA2/3 among the highest scoring proteins.

The BioID list also included low counts for the known PYGO2 binding partner ChiLS (both SSDP1/2 and LDB1 display <10 spectral counts each), which is in contrast to previous BioID studies where LDB1 scored much higher (van Tienen et al., 2017). My list of candidate interactors generally showed lower counts than the previous data set despite using the same method and bait-BioID1 fusion proteins based on the lines used in this publication.

Conversely, I identified several hits with high TSC that are absent from the previous data set, including SIN3B and the Wnt signalosome proteins DVL2/3. I also found two subunits of the BAF complex (SMARCA5 and SMARCC1) that are not identified by van Tienen et al., although other BAF subunits are listed with high scores. The reason for these discrepancies is unclear but could be related to differences in the state of the cell cultures or the performance of the mass spectrometry instrumentation.

Gene ontology (GO) enrichment analysis using the ShinyGO tool (Ge et al. (2019), available at http://bioinformatics.sdstate.edu/go/) confirmed that the majority of proteins in close proximity with PYGO2 (≥10 spectral counts in PYGO2^{WT} sample) are annotated with transcription-related GO terms including "nucleic acid-templated transcription" (FDR = 2.5E-36, 111 proteins), "transcription, DNA-templated" (FDR = 2.5E-36, 110 proteins) or "regulation of gene expression" (FDR = 2.5E-36, 120 proteins).

The top hit (i.e. with the highest spectral counts, higher even than PYGO2 itself) was the lysine demethylase JMJD1C. JMJD1C was reported to act as a transcriptional coactivator that erases repressive H3K9 methylation (Kim et al., 2010), although this has been challenged in more recent publications (Brauchle et al., 2013). Two important homologues of JMJD1C are the histone demethylases KDM3A/B and KDM6A, both of which also showed high scores in my BioID lists.

Histone modifying enzymes were generally among the highest scoring hits with no apparent dependence on the presence of either PYGO2 domain, i.e. the association was not weakened in either deletion mutant. Among these are known SET-domain histone methyltransferases such as KMT2A/B/C/D, which have been shown to methylate lysine-4 of histone 3, thereby increasing transcriptional activity, and KMT3A/B which specifically mediate H3K36 trimethylation (Edmunds et al., 2008). These proteins are close relatives of SET1 (also known as KMT2F), which was one of the earliest Wnt-dependent coactivators found to be recruited by β-catenin (Sierra et al., 2006).

DOT1L represents another top hit for PYGO2 interactors and this methyltransferase has been implicated in Wnt signalling previously as a known interactor of β-catenin/TCF (Mahmoudi et al., 2010). DOT1L mediates H3K79 methylation which is coupled to active transcription (Steger et al., 2008). The HAT p300 also showed high TSC in all PYGO2 BioID data sets as expected based on its recruitment by β-catenin.

It is striking that all of these histone modifying enzymes are associated with the Wnt enhanceosome prior to Wnt activation, reinforcing the hypothesis that PYGO-bound WREs are poised for transcriptional activation. However, I was also able to identify transcriptional repressors in association with the Wnt enhanceosome, most significantly GSE1, which scored high in the list of PYGO2 interactors and is a subunit of the BRAF35-HDAC1 deacetylase complex (Hakimi et al., 2003). I also identified HDAC1 itself, albeit at low counts.

Table 2.1. Top hits of PYGO2 BioID.

Top hits of BioID of PYGO2^{WT} and N-Box (PYGO2$^{\Delta N\text{-}Box}$) and PHD (PYGO2$^{\Delta PHD}$) deletions. BioID results were pre-sorted for strongest interactors (TSC ≥10) and then filtered for relevant hits including known Wnt enhanceosome components (green), BAF complex proteins (blue), nuclear co-receptor components (orange) and histone modifying proteins (yellow). Hits labelled in red text are either not identified or identified at very low counts in the previous BioID data set (van Tienen et al., 2017). Proteins relevant to Wnt signalling or either of the aforementioned groups were included even if they were identified with low counts and are shown separated by a bold line.

#	Protein ID	PYGO2^{WT}	PYGO2$^{\Delta N\text{-}Box}$	PYGO2$^{\Delta PHD}$
1	JMJD1C	220	258	189
2	**PYGO2**	**206**	**202**	**167**
3	NCOR1	117	146	179
4	ARID1A	110	110	119
5	ARID1B	110	109	119
6	ARID3B	71	60	70
7	ZNF318	65	96	46
8	Histone 1	62	36	53
9	SMARCA4	54	61	62
10	TLE3	53	59	48
11	BPTF	49	66	86
12	RBM14	49	66	86
13	GSE1	41	30	35
14	BRCA2	41	15	0
15	KDM3B	38	70	47
16	SIN3B	36	24	12
17	BCL9	34	20	0
18	KMT3A	29	31	35
19	DVL2	28	34	19
20	TLE1	27	37	26
21	NCOA2	26	20	7
22	NCOA3	26	17	16
23	SMARCA5	25	37	80
24	SMARCA2	25	27	33
25	DOT1L	24	35	19
26	p300	21	14	13
27	NCOR2	16	25	37
28	DVL3	16	22	13
29	NCOA5	15	11	15
30	ISL2	14	3	29
31	KDM3A	13	14	9
32	KMT3B	13	12	19
33	NCOA6	13	12	4
34	XIAP	12	13	29
35	KMT2B	11	17	8
36	TCF7L2	11	16	34
37	FOXK1	11	16	21
38	KMT2D	10	5	3
39	SMARCC1	10	2	0
40	ARID2	9	8	1
41	HAT1	8	14	16
42	SMARCE1	8	9	5
43	FOXC1	7	12	8
44	KMT2A	7	8	19
45	SSDP1/2	6-7	2	12-16
46	LMX1B	6	2	21
47	KDM6A	5	7	6
48	ARID3A	5	4	9
49	KMT2C	5	4	8
50	GATA6	5	4	8
51	SIN3A	5	4	1
52	LDB1	4	5	36
53	SMARCAD1	4	5	7
54	ARID5B	4	4	15
55	BCL9L	4	4	0
56	CTBP2	3	8	8
57	FOXK2	3	5	4
58	HDAC1	3	4	4
59	NCOA1	3	4	0
60	SMARCAL1	2	6	6
61	CBP	0	0	0
62	UBR5	0	0	0

Wnt enhanceosome
BAF complex
Nuclear co-receptor components
Histone modifiers

2.2.2. PHD-dependent PYGO2 interactors

To determine which protein interactors of PYGO2 are dependent on the PHD domain, results were sorted for fold change of $PYGO2^{WT}$ over $PYGO2^{\Delta PHD}$ (= WT/ΔPYGO2) and a cut-off was set for ≥5-fold change of WT vs. mutant (Table 2.2). As expected based on the interaction of BCL6-HD1 with the PHD finger, spectral counts for both BCL9 paralogues are zero following deletion of PYGO2-PHD (BCL9 TSCs: WT = 34, ΔPHD = 0; BCL9L TSCs: WT = 4, ΔPHD = 0).

Strikingly, this analysis also revealed the DNA repair protein BRCA2 as strongly dependent on the PHD finger. While BRCA2 was identified with high spectral counts in the WT sample, this interaction was abolished upon deletion of the PHD finger (BRCA2 TSCs: WT = 41, ΔPHD = 0). Note that the association with BRCA2 is also diminished in samples stemming from the $PYGO2^{\Delta N\text{-}Box}$ bait protein, although not as strongly (ΔN-Box = 15). Interaction with the BRCA2-associated protein EMSY also relies on the PHD finger, which is likely indirect due to loss of BRCA2 association itself. Additional components known to be involved in DNA repair also depend on the PHD finger for interaction with PYGO2 (RRP1B, WRNIP1).

Two components of the BAF complex (SMARCC1 and ARID1A) also appear to require a functional PHD finger for interaction with PYGO2.

Table 2.2. PHD-dependent interactors of PYGO2.
Binding to BCL9 and BCL9L is abolished upon loss of the PHD domain. Several proteins of the DNA damage response, most importantly BRCA2, interact with PYGO2 in a PHD-dependent manner. List includes proteins with a ≥5x change over WT PYGO2. Known interactors or proteins relevant to PYGO2 function have been added even if their fold change did not meet the criteria (upper bold line). Interaction with proteins of the ChiLS complex appears strengthened in PHD mutants as indicated by higher TSC in this sample (lower bold line).

#	Protein ID	PYGO2^{WT}	PYGO2$^{\Delta N\text{-}Box}$	PYGO2$^{\Delta PHD}$	Fold Change WT/ΔPHD
1	BRCA2	41	15	0	41
2	**BCL9**	**34**	**20**	**0**	**34**
3	ODF2	25	0	0	25
4	CENPF	20	9	1	20
5	RRP1B	18	6	0	18
6	WRNIP1	17	16	0	17
7	FAM208B	16	16	1	16
8	COPG2	15	8	0	15
9	TTF1	57	37	4	14.25
10	CD2AP	11	6	0	11
11	**SMARCC1**	**10**	**2**	**0**	**10**
12	**ARID2**	**9**	**8**	**1**	**9**
13	SRCAP	17	7	2	8.5
14	EMSY	8	8	1	8
15	NIN	8	0	0	8
16	ZNF326	7	10	1	7
17	ZNF746	7	6	0	7
18	RFX1	6	5	1	6
19	DSG1	5	1	0	5
20	UBA2	5	1	0	5
21	SIN3A	5	4	1	5
22	CTTN	5	3	1	5
23	OGT	5	2	1	5
24	**BCL9L**	**4**	**0**	**0**	**4**
25	**NCOA1**	**3**	**4**	**0**	**3**
26	Histone 3	0	0	0	n/a
27	**LDB1**	**4**	**5**	**36**	**0.1**
28	**SSDP1**	**6**	**2**	**16**	**0.375**
29	**SSDP2**	**7**	**2**	**12**	**0.583**

Wnt enhanceosome BAF complex Nuclear co-receptor components

In addition to protein interactions that are abolished in PHD mutants, there are also a number of interactors that yield higher scores upon loss of PHD. GO enrichment analysis revealed these novel interactors to be mostly involved in nucleic acid

metabolism, RNA processing, regulation of gene expression as well as chromosome organisation and similar, which may reflect displacement of PYGO2$^{\Delta PHD}$ from WREs.

An unexpected hit amongst the proteins whose interaction is enhanced upon loss of the PHD finger is the ChiLS complex, where both subunits show a stronger interaction with PYGO2$^{\Delta PHD}$ than PYGO2^{WT}: LDB1, which is strongly (9x) elevated in the ΔPHD-bait sample and SSDP1/2 which yield ~2x more spectral counts in mutant vs. WT sample (see Table 2.2 and discussion).

2.2.3. N-Box-dependent PYGO2 interactors

Similar to the analysis for PHD-dependent interactors, the fold change between PYGO2^{WT} and PYGO2$^{\Delta N\text{-}Box}$ was calculated and top hits with a fold change ≥5 used for downstream analysis (Table 2.3). This revealed a short list of 8 proteins that show decreased spectral counts in ΔN-Box compared with WT PYGO2.

The majority of these proteins are also decreased in PHD deletions (ODF2, NIN, DSG1, UBA2 and SMARCC1), while only DDX27, TP53BP1 and WRAP73 are specifically lost upon deletion of the NPF motif. None of these factors are annotated as involved in transcriptional regulation or have been reported as relevant to Wnt signalling and show very low overall counts. Based on these arguments, neither of the putative N-Box-dependent interactors were addressed in follow-up experiments.

Table 2.3. N-Box-dependent interactors of PYGO2.
Few protein interactors are lost upon deletion of the PYGO2-NPF motif. LDB1, a known direct binder of the PYGO2-N-Box does not show a decrease in TSC compared with WT PYGO2. Hits above the bold line are top hits, while LDB1 was added due to its known binding to PYGO2-N-Box. The Venn diagram depicts the strong overlap between interactors lost in PHD and NPF mutants.

#	Protein ID	PYGO2^{WT}	PYGO2$^{\Delta N\text{-Box}}$	PYGO2$^{\Delta PHD}$	Fold Change WT/ΔN-Box
1	ODF2	25	0	0	25
2	NIN	8	0	0	8
3	DDX27	5	0	4	5
4	SMARCC1	10	2	0	5
5	DSG1	5	1	0	5
6	UBA2	5	1	0	5
7	TP53BP1	5	1	3	5
8	WRAP73	5	1	6	5
9	SSDP1	6	2	16	3
10	SSDP2	7	2	12	3.5
11	LDB1	4	5	36	0.8

Wnt enhanceosome

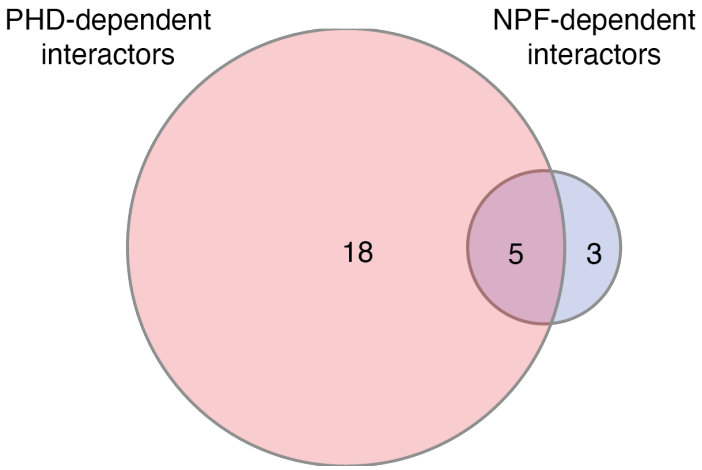

Taken together, my analysis of BioID experiments conducted with deletion mutants of PYGO2 reveals few previously unknown interactors that are dependent on the presence of either the NPF motif or the PHD domain for association with PYGO2. Among these proteins, BRCA2 is an interesting candidate that might specifically interact with the PYGO2-PHD domain. Future experiments are required to determine whether this putative interaction is important for Wnt signalling or other cellular processes.

2.3. Results II: BioID with TLE3

One of the key questions concerning transcriptional control through Wnt signalling is how the corepressor TLE3 is inhibited during active Wnt signalling and how repression is reinstated following a period of active transcription. With the development of the next-generation BioID enzymes it became possible to assess the restructuring of the enhanceosome before, during and after signalling.

I first sought to confirm the applicability of these novel ligases versus BioID1/2 in time courses by verifying their short labelling times in HEK293 cells. To this end, I compared the ability of different eGFP and TLE3 constructs fused to BioID2 or TurboID to generate a strong biotinylation profile at different time points (10 min, 1h, 4h, 8, 12h). BioID2 was chosen for comparability of results since these fusion proteins for BioID studies with eGFP and TLE3 were created before the next-generation enzymes became available.

This experiment revealed striking differences between BioID2, which leads to a clear "biotin smear" only after a minimum of 4 hrs of biotin addition, and the new TurboID, which yielded a strong ladder of biotinylated protein after only 10 min labelling (Figure 2.5, left panel vs right panels, white spots indicate a strong biotin signal leading to bleaching despite limiting exposure to a few seconds). Note that the distinct protein bands in samples without added biotin likely correspond to different naturally biotinylated carboxylases as described in Bramwell (1987), tentatively propionyl carboxylase (70 kDa), β-methyl crotonyl CoA carboxylase (75 kDa) and pyruvate carboxylase (120 kDa).

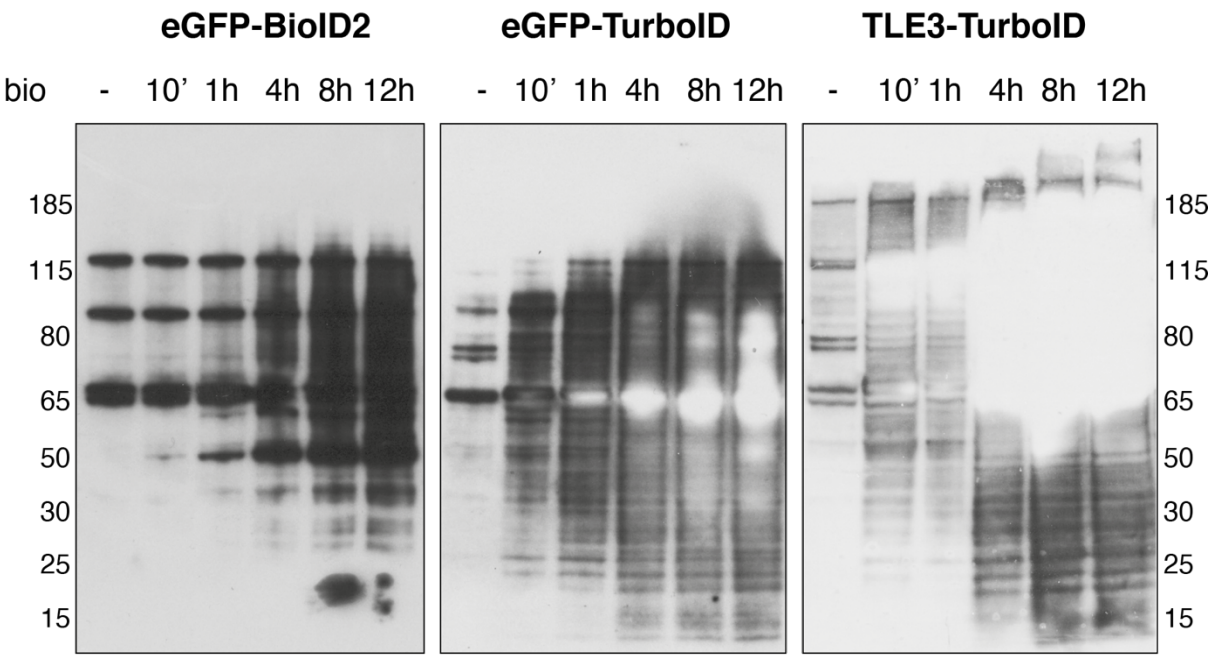

Figure 2.5. Comparison of biotinylation profiles created by eGFP or TLE3 fusions between the classic BioID2 enzyme and the next-generation biotin ligase TurboID.
Stably transfected eGFP-BioID2, eGFP-TurboID and TLE3-TurboID fusion proteins were induced for 12h with tetracycline before addition of 1 mM biotin for the indicated amount of time (10 min, 1 hr, 4 hrs, 8 hrs, 12 hrs). Western blots were developed using streptavidin-HRP and exposed for <10 seconds. Biotinylation profiles of both TurboID lines are consistently stronger than those based on BioID2. White spots in the two right panels indicate overexposure effects due to strong biotinylation. Addition of biotin for 10 min only yields sufficient biotinylation for downstream applications, proving that the next-generation enzymes are indeed superior to the original enzymes.

Based on these results I devised a time course experiment to analyse interactors of TLE3 during different signalling stages. Due to a negative feedback loop based on Wnt-induced expression of the Wnt antagonists *naked* and *Axin2*, β-catenin-mediated expression may be downregulated in cells that receive sustained Wnt stimulation. This feedback loop may have made interpretation of results from BioID experiments based on 12 hrs of Wnt stimulation challenging as these likely represent a convolution of different signalling states.

In order to avoid potential effects of downregulation of Wnt signalling, I chose a 4-hr window for biotinylation during Wnt stimulation using LiCl. Many Wnt target genes including *Axin2* and *TCF7L2* are highly expressed after 4 hrs of Wnt treatment

(Li et al., 2012), but this time point is unlikely to incur changes in the interactome owing to re-silencing. I decided to use LiCl, which activates Wnt signalling by blocking the degradasome at the level of GSK3 and mimics induction with Wnt-conditioned medium (WCM, (Stambolic et al., 1996)).

This led me to develop four different treatments, all preceded by 12 hrs of tetracycline for full induction of the TLE3-TurboID fusion protein: (1) labelling for 4 hrs with LiCl medium to analyse changes to TLE3 interactors upon Wnt induction (4h_LiCl+bio), (2) labelling for 4 hrs with NaCl medium to assess TLE3 interactions before signalling (4h_NaCl+bio), (3) 4 hrs of LiCl followed by 2 hrs of biotinylation to capture processes during immediate re-silencing (4h_LiCl+2h_bio) and (4) a NaCl control equivalent to condition (3) to control for the shorter labelling times (4h_NaCl+2h_bio). LiCl or NaCl-containing medium was washed off before adding biotin for treatments 3 & 4, respectively. Conditions are summarised in Figure 2.6D.

BioID cell lines were constructed to contain a C-terminal TurboID fusion separated by a GS linker and V5 tag from the WD40 domain of TLE3 (Figure 2.6A). I decided to use an eGFP-TurboID construct which was specifically targeted to the nucleus as a control. This is in contrast to previous BioID studies of enhanceosome components, which used a BirA* control that was largely cytoplasmic (van Tienen et al., 2017). I surmised that a nuclear control would be more suitable to subtract background proteins that are highly abundant in the nucleus and therefore become biotinylated by enhanceosome-based bait proteins without any relevance to Wnt signalling (see discussion).

Lines were tested for low background expression and strong biotinylation as before (Figure 2.6B & C). BioID experiments with TurboID were conducted with a lower amount of starting material compared to above described experiments (2 confluent T175 cell culture flasks, approx. 45 x 10^6 cells).

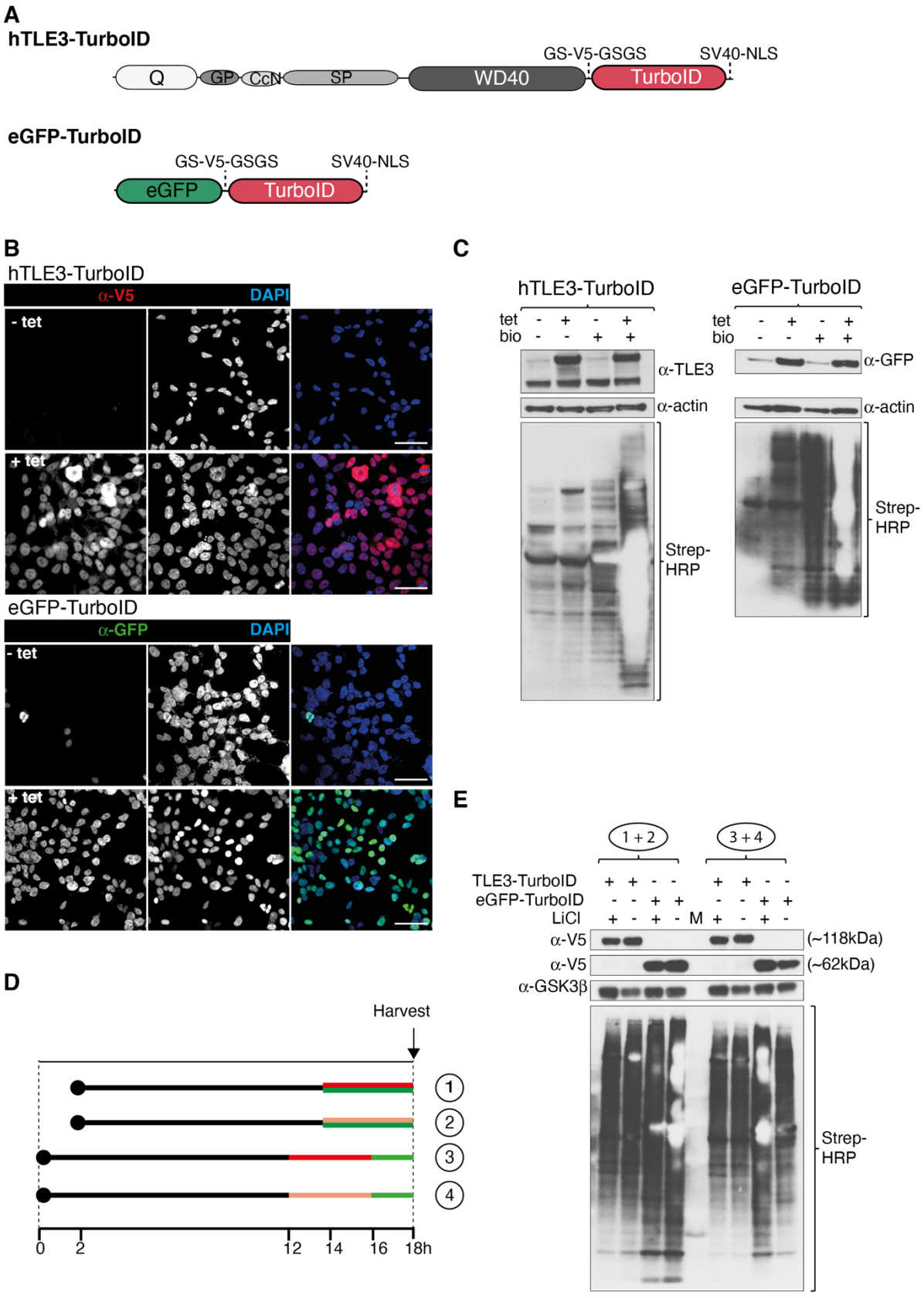

Figure 2.6. Construction and testing of BioID lines for a time course experiment based on TLE3-TurboID and an eGFP-TurboID control.

A) Cartoon of TLE3-TurboID and eGFP-TurboID fusion constructs used in these experiments. Constructs were designed to include GS linkers as well as an internal V5 tag for detection and a nuclear localisation signal from SV40.
B) IF assays of HEK293 Flp-In lines expressing TLE3-TurboID (upper panel) or eGFP-TurboID (bottom panel), with or without tetracycline-mediated induction show that leaky expression is limited to few cells, whereas induction leads to expression of fusion constructs in ≥95% of cells. Scale bars = 50 μm.
C) Western blots of the same lines indicating inducible expression of fusion proteins upon tetracycline addition as well as biotinylation profiles. Background level of expression is very low in both lines. Background biotinylation in uninduced TLE3-TurboID is very low, slightly higher in eGFP-TurboID. Addition of biotin in all samples results in a strong smear of biotinylated proteins. White spots indicate bleaching due to overexposure as before.
D) Time course chosen for this TurboID experiment with TLE3 and eGFP. TLE3 interactors were tested during active Wnt signalling (4h_LiCl+bio), before Wnt signalling (4h_NaCl+bio) as well as in the re-silencing phase after Wnt stimulation is withdrawn (4h_LiCl+2h_bio and a respective NaCl control).
E) Resulting biotinylation smear from the same samples in D). Samples in all lanes lead to approximately the same amount of biotinylated protein following pull-down with Streptavidin. BioID samples were sent for mass spectrometry.

2.3.1. TLE3 interactome

To determine proteins associated with TLE3 in the absence of Wnt signalling, the peptides identified following 4 hrs of biotinylation under NaCl control conditions were compared to the respective eGFP control and the fold change calculated (TLE3-TurboID_4h_NaCl+bio / eGFP-TurboID_4h_NaCl+bio).

This list includes a high number of unrelated cytoplasmic proteins such as carboxylases and therefore required additional filtering for relevant proteins. Relevance was determined using database entries and literature research, with candidates discarded if they were annotated as exclusively cytoplasmic or elements of the cytoskeleton. Raw data of this TLE3 BioID experiment is listed in the appendix (8.8) with a cut-off at TSC ≥ 3 but without pre-selection of relevant interactors.

To compare this list with TLE3 interactors during the ON phase of Wnt signalling, the same procedure was applied to the sample treated with LiCl for 4 hrs and high-scoring proteins (TLE3-TurboID_4h_LiCl / eGFP-TurboID_4h_LiCl ≥ 10) of relevance

were added to the list of top hits. None of the top scoring proteins show significant change (≥ 4x) in spectral counts following stimulation with LiCl for 4 hrs (Table 2.4).

Potentially interesting candidate interactors of TLE3 are shown in Table 2.4, topped by TLE3 itself. Specific interactors include several Wnt pathway components such as TCF7L2 (TCF4) and LEF1 as well as p300, ChiLS and C-terminal binding protein (CTBP). Neither of the BCL9 paralogues was identified in any of my samples, despite TLE3 scoring very high in the BCL9 BioID lists published in van Tienen et al. (2017).

As before, several components of the nuclear co-receptor network and the BAF complex are associated with TLE3, although the latter components are present at lower scores compared with PYGO2 (see above) and BCL9 BioID experiments (van Tienen et al., 2017). This could indicate a higher distance between TLE3 and the BAF complex owing to the conformation of the enhanceosome.

My BioID list also confirms GSE1 as a closely associated protein of the Wnt enhanceosome, which is identified with high confidence in all enhanceosome-based BioID experiments to date (see above). I also found a strong and specific association of TLE3 with DVL2 & 3, which is unexpected given the different cellular compartments that these proteins localise to. Specific interactors of TLE3 also include proteins from different signalling pathways such as YAP1 (Hippo pathway) and HES1 (Notch signalling), the latter of which is a known TLE3 interactor (Jennings et al., 2006).

Among the highest scoring interactors are the ubiquitin associated proteins 2 and 2L (UBAP2 & UBAP2L). These interact with the Polycomb group protein BMI, which itself binds to UBR5, the E3 ubiquitin ligase responsible for TLE3 inhibition during active Wnt signalling. This association of BMI and UBR5 appears to be DNA damage-dependent (Bordeleau et al., 2014; Sanchez et al., 2016) and UBAP2L has been described to control the expression of genes involved in EMT in different cancers (Ye

et al., 2017). Strikingly, UBR5 itself is absent from all of my BioID lists for TLE3, which may be due to technical reasons (see 2.4.4.). PRRC2A/B, which are also top hits for TLE3 interactors, are thought bind to UBAPL proteins based on yeast-two-hybrid assays (Lehner et al., 2004), which may explain their association with TLE3 in BioID.

In addition to these factors, the highest scoring TLE3-specific protein hits include several Zinc finger proteins, most notably ZNF703 (also known as Zeppo1), which has been described as a direct binder of TLE3/Groucho and represses Wnt reporter expression (Slorach et al., 2011).

Based on specificity and a high TSC, the Forkhead box protein FOXK1 as well as its paralogue FOXK2 pose interesting top hits for novel interactors of the Wnt enhanceosome. Note that both FOXK1/2 are also found in the PYGO2 BioID list shown in section 2.2.1. and in other BioID studies focusing on Wnt pathway components (van Tienen et al., 2017, Melissa Gammons, Bienz Lab, MRC LMB, unpublished observations, see Chapter 3).

As mentioned, the overall TLE3-TurboID dataset included several cytoplasmic proteins, most of which are likely not relevant to Wnt-mediated transcriptional regulation. I was, however, intrigued by the identification of several subunits of the TCP1 ring complex/chaperonin-containing TCP1 (TRiC/CCT) chaperone: CCT1, 2, 5 & 6 all show a fold change of ≥9 compared with the eGFP control. The TRiC/CCT chaperone has previously been described as required for folding of other WD repeat proteins and so is likely to mediate folding of TLE3 (Miyata et al., 2014).

Table 2.4. Top hits of TLE3 BioID.

Top hits of BioID with TLE3-TurboID with a fold change of ≥10 over a nuclearly localised eGFP-TurboID control. BioID results were filtered for interesting hits including known Wnt enhanceosome components (green), BAF complex proteins (blue), nuclear co-receptor components (orange) and the WD40-specific chaperon CCT (pink). Proteins relevant to Wnt signalling or either of the aforementioned groups were included even if they were identified with low counts, and are separated by a bold line.

#	Protein ID	TLE3	eGFP	TLE3	eGFP
		+ NaCl	+ NaCl	+ LiCl	+ LiCl
1	TLE3	214	2	227	1
2	NCOR1	96	1	91	1
3	TLE1	81	1	86	1
4	TLE4	81	1	85	1
5	GSE1	77	1	53	1
6	UBAP2L	67	1	46	1
7	PRRC2A	52	1	49	2
8	PRRC2B	49	1	49	1
9	UBAP2	34	1	29	1
10	NCOR2	26	1	21	2
11	ZNF703	26	1	18	1
12	RMB12	25	1	24	1
13	BCORL1	25	1	22	1
14	ZNF148	22	1	22	2
15	PFDN2	22	1	8	1
16	CCT6A	21	1	9	1
17	ATXN2L	19	1	5	1
18	IRF2BP2	18	3	11	1
19	NCOA2	17	1	16	1
20	YAP1	17	1	15	1
21	DVL2	17	1	11	1
22	PIAS	16	1	21	1
23	ARID3B	15	1	27	1
24	CCT5	15	1	6	1
25	RANBP2	42	1	46	1
26	p300	14	1	17	1
27	ATN1	14	1	9	1
28	DVL3	13	1	11	1
29	IRF2BP1	13	1	8	1
30	CCT2	13	1	5	1
31	KMT2D	12	1	15	1
32	TCF7L2	12	1	13	1
33	HES1	12	1	11	1
34	FOXK1	34	3	39	6
35	ZMIZ2	11	1	11	1
36	ZMIZ1	11	1	11	1
37	LEF1	11	1	9	1
38	ATXN1L	11	1	3	1
39	CCT1	9	1	11	1
40	FOXK2	17	2	11	2
41	KDM1A	8	1	9	1
42	DOT1L	8	1	3	1
43	DPF1	7	1	11	1
44	LDB1	7	1	8	1
45	HAT1	7	1	5	7
46	CTBP1	6	1	11	7
47	JMJD1C	6	1	8	1
48	NCOA3	6	1	2	1
49	NR3C1	5	1	11	1
50	SMARCA2	4	1	4	6
51	KMT2C	3	1	11	1
52	SSBP3	3	1	2	1
53	ARID1A	5	2	4	1
54	SMARCD3	2	1	6	1
55	SMARCE1	2	1	2	1
56	NCOA7	2	1	1	2
57	SMARCB1	1	1	1	1
58	FOXC1	4	0	4	0
59	CTNNB	0	0	0	0
60	BCL9	0	0	0	0
61	BCL9L	0	0	0	0
62	UBR5	0	0	0	0

Wnt enhanceosome BAF complex Nuclear co-receptor components CCT Chaperone

2.3.2 Cessation of Wnt signalling affects a small fraction of TLE3 interactors

In order to determine which TLE3 interactors are lost or gained during downregulation of transcription after Wnt signalling ceases, I compared the top hits listed above with the spectral counts resulting from the sample which was supplied with biotin only after LiCl exposure for 4 hrs had been terminated (TLE3-TurboID_4h+LiCl_2h Bio) (Table 2.5). Most interactions are unchanged in this condition and only 9 proteins are identified as reduced by a factor of ≥ 5x following cessation of Wnt signalling compared with either of the two 4-hr samples.

Importantly, TCF7L2 (TCF4) is decreased in this sample if compared to both the Wnt OFF (NaCl_4h) and the Wnt ON (LiCl_4h) samples. At the same time, CTBP1 is also decreased. This could indicate that β-catenin-mediated transcription is still active at this time (see discussion below).

Table 2.5. Top hits for TLE3 interactors altered after Wnt signalling ceases.
Few protein interactors are lost and none are gained in the phase of putative re-silencing following termination of Wnt signalling. The most interesting change in TSC is seen for TCF7L2, which loses its association with TLE3 after 4 hrs of Wnt stimulation.

#	Protein ID	TLE3	GFP	TLE3	GFP	TLE3	GFP	TLE3	GFP
		+ NaCl	+ NaCl	+ LiCl	+ LiCl	+ NaCl	+ NaCl	+ LiCl	+ LiCl
1	KMT2D	12	1	15	1	5	3	1	2
2	KMT2C	3	1	11	1	4	1	1	3
3	DPF1	7	1	11	1	5	2	1	3
4	KDM1A	8	1	9	1	2	1	1	1
5	**TCF7L2**	**12**	**1**	**13**	**1**	**8**	**1**	**2**	**1**
6	SMARCD3	2	1	6	1	2	1	1	1
7	CTBP1	6	7	**11**	1	5	3	**2**	1
8	PRRC2A	52	2	49	1	11	1	9	2
9	ARID3B	15	1	27	1	19	4	5	1

2.4. Discussion

The new BioID data sets described in this chapter largely validate previous results, while also identifying potential novel interactors and giving an insight into the dynamicity of the enhanceosome conformation during signalling. However, my experiments also highlight the practical constraints of BioID assays and their interpretation.

2.4.1. Interactions within the Wnt enhanceosome

Most importantly, the data presented here underscore the results by van Tienen et al. (2017) showing that most interactions within the enhanceosome are constitutive and do not change majorly upon β-catenin binding.

I was also able to confirm the BAF complex as a key unit of transcriptional regulation of Wnt target genes. BAF or SWI/SNF (Switch/Sucrose Non-Fermentable) complexes are ATP-dependent chromatin remodellers that have been found to play an important role in many cancers (Kadoch and Crabtree, 2015) and mutations in several subunits have *wg*-like phenotypes in *Drosophila* (Collins and Treisman, 2000). While there is now robust evidence for BAF complex association with Wnt target genes, further analysis is required to assess how its activity is controlled and whether subunits are exchanged upon signalling changes. These questions could be addressed by correlating changes in Wnt target gene expression in different cancer lines with BAF complex mutations or by analysing subunit binding patterns before, during and after Wnt signalling.

Similarly, the association of nuclear co-receptors is reproducible using different enhanceosome components as bait, but there are currently no mechanistic insights into whether and how they are involved in regulation of Wnt target gene transcription. Nuclear co-receptor proteins are recruited to loci by DNA-binding

transcription factors and act either as corepressors (e.g. NCOR and NCOR2/SMRT) or coactivators (including NCOA1-6). Factors are exchanged depending on the presence of different hormones such as androgen or estrogen, and aid transcriptional repression or activation by presenting docking sites to histone modifiers (reviewed in Watson et al. (2012) and Dasgupta et al. (2014)).

Cross-linking experiments in the Bienz group (e.g. RIME, see van Tienen et al., 2017) with B9L did not verify either of these proteins as direct binders of BCL9. However, TLE3 has been shown to be required for recruitment of ER to chromatin at specific loci and accordingly for transcription of a subset of ER-dependent genes (Holmes et al., 2012). The association of nuclear co-receptors with the Wnt enhanceosome is thus likely to be due to binding of TLE. Future experiments could address transcriptional activity at WREs following loss or inhibition of these co-receptors by tracking transcripts of target genes to address whether these proteins also play a role in Wnt target gene expression.

2.4.2. The interactome of PYGO2

The analysis of PYGO2 interactors resulted in the identification of several candidates for novel interactors for PYGO2 or one of its domains, with BRAC2 and JMJD1C being the most intriguing candidates.

PYGO2 interaction with ChiLS

It was unexpected that the association of PYGO2 with the ChiLS complex is seemingly unaffected by loss of the NPF motif (see Table 2.3), whereas it appears to be significantly strengthened in the PHD deletion sample compared with the WT sample.

Based on previous direct protein interaction studies including tandem affinity purification, coIP and NMR, we know that the association between PYGO2 and the ChiLS complex is mediated by direct binding between PYGO2-NPF and the LDB1 subunit (Fiedler et al., 2015). This was further underscored by the earlier PYGO2-BioID data set by van Tienen et al. (2017) which found relatively high counts for both ChiLS components.

I surmise that the low counts assigned for SSDP1/2 and LDB1 in my WT sample are erroneous and that the score reached in the ΔPHD sample (36 spectral counts) more accurately reflects the interaction of PYGO2 containing a WT NPF motif with ChiLS. Thus, if the comparison of ChiLS-derived TSC is done between the ΔPHD and the ΔN-Box mutant, the decrease in ChiLS counts for the ΔN-Box mutant is as expected, underscoring the NPF-dependence of PYGO2-LDB1 binding.

Given the strong presence of the BAF complex at WREs in association with PYGO2 and BCL9 (and, to a lesser extent, TLE3) we wondered if PYGO2 and the BAF subunit ARID1/Osa compete for binding to ChiLS (note that both interactions are mediated by NPF motifs in PYGO2 and ARID1/Osa). This could be a mechanism by which re-silencing of transcription is achieved following a period of active Wnt signalling by exchanging activating for silencing factors via the ChiLS complex.

To test this, Juliusz Mieszczanek (Bienz Lab, MRC LMB) and I designed an assay based on monitoring the effect of overexpression of either Pygo or Osa or both at the same time on expression of *Ubx* in the midgut of *Drosophila*. Overexpression of Osa alone has been shown to diminish *Ubx* expression as expected based on its antagonistic role (Collins and Treisman, 2000), which we were able to confirm.

Our preliminary results suggest that overexpression of $Pygo^{WT}$ can partially rescue this effect of Osa-OE but use of a $Pygo^{\Delta N\text{-}Box}$ mutant did not reveal a competition for ChiLS binding: the ability of Pygo-OE to rescue the Osa-OE phenotype was not

affected by loss of the NPF motif. This apparent lack of competition for the NPF-binding site of LDB1 can be explained by the multimeric architecture of the ChiLS complex which would allow simultaneous binding of both factors. However, this experiment needs to be repeated before I would be confident in drawing a conclusion.

BRCA2 as a novel enhanceosome interactor

I identified a strong and PHD-dependent interaction of PYGO2 with the DNA damage regulator BRCA2, which is in line with the previously published data set where BRCA2 counts were also high (van Tienen et al., 2017). This result is particularly interesting as previous experiments addressing aneuploidy in tumours found that loss of BCL9L increases tolerance to genome instability following unresolved DNA damage, which is an important driver of tumour evolution (López-García et al., 2017). The authors show that BCL9L deficiency results in decreased transcription of the Wnt target gene *caspase2*. Caspase2 regulates apoptosis via two separate mechanisms (p53-mediated and p53-independent pathways) and cells expressing low amounts of Caspase2 fail to induce apoptosis as needed. The authors speculate that a sensor of DNA damage controls *caspase2* expression via BCL9.

BRCA2 is known to regulate the cellular DNA damage response by controlling p53-mediated transcription as well as binding to RAD51 and recruiting this protein to damaged loci resulting in repair by homologous recombination (Mamorstein et al., 1998; reviewed in San Filippo et al., 2008). I speculate that BRCA2 interaction with the enhanceosome – whether through PYGO2-PHD or BCL9 – functions as the postulated sensor for genome instability, resulting in upregulation of apoptotic genes. If this interaction is lost, decreased *caspase2* expression could be the

consequence and cells become tolerant to aneuploidy resulting in increased tumour survival.

CoIP studies or direct protein interaction studies with purified protein are required to verify this interaction and determine whether BRCA2 is a direct or indirect binding partner of PYGO2-PHD. Furthermore, it would be interesting to test a C-terminal truncation or PHD deletion in mammalian cells under conditions in which DNA repair is required such as following radiation or bleomycin treatment (which induces double strand breaks (Lloyd et al., 1978)). Cancer cells, e.g. the colorectal cancer cell line SW480, are most suitable for these experiments due to their natural predisposition for genomic instability. Survival or IF assays could determine whether *PYGO*$^{\Delta PHD}$ cells tolerate aneuploidy better than WT control lines and whether recruitment of RAD51 to DNA damage is impaired following truncation of PYGO.

Given that the Swanton lab showed that siRNA-knockdown of BCL9L or C-terminal truncations are sufficient to inhibit *caspase2* expression (López-García et al., 2017), it is possible that PYGO2 is dispensable for this process. However, based on its function in tethering BCL9 to the enhanceosome, subtle effects on DNA damage response are conceivable even if the interaction with BRCA2 is mediated through BCL9/B9L. Note that BCL9L knockout cells are not viable (Mieszczanek et al., 2019) and so cannot be used in equivalent assays.

Histone modifying enzymes are in proximity to PYGO2

My BioID study with PYGO2 as the bait protein identified several histone modifiers, many of which are involved in transcriptional activation. Their association with PYGO2 is surprising given that these BioID experiments were carried out in the absence of Wnt stimulation. It is possible that this is a result of high abundance of these proteins within the nucleus paired with the long labelling times which may have

led to overestimation of these proteins (see below). Future studies are required to clarify whether this association with WREs is real and constitutive even in the absence of nuclear β-catenin. If so, these proteins would not be expected to be active at WREs prior to Wnt stimulation.

JMJD1C show the highest TSC in all three PYGO2 BioID experiments and also scored highly in previous data sets by van Tienen et al. (2017). This may be due to the fact that this histone demethylase is a very large protein (2,540 aa) and contains a high number of lysines (205aa). Analysis of the published protein structure of JMJD1C (PDB: 2YPD) revealed that many of these lysines are on the surface of the protein and are thus likely to be accessible for biotin ligases (see below).

While the amino acid composition of the protein might account for the high spectral counts, JMJD1C has also been reported to associate with nuclear co-receptors (Lempiäinen et al., 2017) and RUNX proteins (Chen et al., 2015a), and RUNX proteins have been previously indicated as putative components of the Wnt enhanceosome (Fiedler et al., 2015). Biophysical assays found an interaction of Runt with the ChiLS core module and RUNX proteins have been shown to regulate transcription in cooperation with TCF in different developmental contexts (Fiedler et al., 2015). However, RUNX proteins have not been confirmed as interactors in BioID studies (van Tienen et al., 2017 and my results), although this may be due to technical reasons (see below). It is also possible that RUNX binding profiles vary according to the differentiation status of the cell lines since they are known as lineage-specific factors (e.g. Lee et al., 2019). Use of undifferentiated cell lines in protein interaction studies to analyse RUNX association with Wnt enhanceosome proteins or occupancy at WREs should help clarify this question.

JMJD1C is also an interesting candidate for a histone demethylase that could aid in a PYGO2-mediated adaptation of the methylation status of histone 3. A similar concept has been proposed by Miller et al. (2013), although it is unclear what the

consequence of binding of PYGO2-PHD to the repressive chromatin mark H3R2me2 is: either binding of PYGO2 masks the chromatin mark and attenuates demethylation (thereby delaying transcription), or PYGO2 recruits demethylases and exposes methylated arginines to favour removal of repressive chromatin marks before trimethylation of H3K4 further facilitates transcription.

Demethylation assays based on JMJD1C or other jumonji-containing demethylases should elucidate whether these enzymes display a preference for H3R2 methylation and whether their activity or recruitment is steered by PYGO2. For example, efficiency of JMJD1C-binding to different chromatin marks in the presence or absence of PYGO could be monitored via ITC assays as previously done for other jumonji domain enzymes and putative cofactors or inhibitors (Horton et al., 2010).

2.4.3. TLE3 interactors

One major conclusion from my TLE3 BioID is that there is little change of the TLE3 interactome upon activation of Wnt signalling. As I did not recover the UBR5 ubiquitin ligase in my experiments, I cannot draw conclusions on the dynamics of TLE3 inhibition. It thus remains elusive whether one or several mechanisms are required to inhibit TLE3. Additionally, I recovered known and novel TLE3 interactors.

Dynamics of TLE3-TCF association

I did notice an intriguing decrease in TSCs of two TCF proteins as well as CTBP1 following termination of Wnt signalling in my time course experiment. These findings indicate that the period of biotin labelling in this sample (4h_LiCl+2h_bio) is likely still within the ON phase of Wnt signalling. It is interesting to speculate that TLE3 is displaced from TCF only after prolonged Wnt signalling (> 4 hrs), but not in the initial

phase (4h_LiCl+bio) during which it may merely be inhibited. I surmise that the experimental setup, in which biotin labelling was induced right after removing LiCl-medium, failed to terminate Wnt signalling immediately and that my BioID sample derived from this treatment still contains sufficient intracellular LiCl to sustain Wnt signalling further.

It is possible that TLE3 is regulated through distinct mechanisms in the initial phase vs. extended periods of signalling and such a model could explain and consolidate different mechanisms that have been described for TLE3 inhibition. Interestingly, in my own preliminary experiments, this displacement was not seen in a sample where Wnt signalling was active for 12 hrs while biotinylation was ongoing. Reproducibility of this phenomenon might argue that after 4 hrs of Wnt stimulation transcriptional activation is not fully activated or that the enhanceosome conformation changes to allow sustained signalling only within hours of Wnt activation. Rearrangements forcing the enhanceosome back into the OFF state would then only be induced several more hours later so that TLE3 binding to TCF is reinstated after 12h. Since TLE3 remains associated with other components of the Wnt enhanceosome throughout extended periods of signalling (van Tienen et al., 2017), it is conceivable that the interaction with TCF is inhibited at specific stages during signalling, but that TLE3 does not dissociate from the enhanceosome complex itself (possibly by tethering through BCL9 or ChiLS (van Tienen et al., 2017)).

This hypothesis is underscored by the finding that CTBP1 follows a similar pattern as TCF: the association of CTBP1 is strong in the absence of Wnt signalling (i.e. under NaCl conditions) and after 4 hrs of Wnt activation but appears weakened following cessation of Wnt signalling. High TSC are found again after 12 hrs of prolonged signalling.

It will be interesting to test different time points in between 4 and 12 hrs and assess interaction of TLE3 with TCF7L2 (and CTBP1) using a combination of BioID and

coimmunoprecipitation (BioIP) to gain experimental support for this hypothesis. Here, BioID constructs are expressed and lead to labelling of the interactome as before, but rather than measuring all proteins in the sample, specific interactors can be tested by CoIP using specific antibodies following streptavidin pulldown. Such a refined time course might be able to confirm whether different modes of TLE3 inhibition act in succession.

Novel candidate interactors for TLE3 in Wnt signalling

Even though I did not observe strong changes in the enhanceosome conformation upon activation of the pathway, the BioID approach had other exciting outputs. Specifically, I was able to identify novel candidate components of the Wnt enhanceosome.

Previous reports have already indicated ZNF703/Zeppo1 as a transcriptional repressor that targets β-catenin/TCF complexes (Kumar et al., 2016) and it was also shown to bind to TLE3 and promote tumour metastasis by regulating EMT (Slorach et al., 2011). Like TLE3, the repressive function of ZNF703 is mediated by recruitment of histone deacetylases (Nakamura et al., 2008) and it is required for repression of at least a subset of Wnt target genes, including E-cadherin and TGFβ (Slorach et al., 2011). Given the high prevalence for mutations in this gene in different types of cancers (Holland et al., 2011; Ma et al., 2014) it would be interesting to assess this interaction as a potential therapeutic target.

I also show a robust interaction of TLE3 with the TRiC/CCT chaperone. This complex was shown to facilitate folding of newly made proteins and is specifically required for complex structures such as WD40 repeats (Miyata et al., 2014; Yam et al., 2008). The chaperone is thus likely required for correct folding of the WD40 domain of TLE3. So far, my results do not indicate an increase or decrease in TLE3 interaction with this

chaperone at different stages of Wnt signalling (but note that my time points might not be suitable to resolve these changes, see above). A temporal pattern of association with CCT could indicate increased translation of TLE3 at specific signalling stages. Further time course experiments or generation of CCT knockout lines followed by studying the effect on TLE3 stability and Wnt repression would allow a refinement of this interaction.

Future experiments should also address the apparent interaction between TLE3 and DVL paralogues. It is unclear how and where TLE3 interacts (directly or indirectly) with DVL2/3. It is possible that they come into proximity in the cytoplasm during the folding process of TLE3. Alternatively, some reports suggest a nuclear function of DVL (see Chapter 4), which could explain the interaction.

Additionally, I repeatedly found the Forkhead box factors FOXK1/2 in my BioID lists, most prominently using TLE3 as bait, but also with PYGO2. Other BioID studies in the Bienz lab have also identified FOX factors in association with Wnt proteins. Taken together with their putative function as pioneer proteins as well as previous publications indicating a potential role in Wnt signalling (see Chapter 3), I decided to further investigate FOXK1/2 as novel candidates for Wnt enhanceosome components.

2.4.4. Limitations of BioID studies

A main aspect when designing BioID experiments is the selection of a suitable control to allow subtraction of highly abundant but unrelated background proteins. My experiments underscore the importance of using a control construct which is targeted to the correct cellular compartments. Several proteins that appeared highly specific for BCL9 or PYGO2 in previous BioID studies, which made use of a cytoplasmic BirA* control (van Tienen et al., 2017), proved to also be biotinylated by

a nuclear BioID control. One examples of such an unspecific interaction in my experiments is the RNA-binding protein RBM14 which was originally included as a Wnt-inducible top hit for BCL9 (TSC = 32 in unstimulated vs. TSC = 67 in stimulated cells in van Tienen et al., 2017) and which is also highly abundant in my PYGO2 BioID lists. However, my controlled experiments with TLE3 revealed that this protein is also pulled down strongly using an eGFP-TurboID construct (TSC = ~50 in all samples tested for TLE3- and eGFP-BioIDs), suggesting that it is simply abundant in the nucleus. Future BioID experiments should take this into account and only carefully selected control constructs will allow conclusions on candidate interactors.

An additional caveat of BioID-based studies is that interactions can be missed or overestimated due to technical errors. For example, we failed to observe several known binding partners in our BioID lists. Lack of identification can be due to several reasons including limited availability of accessible lysines on the partner protein. This could explain the absence of histone 3 in my PYGO BioID data, which is unexpected given the direct interaction of the PYGO PHD finger with methylated lysine and arginine residues of H3 (Fiedler et al., 2008). However, biotinylation can only occur at free lysines and it is conceivable that naturally occurring histone modifications and BioID-mediated biotinylation are mutually exclusive.

Additionally, BioID does not capture binding partners if the interaction is affected by fusion of the bait protein to the BirA* or owing to masking of binding sites following self-biotinylation of the fusion protein. This might explain why BCL9 paralogues as well as the E3 ubiquitin ligase UBR5 are absent from my TLE3 BioID results (note that the reciprocal BioID with BCL9 yielded strong spectral counts for TLE3). Due to technical difficulties in transiently transfecting HEK293 Flip-In lines, I was unable to assess the functionality of the TLE3-TurboID fusion protein in a His-Ubiquitin pull down assay. This assay has been previously used to verify WT ubiquitination of

different proteins (Mund and Pelham, 2009) and could have been used as an indicator for correct function of my TLE3 fusion proteins.

Taken together, these examples explain why BioID experiments do not yield an exhaustive list of interactors.

Overall, these BioID studies support the hypothesis that most components of the Wnt enhanceosome are constitutively associated with it and only undergo subtle changes. Additionally, I have identified novel factors that need to be validated in future experiments. As the Forkhead box factors FOXK1/2 have not previously been described for a function in the Wnt enhanceosome but were found in several of our lab's BioID studies, we decided to take this project forward and these experiments will be described in the following two chapters.

3. FOXK in Wnt/Wg Signalling

As laid out in the previous chapter, my studies of the interactome of the Wnt enhanceosome indicated a potential function for Forkhead box (FOX) factors of the subfamily K. The following two chapters will describe my work concerning two mechanisms through which FOXK factors could be involved in Wnt/Wg signalling: as a regulator of Wg target genes through binding to or priming of Wg target loci (this chapter), or through interaction with DVL (Chapter 4).

3.1. Introduction

FOX proteins are a superfamily of transcription factors with over 50 described members in the human genome that all share a highly conserved DNA-binding domain, the forkhead box or "winged-helix" domain (FKH). The FKH domain was first described in the *Drosophila forkhead* mutant, which shows the eponymous phenotype (Jürgens and Weigel, 1988). Structurally, this DNA-binding motif contains three α-helices, three β-strands and two loops – or wings – that give the domain its characteristic butterfly-like look (Clark et al., 1993) (Figure 3.1A & C).

FKH domains have been reported to bind to regulatory sequences of target genes via the consensus sequence RYAAAYA (where R = purine and Y = pyrimidine), although most FOX proteins allow some degree of degeneracy and some show differential specificity for the adjacent bases (like FOXK2 (Chen et al., 2015b), see Figure 3.1B). Due to the high conservation of this DNA-binding domain, genome-wide binding profiles of different FOX factors substantially overlap (Chen et al., 2015b).

Based on sequence homology, at least 19 subfamilies of FOX proteins have been identified in the genomes of bilaterian animals (FOXA to FOXS) (Shimeld et al., 2010). Historically, many FOX proteins were identified and named for their respective

functions or expression domains (e.g. FOXK1, which is also known as Myocyte Nuclear Factor (MNF)) but their nomenclature has since been consolidated by Kaestner et al. (2000).

In addition to the FKH domain, FOX factors commonly have two or more nuclear localisation sequences (NLS) (Hancock and Oezkaynak, 2009; Romanelli et al., 2003) and may contain other motifs such as transactivation domains (Figure 3.1E).

Notably, FOX proteins of the subfamily K (e.g. FOXK1 and FOXK2 in humans (collectively referred to as FOXK1/2 unless specified), FoxK in *Drosophila*,) differ from other FOX factors in that they contain an additional domain, the Forkhead-associated domain (FHA). FHA domains are also found in unrelated regulatory proteins in both eukaryotes and prokaryotes (Hofmann and Bucher, 1995) and have been shown to bind to phosphothreonine epitopes on proteins (Durocher et al., 1999).

In addition to their DNA-binding property, FOX proteins associate with coactivators or corepressors or, in some cases, form homo- or heterodimers, and these interactions are likely to play a role in target selection and function (Chae et al., 2006). Different post-translational modifications have been reported and determine the cellular localisation of many FOX proteins, thus regulating their activity (Brent et al., 2008).

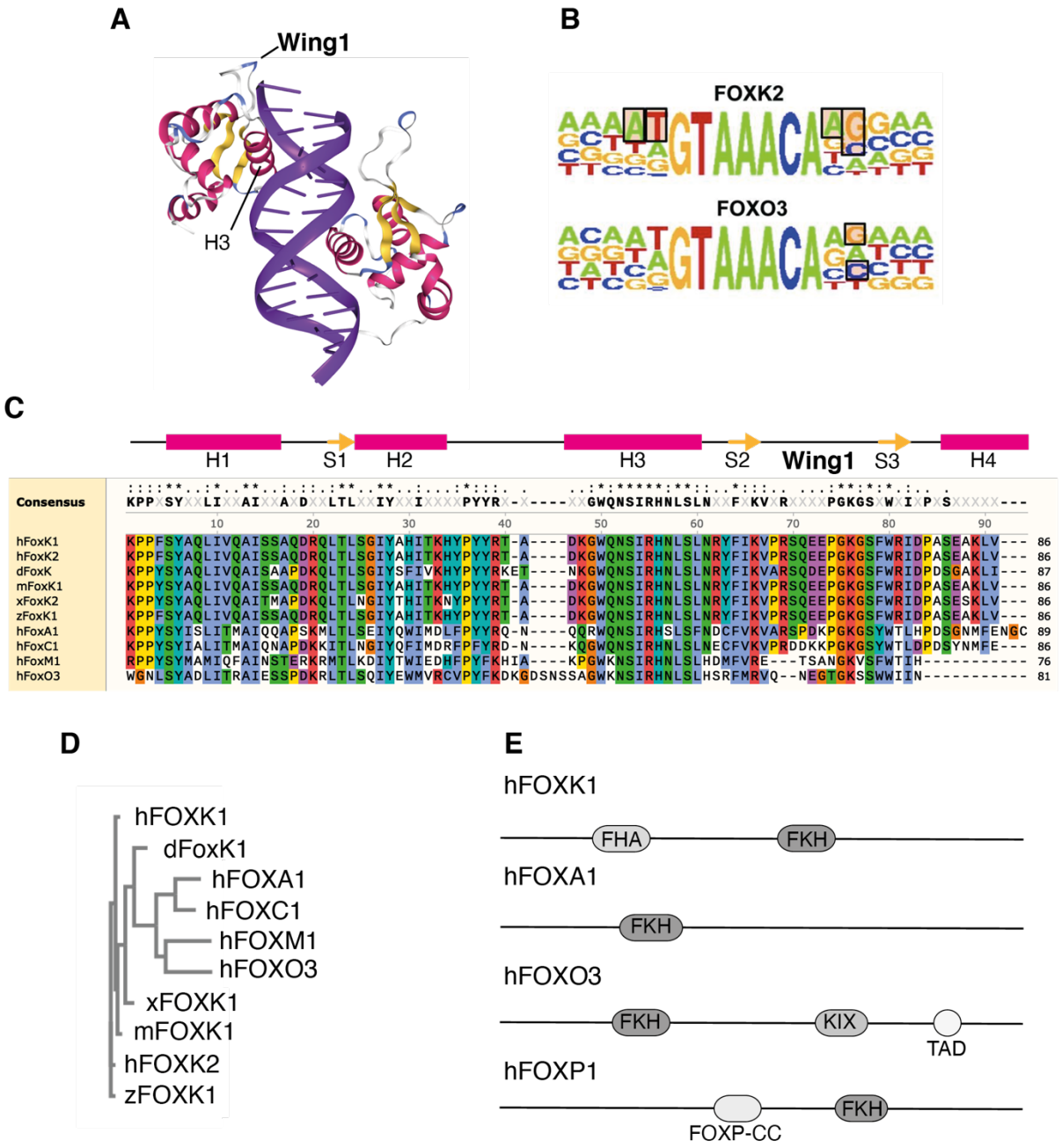

Figure 3.1. FOX proteins share a highly conserved Forkhead box domain (FKH) which binds to the consensus sequence RYAAAYA.

A) FKH domain of FOXK2 bound to DNA; PDB 2C6Y by Tsai et al. (2006).

B) FOX proteins share a conserved DNA binding site but may have different specificities for surrounding sequences. Figure taken from Chen et al. (2015b).

C) and D) Amino acid alignment and phylogenetic tree of the FKH domain of a selection of FOX proteins showing strong sequence alignment between different subfamilies as well as between species (human FOXK1, human FOXK2, *Drosophila* FoxK, mouse FOXK1, *Xenopus* FOXK2, zebrafish FOXK1, human FOXA1, human FOXC1, human FOXM1, human FOXO3). Cartoon in C) indicates structural elements corresponding to structure in A). Multiple alignment made using Snapgene software, phylogenetic tree done with “Simple Phylogeny” Tool from EMBL-EBI.

E) In addition to the conserved FKH domain, some FOX factors contain additional domains (FHA = Forkhead-associated domain; KIX = KIX-binding domain; TAD = trans-activating domain; FOXP-CC = coiled-coil domain).

3.1.1. FOX proteins in development and disease

FOX factors are involved in a spectrum of cellular processes including differentiation (Kaestner, 2010), cell proliferation (van der Heide et al., 2015) and autophagy (Mammucari et al., 2007), and a wealth of publications has focused on their role in development. While some FOX factors are expressed in selective tissues, many show broad expression and there is thus considerable overlap of FOX expression domains (Chen et al., 2015b).

In *Drosophila*, the original *forkhead* gene was found to promote terminal identity and was recognised for its role during salivary gland development (Weigel et al., 1989). The fly FOXG homologues sloppy-paired 1 & 2 (slp1/2) are expressed in stripes to maintain parasegment boundaries, and *slp1/*2 double mutants show the classic denticle lawn phenotype of loss of *wg* (Grossniklaus et al., 1992) (see below). *Biniou* (*Drosophila* FOXF) is a critical factor during mesoderm development and midgut morphogenesis as a mediator of Dpp signalling (Zaffran et al., 2001) and this function is conserved in mammals (Ormestad et al., 2006). Fly FOX proteins also have roles in the establishment of head structures (*crocodile,* or FOXC (Häcker et al., 1995)) or neuronal differentiation (*jumeaux*, or FOXN1 (Cheah et al., 2000)).

FOX factors have also been linked to different cancers, for example breast (e.g. FOXA (Miyamoto et al., 2005), FOXC (Han et al., 2015) and FOXM (Ahn et al., 2015)), colorectal (Laissue (2019) for review) and hepatocellular cancer (FOXC1 (Xia et al., 2014). For instance, FOXA has a significant function in different cancers, where it acts as a pioneer factor (see 1.5) and cooperates with estrogen receptor (ER) to regulate target gene transcription (reviewed in Zaret and Carroll, 2011). In many cases there

is conflicting evidence as to whether a specific FOX factor functions as a tumour suppressor or an oncogene and it is incompletely understood whether high or low levels are associated with a better prognosis.

3.1.2. Forkhead box factors and Wnt/Wg signalling

Previous studies have linked several subfamilies of FOX factors to the Wnt pathway, most notably FOXP and FOXO. These interactions are very diverse, and different mechanisms can be summarised as follows: 1) FOX factors that have an effect on Wnt activation, 2) FOX factors that are themselves direct or indirect target genes of Wnt and, most interestingly from my perspective, 3) FOX proteins that form a complex with nuclear Wnt pathway components to drive gene expression.

FOXL indirectly activates Wnt signalling by acting on the expression of extracellular proteoglycans that function as Wnt co-receptors (Perreault et al., 2001; Tsuda et al., 1999). This network was found to be important in cancer, as $APC^{+/MIN}$ $foxl1^{-/-}$ double mutants were reported to display increased tumour load compared with $APC^{+/MIN}$ mice (Perreault et al., 2005). The opposite effect has been described for FOXF, which negatively regulates expression of Wnt5a through induction of BMP4, which in turn represses Wnt. *Foxf* mutants have been reported to have increased Wnt expression and associated over-proliferation, which can contribute to tumorigenesis (Ormestad et al., 2006).

Early reports for FOX expression regulation by Wnt/Wg came from studies in *Drosophila*, where researchers uncovered that expression of the FOXG homologues *slp1/2* is activated by Wg signalling (Lee and Frasch, 2000), and in turn upholds *wg* and restricts *en* expression within their appropriate parasegments (Cadigan et al., 1994).

FOXO is under context-dependent control by the Wnt target gene SGK1 (serum and glucocorticoid-inducible kinase 1), which is highly expressed upon aberrant Wnt signalling. SKG1 acts to phosphorylate FOXO3a leading to FOXO3a exclusion from the nucleus (Dehner et al., 2008). Due to FOXO's pro-apoptotic function, this exacerbates the cancer phenotype as apoptotic genes such as BIM and $p27^{KIP1}$ remain unexpressed and cancerous cells do not undergo apoptosis.

Compelling evidence for a direct interaction of a FOX factor with Wnt pathway components has been published by Walker et al. (2015), who identified FOXP as a transcriptional enhancer of β-catenin-mediated signalling. The authors demonstrate that FOXP forms a complex with β-catenin, TCF4 and CBP in a Wnt-dependent manner and that this complex binds to and regulates Wnt target genes. Chromatin immunoprecipitation sequencing (ChIP-Seq) analysis confirmed a strong enrichment of FOXP binding sites close to TCF4 genomic sites and protein-based studies revealed that FOXP-dependent recruitment of CBP leads to acetylation of β-catenin thereby enhancing target gene expression.

Another example of direct interaction of FOX factors with nuclear Wnt effectors is the interaction between FOXO3a and β-catenin, which leads to a change in the FOXO3a expression profile from a pro- to an anti-apoptotic programme (Tenbaum et al., 2012). These results also reconcile evidence that FOXO3a can act either as a tumour suppressor or an oncogene. While nuclear FOXO3a on its own functions as a tumour suppressor by inducing apoptosis, in cells with combined mutations in the Wnt pathway as well as in the PI3K-AKT-FOXO3a network (resulting in high nuclear β-catenin and FOXO3a) FOXO3a acts as an oncogene.

Taken together, these reports suggest intriguing mechanisms through which FOXK1/2 could function during Wnt signalling.

3.1.3. Current knowledge of FoxK in *Drosophila*

Drosophila FoxK was originally named myocyte nuclear factor (MNF) after its mammalian homologue which was first described in muscles. FoxK remained largely unstudied until 2008, when Casas-Tinto et al. (2008) published work on the role of the protein during development of the embryonic midgut endoderm. Here, FoxK mediates Dpp signalling: Dpp induces expression of *foxK* in the midgut endoderm and FoxK in turn binds to and activates expression from the *labial* enhancer.

The authors generated two mutant alleles, $foxK^{16}$ and $foxK^{44}$, using mobilisation of a nearby *P* element and found that zygotically homozygous mutant embryos fail to generate the middle midgut constriction, essentially phenocopying several *wg* mutants including *armadillo* and *pygo* mutants (see chapter 1.6, Figure 3.2A & B). Casas-Tinto et al. further used RNA interference (RNAi) to verify FoxK function during early embryo development and observed that embryos lacking maternal *foxK* contribution (*foxKi*) stopped developing at stage 13 and showed dramatic alteration of Engrailed staining.

$FoxK^{16}$ embryos were found to lack *labial* expression in the midgut endoderm which was confirmed by expression of an endoderm-specific RNAi construct (Figure 3.2C). In contrast, endoderm-specific overexpression of *foxK* was not sufficient to upregulate *labial* expression, and *Dpp* overexpression in a *foxK* mutant background also failed to induce *labial* expression. The authors speculate that both pathways act in parallel to drive *labial* expression.

Analysis of the *labial* enhancer revealed FKH binding sites and reporter assays confirmed that FoxK can drive expression from the respective enhancer fragment. Casas-Tinto et al. conclude that *Drosophila* FoxK fulfils a crucial role during embryogenesis and is part of a gene regulatory network, in line with previous findings for its mammalian counterparts.

A second publication shows a requirement of FoxK during antiviral response in *Drosophila*, where FoxK allows Nup98 to access chromatin of antiviral genes to allow rapid induction of gene expression upon infection (Panda et al., 2015). This underscores the hypothesis of FoxK as a pioneer factor that, depending on cell type and condition, may regulate gene expression in cooperation with other factors.

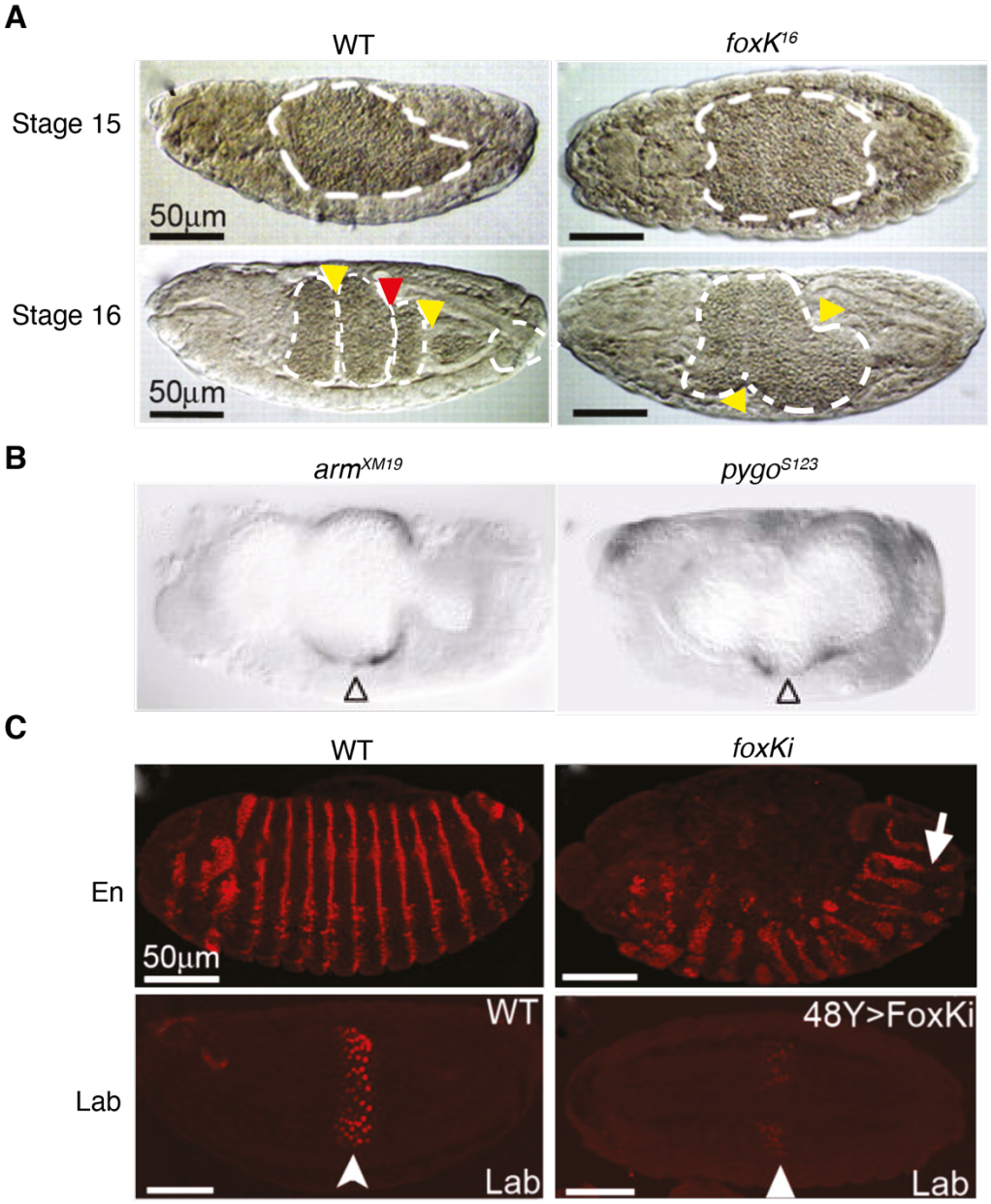

Figure 3.2. Published evidence that FoxK mediates Dpp signalling in the *Drosophila* embryo and is required for the middle midgut constriction as well as *labial* expression. A & B) Casas-Tinto et al. (2008) reported a midgut constriction phenotype of their *foxK*^{16} allele, zygotically homozygous mutants of which fail to form the middle midgut constriction (red arrowhead), whereas the first and third constrictions (yellow arrowheads) start to form before

development arrests (see stages 16 & 17 in A, adapted from Casas-Tinto et al. (2008)). This is similar to other *wg* mutants such as *armadillo* or *pygo* mutants (B, adapted from Thompson et al. (2002)).
C & D) Maternal expression of an RNAi construct against *foxK* (*foxKi*) confirms its function in early embryo patterning as *engrailed* and *labial* expression (red) are disrupted (left: WT, right: *foxKi*, adapted from Casas-Tinto et al., (2008)).

3.1.4. Current knowledge of FOXK in mammalian cells

Mammalian FOXK1/2 homologues were originally described in the 1990s as myocyte nuclear factors (MNF) with high sequence similarity to yeast FKH proteins and hepatocyte nuclear factor-3 (HNF-3, later renamed FOXM1) (Bassel-Duby et al., 1994).

Since then, studies have identified FOXK1/2 as components of the Sin3A complex to exert transcriptional repression during myogenic differentiation (Shi et al., 2012). Bowman et al. (2014) describe regulation of FOXK1/2 via mTOR signalling and showed that starvation-induced cytoplasmic translocation displaces FOXK-Sin3A complexes from the respective enhancer/promoter regions that are subsequently bound by FOXO3a to elicit an autophagy response.

A recent review by Liu et al. summarises evidence for a role of FOXK1/2 in cancer (Liu et al., 2019), collating studies that describe roles for FOXK1/2 in breast cancer, colon cancer, lung cancer and others. These data sets show a drastic difference between cancer types in terms of whether high levels of FOXK1/2 are associated with a better or worse prognosis. The review also summarises data indicating roles for FOXK1/2 in EMT and metastasis.

I was intrigued by data by Wang et al. (2015), who describe an interaction of FOXK1/2 with DVL that is required for full Wnt activation. Here, the authors performed tandem affinity purification to identify novel binding partners of DVL to elucidate the putative nuclear translocation of DVL during Wnt signalling. They found

a specific interaction with FOXK1/2, whereas other FOX factors did not bind to DVL in co-immunoprecipitation assays. Using IF assays under overexpression of FOXK1 or FOXK2, the authors observed nuclear accumulation of DVL leading to a concomitant increase in nuclear signalling as measured by luciferase reporter assays (TOPFLASH, see 6.7) and target gene expression (Figure 3.3B & D).

Pull down assays in conjunction with different DVL and FOXK1/2 truncation mutations were used to map the interaction to the DVL PDZ domain and an adjacent IVLT motif as well as the FHA domain of FOXK (Figure 3.3C). ShRNA-mediated knockdown of FOXK1/2 reduced Wnt-mediated induction of target genes in luciferase reporter assays (Figure 3.3D). Inhibition of induction was also observed for native target genes (e.g. *AXIN2* and *MYC*). The stimulatory function of FOXK1/2 was independent of their DNA-binding properties, as mutants lacking DNA-binding activity were still able to bind to DVL and facilitate Wnt signalling.

A DVL construct fused to an NLS sequence bypassed the requirement for FOXK1/2 to some extent, indicating that the positive effect of FOXK1/2 is largely due to its role in translocation of DVL into the nucleus. The apparent positive effect of nuclear DVL is separate from its function in signalosome formation in the cytoplasm as Wnt stimulation is still required for nuclearly targeted DVL-NLS to induce a strong Wnt response. This observation led to the conclusion that nuclear translocation of DVL is independent of stabilisation and translocation of β-catenin itself.

The authors further assessed a requirement for FOXK1/2 in the colorectal cancer cell lines HT29 and DLD-1, demonstrating that loss of either FOXK paralogue by CRISPR editing leads to a reduced Wnt response (Figure 3.3E), decreased cell proliferation and lower tumour growth rates. This requirement of FOXK1/2 for Wnt signalling was underscored by *in vivo* studies using axis duplication assays in *Xenopus* eggs and xenograft experiments in mice, as well as conditional FOXK2 overexpression in

mouse intestines (Figure 3.3F) – all of which are in line with a function for FOXK1/2 as positive Wnt regulators by promoting DVL nuclear translocation.

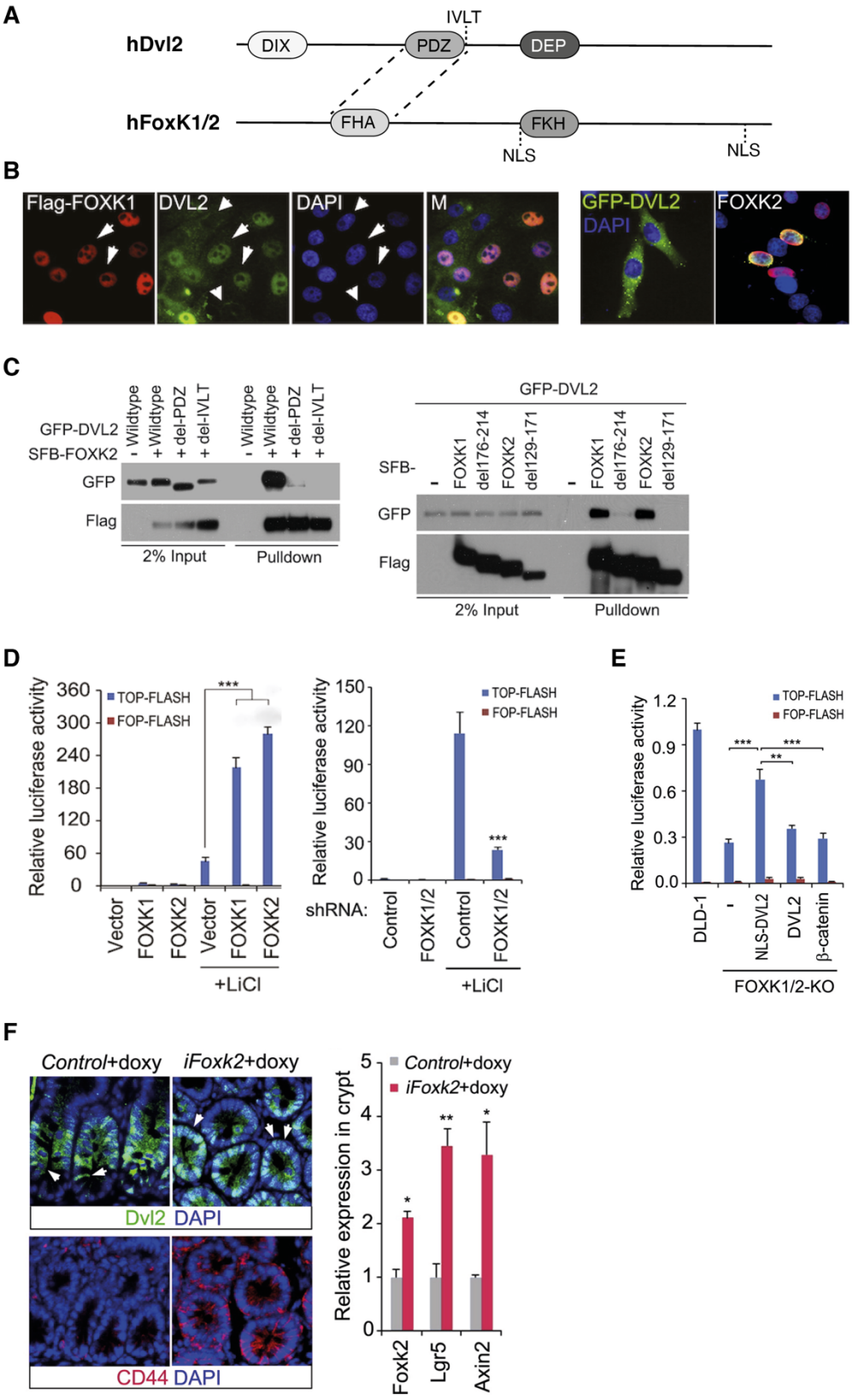

Figure 3.3. Evidence for an interaction of DVL with FOXK1/2 described by Wang et al. (2015).

A) Cartoon of human FOXK1/2 and DVL2 with respective domains and the interacting regions (dotted lines) as proposed by Wang et al. (2015). Nuclear localisation signals (NLS) in FOXK1/2 as predicted using the NLS mapping tool by the Yanagawa lab (Kosugi et al., 2009).
B-E) Excerpt from Wang et al. (2015) detailing their work on a potential DVL-FOXK interaction.
B) IF assays suggest translocation of endogenous (left) as well as overexpressed (right) DVL to the nucleus upon overexpression of FOXK.
C) Coimmunoprecipitation experiments between different DVL and FOXK truncations indicate an interaction between FOXK-FHA and DVL-PDZ as well as the IVLT motif.
D) Overexpression or siRNA-mediated knockdown results in increased or reduced luciferase activity from a TCF reporter plasmid (TOPFLASH), respectively.
E) CRISPR-mediated knockout of FOXK1/2 in DLD-1 cancer cells results in a decreased TOPFLASH response that can be partially rescued by a DVL-NLS construct.
F) Conditional expression of FOXK2 in mouse intestinal epithelial cells results in nuclear translocation of DVL2 that is largely cytoplasmic in control intestines. This translocation is concomitant with an increase in CD44 staining indicating increased proliferation (left). Overexpression of FOXK2 in mouse intestines also leads to increased expression of Wnt target genes *Lgr5* and *Axin2* (right).

In conclusion, Wang et al. report strong evidence for a role of FOXK1/2 in Wnt signalling in mammalian cells and attribute this role almost exclusively to a requirement for nuclear translocation of DVL. While nuclear DVL has been reported several times in the past, the mechanistic details during Wnt signalling remain unsolved and have been a matter of debate within the Wnt field. This controversy will be further discussed in Chapter 4, which focuses on the putative DVL-FOXK interaction.

3.1.5. A potential role of FOXK in Wnt/Wg signalling

We decided to assess a potential role for FOXK in Wg signalling based on our own findings obtained through proximity labelling using different Wnt pathway components as baits. As mentioned above, both human FOXK paralogues were found in several BioID data sets in the Bienz lab, including my own experiments using TLE3 and PYGO2 as bait proteins (see Chapter 2). Interestingly, I observed an increase in FOXK spectral counts upon Wnt induction in my TLE3 data set. Additionally, unpublished data by Melissa Gammons showed an interaction between

FOXK1/2 and WT-DVL2, which is abrogated in a PDZ deletion mutant (DVL2$^{\Delta PDZ}$). This strict dependence for the interaction between FOXK1/2 with DVL on the presence of the PDZ domain indicates a potential interaction surface. Table 3.1 summarises these different data sets.

Table 3.1. Proximity labelling using several known Wnt pathway components as bait captures FOXK1/2 in a Wnt- and PDZ-dependent manner.
For comparison, total spectral counts are shown without background normalisation as not all experiments were done using a control construct. Where experiments included a nuclear GFP-BirA* construct, these results are listed below to indicate background counts. Experiments were either conducted under addition of NaCl (no Wnt activation) or LiCl (Wnt stimulation). DVL data set from Melissa Gammons.

		1 mM LiCl	1 mM NaCl
TLE3-BIOID2			
	FOXK1	27	5
	FOXK2	0	1
EGFP-BIOID2			
	FOXK1	5	6
	FOXK2	0	3
TLE3-TURBOID			
	FOXK1	73	21
	FOXK2	32	12
EGFP-TURBOID			
	FOXK1	7	7
	FOXK2	2	0
PYGO2-BIOID1			
	FOXK1	n/a	13
	FOXK2	n/a	4
PYGO2$^{\Delta N\text{-}BOX}$-BIOID1			
	FOXK1	n/a	15
	FOXK2	n/a	9
PYGO2$^{\Delta PHD}$-BIOID1			
	FOXK1	n/a	20
	FOXK2	n/a	6
DVL2-BIOID1			
	FOXK1	n/a	15
	FOXK2	n/a	35
DVL2$^{\Delta PDZ}$-BIOID1			
	FOXK1	n/a	0
	FOXK2	n/a	0

Taken together with the publications described above, we decided to assess the function of FOXK in Wnt/Wg signalling following two lines of investigation: 1) To phenotypically and genetically assess FoxK during *Drosophila* development, and 2)

to investigate the link between FOXK1/2 and DVL2 using mammalian cell lines. Results concerning the former strand of investigation are described in this chapter, whereas Chapter 4 deals with the interaction between FOXK and DVL.

3.2. Results

3.2.1. Forkhead box protein binding sites are required for expression from a minimal *Ubx* enhancer fragment

My initial approach was to ask whether FOX factors in general act in cooperation with Wnt signalling and are required for expression of Wnt target genes. As the read-out, I chose an established assay to analyse expression of a Wg target gene in the embryonic midgut of *Drosophila*.

As described in the introduction (see 1.6), expression of *Ubx* in parasegment 7 in the visceral mesoderm is regulated by *wg* expression and loss of Wg eliminates the middle midgut constriction (Thüringer and Bienz, 1993). Based on the high sensitivity of *Ubx* expression to small changes in Wg signalling levels, the *Ubx* enhancer is an effective tool to assess the effect of mutations in putative Wg pathway components.

A minimal *Ubx* enhancer fragment of 250 bp is sufficient for Wg- and Dpp-mediated expression in the midgut as shown using a LacZ fusion construct (Thuringer et al., 1993). This minimal *Ubx* control sequence, termed *UbxB*, has since been used by the Wnt community as a β-galactosidase (β-gal) reporter in the midgut ($LacZ^{Ubx.Bhz}$) (Thuringer et al., 1993) for example in studies on Pygo (Mieszczanek et al., 2008) and Runt (Fiedler et al., 2015).

Analysis of the minimal enhancer fragment revealed two highly conserved putative FOX binding motifs and several less conserved sites (Figure 3.4A & C). Putative binding sites were replaced by random sequences to prevent binding of FOX proteins in order to assess the effect on *β-gal* expression. I generated two different constructs, one carrying mutations only in the two highly conserved binding motifs ($UbxB^{\Delta FOXK\text{-}BS\_1}$) and one with all six potential binding motifs mutated ($UbxB^{\Delta FOXK\text{-}BS\_2}$).

To avoid interference with other binding sites or gain of new transcription factor binding sites, the proposed mutations in the minimal *Ubx* enhancer sequence were

subjected to a transcription factor binding site prediction programme (PROMO (Messeguer et al., 2002); http://alggen.lsi.upc.edu) and the transcription factor binding profiles compared to the original *UbxB* binding sites. No new binding sites were created, and both constructs were transformed into *Drosophila* using random *P*-element-mediated integration.

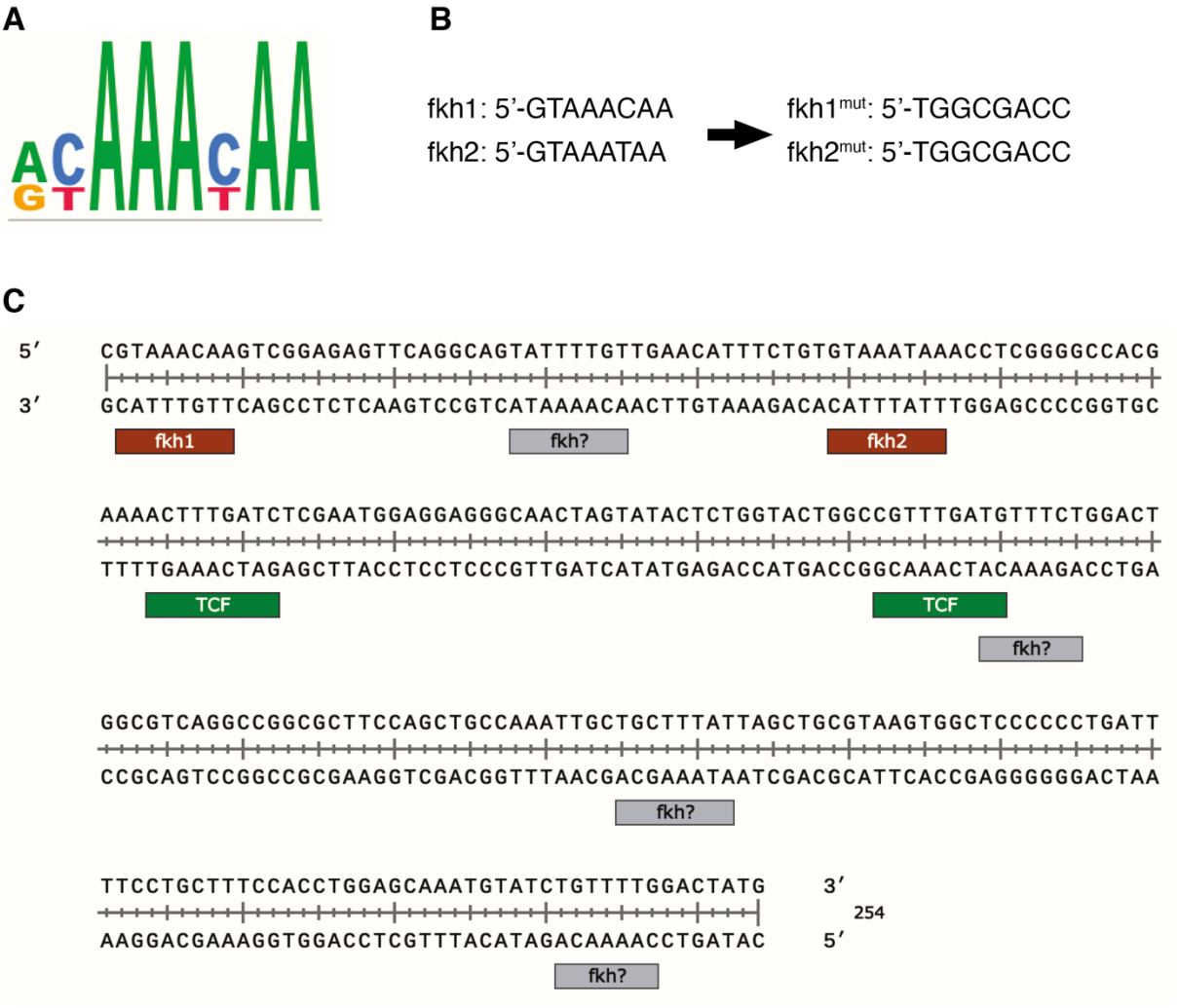

Figure 3.4. Mutation of FKH binding sites in the minimal *Ubx* reporter *UbxB*.
A) FKH-containing proteins bind to the consensus sequence (A/G)(C/T)AAA(C/T)AA.
B and C) Two strongly conserved and four somewhat degenerate binding sites for FKH binding (brown and grey in C, respectively) were identified in the minimal *Ubx* enhancer and selected for mutation to random sequences. B) exemplifies mutation of the two strongly conserved binding sites for construct $UbxB^{\Delta FOXK\text{-}BS\_1}$. Known binding sites for TCF are marked in green.

Analysis of embryos carrying the WT *UbxB* enhancer construct by DAB staining (see 6.15) showed the expected strong *β-gal* expression in parasegment 7 of the midgut throughout all examined stages (stage 14-16, Figure 3.5, left panels). To minimise potential effects of random integration into the genome, 3 independently generated lines carrying the FKH-mutant enhancer were analysed for *β-gal* expression. This revealed complete loss of LacZ staining in the midgut upon mutation of FKH binding sites.

No difference was found between the two constructs carrying mutations of two (Figure 3.5, right panels) or all FKH binding sites (data not shown) leading me to conclude that loss of only the two highly conserved binding sites in $UbxB^{\Delta FOXK\text{-}BS\_1}$ is sufficient to abolish *β-gal* expression from the minimal *UbxB* enhancer entirely.

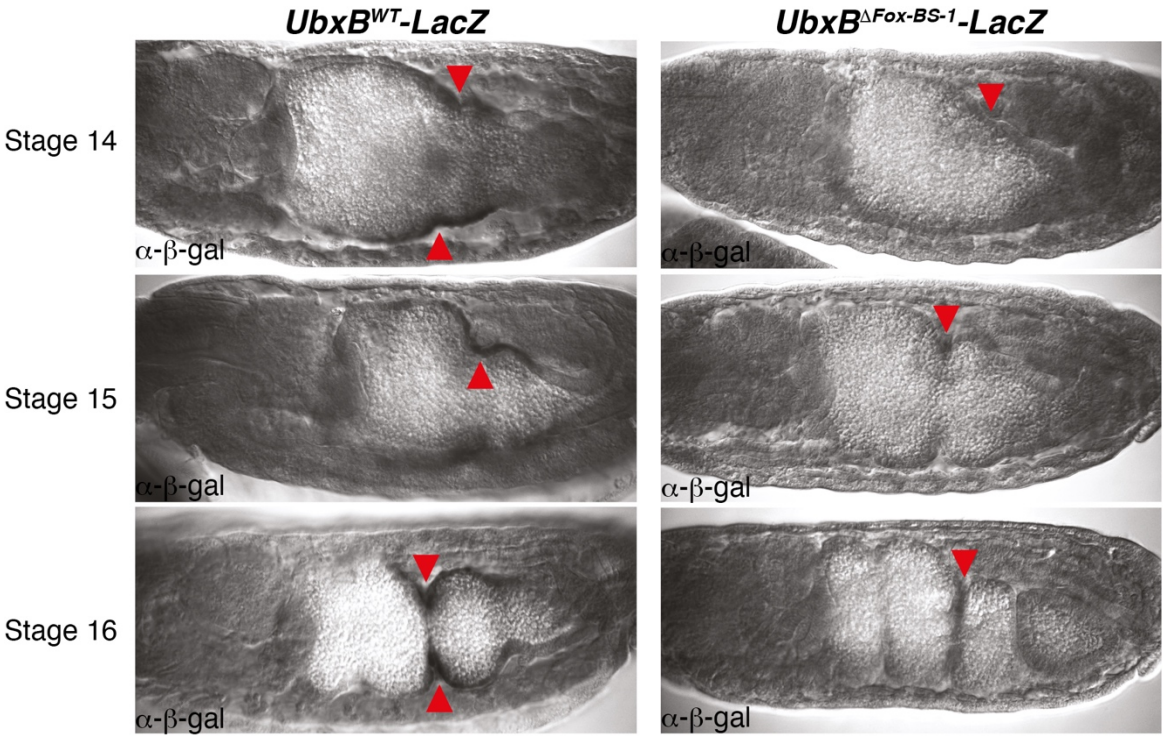

Figure 3.5. Binding sites for FOX transcription factors are required for expression from a *UbxB* reporter plasmid.
WT or mutant *UbxB* reporter plasmid was inserted randomly into the *Drosophila* genome and *β-gal* expression monitored in the midgut of embryos of stage 14-16, where expression from the minimal enhancer is strongest. As expected, the WT enhancer fragment yields strong expression at the boundary between parasegments 7 and 8, marking the constricting midgut (left panels, red arrows). In contrast, no *β-gal* expression is found in embryos carrying a *UbxB*

construct with mutations in the conserved FKH binding sites (*UbxB*$^{\Delta FOXK\text{-}BS\_1}$, right panels, red arrows).

Loss of expression from the *UbxB* reporter construct upon mutation of FKH binding sites supports the hypothesis that FOX proteins function at Wnt/Wg target loci. Since FOXK proteins were predominantly found in association with Wnt enhanceosome bait proteins, I focused my analyses on the FOXK family of FOX factors.

3.2.2. *FoxK*^{16} embryos show a low-penetrance midgut constriction phenotype but wild-type cuticles

Based on the FoxK study by Casas-Tinto et al. (2008), we decided to use their *foxK*^{16} fly strain to assess in more depth a connection between FoxK and Wg signalling.

I first attempted to confirm the failure of homozygous *foxK*^{16} flies to form the middle midgut constriction as described above (Figure 3.2A, Figure 3.6A). This was achieved by using a *foxK*^{16} line balanced over *TM6-twi::LacZ*, which expresses *β-gal* from a *twist* promoter. Balanced, heterozygous embryos (β-gal^{+}) can accordingly be distinguished from *foxK*$^{16/16}$ homozygous mutant embryos (β-gal^{-}) using 3,3'-Diaminobenzidine (DAB) staining on stage 14-18 embryos (see 6.15).

I was able to corroborate the reported phenotype in a small minority of homozygous embryos (Figure 3.6B) that lack the middle midgut constriction but begin the first and third constriction prior to developmental arrest around stage 16. However, the penetrance of this phenotype was very low (5 out of ~200 embryos, approx. 2.5%) and most β-gal^{-} embryos developed normally and even hatched into larvae.

To confirm that zygotically homozygous *foxK*^{16} larvae are indeed viable, a *TM6-twi::GFP*-balanced *foxK*^{16} strain was used. Of the progeny (n = 427), 98 1st and two 2nd instar larvae without GFP expression (*foxK*$^{16/16}$) were identified (23.4%), which is

not substantially lower than the expected Mendelian ratio of ~25% (*TM6-GFP* balancer used here is larval lethal). This observation reveals that the *foxK*^{16} allele is not substantially embryonic lethal, in contrast to my expectation based on the study by Casas-Tinto et al. However, 3rd instar homozygous *foxK*$^{16/16}$ larvae were never observed, indicating high lethality during the 1st/2nd instar stage.

The f*oxK*^{16}*/TM6-twi::GFP* strain was also used to assess any phenotypic changes of the denticle pattern, which is a process regulated by Wg signalling (see 1.6). (Recall that embryos overexpressing Wg or any of its positively acting components have a denticle lawn with no distinguishable denticle belts, whereas loss of *wg* or overexpression of antagonistic proteins can lead to naked cuticle.)

Embryos were collected overnight at 18°C, those without GFP expression (*foxK*$^{16/16}$) selected and cuticles prepared as described (6.16). Analysis by light microscopy did not indicate any anomalies in the denticle pattern when compared with similarly staged control (*white)* embryos (Figure 3.6C).

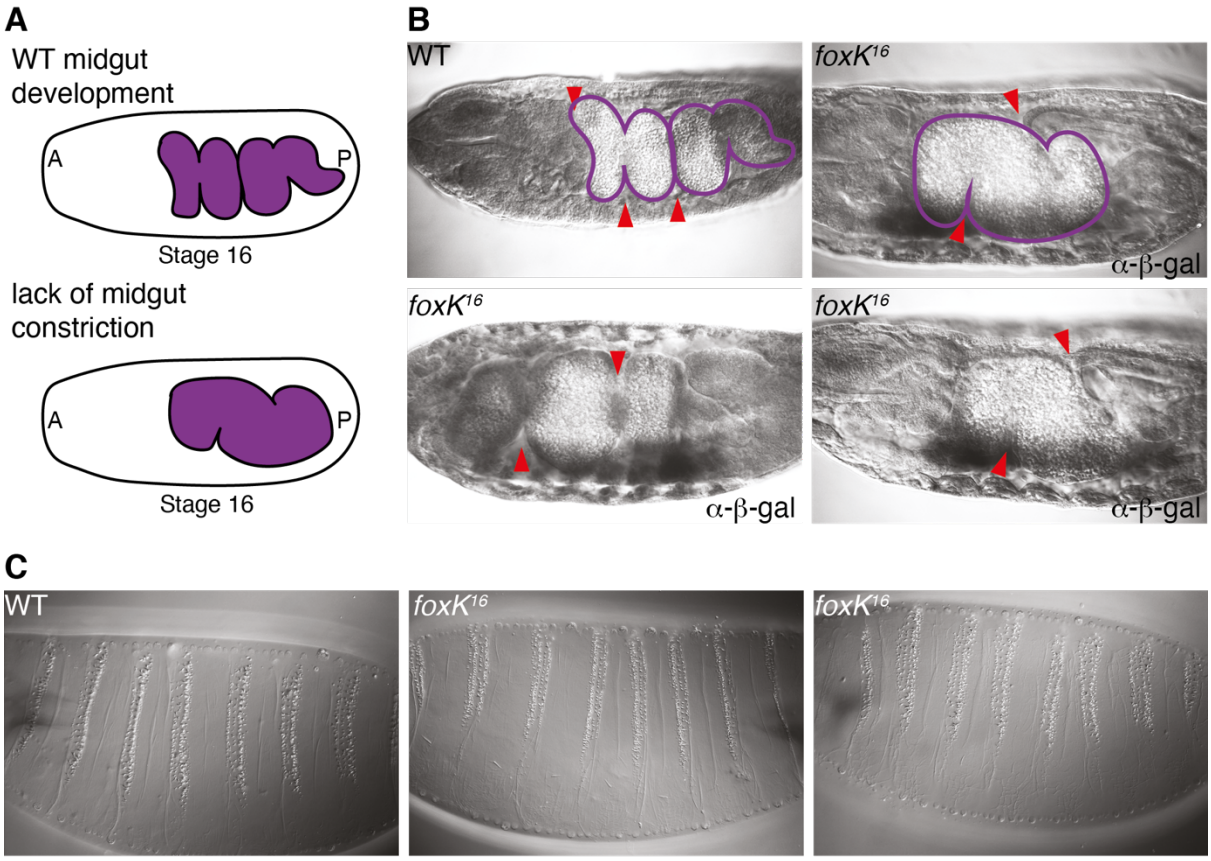

Figure 3.6. Phenotypic analysis of the *foxK[16]* mutation in embryo development.
A) Cartoon of WT and mutant midgut constriction formation. WT embryos form the middle midgut constriction first, before the 1st and 3rd constriction begin to invaginate. Embryos mutant for several components of the Wg signalling pathway or *foxK* as reported by Casas-Tinto et al. fail to form the middle constriction and development arrests soon after.
B) Analysis of the middle midgut constriction in zygotically homozygous *foxK[16/16]* embryos. Embryos of a *foxK[16]/TM6-twi::LacZ* strain were collected overnight at 18°C (stage 14-18) and subsequently stained for *β-gal* expression to distinguish homozygous mutant embryos. Only 5 out of ~200 embryos failed to form the middle midgut constriction and arrested during embryonic development, whereas most embryos hatched into 1st instar larvae.
C) Cuticle preparations of WT (*white*) and *foxK[16/16]* mutant embryos. Embryos of a *foxK[16]/TM6-GFP* strain were collected overnight at 18°C and homozygous mutant, GFP-negative embryos picked under a fluorescent microscope. The denticle pattern shows no difference compared to WT embryos.

3.2.3. *FoxK[16]* homozygous clones in the wing lead to wing notches

Additionally, I used clonal analysis to assess phenotypes in larval or adult tissues homozygous for the *foxK[16]* allele following recombination of the mutant allele onto FRT lines (see 6.19). Complementation assays with the original *foxK[16]/TM6b* strain

were used to determine if the *foxK*^{16} allele was present on the recombinant chromosomes. At least three independent recombinant lines were tested for clones in wing discs as well as adult wings by crossing to a strain carrying *FRT2A* linked to a nuclear GFP construct and a heat-shock (HS)-inducible flippase insertion (*hsFlp;; FRT2A, GFP.nls*).

In discs, I observed a high number of small mutant clones across the presumptive wing blade as well as in future hinge and notum tissues. Clones and corresponding twin spots approximately matched in size, indicating that growth of homozygous *foxK*^{16} tissue was not significantly affected. Clones found directly adjacent to the Wg stripe did not lead to visible changes in *wg* expression (Figure 3.7A, see closeup of Line 2), a phenotype previously described for various *wg* mutants (e.g. Flack et al., 2017).

Adult wings of larvae treated with the same HS protocol displayed notches along the margin as well as defects of vein formation. These notches differed in size and were most frequently observed along the posterior margin but occasionally appeared anteriorly (Figure 3.7B). Defects in vein formation usually resulted in gain of vein-like tissue; however, shortened veins (mostly of L5) occurred with lower frequency.

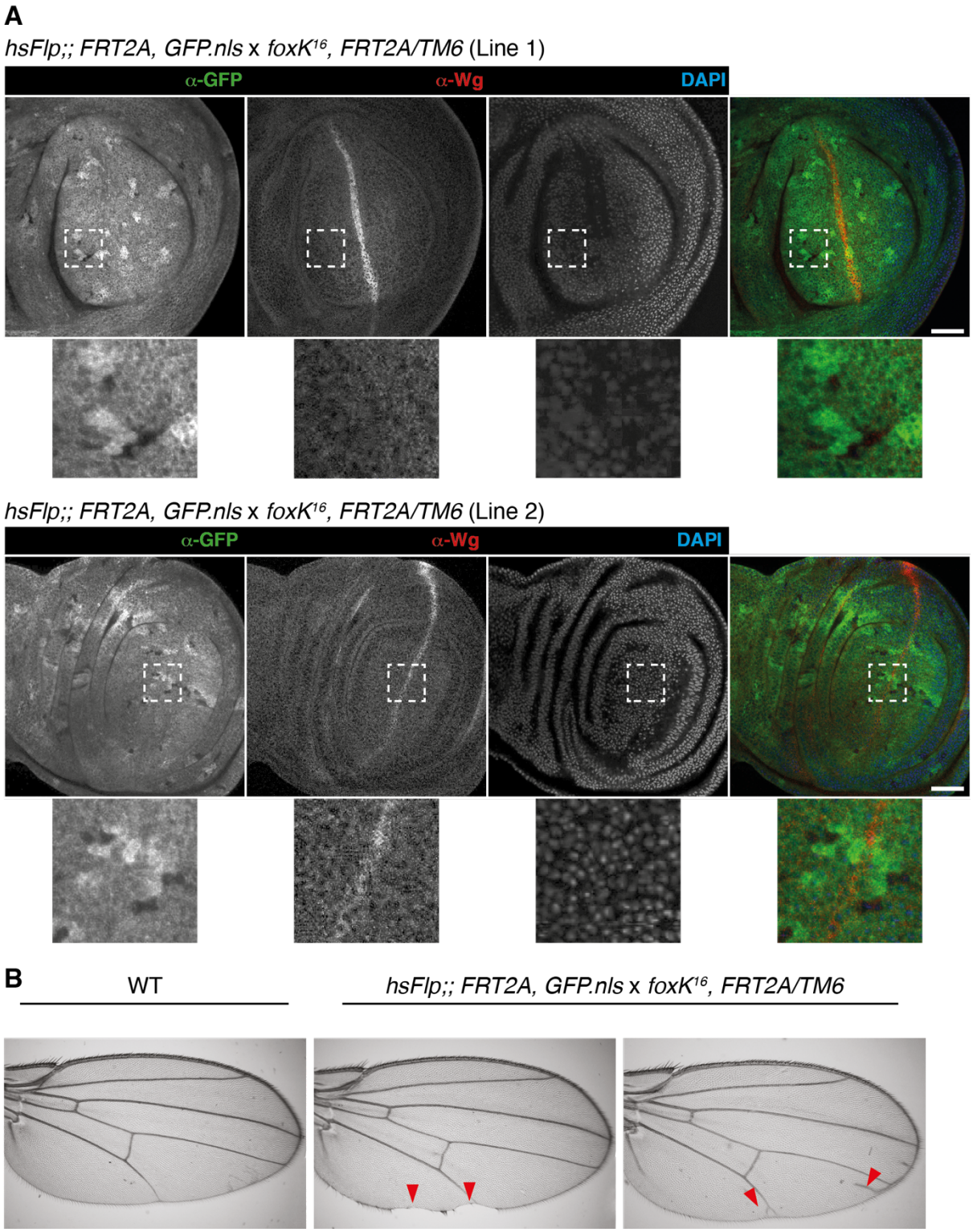

Figure 3.7. Analysis of *foxK*$^{16/16}$ mutant clones in wing discs and adult wings.
A) Wing discs of 3rd instar larvae 2 days post-HS of a cross of *hsFlp;; FRT2A, GFP.nls* to *foxK*^{16}*, FRT2A/TM3*. Mutant clones (GFP^{-}) and twin spots (GFP^{++}) are of approximately the same size. *Wg* expression is not perturbed by nearby *foxK*$^{16/16}$ clones. Magnifications are 4x the original size.
Scale bar = 50 μm. α-GFP (green), α-Wg (red), DAPI (blue).

B) Adult wings of the same cross showing wing notches, predominately on the posterior margin, as well as excessive vein tissue. Defects are indicated by red arrows.

3.2.4. The *foxK*^{16} allele does not carry the molecular lesion described

The low penetrance of the midgut constriction phenotype of *foxK*^{16} zygotic mutants led me to re-assess this mutation to verify *foxK*^{16} as a null allele.

Casas-Tinto et al. describe the molecular basis of the *foxK*^{16} allele to be a 962 bp deletion and 4 bp insertion affecting exons 2 and 3 and resulting in a truncated protein that only shares the first 26 amino acids with WT FoxK (Figure 3.8A & B).

I developed a PCR assay with oligonucleotide primers binding upstream and downstream of the mutation to amplify the affected genomic region. This analysis was performed on heterozygous flies, and was expected to yield two bands on a separating agarose gel: a WT band of 1900 bp, as well as a band corresponding to the *foxK*^{16} allele of 944 bp.

Repeated PCR assays under different conditions (e.g. time of elongation, temperature etc.), did not yield the expected *foxK*^{16} band, while the WT allele amplified without issues. An additional, unspecific band of approximately 1 kb was observed in all samples (WT and *foxK*^{16}/*TM6*, Figure 3.8C). Sequencing of the main band at 1.9 kb with an internal sequencing primer confirmed this as the expected amplification product of the WT allele. Sequencing of PCR-purified samples also did not reveal any trace of an additional allele other than the WT sequence.

Given these difficulties to confirm the *foxK*^{16} allele, I attempted to verify the lethality associated with the *foxK* genomic locus using deficiency strains available at Bloomington (BSC817, BSC753 & ED4470). Adult flies transheterozygous for each of the deficiency chromosomes and *foxK*^{16} were viable and fertile and did not show any overt defects over several generations (Figure 3.8D).

These results suggest that the observed larval lethality in homozygous *foxK*^{16} offspring was due to a mutation elsewhere in the genome.

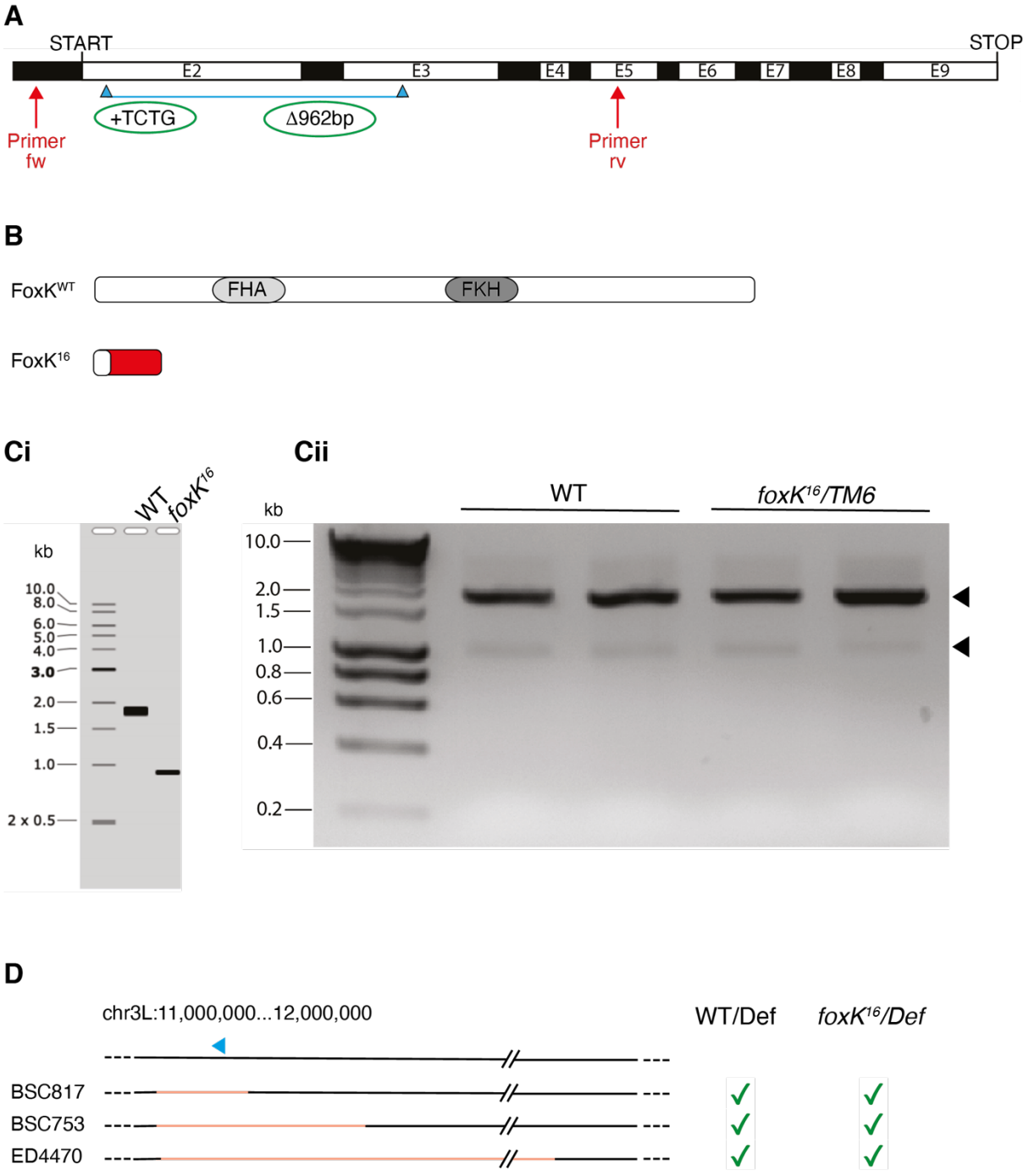

Figure 3.8. Molecular analysis of the *foxK*^{16} allele.
A) Intron-exon sequence of *foxK* marking the reported mutation *foxK*^{16} (blue). Mobilisation of the *P* element reportedly led to an insertion of TCTG in exon 2 followed by a deletion of 962 bp affecting exons 2 and 3 and causing a frame shift. PCR amplification oligonucleotides were designed to bind in the 5'-UTR and exon 5 (red).

B) Predicted protein size of FoxK^{16} protein in comparison to WT FoxK. Grey: first 26 amino acids are shared between WT and FoxK^{16}. Red: novel sequence in FoxK^{16} generated by frameshift. Stability of this protein fragment is unknown.
Ci) Agarose gel (1%) with DNA fragments by amplification using primers fw and rv (red, see A) simulated using SnapGene.
Cii) Amplification of *Drosophila* DNA from 2 WT flies and 2 *foxK^{16}*/*TM6* flies using the same primers. A main band at 1.9kb corresponding to the WT allele was found in all samples and an additional unspecific band at approx. 1kb was observed in most samples, but no distinct amplification was found for the *foxK^{16}* allele (944 bp) in either of the 4 samples.
D) Deficiency analysis using three distinct deficiency lines showed that *foxK^{16}* is a viable allele when transheterozygous over either deficiency (green ticks). Red area in deficiency lines indicates area of deletion, each covering the *foxK* locus (blue triangle).

The molecular basis of the f*oxK^{16}* allele could thus not be confirmed and bearing in mind the surprisingly low penetrance of the midgut constriction phenotype, I decided to generate a new f*oxK* allele using CRISPR/Cas9-mediated editing.

3.2.5. Generation of *foxK^{KO}* alleles using CRISPR/Cas9

I designed several different guide RNAs (sgRNAs, see 6.12) using online resources (www.crisprflydesign.org) to target the N-terminal region of *foxK*, with the aim of generating a full knockout allele. Originally, I selected three sgRNAs binding in the very N-terminal part of the protein within 100 bp of the transcription start site (TSS) to produce an allele that results in nonsense-mediated decay rather than leading to translation of truncated but potentially stable protein (sgRNAs 1-3, Figure 3.9A).

sgRNA2 led to successful editing as verified by sequencing analysis, and several different alleles predicted to carry frameshift-causing insertion/deletion mutations (Indels) resulting in premature STOP codons were recovered. Despite the fact that all of these new alleles carry a lethality on chromosome 3, use of the above-mentioned deficiency strains (Figure 3.8D) showed that this is not due to loss of FoxK. Complementation assays between these different alleles revealed that use of

sgRNA2 resulted in at least two different lethal off-target effects on chromosome 3 in addition to non-lethal editing in the *foxK* locus.

To test if WT FoxK protein is produced from the CRISPR mutant alleles, I generated a new FoxK antiserum using FoxK$^{216-417}$ as the antigen (see 6.20). As expected, this antiserum binds to both splice variants (~72 and ~81 kDa, respectively) described by Casas-Tinto et al. (2008), reflected by two bands on western blot for WT samples.

All lines edited with the N-terminal sgRNA2 were tested as transheterozygotes over a deficiency chromosome and found to produce a ~70-75 kDa FoxK protein (see results for *foxK^{2}/BSC817* and *foxK^{10}/BSC817* in Figure 3.8D). It was not determined whether this protein species is one of the known FoxK variants found in WT flies and thus corresponds to the lower molecular weight band seen in WT sample or whether it is a differently truncated variant. Given that the alternative splicing affects exons 8 and 9, it seems unlikely that editing in exon 2 should generate the same protein.

I concluded that this protein species is likely different from the smaller splice variant and could derive from picking up another translational initiation codon that reads into the *foxK* open reading frame. Such a scenario has been observed on multiple occasions in the Bullock lab at MRC LMB (Simon Bullock, personal communication). The extensive protein-coding capacity of the *foxK^{2}* and *foxK^{10}* mutant alleles suggests that they are unlikely to represent null mutations.

In order to circumvent this putative alternative reading frame, I designed several additional sgRNAs to bind further downstream, closer to the FHA domain (sgRNAs 4-6).

SgRNA5 and sgRNA6 led to frequent editing events and I recovered multiple alleles with predicted frameshift mutations as exemplified for *foxK^{42}* (Figure 3.9B & C). Animals homozygous for these alleles are not embryonic lethal but die as pupae (see below). Western blot analysis with FoxK antiserum confirmed that homozygous 3rd

instar (climbing) larvae do not produce any FoxK protein ((Figure 3.9D), lanes for FoxK^{11}, FoxK^{23} and FoxK^{42}). Additionally, the deficiency lines described above were used to demonstrate that the lethality was indeed due to a lesion at the *foxK* locus.

I was thus able to generate three novel *foxK^{KO}* alleles stemming from two independent sgRNAs, which are likely to represent null alleles. These knockout alleles were used for additional experiments in *Drosophila*. Sequences of all mutant *foxK* alleles can be found in the appendix (8.4).

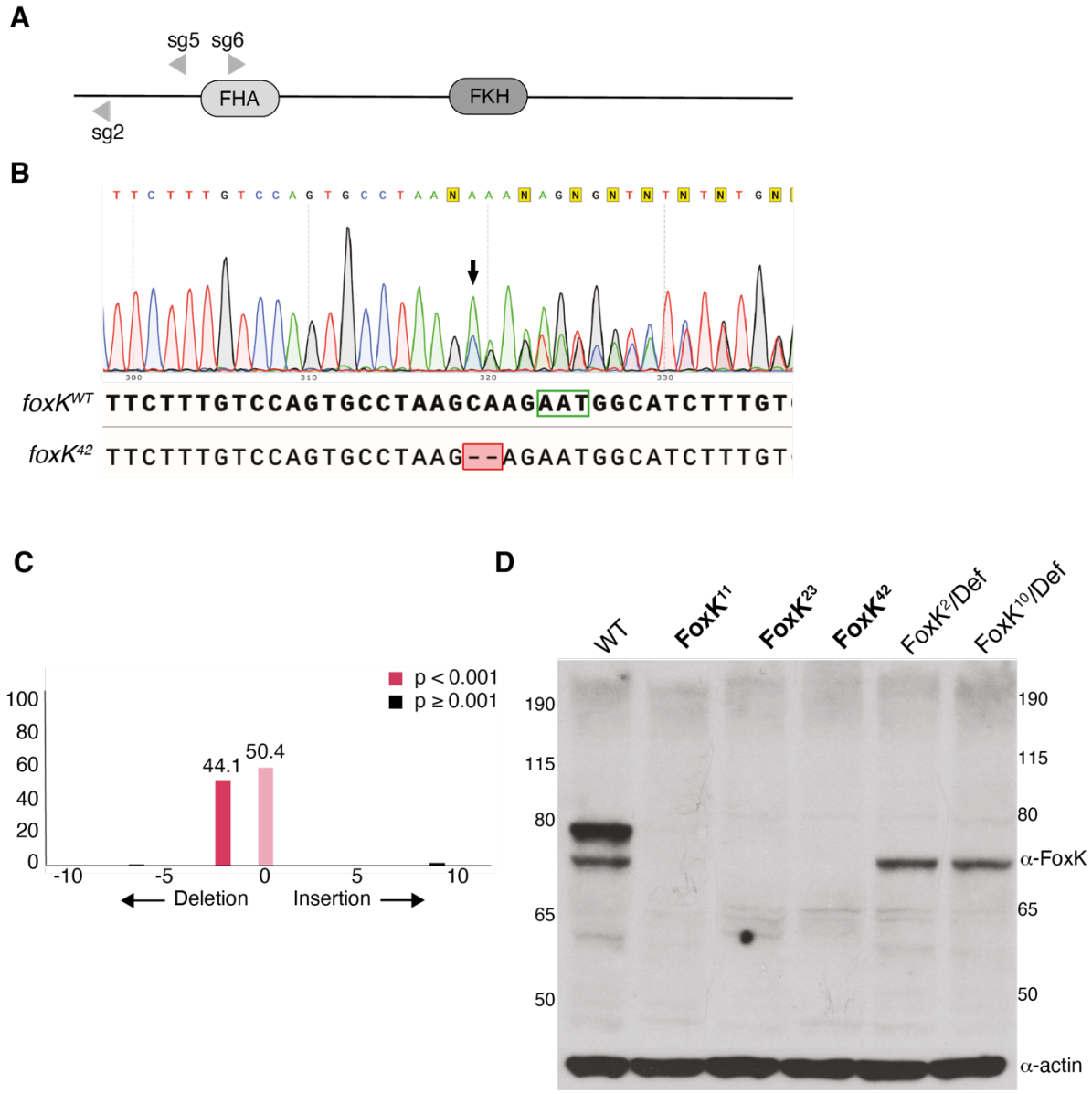

Figure 3.9. CRISPR/Cas9-mediated knockout of *Drosophila* FoxK.
A) Cartoon of *FoxK* with positions of sgRNAs used to generate edited alleles of *foxK.*

B) Typical sequencing chromatogram of a heterozygous line with editing leading to a 2 bp deletion roughly 5 bp away from the PAM site (green box). Shown here is line *foxK*^{42}*/TM6*.
C) The online resource Tide-Seq was used to determine the Indel mutation generated through editing (shown here is the same 2 bp deletion as in B).
D) Western blot analysis of 3rd instar larval tissue of animals with different *FoxK* alleles. From left to right: WT, *foxK*$^{11/11}$, *foxK*$^{23/23}$, *foxK*$^{42/42}$, *foxK*^{2}*/BSC817* and *foxK*^{10}*/BSC817*. WT FoxK is expressed as two isoforms of 71 and 82 kDa, respectively. Full knockouts (*foxK*^{11}, *foxK*^{23} and *foxK*^{42}) do not form any detectable protein, whereas lines *foxK*^{2} and *foxK*^{10} yield a truncated but functional protein.

3.2.6. Zygotically homozygous *foxK*^{KO} flies are pupal lethal and have deformed wing discs

As described previously, the published *foxK*^{16} allele causes developmental arrest at around embryonic stage 16. Contrary to the embryonic lethality of *foxK*^{16}, *foxK*^{KO} animals were found to develop normally until pupariation, at which point development stopped. No homozygous adult flies hatched from any of the knockout lines. This pupal lethality is reminiscent of other mutants of Wg pathway components such as the Pygo mutant *pygo*^{S123} (Figure 3.10A, Thompson et al., 2002). Additionally, zygotically homozygous *FoxK*^{KO} larvae were developmentally delayed and reached the pupal stage approximately 5-6 days later than WT or heterozygous animals (Figure 3.10B).

Interestingly, when dissecting homozygous, climbing 3rd instar larvae from *foxK*^{KO}*/TM6-GFP* strains, I found that wing discs are significantly smaller than in WT animals (Figure 3.10C). Other discs as well as the larval brain were not affected in size (data not shown). Anatomically, the homozygous mutant wing discs appear to lack presumptive wing blade tissue, while the hinge and notum regions develop relatively normally. The developmental delay described above is likely secondary to the growth impairment of the wing discs, as such an effect has been previously described for mutants affecting larval growth (Colombani et al., 2012).

Staining of discs for Wg and dMyc, a Wg target gene (Duman-Scheel et al., 2004), revealed that, while both proteins are expressed in *foxK*^{KO} discs, Wg does not localise in the typical stripe across the presumptive blade that occurs in 3rd instar WT discs and specifies the future wing margin.

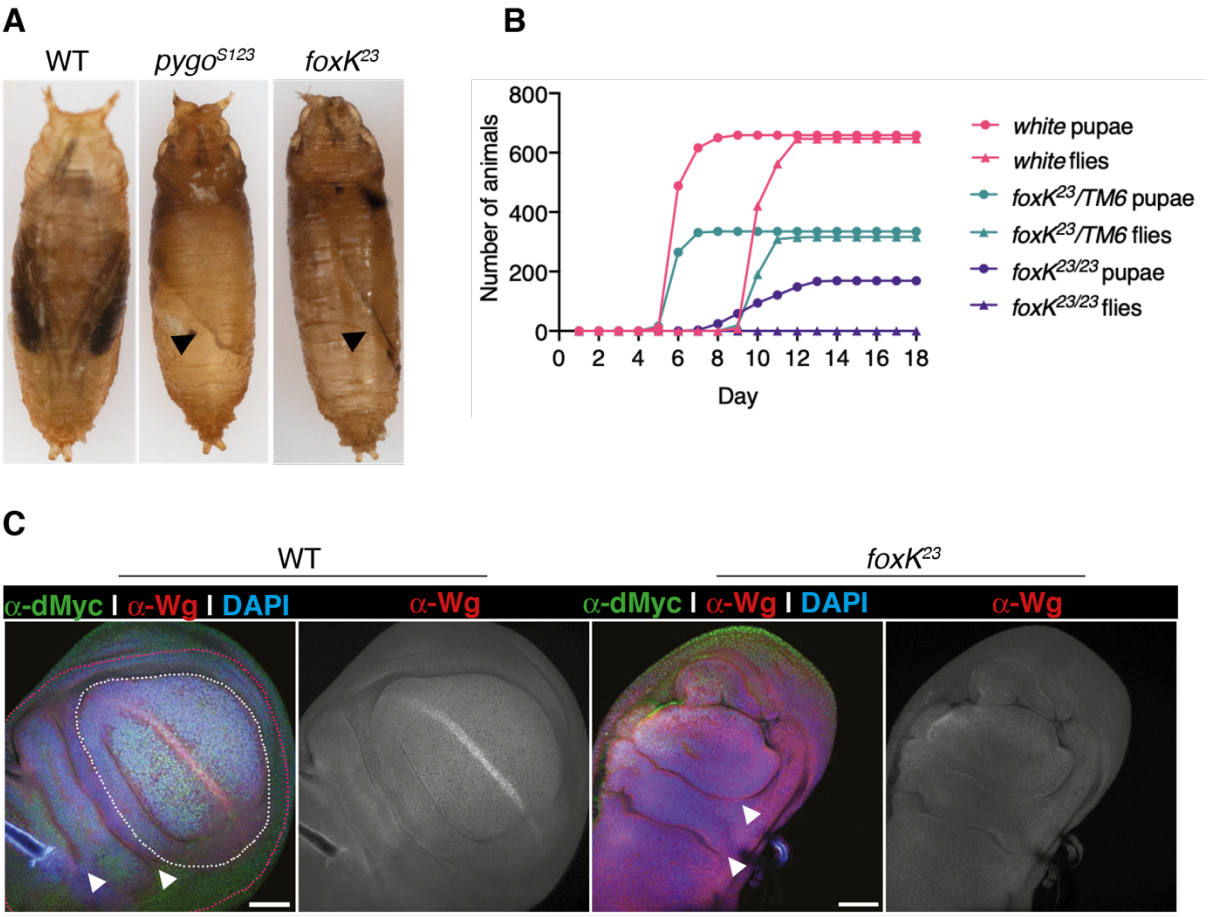

Figure 3.10. Phenotypes of zygotically homozygous *foxK*^{KO} mutants.
A) Zygotically homozygous *foxK*^{KO} mutants die shortly after pupariation, and this phenotype is similar to several mutants of the Wg pathway such as *pygo*^{S123} (allele generated by Thompson et al., 2002). Black arrow indicates dead animals within the pupal cocoon.
B) Homozygous *foxK*^{KO} mutants are developmentally delayed and reach pupal stages approximately 5-6 days later than WT or heterozygous animals. Lines indicate total number of animals of a *white* control (pink), *foxK*^{23} heterozygous progeny balanced over TM6 (turquoise) as well as *foxK*^{23} homozygous progeny (purple). All progeny was counted each day and developmental stages were recorded for each line (pupae or adult fly, circles or triangles, respectively).
C) 3rd instar larvae of *foxK*^{KO} mutants (right) show deformations of wing discs, possibly restricted to the presumptive wing blade. WT wing disc (left) depicting the future blade (white circle) and hinge tissues (red circle). Images are taken while focused on the plane of the Wg stripe.
Scale bar = 50 μm. α-dMyc (green), α-Wg (red), DAPI (blue).

3.2.7. FoxK is ubiquitously expressed in nuclei during *Drosophila* development

I next used the antiserum I generated (see 6.20) to ask whether FoxK shows differential localisation during development and is specifically expressed in some tissues but not others. An expression pattern similar to Wg would hint at a function related to Wg signalling.

I assessed FoxK localisation during different stages of embryonic development as well as in context with different Wg pathway proteins. FoxK localises to the nucleus in a ubiquitous fashion throughout all stages of embryogenesis and is not enriched in parasegmental stripes (Figure 3.11Ai-iii). This is expected based on mRNA expression pattern from the Berkeley *Drosophila* Genome Project (insitu.fruitfly.org), which revealed that FoxK mRNA is also ubiquitously expressed. FoxK expression overlaps with that of Pygo, which is also ubiquitous and nuclear.

I was able to confirm that Pygo is expressed ubiquitously and localises to the nucleus. I also found that subcellular distribution of Armadillo does not affect localisation of FoxK. While Armadillo is ubiquitously found at the plasma membrane, a fraction of the Armadillo pool moves into the nucleus in cells stimulated with Wg (Figure 3.11Bi-iii).

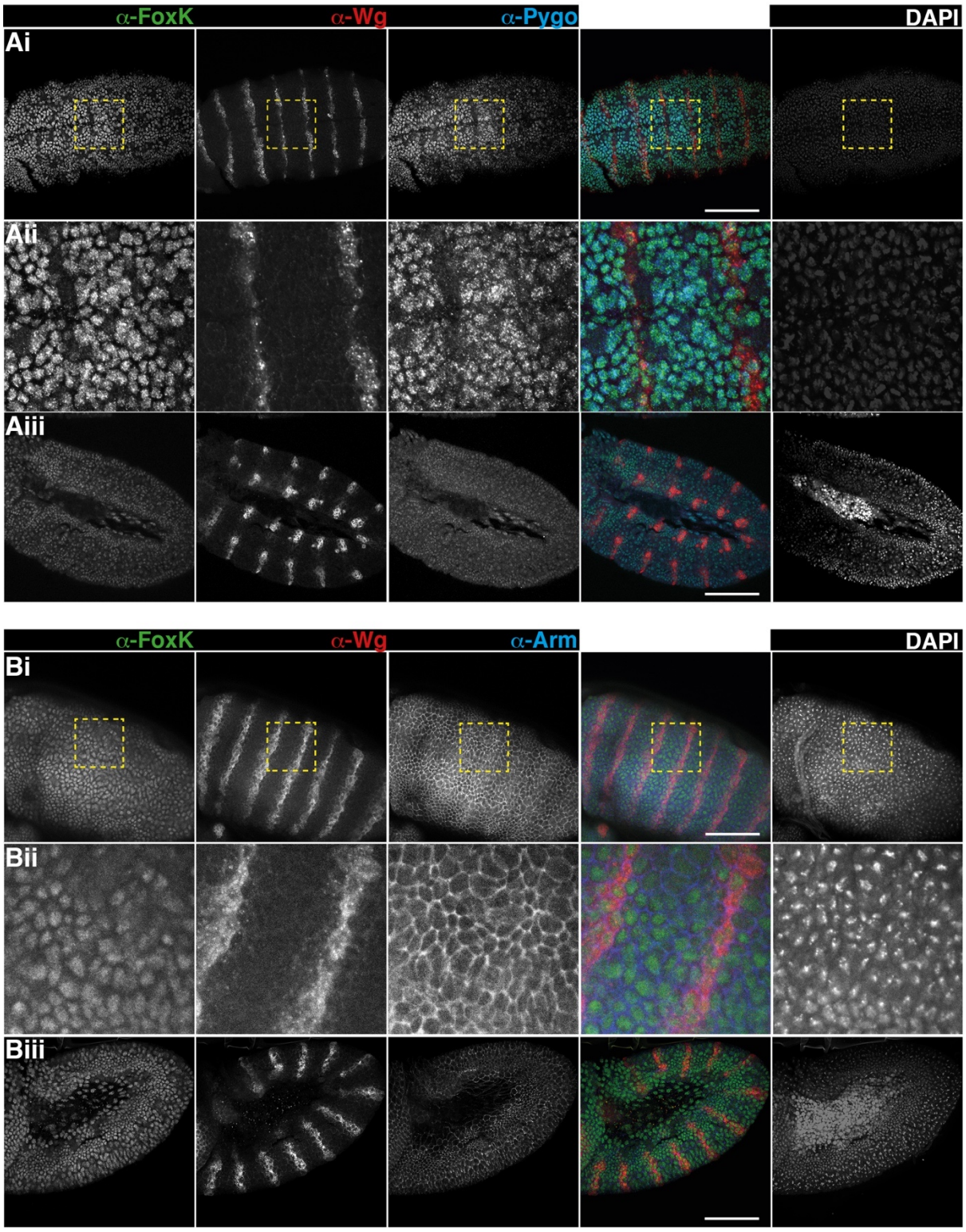

Figure 3.11. Embryonic localisation pattern of *Drosophila* FoxK, Wg, Pygo and Armadillo.

A) *Drosophila* embryos stained for FoxK, Wg and Pygo. Ai & Aii) ventral view, Aii) side view. B) *Drosophila* embryos stained for FoxK, Wg and Armadillo. Ai & Aii) ventral view, Aii) side view.

All embryos between stage 9-11. Scale bar = 100 μm. Aii) and Bii) 4x magnification of Ai) and Bi) respectively. Ai), Aiii) & Bi) were taken as z stacks and appropriate imaging slices collapsed using ImageJ software. Anterior left, posterior right in all images.
α-FOXK (green), α-Wg (red), α-Pygo (blue in A), α-Arm (blue in B), DAPI (grey).

Next, I sought to determine whether FoxK specifically localises to the presumptive blade tissue in wing discs given the deformed blade in zygotically homozygous FoxK mutants (Figure 3.10C). Figure 3.12 shows the localisation of FoxK in third instar wing discs (n = 10), where it is ubiquitous and nuclear across presumptive blade, hinge and notum regions. Note that the reduced staining adjacent to the Wg stripe in the anterior wing blade compartment (arrowheads in Figure 3.12A) is mirrored in both FoxK and DAPI channels and therefore likely represents differences in antibody accessibility or nuclear localisation.

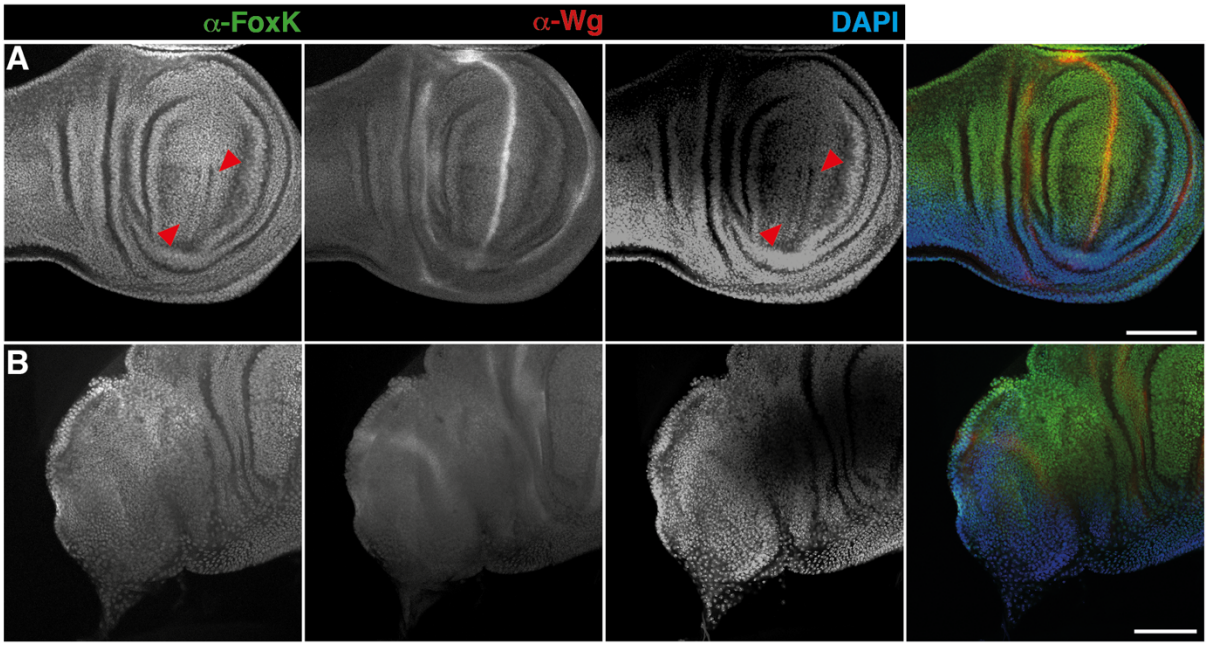

Figure 3.12. Endogenous FoxK is ubiquitously localised to nuclei across 3rd instar wing discs.
A) Prospective wing blade of a 3rd instar wing disc showing ubiquitous FoxK staining in nuclei. Red arrowheads denote areas adjacent to the Wg stripe with lower signal in the FoxK and DAPI channel.
B) Hinge and notum regions of 3rd instar wing disc, staining as above. FoxK expression does not differ between presumptive blade, hinge and notum areas.
Scale bar = 100 μm. Images are maximum intensity projections of appropriate z-stack slices using ImageJ software. α-FoxK (green), α-Wg (red), DAPI (blue).

3.2.8. *FoxK^{KO}* clones show impaired survival in the presumptive wing blade tissue

Given the apparent specificity for FoxK requirement during wing development seen in zygotic larvae, I sought to examine *foxK^{KO}* clones in wing discs and adult wings.

In order to assess the consequence of homozygous loss of FoxK in larval and adult tissues, I recombined independently generated *foxK^{KO}* alleles onto FRT lines as before and crossed the recombinant progeny to a *hsFlp;; FRT2A, GFP.nls* line (see above).

The standard protocol to induce mutant clones in wing discs was a 30-min HS at 37°C on the 3rd day post laying (early 3rd instar larvae, Figure 3.13A). Climbing 3rd instar larvae were dissected and stained for GFP and Wg expression. Using this protocol, a very small number of mutant clones of only about 2-4 cells in size were recovered in the blade region, whereas clones in the hinge area grew to be substantially larger (Figure 3.13B). Additionally, despite a large sample size (> 50 wing discs), no mutant clones were found on the presumptive margin, i.e. correlating with Wg-expressing cells.

As this lack of clones in the blade makes interpretation of an effect of loss of *foxK* on *wg* expression difficult, I decided to adjust the HS protocol to favour induction of larger clones by applying a longer HS (60 min) to younger, 2nd instar larvae (2 days post laying). This revised HS protocol resulted in the induction of large clones in the hinge and notum that corresponded in size to their respective twin spots.

Strikingly, the pouch itself did not contain any mutant clones, even though the corresponding twin spots were clearly visible and spanned >20 cells in diameter (Figure 3.13C). This observation indicates that *foxK^{KO}* clones are not viable in the pouch and are likely extruded from the wing blade (see below). Based on the absence of mutant clones in this region, assessment of the classic Wg target

s*enseless*, which is commonly analysed to link mutations to Wg signalling (see 1.6), was not possible.

Please note that all images shown in Figure 3.13 have been taken in the plane of the clones in the wing pouch rather than as z-stacks to allow easier visibility of clones and twin spots. The Wg stripe across the dorsoventral margin is therefore not visible in selected images but was found to be unaltered.

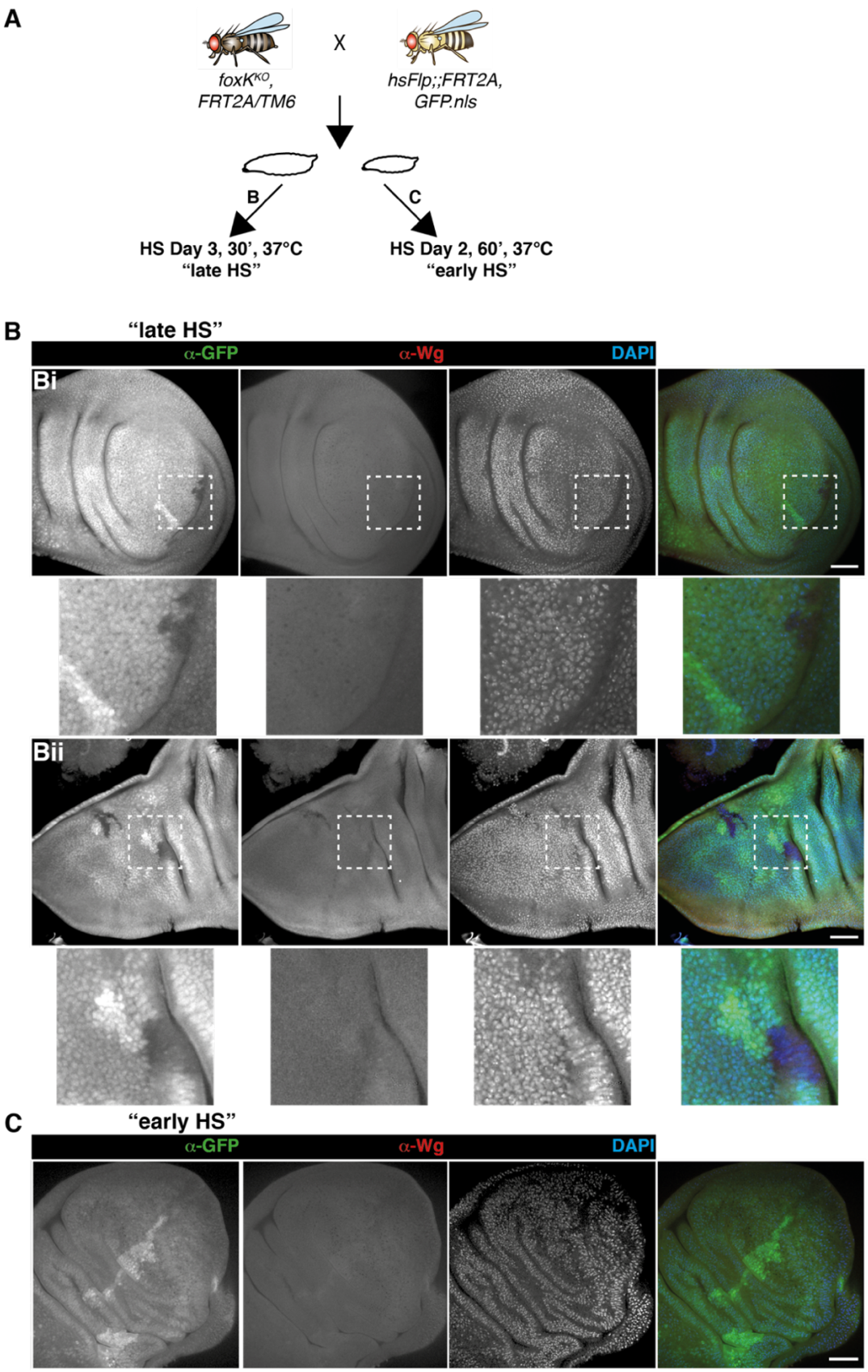

Figure 3.13. *FoxK^KO* clones in wing imaginal discs are lost from the presumptive blade tissue but survive in the hinge and notum area.

A) Schematic description of the HS protocol used for generation of mutant clones.
B) If a late HS is applied on day 3 of larval development (3rd instar stage), small, infrequent clones are generated in the future blade (red arrow), whereas slightly bigger clones can be found in the hinge and notum (black arrows). Magnified images are 3x the original size.
C) Earlier HS applied for a longer time frame is expected to increase the size of clones. While the respective twin spots reach a large diameter, no corresponding clones are found in the blade area. In the future hinge however, growth of *foxK*^{KO} clones is not impeded and they reach a size corresponding to their twin spots.
Scale bar = 50 μm. α-GFP (green), α-Wg (red), DAPI (blue). Images are taken in the plane of clones in wing blade, not as z-stacks (see text).

3.2.9. *FoxK*^{KO} clones in adult wings lead to perturbed vein structures

I next sought to determine whether induction of *foxK*^{KO} clones during imaginal development leads to visible phenotypes in adult appendages such as wings, legs or eyes. By applying the same HS regimes described above I was able to generate clones with phenotypes in the adult wing.

In contrast to clones of other mutations that disrupt *wg* functions, *foxK*^{KO} clones do not cause notches of the wing margin but rather show vein deletions and duplications (Figure 3.14B & C). This result prompted me to examine whether these vein defects are a direct effect of loss of functional FoxK protein or whether they result indirectly from loss of *foxK*^{KO} tissue. To distinguish between these possibilities, I made use of an *FRT2A* line carrying a *multiple wing hair* (*mwh*) marker which marks tissue in the blade with additional wing hairs (Wong and Adler, 1993) (Figure 3.14D).

I was thus able to identify twin spot tissue in the adult wing as these display the *mwh*$^{-}$ phenotype, whereas homozygous mutant and heterozygous tissues are *mwh*$^{+}$. This allowed me to distinguish whether the defects in vein formation correlate with twin spot tissue (mwh^{-}, indirect effect of FoxK loss) or with mwh^{+} tissue, which would likely indicate a direct effect of loss of FoxK on vein formation.

I found that vein defects are limited to areas carrying multiple wing hairs (*mwh*$^{-}$) and are thus formed by twin spot tissues. My observations further showed that the defect

itself often directly abutted the boundary between *mwh*$^{-}$ and WT wing tissue (Figure 3.14E). Loss of *foxK* therefore indirectly affects vein formation.

The *mwh, FRT2A* line additionally carries a *yellow*$^{+}$ marker such that mutant clones are marked with *yellow*$^{-}$ in an otherwise WT background. This marker is only visible in the wing margin due to lack of pigmentation of the blade itself but allowed me to assess survival of *foxK*$^{-/-}$ clones specifically at the dorso-ventral boundary.

Indeed, I was able to recover small clones stretching between 1-7 bristles in a number of wings (Figure 3.14F & G) regardless of when during development the HS was applied. While the *yellow*$^{-}$ bristles appear slightly shorter and thinner than neighbouring WT bristles, this is likely due to the *yellow*$^{-}$ mutation itself rather than loss of *foxK*, as we have observed this effect in other experiments as well (Juliusz Mieszczanek, Bienz Lab, unpublished observations).

As I made use of a flippase line activated ubiquitously by HS rather than driven in specific tissues (such as a *vestigial::flippase* line leading to wing-specific expression), clones should be induced in other organs as well. Since *wg* is expressed in other imaginal discs such as the eye or leg discs and mutants of the Wg pathway have been reported to lead to deformations in these organs (see for example Legless mutants, van Tienen et al., 2017), an adult phenotype in other appendages might be expected.

Despite screening a large sample of adult flies post HS ($n > 300$), I was unable to find discernible mutant phenotypes in any adult tissues other than the wing, which suggests a specificity for FoxK restricted to the wing disc rather than a general requirement of FoxK for development of imaginal discs, in line with the zygotically homozygous visible phenotype in wing discs only.

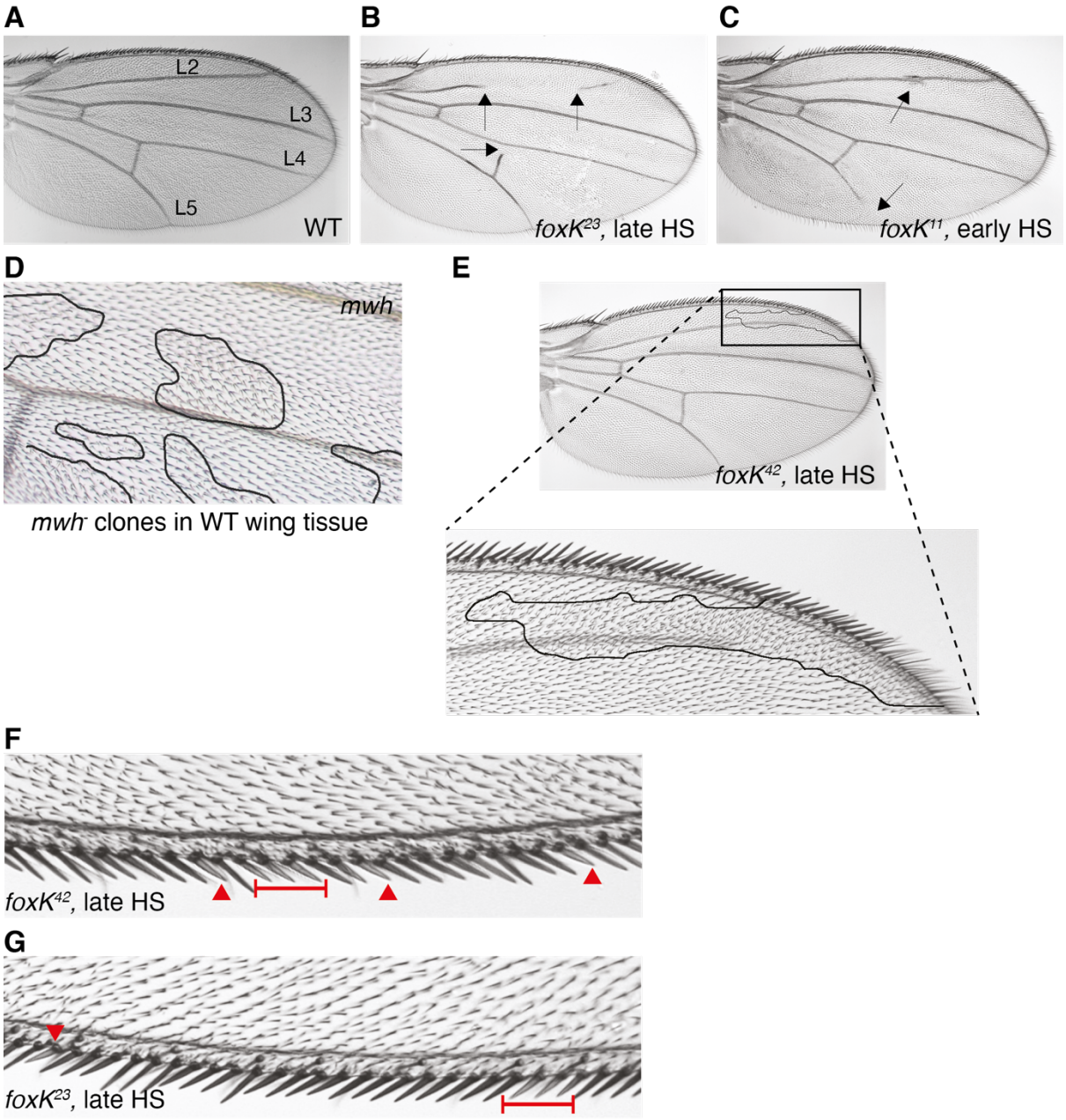

Figure 3.14. *FoxK*^{KO} clones in adult wings lead to vein defects but viable clones are found in the wing margin.

A)-C) Wings of adult flies of A) *white* genotype as control, B) Progeny of *foxK*^{11}*, FRT2A/TM6* x *hsFlp;;FRT2A, GFP.nls* following HS during 2nd instar, and C) Progeny of f*oxK*^{23}*, FRT2A/TM6* x *hsFlp;;FRT2A, GFP.nls* following HS during 3rd instar. Wing vein defects indicated by arrows (black).

D) *Multiple wing hair* clones (black markings) in otherwise wild-type tissue allow identification of twin spots in adult wings.

E) Use of an *mwh*, FRT2A line suggests that loss of vein tissue is indirect through loss of *foxK* clones. Insert shows magnification of a twin spot clone in a wing of progeny of *foxK*^{42}*, FRT2A/TM6* x *hsFlp;;FRT2A, GFP.nls* following HS during 3rd instar.

F) and G) *foxK*^{KO} clones (red arrowheads) are identifiable in the wing margin by a *yellow*$^{-}$ marker in a wild-type background and reach 1-7 bristles in length. Progeny of (F) *foxK*^{23},

FRT2A/TM6 or (G) *foxK*^{42}*, FRT2A/TM6* crossed to *hsFlp;;FRT2A, GFP.nls* following HS during 3rd instar.

3.2.10. Loss of *foxK* partially rescues eye-specific Armadillo overexpression

Having established a requirement for FoxK during wing development, I decided to use a further Wg read-out to analyse FoxK function during *Drosophila* development. An established assay to test for an effect on Wg signalling is the use of a constitutively active Armadillo mutation, *Arm*^{S56F} or F76, driven by an eye-specific promoter (GMR.Gal4, Ray and Lakhotia, 2015) as shown in Freeman and Bienz, 2001.

Overexpression of this construct in the eye leads to a typical rough eye phenotype based on upregulation of apoptosis through high levels of Wg signalling. If combined with loss-of-function mutations in other positively acting Wg components, this phenotype is at least partially suppressed, indicating epistasis, whereas mutations in unrelated genes will result in an unchanged or worsened phenotype.

I thus decided to cross the novel *foxK*^{KO} alleles into the F76 background and assess the effect on eye size in a heterozygous state. For comparison, I selected several loss-of-function alleles from known Wg interactors (*pygo*^{S123}, *ssdp*^{L7} and *chip*^{e55}). Eye area was measured in pixels using ImageJ (yellow markings in Figure 3.15) and statistically analysed via one-way ANOVA using GraphPad Prism. Overall body size of the heterozygous progeny appeared unchanged, but no measurements were undertaken. Eye measurements were done on flies of the same age (2 days post hatching). For simplification, the graph shown in Figure 3.15 includes only data for eyes of female adults; the full data set can be found in the appendix (8.6.). The result is essentially the same for male and female animals.

As expected, heterozygosity of the Pygo mutant allele *pygo*^{S123} essentially rescued the photoreceptor loss of heterozygous F76 to wild-type eye size as originally shown in Thompson et al., 2002. Heterozygosity for either f*oxK*^{KO} allele ameliorated the F76 phenotype substantially (one-way ANOVA, $P<0.0001$). Neither partial loss of Chip nor of SSDP affected eye size to a similar extent, although a significant increase in eye area was measurable in both cases.

These results indicate a function for FoxK downstream of Armadillo and a requirement for FoxK in the eye disc, at least when the Wg pathway is hyperactivated. Recall that clonal induction using a HS-driven FRT element did not result in visible clones in the adult eye. I did not, however, assess clones in the eye disc of late-stage larvae and so it is possible that subtle phenotypes of FoxK loss in the eye were overlooked.

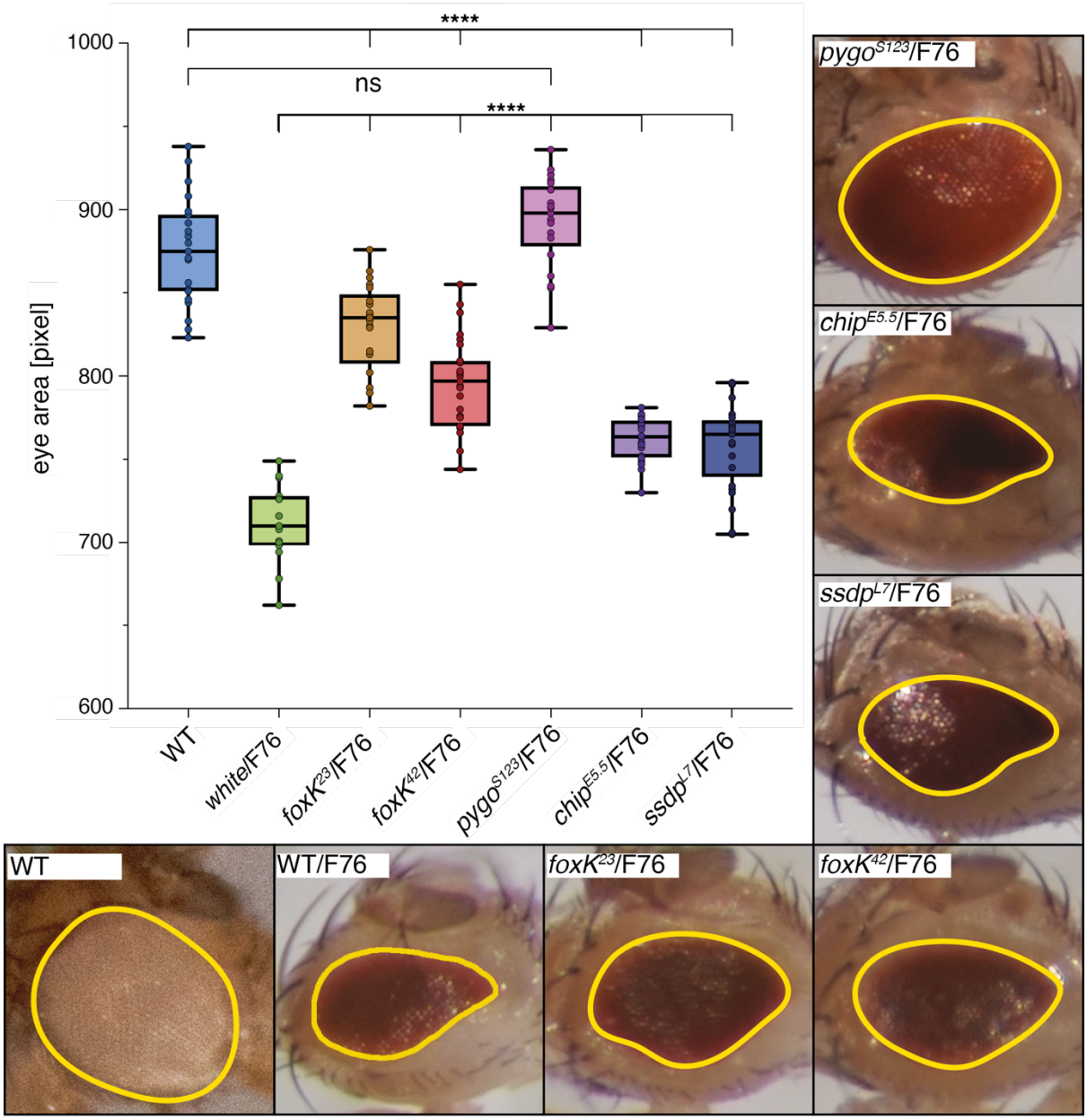

Figure 3.15. Heterozygosity for *foxK^{KO}* substantially ameliorates the rough-eye phenotype of a constitutively active Armadillo mutant.
Flies heterozygous for constitutively active Armadillo (*Arm^{S56E}* or F76, overexpressed using an eye-specific driver (GMR-Gal4)) as well as *foxK^{KO}* alleles (*foxK^{23}* and *foxK^{42}*) or Wg pathway mutants (*pygo^{S123}*, *ssdp^{L7}* and *chip^{e55}*). Area measurements were done in Pixel using ImageJ as shown (yellow marking). Normal distribution and one-way ANOVA analysis including Tukey's multiple comparison tests were done in GraphPad Prism. Heterozygosity of *pygo^{S123}* in a F76 background leads to full suppression of the rough eye phenotype (white vs. *pygo^{S123}*/F76 not statistically significant). Both *foxK* alleles rescue the rough-eye phenotype significantly. *Ssdp^{L7}*/F76 and *chip^{e55}*/F76 are not significantly different from each other. Multiple comparison test showed that all other comparisons are statistically significant by one-way ANOVA. $p < 0.0001$.

3.2.11. *FoxK^{KO}* germ line clones arrest in embryogenesis and show patterning defects

Analysis of *foxK* expression throughout development using my own embryo staining as well as database research indicated a strong maternal contribution of FoxK, which is likely to mask early developmental defects in zygotically homozygous mutant animals. To circumvent this, I generated germ line clones (glc) based on *ovo^{D}*/Flp recombination (Chou et al., 1993) (see 6.19) and assessed cuticle and gut development, as well as general patterning, of embryos null for *FoxK*.

Cuticles of the GFP-negative (GFP^{-}) progeny of a cross between glc-bearing females and *foxK^{KO}/TM6-twi::GFP* males, i.e. *foxK^{null}* embryos, were not fully formed and exhibited extreme malformations and developmental arrest during early embryo development (n = 18, Figure 3.16C & D). GFP^{+} progeny of the same cross, which is expected to express FoxK^{WT} protein from a paternally contributed copy later during embryogenesis, showed no significant difference to *foxK^{null}* mutants and no larvae hatched after >7 days at 25°C (n = 43, Figure 3.16B).

Many of these embryos showed abnormal denticle belts and were shorter than WT embryos, indicating potential loss of segments that ultimately lead to fusion of denticle belts. Despite a large number of glc-bearing females (~200) used for this cross, only very few eggs were recovered and only roughly half of these contained fertilised embryos for analysis.

Despite these strong malformations I decided to assess the midgut development as an additional Wg read-out by staining progeny of a cross between glc-bearing females and *foxK^{KO}/TM6-twi::LacZ* flies with DAB (see 6.15) to distinguish between homozygous mutant and heterozygous, balanced embryos as before (3.6).

Unexpectedly, I was not able to recover progeny that remained unstained (see Figure 3.16Ei & Eiii) and thus was unable to assess *foxK^{null}* mutant embryos in this assay.

Since I find homozygous mutant embryos in the progeny of glc-bearing females crossed to *TM6-GFP*-balanced *foxK*^{KO} flies, this is unlikely to be due to a lack of null embryos. It is possible that this phenomenon was the result of overstaining of unbalanced embryos since only a low number of embryos was available for staining.

The paternally rescued progeny of this cross failed to develop midgut structures, and only very few embryos were found with structures vaguely resembling potential midgut primordia (~5% of β-gal-expressing embryos, see arrowheads in Figure 3.16E).

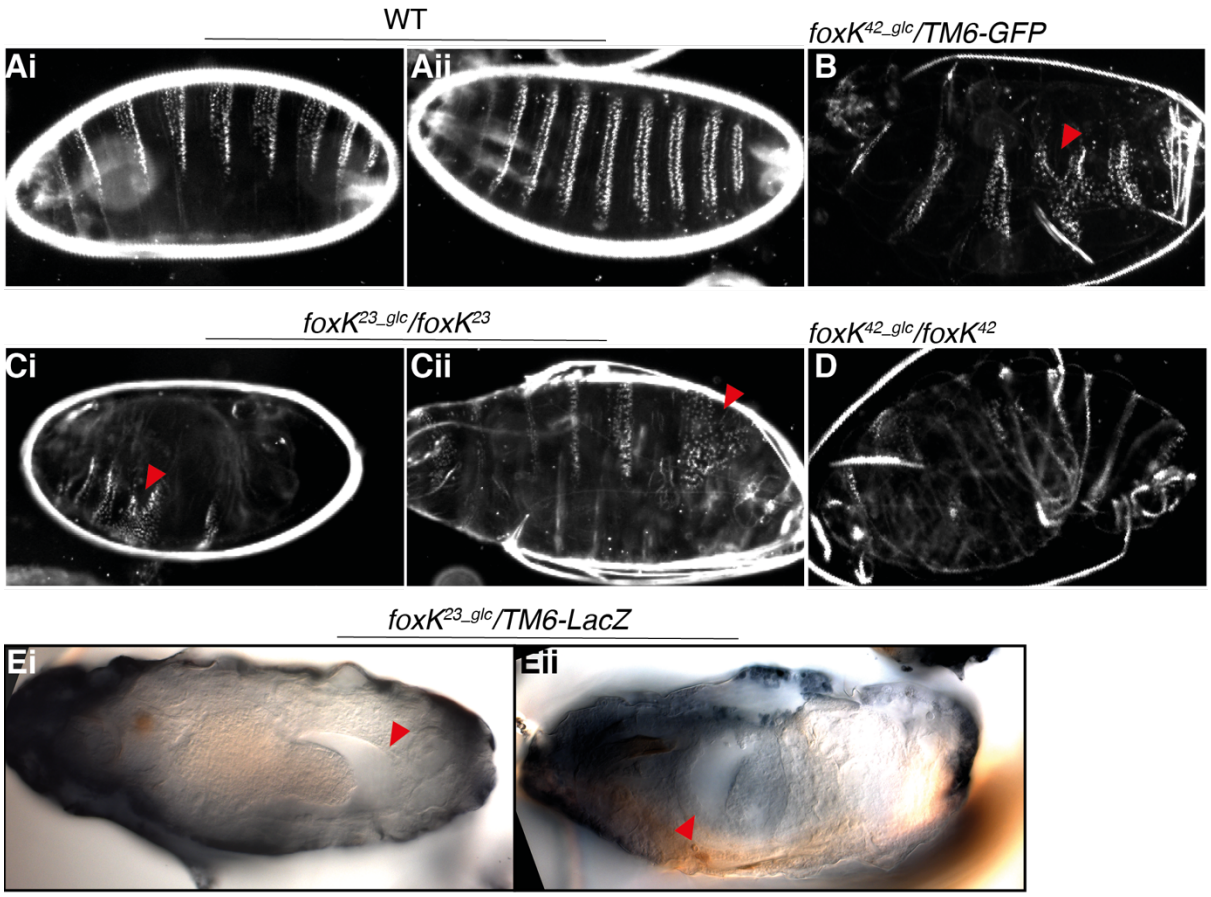

Figure 3.16. Germ line clone-derived embryos show a range of deformations including cuticles with fused denticle belts, and fail to specify midgut structures.
Ai & Aii) Cuticles of WT embryos with denticle belts separated by naked cuticle as described in 1.6.
B) Glc-derived embryos with a paternally contributed *foxK*^{WT} copy (*foxK*$^{42\_glc}$*/TM6-GFP*) show morphological abnormalities and partial fusion of denticle belts (red arrowheads).
C & D) *FoxK* null mutant embryos show deformations, partially fused denticle belt (red arrowheads) and are often shorter than WT embryos. Null embryos of *foxK*^{23} in Ci & Cii), of *foxK*^{42} in D).

E) Glc-derived embryos with a paternal *foxK*^{WT} copy (*foxK*$^{23\_glc}$/*TM6-LacZ*) stained with DAB reveal failure to form a midgut primordium. Red arrowheads indicate structures resembling a midgut cavity.

As these morphological markers proved difficult to analyse, I decided to investigate earlier embryonic developmental steps by analysing expression of patterning genes in glc-derived embryos. To this end, embryos were collected overnight to obtain a range of developmental stages, fixed and stained with different markers for IF-based analysis. WT embryos were used as comparison for staining patterns of different developmental stages (Figure 3.17).

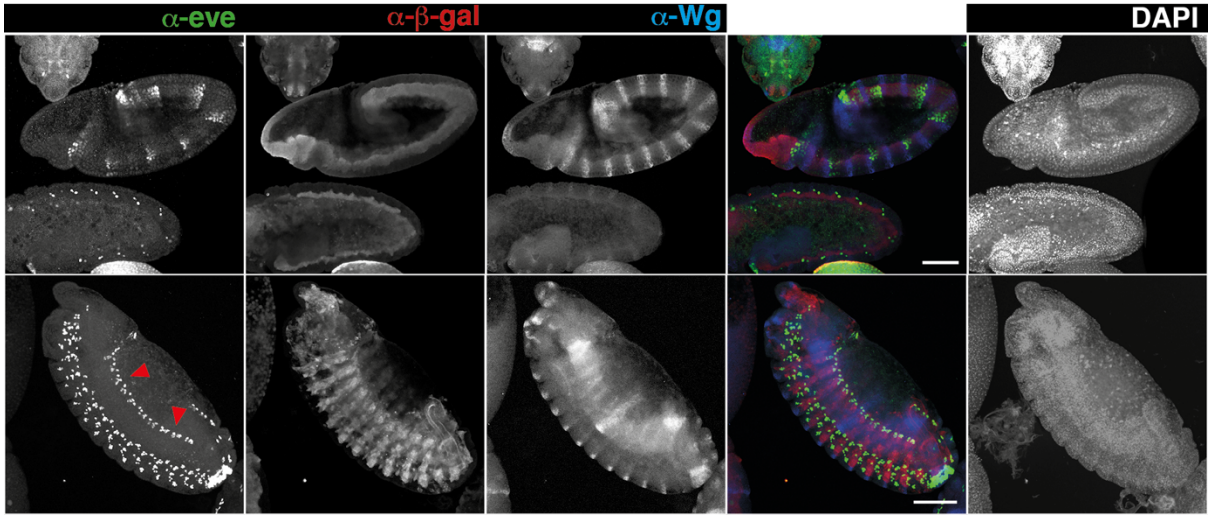

Figure 3.17. Staining pattern of even-skipped, β-gal and Wg in WT embryos.
Embryos stained for embryonic markers as well as for a *twi::LacZ* balancer chromosome during early embryonic development (stage 10-11, upper panel) and later stages of development (stage 13-14, lower panel). *β-gal* expression from the balancer is visible throughout different developmental stages, allowing distinction of null embryos from embryos carrying a paternal *foxK*^{WT} copy. Red arrowheads indicate pericardial expression of *eve*. Scale bar = 100 *μ*m. α-eve (green), α–β-gal (red), α-Wg (blue), DAPI.

Based on *twi::LacZ* expression I was able to distinguish null embryos from embryos with paternally contributed *foxK*. Analysis of glc embryos revealed a striking loss of Wg staining in null embryos, where only occasional traces of Wg protein could be detected (arrowheads in Figure 3.18Ai & Aii).

Note that the pericardial expression of even-skipped (eve) (arrowheads in Figure 3.17) is also lost in *foxK*^{null} embryos. *Eve* expression in these presumptive heart cells requires Wg (Wu et al., 1995) and Dpp (Knirr and Frasch, 2001) signalling and is consequently lost in *wg* or *pygo* mutants (Parker et al., 2002). Expression of *eve* is reinstated to varying degrees in paternally rescued embryos (red arrowheads in Figure 3.18Bi & Bii).

Embryos lacking maternal and paternal contribution of *FoxK* further show a range of morphological deformations as before, often leading to shorter embryos. *Eve* expression in the CNS appears unaffected by loss of *foxK* (as in *pygo* glc (Parker et al., 2002)) and this staining can thus be used as a marker for segmentation. This analysis shows that while some embryos specify embryonic segments largely correctly (e.g. Figure 3.18Aiii), the majority of embryos fail to form the appropriate segments and therefore do not complete gastrulation (Figure 3.18Ai & Aii).

Embryos expressing paternally contributed *foxK* similarly show a range of defects, whereby some appear to segment normally (Figure 3.18Bii & Biii), while others are shorter and deformed. Wg staining is very variable in these embryos, ranging from only traces of staining (Figure 3.18Bi) to almost wild-type arrangement of Wg stripes in Figure 3.18Biii. Generally speaking, the amount and pattern of Wg staining appear to correlate with the overall degree of morphological deformation.

Due to the small number of developing embryos, statistical analysis of the abnormal protein localisation phenotype, as well as meaningful measurements of embryo length, were not possible.

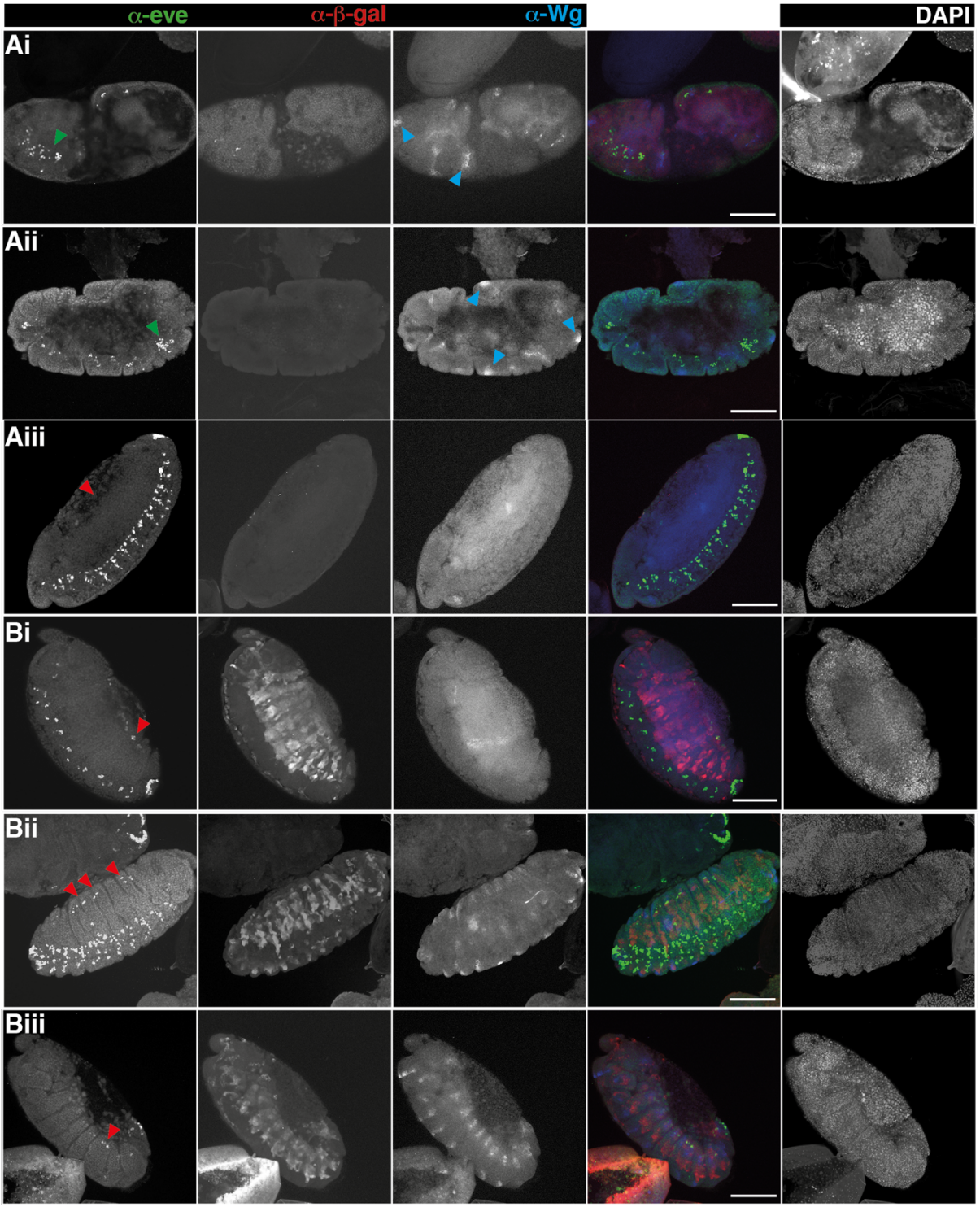

Figure 3.18. Germ line clone-derived embryos of *foxK*^{KO} show morphological deformations and reduced Wg staining.

Ai-Aiii) Embryos derived from glc-bearing mothers without a paternally contributed WT copy of *foxK* (as distinguished by absence of twi::LacZ staining) lack Wg and pericardial Eve staining (red arrowhead in Aiii). These embryos show a range of morphological deformations and often fail to form correct segments. Ai & Aii show strongly deformed embryos that are much shorter than WT embryos, whereas the embryo in Aiii) specifies wild-type-like segments.

Bi-Biii) glc-derived embryos carrying a paternally contributed copy of *foxK*^{WT}, which results in a partial rescue of the null phenotype. While some embryos (Bi) remain strongly deformed and lack Wg staining, others specify the correct number of segments and show partially restored *wg* expression (Bii & Biii). Pericardial Eve staining is partially rescued in these embryos (red arrowheads).
Scale bar = 100 μm. Eve = even-skipped, β-gal = β-galactosidase, Wg = Wingless.

Based on the apparent lack of *wg* expression in several germ line clone embryos and the fact that *wg* expression is maintained in part through a positive feedback loop (see Introduction), I decided to analyse whether the Wnt enhanceosome itself is established in *foxK*^{null} embryos.

Due to practical constraints, i.e. the very low number of glc-derived embryos available for staining, I was only able to obtain preliminary data regarding the expression and subcellular localisation of Pygo. Compared with WT embryos (see Figure 3.11Ai-iii), Pygo staining is unaffected in null embryos (Figure 3.19).

I was further able to show loss of FoxK staining in glc-derived embryos without paternally contributed *foxK*^{WT}, confirming the quality of the newly generated antibody (Figure 3.19, left panel).

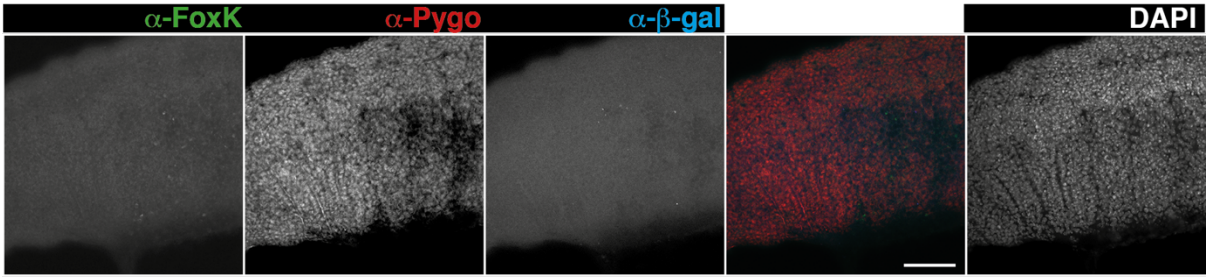

Figure 3.19. *Pygo* expression and nuclear localisation are unaffected in *foxK*^{null} embryos.
foxK^{null} mutants do not show FoxK staining using the antibody generated in this study (see M&M), but Pygo staining is as in WT embryos (cp. Figure 3.12).
Scale bar = 100 μm.

3.3. Discussion

The data described in this chapter underscore the importance of FoxK for *Drosophila* development and indicate roles for this protein in patterning during early embryogenesis as well as for wing blade formation. I further demonstrate a requirement for FOX binding sites in the minimal enhancer of the Wg target gene *Ubx* for expression from a reporter construct during midgut development.

3.3.1. FOX proteins might bind to and regulate Wnt responsive loci

My analysis of a mutant *Ubx* enhancer lacking FKH binding sites suggests a function for FOX proteins in Wg/Wnt signalling (Figure 3.5) but, bearing in mind the high sequence conservation of the FKH domain and the respective consensus sequence, this does not allow me to conclude an involvement of FoxK specifically.

Specificity may arise through differential expression of FOX proteins in different tissues, but previous analysis of expression patterns showed large overlap (see review by Lee and Frasch, 2004). It thus remains unclear if *Ubx* expression in the midgut is regulated by FoxK in particular or other FOX factors, and whether they can act redundantly.

Future analysis is required to narrow down which FOX proteins specifically impinge on Wg/Wnt signalling in different tissues. Generation of ChIP-Seq data in mammalian or insect cells based on differential activation of the Wnt pathway would help elucidate FOXK occupancy at WREs. Specifically, the use of undifferentiated cell lines such as embryonic stem cells or induced pluripotent stem (iPS) (Takahashi et al., 2007) cells will be useful to infer a pioneering role for FOXK factors if a requirement for sequential binding of transcription factors led by FOXK can be confirmed.

Overlap of chromatin binding of FOXK and TCF or PYGO could alternatively be assessed in *Drosophila* polytene salivary gland chromosomes as done previously for Pygo, Groucho and dTCF (de la Roche and Bienz, 2007; Mieszczanek et al., 2008).

If further studies can indeed underscore the hypothesis that FoxK binds to TCF loci, their role as pioneer factors can be analysed using compacted nucleosome arrays. These arrays are assembled *in vitro* using DNA templates and purified histones. DNase I footprinting assays of compacted nucleosomes yield a regular cleavage pattern and this pattern is affected by addition of factors that remodel nucleosomes such as pioneer factors. Similar assays have been used previously by the Zaret lab to highlight FOXA's propensity to bind to compacted chromatin and open it for binding of downstream transcription factors (Cirillo et al., 2002).

3.3.2. Generation of a *foxK* knockout allele

Assessment of the FoxK knockout phenotype in *Drosophila* was complicated by issues with the existing $foxK^{16}$ fly strain, and subsequently delayed by off-target effects during the initial round of CRISPR.

I was able to conclusively show that the $foxK^{16}$ allele available at this time is not a *foxK* null allele (Figure 3.8). This could either be because the original allele was lost over time in storage or because imprecise excision of the *P* element and subsequent errors in genotyping meant the original mutation on chromosome 3 was falsely annotated as a *foxK* mutant.

Arguing against the second scenario, Casas-Tinto et al. used Southern blotting, PCR-based genotyping as well as antibody staining for FoxK (directed against amino acids 414-654 and spanning the FKH domain) antiserum to confirm their mutant alleles. Unfortunately, depletion of their FoxK serum meant that I was not able to try to reproduce their results using their antibody. It is possible that their antiserum was

not suitable to test loss of FoxK if the *P* element disrupted the antigen site but allowed production of a functional FoxK protein. Due to time limitations I did not test the *foxK*^{16} line with my new antibody, but PCR-based genotyping and analysis using deficiency chromosomes conclusively showed that the *foxK*^{16} allele available at this time is not a null allele.

To verify their *foxK* knockout analysis, Casas-Tinto et al. also used RNA interference (RNAi) to generate embryos lacking maternally contributed FoxK protein by driving the RNAi construct in the maternal germ line using *tub-GAL4-VP16*. Because embryos lacking maternal contribution do not develop into later stages of embryogenesis, as confirmed by my own germ line clone-derived knockout mutants, assessment of a midgut phenotype was impossible using an approach relying on maternally expressed RNAi. They thus used an endoderm-specific driver to assess FoxK requirement in later stages of embryogenesis, confirming the reduction in *labial* expression but not the midgut phenotype.

Based on the inconsistencies of the previously published *foxK* allele it was imperative to generate novel *foxK* alleles. For this, I used CRISPR-Cas9 mutagenesis. Although this method is generally thought to have few off target effects in *Drosophila* (Port et al., 2015), I found off-target effects in my first round of experiments aimed at producing *foxK* null alleles. My initial CRISPR experiment led to the generation of at least two different off-target lethalities with just one sgRNA (sgRNA2; the other N-terminal sgRNAs 1 & 3 did not yield editing). As my initial approach included pre-screening of edited lines for embryonic lethality, I have likely increased the detection of such off-target events (Simon Bullock, personal communication). An unbiased approach based on sequencing of random progeny proved more successful during my second round of CRISPR-mediated knockout of f*oxK*.

My initial round of mutagenesis also highlighted the risk of alternative (often non-annotated) start sites that might lead to functional protein despite successful editing

detected in sequencing assays. Such issues can be circumvented by designing sgRNAs to target further downstream, an approach I used in my second round of screening, or by using two sgRNAs binding roughly 500 bp apart in tandem to create a larger deletion through induction of DNA double strand breaks at both binding sites.

3.3.3. FoxK requirement for wing blade development

My work on the novel *foxK*^{KO} alleles indicates a requirement for FoxK specifically during the development of the wing blade in *Drosophila* (Figure 3.10, Figure 3.13, Figure 3.14). As described above, wing blade development is highly regulated by the Wg pathway, but also by Notch and Dpp signalling.

Moreover, the vein defects seen in adult flies post induction of recombination might indicate an interplay with EGFR signalling. Analysis of different pathways is complicated because clonal induction at an early stage during disc development likely leads to loss of *foxK*^{KO} clones by extrusion from the blade. This extrusion is known to occur for mutant clones that stop proliferating such as *Frizzled* clones (Chen and Struhl, 1999). It will be interesting to confirm loss of *foxK*^{KO} clones using apoptotic markers such as Caspase-3 staining.

Additionally, as I am able to recover small clones localised to the blade following induction in later stages of development, there might be a temporal requirement for FoxK restricted to early wing patterning genes. Use of a Minute marker (Lawrence et al., 1986) recombined into the *foxK*^{KO}*/FRT2A* line should allow generation of larger clones that grow faster than surrounding heterozygous tissues and twin spots. Temporal control of induction of recombination might reveal whether *foxK* null clones are able to grow during late development or whether they become apoptotic as equivalent clones do in younger tissues.

Alternatively, overexpression of FoxK (*foxK*^{OE}) in parts of the wing disc (i.e. by driving a *FoxK*^{OE} construct using a *patched-GAL4* driver or induction of *FoxK*^{OE} clones across the disc) can be used to assess the response of expression of *wg* itself or its target genes to high levels of FoxK.

As mentioned above, *wg* is initially expressed across the whole wing disc during the 1st and 2nd instar before becoming largely restricted to the dorso-ventral boundary. In zygotically homozygous mutants this stripe of Wg across the wing blade is lost (Figure 3.10C), but it remains to be determined whether *wg* expression is wild-type in earlier stages of disc development.

Wg target genes can be placed into two classes, whereby the first class is induced by early *wg* expression and the second class is expressed at different thresholds within the blade tissue of 3rd instar discs. While *senseless* and *distalless* are commonly used to assess Wg pathway mutants during later stages, early targets are interesting candidates for FoxK-mediated regulation.

The earliest known Wg target in the wing disc is *zfh-2*, which is initially expressed across the wing primordium and later becomes restricted to the proximal wing blade by Vestigial (Whitworth and Russell, 2003), which in turn is regulated by Wg and Notch. Dissection of 2nd instar wing discs bearing *foxK*^{KO} clones or analysis of zygotically homozygous mutant discs for expression of *zfh-2* and other Wg target genes will be insightful.

Preliminary observations of the Wg target gene *dMyc* suggest it is expressed in zygotically homozygous mutant wing discs (Figure 3.10C), although future experiments are required to confirm that *dMyc* expression follows its dynamic wild-type patterning in these discs. As dMyc is a growth regulator and substantially involved in determining size and proportion of the *Drosophila* wing (Wu and

Johnston, 2010), any changes in its expression level could result in lack of proliferation and hence account for deformations of the blade region of the disc.

My evidence largely indicates a specific requirement for FoxK during wing blade development as indicated by lack of phenotypes in legs or eyes of animals post-HS (see 3.2.9). However, my experiments using heterozygosity of *foxK*^{KO} alleles with eye-driven overactivated Armadillo argue that FoxK acts downstream of Arm in this tissue. Therefore, clonal induction in eyes should be revisited by assessing growth of mutant clones and expression of Wg target genes in *foxK*^{KO} tissue.

3.3.4. FoxK germ line clones

The strong morphological phenotype and early developmental arrest of f*oxK*^{null} embryos confirm an important role of FoxK during development. Thus, there is not full redundancy of FOX family members at these stages.

The most striking result of this analysis was the severe disruption of *wg* expression to varying degrees in glc embryos. This is strongly reminiscent of *pygo* null mutants that were also shown to lack Wg expression during embryogenesis (Parker et al., 2002). A similar phenotype has been described for *ssdp* null mutants (Fiedler et al., 2015) and loss of ChiLS results in a denticle lawn due to loss of Wg signalling.

Recall that *wg* expression is restricted by the pair rule genes *even-skipped* (*eve*) and *fushi tarazu* (*ftz*) during early patterning in the embryo (Ingham et al., 1988; Manoukian and Krause, 1992) and its expression is maintained by a positive feedback loop along with other mechanisms. Analysis of upstream genes that control *wg* expression such as *odd-paired* will be pivotal in determining whether this requirement for FoxK is direct or secondary due to loss of pair rule genes.

Rescue of *wg* expression to near-wild-type levels in some glc-derived embryos carrying a WT *foxK* copy through their paternal genome can be explained by the onset of zygotic gene expression from cycle 8 onwards (Pritchard and Schubiger, 1996). It would be interesting to test *wg* RNA levels in null embryos by FISH or similar methods to determine whether transcription or protein stability are affected by loss of *foxK*.

Additionally, loss of maternal and zygotic *foxK* results in loss of pericardial *eve* expression, which is also seen in *pygo* glc embryos (Parker et al., 2002). Eve expression is similarly disrupted in embryos null mutant for *ssdp* or *chip*. The apparent specificity of FoxK requirement for *eve* expression in only these cells is interesting because mesodermal *eve* expression in heart progenitor cells is regulated by Wg and Dpp (Knirr and Frasch, 2001), whereas *eve* expression in the CNS is not under control by Wg. This combinatorial regulation of *eve* by Wg and Dpp in pericardial cells parallels the regulation of *labial* expression in the midgut endoderm (Yu et al., 1996). The expression of *labial* has previously been shown to be affected in *foxK* loss-of-function experiments (see Figure 3.2C).

FoxK might function to combine signals from Wg and Dpp (or other pathways) or to relay signals from only one pathway. Note that while many Wg signals are commonly mediated through sloppy-paired (e.g. during the mesodermal restriction of *bagpipe,* (Lee and Frasch, 2000)), *eve* expression has been shown to be independent of slp function (Lee and Frasch, 2000). These observations suggest an intriguing mechanism by which FoxK rather than slp may mediate Wg signalling in specific tissues (i.e. control via one FOX protein is exchanged for another). However, observations by Knirr and Frasch (2001) revealed that mutation of the FKH binding site in the *eve* promoter did not abrogate expression from a minimal reporter. Of note, FoxK has been noted as expressed in heart tissues in a genome-wide DNA binding screen for cardiac transcription factors in *Drosophila* (Busser et al., 2015).

Embryos with a paternal *foxK* copy rescue *wg* expression partially and while this appears concomitant with a partial rescue of *eve* expression in the pericardial cells, the extent of rescued expression appears lower for *eve* than *wg* (Figure 3.18Biii).

Due to the small number of embryos recovered from glc-bearing mothers I was unable to confirm the disruption of Engrailed and Labial staining upon loss of FoxK as demonstrated by Casas-Tinto et al. (cp. Figure 3.2D). *Engrailed* expression is partially reliant on continued *wg* expression and is initiated but not maintained in *wg* mutants (Bejsovec and Arias, 1991). Loss of Engrailed stripes during later development stages would therefore emphasise a role of FoxK in mediating Wg signals.

Future experiments should also assess expression from the minimal *Ubx* enhancer (*UbxB*) in null embryos of *foxK*, which can be crossed into the background of the *foxK* mutant line.

I did not detect a loss or subcellular redistribution of Pygo which implies that its nuclear localisation is unaffected by loss of FoxK, although this does not confirm whether Pygo binds to WRE in the absence of FoxK. It is imperative to examine the DNA binding of TCF/Pangolin itself to address whether loss of FoxK results in failure of TCF to bind to the Wnt enhanceosome or in failure to establish the Wnt enhanceosome itself at the correct WREs as would be expected if FoxK acts as a priming factor during early development.

In summary, my work on *Drosophila* FoxK has uncovered an interesting link to Wg signalling during embryogenesis, as well as during the development of the eye and wing primordia. Future studies are required to determine whether FoxK directly controls expression of *wg* itself or of Wg target genes and if this requirement is restricted temporally during development. Specifically, several strands of

investigation indicate a potential crosstalk between the Wg and Dpp signalling pathways and future experiments should address whether *foxK* expression is required for either pathway or whether FoxK combines input from both to regulate expression of common target genes of Wg and Dpp.

4. Interaction between FOXK and Dishevelled

4.1. Introduction

As described above, we found human FOXK1/2 associated with Dishevelled in a PDZ-dependent manner in BioID studies of mammalian cells (Melissa Gammons, unpublished results). Taken together with evidence of a direct interaction between FOXK1/2 and DVL published by Wang et al. (2015), which I summarised in section 3.1.4, we aimed to further investigate the DVL/FOXK interaction in mammalian cells and *Drosophila* using IF and reporter assays *in vivo*.

The following sections will introduce DVL function and the current state of research concerning this crucial signalosome protein.

4.1.1. Role of Dishevelled in Wnt/Wg signalling

DVL plays a pivotal role during both canonical and non-canonical Wnt signalling and its function has been extensively studied. Particularly relevant to its role is its propensity to form polymers. These structures result in the formation of signalosome complexes upon Wnt ligand binding, which are often visible as punctate condensates both in endogenous settings (Schwarz-Romond et al., 2007a; Yanagawa et al., 1995) and after overexpression (Axelrod et al., 1998).

Polymerisation-dependent signalling has been described previously (e.g. through SAM domains (Kim et al., 2001)) and in Wnt signalling is mediated mainly through the DIX domain (Schwarz-Romond et al., 2007b), which is exclusive to the Wnt pathway and is found in the key components DVL and Axin as well as CCD1 (Coiled-Coil protein DIX1), a regulator of DVL polymers (Liu et al., 2011).

Like many signalling proteins, DVL consists of several structured domains connected by largely unstructured regions. In the case of DVL, the structured regions are the DIX, PDZ and DEP domains (Figure 4.1). During Wnt signalling, the N-terminal DIX domain forms protein assemblies through head-to-tail polymerisation (Schwarz-Romond et al., 2005).

More recently, the Bienz lab has shown that the DEP domain plays a previously underappreciated role in this process by dimerising through domain swapping, which triggers subsequent DIX polymerisation during signalosome formation (Gammons et al., 2016b). DEP domain swapping occurs subsequent to DEP binding to the Frizzled receptor (Tauriello et al., 2012) and thus provides the immediate switch to signalosome formation and active signalling upon Wnt binding.

The high local concentrations of DVL result in increased avidity for its binding partner Axin, which is recruited by its own DIX domain (Axin-DIX, also known as DAX) to form heteropolymers with DVL-DIX (Schwarz-Romond et al., 2007a). Crucially, this "head-to-tail" DIX polymerisation overcomes the low cellular concentration of interactors as well as their low affinity to each other resulting in a rapid response. Due to the dynamic nature of the polymerisation process this switch is reversible to prevent hyperactivation of the pathway (Bienz, 2014). This sequence of events ultimately inactivates the degradasome complex, leaving β-catenin free to translocate to the nucleus as described (1.3).

Lastly, the DVL-PDZ domain offers an interaction platform for proteins such as Naked, which was recently found to be required for sustained Wnt signalling by facilitating Axin2 degradation after onset of signalling (Melissa Gammons, Miha Renko, Bienz Lab, unpublished results). The PDZ domain is also thought to interact with components of the planar cell polarity (PCP) pathway and was shown to mediate interaction with the negative Wnt regulator Dapper (Cheyette et al., 2002) (see below).

DVL is not only crucial for Wnt-activated signalling in healthy tissues, but is also involved in cancer development and has been found to be highly expressed in colorectal cancer tissues (Metcalfe et al., 2010). High levels of DVL can enhance Wnt signalling by freeing up more β-catenin through signalosome formation and Axin sequestration independent of Wnt ligand binding.

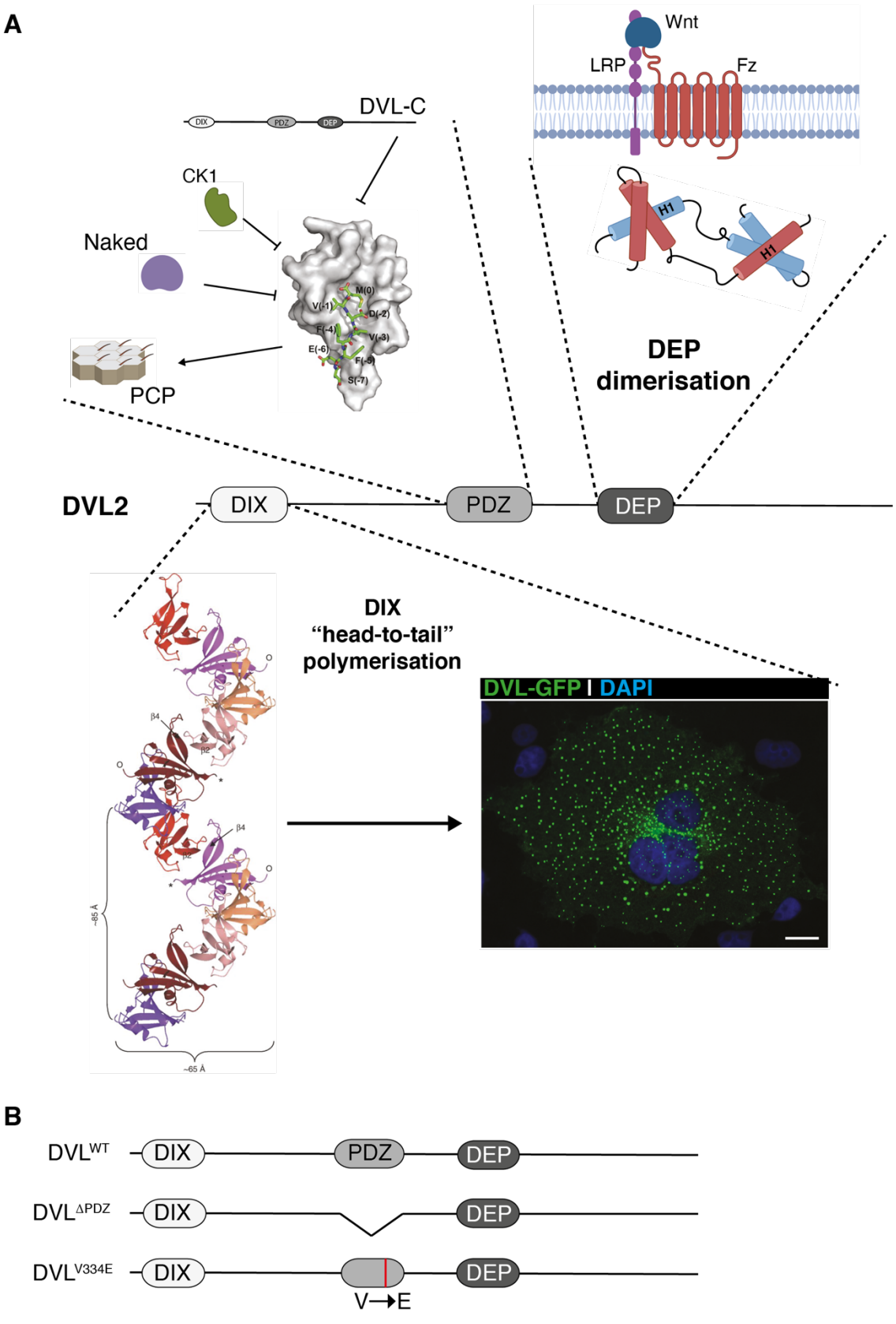

Figure 4.1. Dishevelled facilitates signalosome formation through domain swapping of its DEP and polymerisation of its DIX domain.

A) “Head-to-tail” polymerisation of DIX leads to the formation of oligomers that function as signalling platforms and are visible as puncta in cells. The PDZ domain is thought to interact with components of the planar cell polarity (PCP) pathway and negative Wnt regulators including Dapper, Naked and the DVL-C-terminus itself. DEP mediates the interaction with Wnt receptor Frizzled and forms dimers through domain swapping, which precedes the formation of DIX-mediated polymers.
DIX assembly from Schwarz-Romond et al. (2007b); PDZ structure with ligand from Lee et al. (2015), DEP dimerisation based on Gammons et al. (2016b). PCP cartoon in A) taken from Maung and Jenny (2011).
Scale bar = 20 μm. α-DVL-GFP (green), DAPI (blue).
B) DVL WT and PDZ mutants used in this work: $DVL^{\Delta PDZ}$ lacking the full PDZ domain and DVL^{V334E} with a single amino acid substitution (V→E) in the PDZ cleft at residue 334, which was shown to abolish cleft binding.

4.1.2. Nuclear functions for Dishevelled

While DVL is mostly known for its cytoplasmic functions, evidence for a nuclear role of this protein has been reported by several groups.

Itoh et al. (2005) identified an unusual NLS sequence carboxy-terminal to the PDZ domain containing an IVLT motif which was required for nuclear translocation. Nuclear translocation was found to be essential for full activation of Wnt targets as studied by luciferase reporter analysis and axis duplication assays in *Xenopus*. The authors suggested a stabilising role whereby DVL affects β-catenin stability by interacting with proteins known to sequester β-catenin in the nucleus, such as APC; however, they provide no insight into the underlying molecular mechanism.

Gan et al. (2008) reported a surprising requirement for DVL in SW480 cells. This cell line is derived from a colorectal cancer patient and carries an inactivating mutation in APC resulting in constitutive nuclear translocation of β-catenin which should bypass the need for signalosome formation and therefore DVL. The same authors found DVL associated with Wnt target loci such as the *c-myc* promoter to which it was shown to be recruited in a Wnt-dependent manner. This led Gan et al. to conclude that nuclear DVL might function to stabilise TCF-β-catenin complexes.

Other labs have identified an interaction between Wnt signalling and the Hippo pathway where the Hippo effectors TAZ (Varelas et al., 2010) and YAP (Barry et al., 2013) inhibit DVL phosphorylation and DVL nuclear translocation, respectively. The latter study by the Camargo lab describes nuclear DVL in intestinal crypt cells which is controlled by YAP; this interaction was shown to be crucial during cancer development. The evidence by Wang et al. corroborates these findings based on overexpression studies and IF analysis coupled with luciferase reporter assays (see 3.1.4.).

Contrary to these publications many labs, including the Bienz lab, have not been able to reproduce robust nuclear DVL localisation and thus these findings have been a matter of controversy in the field that is yet to be resolved. For instance, a study by Schwarz-Romond et al. (2007a) failed to reproduce the nuclear DVL staining using the same antiserum and conditions described in Itoh et al.

Other groups identified a likely localisation of DVL overexpression puncta near the nucleus at the microtubule organising centre (MTOC) (Smalley et al., 2005) or associated with the nuclear envelope (Gammons et al., 2016a) but were unable to show DVL inside the nucleus. Despite extensive efforts to uncover the mechanistic details through which DVL might function in the nucleus, studies to this date fail to conclusively prove this nuclear role.

4.1.3. Binding properties of DVL-PDZ

As detailed in Chapter 3, Wang et al. mapped the interaction between FOXK and DVL to the FOXK FHA-spanning region and the DVL-PDZ domain as well as an upstream motif (IVLT), which has previously been described as required for nuclear translocation of DVL (Itoh et al., 2005) (see above).

It is somewhat unusual for PDZ domains to bind to internal sequences as the evidence for binding to the FHA domain would suggest, since many PDZ domains studied to date tend to bind to C-terminal motifs (Tonikian et al., 2008). However, Zhang et al. (2009) have described the DVL-PDZ domain as particularly flexible, possibly allowing binding of internal peptide sequences.

This property of DVL-PDZ has been demonstrated *in vitro* for its interaction with Frizzled (Wong et al., 2003), but the physiological relevance of this interaction is unclear: the PDZ domain was found to be dispensable for β-catenin stabilisation and NMR experiments were unable to confirm PDZ binding to Frizzled (Gammons et al., 2016a).

Thus far, the only verified DVL-PDZ binding partners include C-terminal motifs such as in Dapper (Cheyette et al., 2002) and the DVL-C-terminus itself (Lee et al., 2015), both of which are negative regulators.

4.2. Results

I was intrigued by the results presented in Wang et al. (2015), who describe a FOXK1/2-dependent recruitment of DVL into the nucleus which they show is required for full activation of Wnt target gene transcription (summarised in Figure 3.3). I decided to reproduce their results, mainly by focusing on the immunofluorescence and TCF reporter assays. Additionally, I assessed a potential C-terminal PDZ binding motif in *Drosophila* FoxK, which was identified by Melissa Gammons.

Some of the experiments presented in this chapter were carried out in collaboration with Melissa Gammons, as indicated below.

4.2.1. A *Drosophila* FoxK$^{\Delta C\text{-}Term}$ truncation does not have a mutant phenotype

Since it remains controversial whether DVL-PDZ binds to internal sequences *in vivo* and therefore is likely to bind FOXK through the FHA domain, Melissa Gammons decided to search for additional PDZ binding motifs in different FOX factors. She identified a putative PDZ binding motif in the C-terminus of *Drosophila* FoxK, which she analysed via NMR spectroscopy (with Trevor Rutherford, MRC LMB). Spectral changes in NMR assays with bacterially expressed FoxK$^{C\text{-}term}$ and DVL-PDZ peptides indicated interaction between the two peptides (unpublished results) and I thus decided to generate a C-terminal FoxK truncation to delete this putative interaction site in *Drosophila* and assess its consequence on development.

To this end, Cas9-expressing fly embryos were injected with an sgRNA-expressing plasmid targeting ~20 nucleotides upstream of the putative binding site, and a repair template to introduce several STOP codons in place of the 8 amino acids of the C-terminal binding site (Figure 4.2).

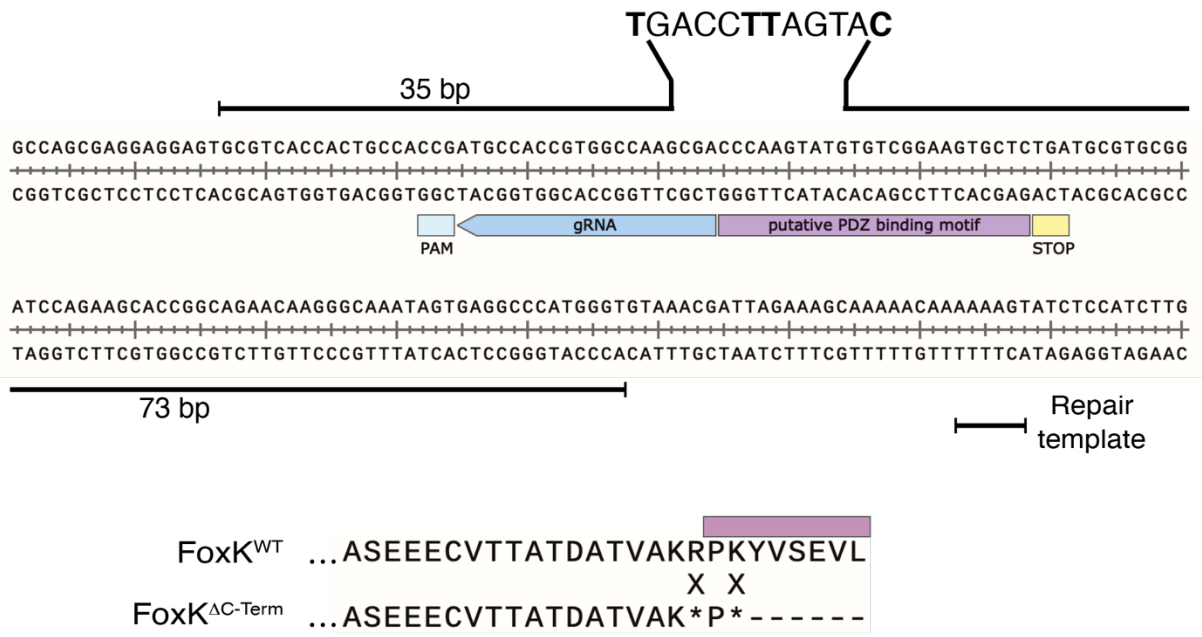

Figure 4.2. CRISPR-mediated truncation of FoxK to eliminate the putative PDZ binding motif.
An sgRNA (blue) was designed to guide Cas9 to a PAM site (light blue) just downstream of the putative PDZ binding motif (purple). A repair template carrying point mutations was used to generate STOP codons at the beginning of the motif leading to the C-terminal truncation as shown below, leaving the remainder of the protein intact.

Homozygous flies carrying this truncation did not have any mutant phenotype nor were they developmentally delayed in any way. Hence, if there is indeed binding between FoxK and the fly ortholog of DVL, Dsh, through the C-terminus of FoxK, it does not appear to impact on the function of either protein in a way that would visibly affect development. Due to the lack of a phenotype, this mutant was not analysed further, and I decided to focus on validating the DVL-FOXK1/2 interaction in mammalian cells.

4.2.2. FOXK1/2 localise to the nucleus of mammalian cells

To this end, I attempted to replicate the findings reported by Wang et al. I was particularly intrigued by their conclusion that DVL is transported into the nucleus through FOXK1/2, as our lab has not been able to find conclusive evidence for

nuclear DVL. Recall that Wang et al. used overexpression of DVL and FOXK1/2 as well as other FOX factors to show that FOXK1/2 specifically facilitate nuclear translocation of DVL (Figure 3.3B). I aimed to validate these results by assaying subcellular localisation of DVL and FOXK1/2 both in endogenous settings as well as following overexpression of either protein.

In the first instance, I decided to verify nuclear localisation of both FOXK1/2 under endogenous as well as overexpression conditions in different cell types (HEK293T, Cos-7 and HeLa cells) using specific antibodies for both proteins. The objective for this experiment was to clarify whether overexpression of FOXK1/2 or activation of Wnt signalling affects localisation of either paralogue as well as to ensure that overexpression does not cause high levels of cell toxicity.

IF experiments with FOXK1/2 showed a strictly nuclear localisation for endogenous FOXK1, and a mostly nuclear staining of endogenous FOXK2 with some diffuse cytoplasmic localisation. Representative images for these analyses are shown for HEK293T cells in Figure 4.3; no difference was seen for different cell types.

Next, I asked whether activation of Wnt signalling affects the expression pattern of either human FOXK1/2 protein by supplying the cells with WCM or LiCl-added medium for 6 or 4 hrs before fixation, respectively. In this case, it is crucial to test both WCM and LiCl, as the latter inactivates the degradasome and bypasses DVL requirement which may result in underestimation of potential DVL-mediated effects that require induction of polymerisation by Wnt ligand binding. I found that neither LiCl nor WCM affect the localisation of either FOXK1 (Figure 4.3B & C) or FOXK2 (not shown).

Additionally, I used this assay to confirm that both overexpression constructs of FOXK1/2 (kindly provided by the Sharrocks lab, University of Manchester) show the same subcellular localisation of endogenous protein. Lack of apoptotic cells in IF

assays as judged by cell morphology and DAPI staining indicated that cell viability was not affected following transfection of 200 ng of FOXK1/2 plasmid.

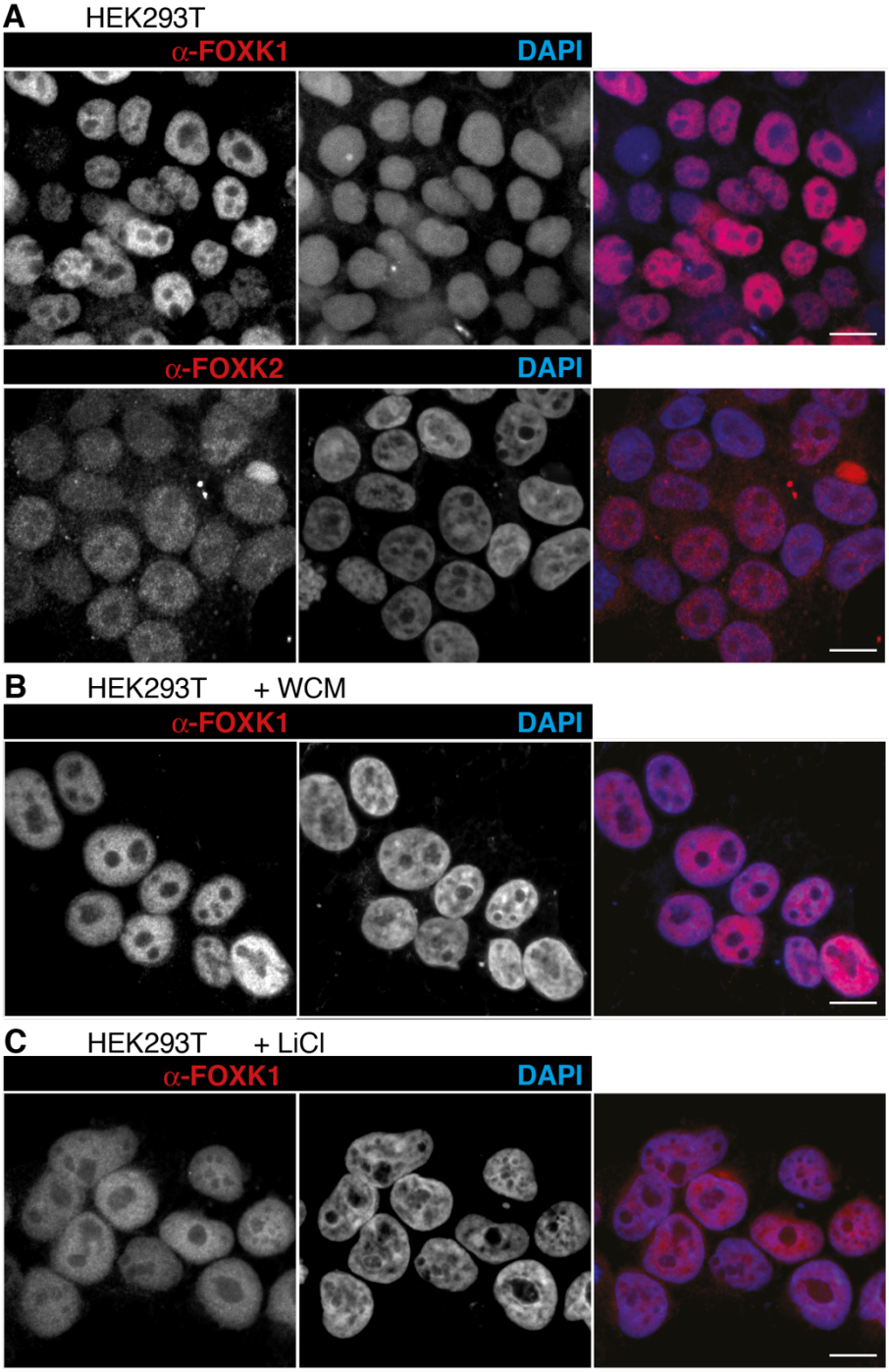

Figure 4.3. Localisation of endogenous FOXK1 and FOXK2 under different conditions.
A) Both FOXK1 and FOXK2 are localised largely to the nucleus under endogenous conditions in HEK293T cells.
B) & C) Induction of Wnt signalling either at the level of the signalosome (+ WCM, B) or by blocking the degradasome (+ LiCl, C) does not change FOXK1/2 nuclear localisation.
Scale bar = 10 μm. α-FOXK1/2 (red), DAPI (blue).

I also set out to determine whether loss of all three DVL proteins (DVL1, DVL2 and DVL3) affects FOXK1/2 localisation, which would imply a functional connection between the proteins. To this end, I used a DVL triple knockout cell line (DVL-TKO, $\Delta DVL^{1/2/3}$) established by Melissa Gammons in a HEK293T background (Gammons et al., 2016a) and assessed localisation of both endogenous (not shown) and overexpressed, FLAG-tagged FOXK1/2 (Figure 4.4) in control medium (CM) as well as under activation of Wnt signalling. FOXK1/2 localisation was found to be unaffected by loss of DVL under either condition.

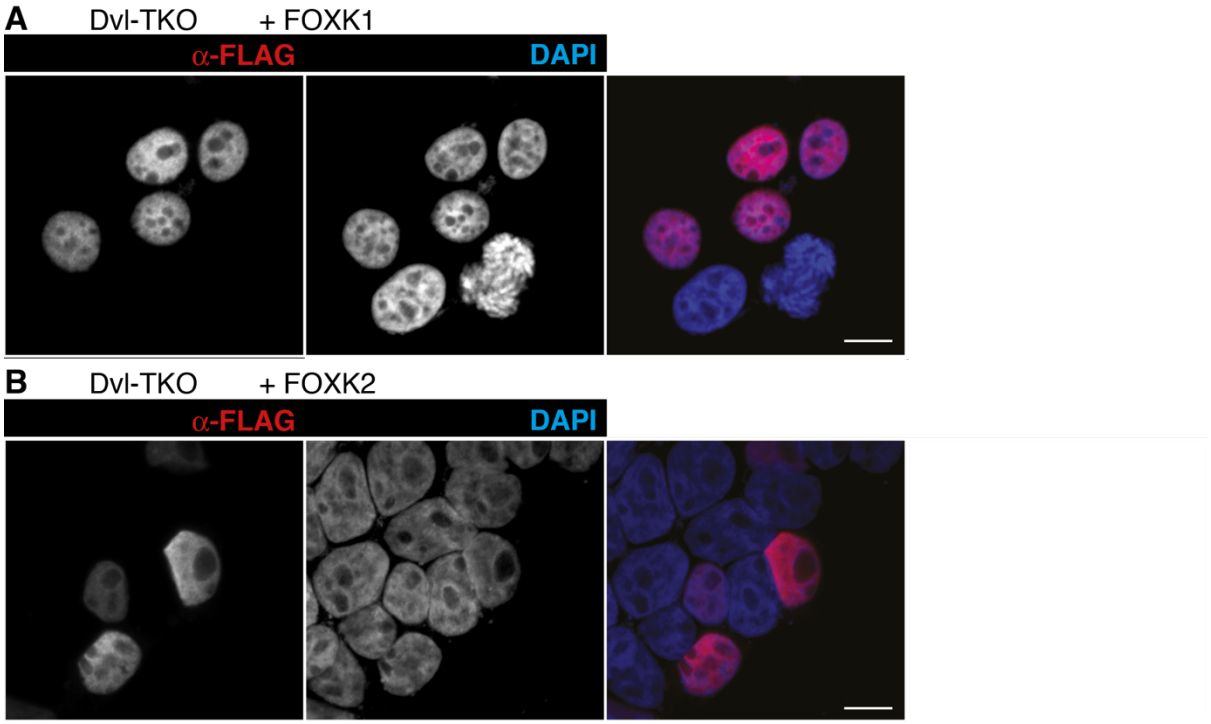

Figure 4.4. Loss of all three DVL paralogues does not affect localisation of FOXK1/2.
DVL-TKO cells were transfected with FOXK1 (A) or FOXK2 (B) and localisation analysed by IF. Nuclear localisation of FOXK1/2 is unaffected by loss of DVL1/2/3. Scale bar = 10 μm. α-FLAG (red), DAPI (blue).

From these experiments I concluded that FOXK1/2 are nuclear proteins that do not require endogenous DVL for correct subcellular localisation. I next asked whether

FOXK1/2 localisation would be affected by overexpression of DVL, or vice versa, as shown in Wang et al. (2015).

4.2.3. Co-overexpression of hDVL2 and FOXK1/2 does not result in co-localisation of both proteins

DVL-overexpressing cells form typical punctate DVL assemblies in the cytosol (Schwarz-Romond et al., 2005) and this has been used in the past to assess recruitment of DVL interactors into DVL puncta (Schwarz-Romond et al., 2007a). Wang et al. show a nuclear translocation of DVL upon overexpression of FOXK but do not find FOXK1/2 in DVL puncta, which appear completely dissolved following FOXK1/2 overexpression (Figure 3.3B, left panel). Given the controversy in the field on whether or not DVL can translocate into the nucleus to regulate Wnt target gene expression, I decided to replicate the assay used by Wang et al.

In collaboration with Melissa Gammons, we adjusted the DVL puncta assay to assess FOXK1/2 recruitment under overexpression of GFP-tagged constructs based on WT-DVL and a DVL-PDZ mutant (Figure 4.1B), both of which form punctate structures as their DIX domain is intact. Experiments were done in three different cell types (HEK293T, HeLa and Cos-7) to exclude cell type-specific effects, and with or without activation of Wnt signalling (i.e. in CM, WCM and LiCl) as well as in biological duplicates. I used a primary α-GFP antibody for staining of DVL-GFP protein rather than imaging endogenous GFP fluorescence in order to amplify signal strength.

Stimulation of Wnt signalling did not affect localisation of either protein under any condition or in any of the cell types and representative images are therefore shown (Figure 4.5).

Overexpression of DVL^{WT} or $DVL^{\Delta PDZ}$ in HEK293T cells did not change the localisation of endogenous or overexpressed FOXK1/2, which remained largely nuclear and did

not co-localise with DVL puncta (Figure 4.5A & B). While I obtained structures resembling punctate assemblies in a small number of cells overexpressing either FOXK paralogue (Figure 4.5C, 1-2% of total cells analysed, n > 1000), these FOXK1/2 "puncta" did not overlap with DVL puncta. Given their rarity, it is conceivable that these dots do not represent physiological protein condensation but are an artefact of fixation or staining. I also did not observe robust nuclear DVL-GFP using this assay (see below).

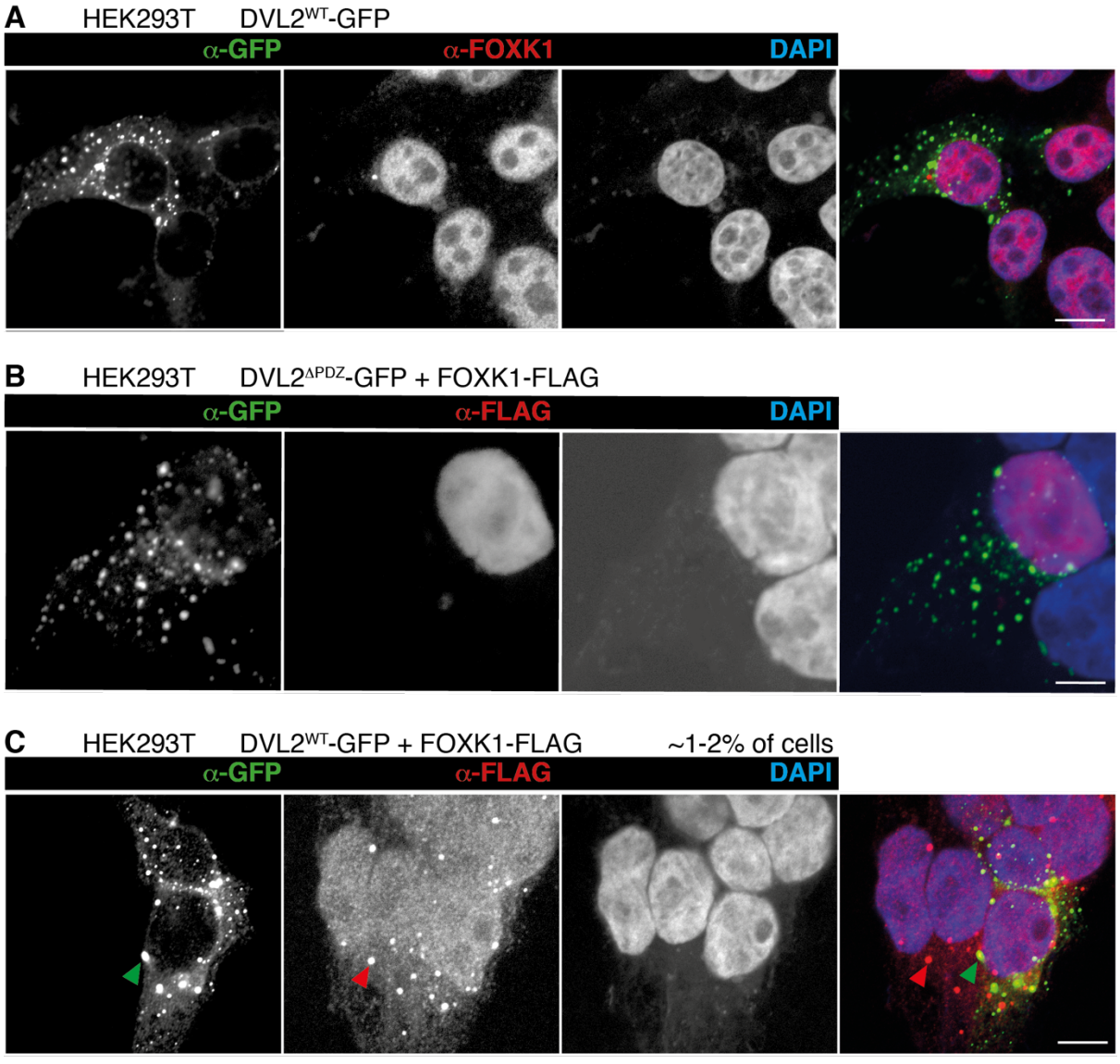

Figure 4.5. DVL^{WT} or DVL$^{\Delta PDZ}$ and FOXK1/2 do not co-localise in HEK293T cells under endogenous or overexpression conditions.
A) Overexpression of DVL^{WT} results in formation of characteristic puncta without any nuclear staining and does not affect nuclear localisation of endogenously expressed FOXK1.

B) A PDZ mutant of DVL ($DVL^{\Delta PDZ}$) forms cytoplasmic puncta without staining in the nucleus and does not alter nuclear localisation of overexpressed FOXK1-FLAG.
C) A small number of cells overexpressing FOXK1/2 show punctate structures (red arrowhead) resembling overexpression condensates of DVL (green arrowhead), but the two punctate pools do not overlap.
Scale bar = 10 μm. α-GFP (green), α-FOXK1/2 or α-FLAG (red), DAPI (blue).

In addition to HEK293T cells, Cos-7 were chosen as their cell shape, with high cytoplasmic content, allowed easy distinction of DVL puncta. As before, overexpression of DVL^{WT} or $DVL^{\Delta PDZ}$ resulted in cytoplasmic puncta without nuclear staining, while FOXK1/2 remained nuclear in >95% of cells analysed (n > 1000, Figure 4.6A).

Unexpectedly, very large aggregates were visible in a small number of cells (~2-3% of cells analysed) that emit a fluorescence signal in all channels, including in the red (Alexa-546, FOXK) and blue channels (DAPI, Figure 4.6B). Given that these puncta fluoresce very strongly, it is likely that large, DVL-based assemblies trap primary and/or secondary antibodies as well as DAPI during the staining process, resulting in fluorescence emission in all channels without biological interaction of the components. This artefact highlights the caveat of using artificial overexpression systems to analyse protein interaction.

Surprisingly, a very small number of cells (<1%) overexpressing either DVL construct did show nuclear GFP staining, overlapping with nuclear FOXK1/2 staining, in addition to the typical punctate pattern. Note that this appears to coincide with cells showing very low DAPI staining (Figure 4.6C, arrowheads) and was only found in cells overexpressing either FOXK paralogue but not under endogenous FOXK1/2 expression. The phenomenon occurred randomly and was not reproducible in higher numbers.

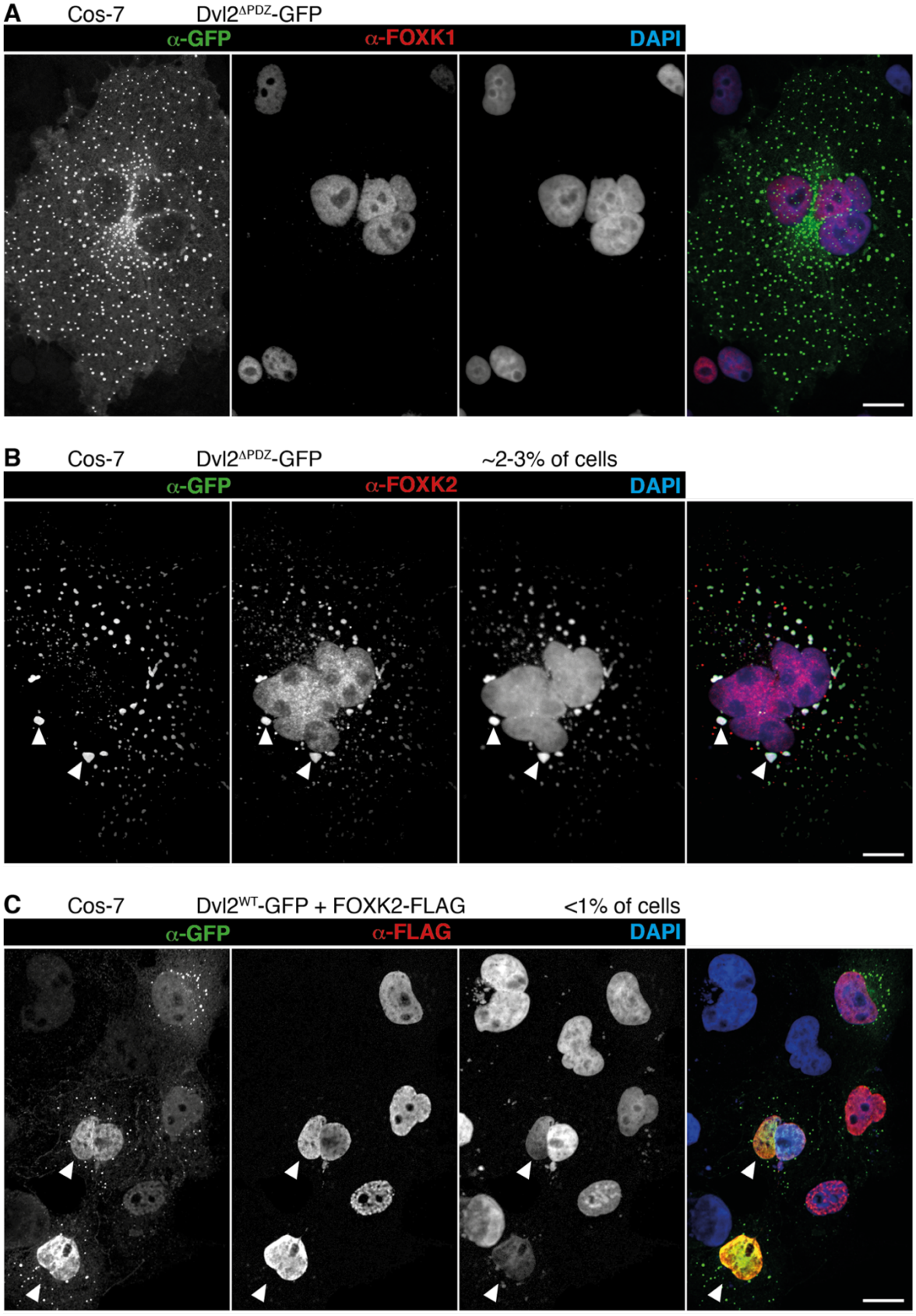

Figure 4.6. DVL^{WT} or DVL$^{\Delta PDZ}$ and FOXK1/2 do not co-localise in Cos-7 cells under endogenous or overexpression conditions.

A) Overexpression of DVL$^{\Delta PDZ}$ leads to characteristic cytoplasmic puncta without nuclear DVL-GFP staining and does not affect localisation of FOXK1.
B) Few cells expressing a high amount of either DVL construct exhibit large cytoplasmic aggregates (arrowheads, 2-3% of cells analysed) that are visible in all channels, including the red (Alexa-546, FOXK) and blue (DAPI) channel.
C) Infrequently, nuclear DVL-GFP staining is observed (<1% of cells analysed) in cells overexpressing either DVL construct and a FOXK paralogue. Note the somewhat reduced DAPI staining in these cells (arrowheads).
Scale bar = 20 μm. α-GFP (green), α-FOXK1/2 or α-FLAG (red), DAPI (blue).

I was thus unable to reproduce the IF-based evidence shown by Wang et al. and could not confirm a robust FOXK1/2-mediated nuclear translocation of DVL. Based on these results, I next asked whether the luciferase reporter assays done in the Wang study would be reproducible in our hands. Wang et al. show that overexpression of FOXK1/2 drastically induces activity of a TCF reporter, whereas FOXK1/2 downregulation conversely decreases reporter activity and that this is largely due to DVL translocation (Figure 3.3D). As I was unable to verify the latter evidence, I decided to examine the effect of overexpression of FOX factors or CRISPR-mediated knockdown on different Wnt readouts to assess whether FOXK1/2 have a DVL-independent role during Wnt signalling.

4.2.4 Overexpression of FOXK1/2 does not result in activation of Wnt signalling

Together with Melissa Gammons, we first asked whether overexpression of FOXK affects cytoplasmic Wnt signal transduction, e.g. by regulating stability of β-catenin itself, or whether FOXK acts further downstream in the pathway to directly influence expression of Wnt target genes.

An effect on β-catenin stabilisation can be assessed by measuring induction of transcriptionally active β-catenin (ABC), which refers to N-terminally dephosphorylated β-catenin (Staal et al., 2002). In untransfected cells, ABC becomes

visible on western blot after induction with WCM or LiCl for ~6 hrs. On the other hand, overexpression of DVL leads to formation of the signalosome in the absence of a Wnt ligand and thereby stabilises β-catenin. Similarly, knockout of degradasome components increases β-catenin stability. In contrast, overexpression of enhanceosome components does not have an effect on β-catenin stability.

We sought to assess whether overexpression of FOXK1/2 variants affects the phosphorylation status of β-catenin by transfecting HEK293T cells with increasing amounts of either FOXK1 or FOXK2, as well as FOXM1 as a control paralogue. No effect on β-catenin stabilisation was seen in comparison with untransfected cells either under activation with WCM or LiCl-containing medium for either of the tested paralogues (Figure 4.7A).

Conversely, we asked whether induction of Wnt signalling affects expression, stability or posttranslational modifications of endogenous FOXK1/2 proteins as this could indicate a role for FOXK1/2 in the Wnt pathway.

No effect of induction of Wnt signalling on FOXK1 could be detected and immunoblotting revealed a band of the expected size of 75 kDa based on molecular weight prediction (Figure 4.7B, left panels). FOXK2 shows two different protein species on western blot, one as expected at ~69 kDa and a slightly smaller variant. While it appears that stimulation of Wnt signalling either by addition of LiCl or WCM induces this lower molecular weight band, longer exposure of the same western blot revealed this protein species to be present in all samples regardless of Wnt stimulation (Figure 4.7B, right panels).

Bearing in mind that Wang et al. reported a strong induction of a standard luciferase reporter assay (TOPFLASH) following overexpression of FOXK1/2 under LiCl induction (see Figure 3.3D for excerpt from their publication), we assessed the effect of different FOX proteins (FOXK1, FOXK2, FOXM1, FOXA1, FOXO3a) on Wnt

signalling under control, WCM and LiCl conditions using a similar TCF reporter (SuperTOP, see 6.7 for comparison).

In contrast to the results published by Wang et al., overexpression of either FOX protein in HEKT293T cells did not significantly affect luciferase activity relative to the empty vector control (ev) following Wnt stimulation (Figure 4.7C, Student's t-test, $n = 5$, $p > 0.05$). Overexpression of FOXK2 and FOXM1 slightly decreased uninduced (i.e. CM) luciferase reporter activity ($p \leq 0.01$) (Figure 4.7C).

If FOXK1/2 proteins stimulated Wnt signalling through affecting DVL localisation or activity, loss of DVL should render FOXK overexpression inconsequential. Alternatively, if FOXK1/2 proteins regulate Wnt signalling through a distinct, cytosol-based process, overexpression might result in partial rescue of Wnt3a-based stimulation in the absence of DVL.

We thus repeated these experiments using the same DVL-TKO cell line described above. Neither FOXK1 nor FOXK2 overexpression significantly affected luciferase activity following induction of Wnt signalling with LiCl (Figure 4.7D, Student's t-test, $n = 3$, $p > 0.05$). Overexpression of FOXK1 and FOXA1 resulted in a slight, but significant increase of luciferase activity in control medium ($p \leq 0.01$) but not after addition of WCM or LiCl. Conversely, FOXM1, FOXA1 and FOXO3a overexpression appeared to result in significantly decreased luciferase activity following induction with LiCl, an effect only seen in DVL TKO cells. It is unclear whether this effect is due to an increase in cell death following overexpression of these particular FOX factors that may have been missed in WT cells due to variation, or whether loss of DVL exacerbated a potential toxicity of FOX overexpression. It is unlikely that overexpression of these FOX factors should repress TCF reporter activity specifically in the absence of DVL.

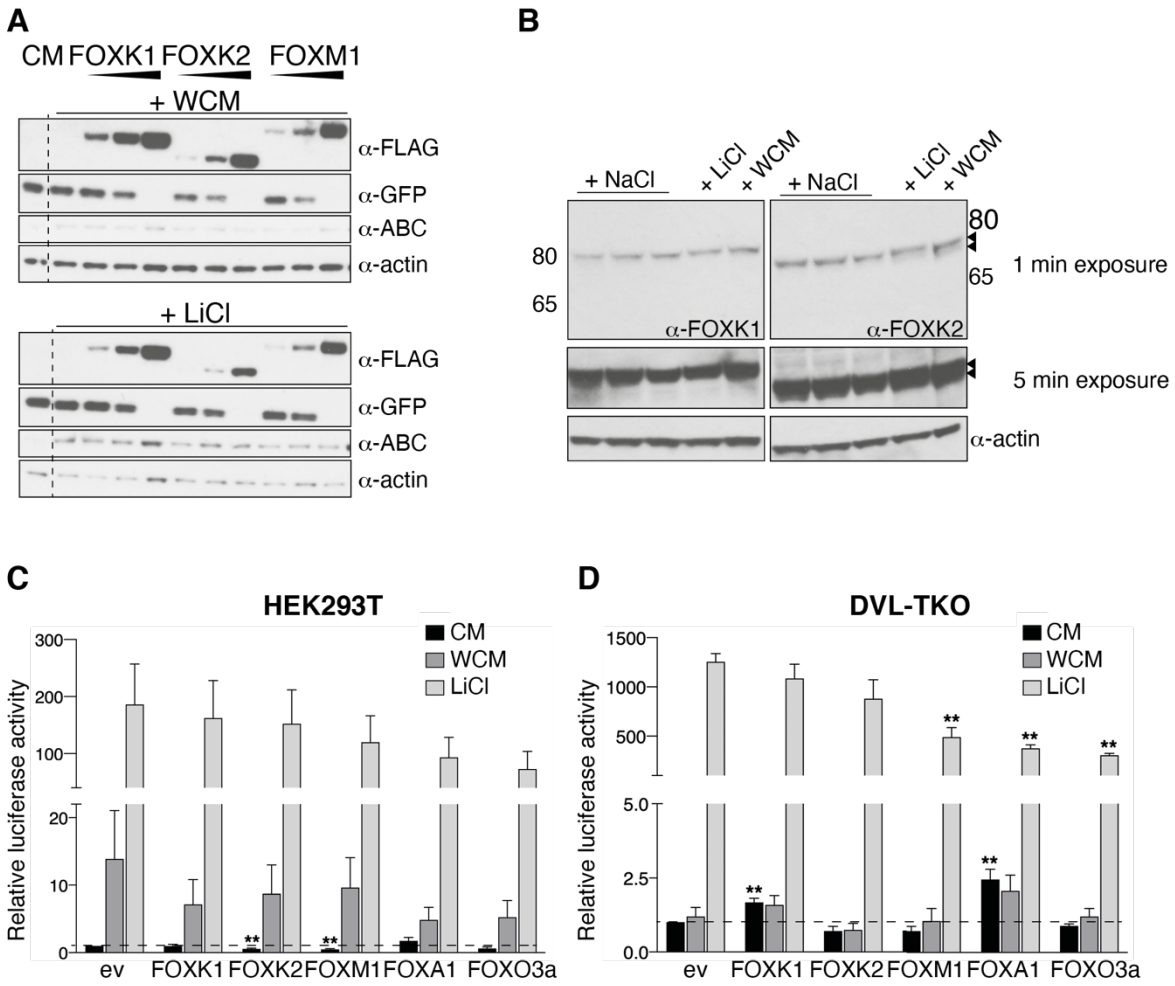

Figure 4.7. Overexpression of different FOX proteins does not lead to increased Wnt signalling.

A) Overexpression of increasing concentrations (50 mM, 100 mM, 200 mM) of FOXK1, FOXK2 and FOXM1 does not affect stabilisation of ABC under Wnt activation with either WCM or LiCl in HEK293T cells in comparison with cells transfected with an empty vector control (ev, GFP vector). Cells were co-transfected with decreasing concentrations of the same empty vector to match the amount of genetic material transfected to 200 ng per well. Western blot done with Melissa Gammons.

B) Induction of Wnt signalling with WCM or LiCl does not affect stability or post-translational modifications of endogenous FOXK1 (left) or FOXK2 (right) in HEK293T cells. Overexpression constructs and endogenous protein show the expected molecular weight of 75 kDa (FOXK1) and 69 kDa (FOXK2). FOXK2 immunostaining results in a second, lower molecular weight band that does not correspond to known splice variants.

C) & D) SuperTOP assays of HEK293T (C) or DVL-TKO (D) cells with overexpression of different FOX proteins following treatment with WCM or LiCl for 4-6 hrs. All experiments normalised to empty vector (ev) control of CM; error bars indicate SEM of ≥3 independent experiments; **p ≤ 0.01. SuperTOP assays were carried out in collaboration with Melissa Gammons.

Based on these experiments, I was unable to reproduce the reporter assays done in Wang et al. (2015) under overexpression of FOX proteins. Since overexpression experiments bear certain caveats that might complicate interpretation and may lead to the discrepancies between my work and the Wang study, I decided to also re-examine their finding that shRNA-mediated knockdown of either FOXK1 or 2 results in a significant reduction in Wnt responsiveness (cp. Figure 3.3D).

4.2.5. Knockdown of FOXK1/2 does not affect activity of a Wnt reporter

To this end, I designed sgRNAs binding in the N-terminal region of either *FOXK1* or *FOXK2* and transfected HEK293T cells with combinations of these to induce simultaneous editing of both *FOXK1/2* paralogues (Figure 4.8A). Emerging double knockdown lines were chosen based on immunoblot analysis and used in downstream assays if FOXK1/2 bands did not appear after long exposure (Figure 4.8B). Lines were further verified using IF with antibodies against endogenous FOXK1/2, confirming no expression of either paralogue.

I subsequently tested several independently generated lines in SuperTOP assays for their response to induction of Wnt signalling. None of the four lines tested revealed any changes in luciferase reporter activity compared with WT HEK293T cells under any condition (CM, WCM or LiCl, Student's t-test, $n = 3$, $p > 0.05$) (Figure 4.8C).

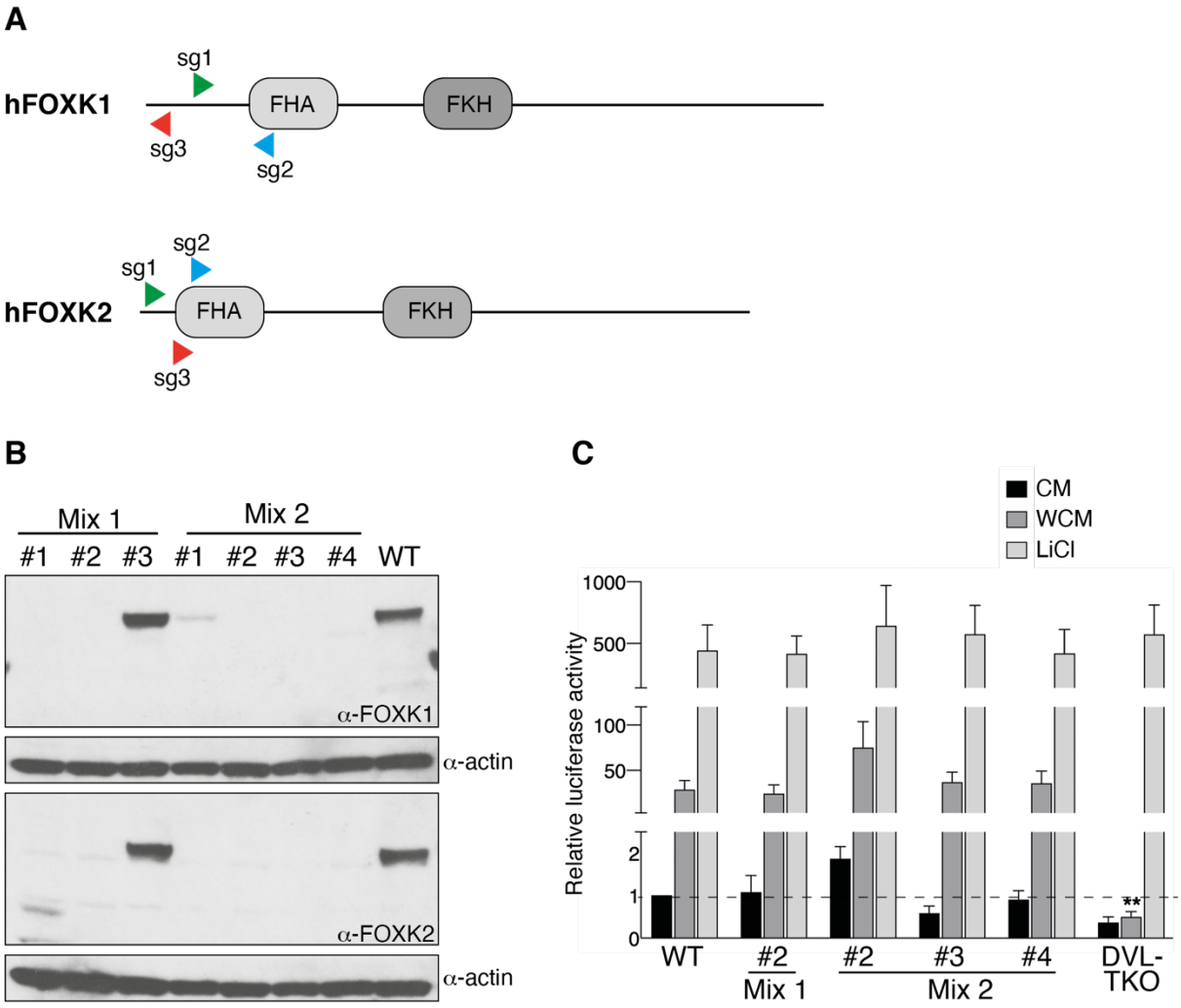

Figure 4.8. CRISPR-mediated knockdown of FOXK1 and FOXK2 does not affect activity of a TCF reporter.

A) sgRNAs were designed to target the N-terminal regions of FOXK1 and 2 and transfected into HEK293T cells in different combinations (Mix 1: FOXK1^{sgRNA1} + FOXK2^{sgRNA2}; Mix 2: FOXK1^{sgRNA2} + FOXK1/2^{sgRNA2}).

B) Immunoblot of different FOXK1/2 double knockdown lines. Mix 1, Line #2 as well as Mix 2, Lines #2-4 were chosen for downstream analysis of Wnt signalling based on immunoblot analysis.

C) SuperTOP assays comparing WT HEK293T, a DVL TKO line and different FOXK1/2 double knockdown lines. Error bars indicate SEM of 3 independent experiments; **p ≤ 0.01.

In summary, my experiments presented in this chapter refute the evidence published by Wang et al. (2015). In the following sections I will discuss these discrepancies and suggest future experiments that should inform on the role of FOXK1/2 in mammalian cells.

4.3. Discussion

While we were unable to reproduce nuclear DVL or a direct effect of overexpression or loss of FOXK1/2 on Wnt reporter assays, BioID studies in our lab indicate a PDZ-dependent interaction of FOXK1/2 with DVL (Melissa Gammons, unpublished results) as well as a consistent association with core components of the Wnt enhanceosome (PYGO2 and TLE3, see Chapter 2). It remains unclear whether and how FOXK1/2 and DVL interact and whether this interaction is required for Wnt target gene transcription, or whether FOXK1/2 act by binding to WREs directly as my results using the *UbxB* reporter in *Drosophila* indicate (Chapter 3).

4.3.1. Putative interaction between FOXK$^{C\text{-}Term}$ and DVL-PDZ

While unpublished results by Melissa Gammons and Trevor Rutherford show an *in vitro* interaction between *Drosophila* FoxK and human DVL mediated by the FoxK-C-terminus and the DVL-PDZ domain, the respective *Drosophila* mutant did not reveal a phenotype indicative of a biological function for this interaction (Figure 4.2). It is possible that while these proteins interact at high concentrations *in vitro*, they do not localise to the same cellular compartment or have a very low binding affinity and therefore do not interact *in vivo*. Based on my experiments I cannot rule out that this protein interaction is biologically relevant but produces an effect that can be compensated for by other FOX homologues or mechanisms. However, our analysis did not indicate that the C-terminal putative PDZ-binding motif is conserved across FOX factors (Melissa Gammons, unpublished results). A cell-based assay to test this interaction directly might be more suitable as known Wnt readouts allow detection of small changes in activity, e.g. by luciferase reporter assays.

Alternatively, DVL and FOXK could interact through the PDZ and FHA domains, respectively, as suggested by Wang et al. (2015). This is possible based on the

flexible structure of the DVL-PDZ domain (Zhang et al., 2009), but DVL-PDZ binding of internal sequences has yet to be shown *in vivo*. Verification of the CoIP studies by Wang et al. (2015) or NMR studies using bacterially expressed FOXK-FHA and DVL-PDZ peptides will be important to assess the requirement of the FHA domain. Additionally, it will be interesting to confirm whether expression of FoxK$^{\Delta FHA}$ protein can rescue the embryonic phenotype of *foxK^{null}* mutants in *Drosophila*.

4.3.2. Co-staining of FOXK1/2 and DVL does not reveal co-localisation and DVL is not found in the nucleus

Despite reports of nuclear DVL (Gan et al., 2008; Itoh et al., 2005), I was unable to robustly reproduce this observation in my experiments nor has this been detected previously by members of the Bienz lab. Of note, tandem affinity purification experiments by Wang et al. did not yield any exclusively nuclear binding partners for DVL as might be expected if DVL were to function as a stabiliser of β-catenin-TCF complexes.

While I find nuclear GFP staining in a very small proportion of cells overexpressing DVL-GFP (Figure 4.6C), this occurrence is too rare to be considered biologically relevant. It is possible that the nuclear GFP staining is caused by cleavage of the DVL-GFP construct resulting in free GFP molecules that can translocate to the nucleus. Given that these cells display reduced DAPI staining it is likely that they are unhealthy or apoptotic cells and a potentially broken nuclear envelope could thus account for the "nuclear" GFP staining. As the cells with nuclear GFP staining tend to occur within close proximity of each other (rather than randomly distributed across slides), it is likely that they stem from a single parental cell that underwent unknown genetic or morphological changes or may have been transfected with an unusually high amount of plasmid leading to cell toxicity due to strong expression.

This effect is not unexpected as high levels of DVL have been found to affect cell division and viability in previous studies, which was hypothesised to increase selective pressure to keep transgene levels low (Gammons et al., 2016a; Smalley et al., 2005). It is unknown whether overexpression of FOXK1/2 may have adverse effects on cells and I did not detect any evidence of cell toxicity upon overexpression of FOXK1/2 alone, but it is conceivable that a combined effect of overexpressed DVL and FOXK1/2 could lead to cell toxicity. Due to lack of reproducibility of this phenomenon it will be difficult to conclusively show which of these possibilities cause the nuclear GFP staining in a minority of cells.

It remains unclear whether the discrepancy in the reported subcellular localisation of DVL by different groups is due to use of different α-DVL antibodies or based on differential overexpression effects. However, Wang et al. work with the same DVL antiserum used in our lab (commercially available from Cell Signalling Technology) and I used a GFP antibody to amplify the signal in my IF experiments using DVL-GFP overexpression to circumvent artefacts based on antisera. These observations argue against a specific effect of a single antibody. Differences in fixation protocols could further contribute to different localisation patterns as described by Torres and Nelson, 2000, who found a significant difference in DVL localisation when glutaraldehyde rather than methanol was used.

My results reinforce the finding that high levels of protein overexpression lead to artificial conditions that do not represent *in vivo* circumstances and need to be interpreted with caution. Gammons et al. (2016a) propose an alternative system based on knockout of proteins in combination with rescue through near-endogenous re-supply of proteins as this is often more suitable and offers a virtually physiological environment. A similar approach is to modify endogenous genes with CRISPR-Cas9.

4.3.3. Overexpression or loss of FOXK does not affect Wnt reporter activity

It is striking that Wang et al. observe a strong induction of TCF reporter activity upon overexpression of FOXK1/2 proteins, which is in stark contrast to our findings, where overexpression of FOXK1/2 did not result in elevated Wnt responses under CM, WCM or LiCl. Unfortunately, Wang et al. (2015) do not disclose the plasmid concentrations used in their IF and TOPFLASH assays, which hinders direct comparison with my results. Given that transfection with 200 ng of FOXK1/2 plasmid led to strong expression of these constructs as documented using immunoblotting (cp. Figure 4.7A), we used this concentration going forward in SuperTOP assays. This is comparable to most experiments based on overexpression in our lab and has been shown to be sufficient for significant induction of TCF-based transcription in our lab.

I was further unable to reproduce Wang et al.'s finding that loss of FOXK1/2 results in a reduction of Wnt signalling. While most of their experiments are based on shRNA-mediated knockdown, I used CRISPR-mediated editing to reproduce their results.

The CRISPR technology holds the caveat of potential compensation mechanisms induced by stable downregulation of protein levels which may not occur in experiments using transient knockdown via siRNA-based approaches. A rescue effect has been shown previously for cell lines as well as model organisms where genetic compensation or transcriptional adaptation can in some cases result in a partial or full rescue of the knockout phenotype (El-Brolosy et al., 2019; Ma et al., 2019). This phenomenon has been observed as early as in the F2 generation of a zebrafish-based study (Buglo et al., 2020).

CRISPR-induced adaptation could partially account for the differences seen in my luciferase reporter assays in comparison with the siRNA-based findings by Wang et

al. However, note that Wang et al. did use CRISPR technology to generate FOXK1/2 knockouts in cancer cell lines and observed reduced TCF reporter activity in culture and suppressed tumour growth in xenografts based on these CRISPR knockout lines.

Moreover, it seems unlikely that other FOX proteins could act redundantly through a mechanism in line with a PDZ-FHA interaction proposed by Wang et al. as the putative interaction motif should not be present in any FOX proteins other than of the K subfamily. Alternatively, if FOX proteins in general function more directly in Wnt signalling through binding of enhancer sequences of WREs, any FKH-containing protein could be expected to act redundantly, and expression levels of other FOX proteins could be adapted to compensate for loss of FOXK1/2.

Use of a more temporary knockdown system such as siRNA-related approaches or CRISPRi (Qi et al., 2013) with concomitant reporter analysis in the F0 generation could be used to clarify this.

In summary, the evidence presented in this chapter refutes a FOXK1/2-mediated recruitment of DVL to the nucleus and challenges the results presented by Wang et al.

5. Conclusions and Future Directions

This body of work has identified putative novel interactors of the Wnt enhanceosome using a proteomic approach (Chapter 2), of which FOXK was selected for further studies in *Drosophila* (Chapter 3) and human cell lines (Chapter 4).

Based on my BioID studies I have uncovered interesting evidence for a potential dynamic of the TLE3-TCF association throughout the signalling cycle, by which different mechanisms of TLE3 inhibition could function consecutively to allow induction and maintenance of transcription from Wnt-dependent enhancers. As discussed in Chapter 2, TLE3 could initially remain associated with TCF but inhibited through mechanisms such as ubiquitylation. Prolonged Wnt activation could then induce a second mechanism by which TLE3 dissociates from TCF, as my BioID results indicate a weakened interaction between the two proteins only after several hours. However, I was unable to repeat my BioID time course with TLE3 due to time limitations and further experimental validation will be required to assess the possibility of such a two-fold mechanism of TLE3 regulation.

Additionally, my enhanceosome studies identified several novel candidate interactors, most importantly BRCA2, JMJD1C and ZNF703/Zeppo1. Future studies should aim at elucidating the roles of these proteins in Wnt signalling (for example using the approaches discussed in Chapter 2). We were intrigued by the repeated occurrence of FOXK proteins in BioID lists using proteins from the Wnt pathway as baits (van Tienen et al., 2017; Melissa Gammons, unpublished results; as well as my own results) and decided to assess the connection between FOXK and Wnt signalling.

My experiments in mammalian cells provided evidence that FOXK1/2 do not affect Wnt signalling responses as monitored by luciferase reporter assays bearing minimal TCF binding sites either with overexpression or following CRISPR-mediated knockdown. A different luciferase reporter assay which combines FKH and TCF

binding sites might be more suitable to analyse an effect of FOX overexpression on TCF-regulated transcription since FOXK proteins are likely to require DNA binding to mediate an effect on gene expression.

Using IF studies we were further unable to reproduce a proposed nuclear translocation of DVL by FOXK1/2, nor do DVL and FOXK1/2 co-localise in cytoplasmic puncta that form upon DVL overexpression. While we identified a putative C-terminal PDZ binding motif in *Drosophila* FoxK (Melissa Gammons, Trevor Rutherford, unpublished results), I was unable to show a requirement for this motif during fly development based on a C-terminal truncation of FoxK.

I did not examine the putative direct interaction between the DVL-PDZ and FOXK-FHA domains, and future studies should address this interaction and the function of the FHA domain in more detail. For example, it would be interesting to analyse expression of an FHA mutant of *Drosophila* FoxK ($FoxK^{\Delta FHA}$) in the background of my null mutants to assess whether this construct is able to rescue loss of *foxK*. Similarly, over- or misexpression of other FOX proteins could be used in this assay to assess whether expression of any FKH-containing protein is sufficient to rescue the embryonic phenotype of *foxK* null mutants.

Alternatively, BioID using a $FOXK^{\Delta FHA}$ construct in comparison to WT FOXK in mammalian cells could elucidate FOXK association with transcriptional regulation. It will be interesting to determine whether FOXK is specific to the Wnt enhanceosome or also interacts with other transcriptional regulators, and whether the FHA domain is required for its association with PYGO, TLE3 and others.

In contrast, my more promising analysis of FoxK in *Drosophila* shows evidence for a specific role of FoxK in the control of certain Wg targets during embryogenesis and wing development. In early embryo patterning, maternal and zygotic loss of FoxK affects *wg* expression itself as well as expression of *eve* in cells where this gene is

under the control of Wg signalling. It remains to be seen whether the same holds true for other targets of Wg in the embryo such as *engrailed* or *labial* (both of which were shown to be reduced in FoxK-RNAi experiments by Casas-Tinto et al. (2008)).

It is crucial to note that several of these FoxK-dependent genes are controlled by both Wg and Dpp signalling in the respective tissues where loss of *foxK* leads to downregulation of these targets. Future experiments should thus address whether FoxK functions downstream of Wg or Dpp, or is able to combine signals from both pathways to regulate gene expression. This seems likely given that Wg and Dpp inputs are often integrated at the level of transcriptional enhancers, as previously described for control of *labial* (Yu et al., 1996) or *eve* (Knirr and Frasch, 2001) expression, but also of *Distal-less*, which is regulated by both Wg and Dpp signals in the wing disc (Estella et al., 2008).

Different enhancers are regulated by Dpp and Wg in distinct ways: for instance, expression of *eve* is thought to require binding of Tinman (a homeodomain protein important for development of the visceral mesoderm (Bodmer, 1993)) and Smad proteins (nuclear effectors of Dpp; reviewed in Affolter et al. (2001)), both of which are direct targets of Dpp. The *eve* enhancer is further bound by TCF and this controls *tin* expression such that expression only proceeds in tissues that receive a Wg signal. In contrast, regulation of *bap*, which is a target of Dpp and Wg in the visceral mesoderm, is indirectly regulated through Wg. Here, Wg induces *slp1/2* expression leading to suppression of *bap* ((Lee and Frasch, 2005), recall that slp1/2 are homologues of mammalian FOXG), such that *bap* is only expressed in tissues without Wg expression. This interplay between Dpp and Wg is largely responsible for the segment-specific differentiation of tissues.

Casas-Tinto describe a model by which f*oxK* expression is directly regulated through the Dpp effectors Mad/Med resulting in its binding to *labial* enhancers to drive gene expression. It will be vital to establish whether FoxK then interacts with TCF through

binding of the same enhancer fragment, thereby integrating inputs from Dpp and Wg signalling. Future experiments should also address which genes specifically require FoxK-mediated regulation.

This putative interplay between signalling pathways could also account for the discrepancy between my results in *Drosophila* and mammalian cells. Such an effect could not be measured using the SuperTOP reporter which only contains TCF binding sites and does not allow signal integration from different signalling pathways (unless these occur upstream of DNA binding).

I further used the *Ubx* minimal enhancer as a reporter system to assess requirement of FOX binding sites in Wnt responsive enhancers. This revealed an absolute requirement of FKH binding sites for expression from this enhancer, but my analysis so far does not confirm a specificity for one individual FOX factor. It will be interesting to analyse whether a specific subset of Wnt target genes is more strongly regulated/bound by one group of FOX factors or whether there is a temporal or tissue-specific dependency during development.

One of the most intriguing unanswered questions is how specific Wnt target genes are differentially regulated in different cellular contexts or time points. This is important not just in relation to FOX proteins but also more generally as it is likely that the composition of the enhanceosome differs between cell types or throughout the differentiation process as well as at different Wnt response elements. In the following paragraphs I suggest two approaches to extend our knowledge on this important question.

With the development of two novel BirA* enzymes, TurboID and MiniID, BioID is now also feasible in *Drosophila*, as these enzymes are much more efficient and require low amounts of biotin (which can be supplied via food (Branon et al., 2018)). Such a setup has the advantage that different developmental stages can be assessed

relatively easily using GAL4 drivers to express the BioID constructs at distinct time points. By assessing core proteins of the enhanceosome as well as potential pioneer factors (FOXK, Runt or others), the assembly and composition of the enhanceosome can be tracked over time.

Alternatively, the so-called CasID approach (Schmidtmann et al., 2016), which combines Cas9/sgRNA-mediated recruitment to specific loci with a BioID-based proteomic pull-down of interactors, would allow us to elucidate potential differences of enhanceosome composition at specific loci. CasID as well as the related C-BERST method (which relies on Cas9-APEX to label interactors) have been previously proven successful in studying the proteome associated with centromeres and telomeres (Gao et al., 2018; Schmidtmann et al., 2016).

The method relies on a catalytically dead Cas9 enzyme (Qi et al., 2013), which interacts with sgRNAs recruited to any target locus. The Cas9 is fused to a biotin ligase leading to biotinylation of proteins associated with a specific locus. This experimental setup requires careful consideration of control loci to be used so that background normalisation can be achieved to subtract proteins binding to a broad range of loci.

A CasID approach requires generation of stable cell lines expressing the Cas-BioID construct at low levels but then can be adapted to different loci relatively quickly by transient transfection of sgRNAs. Once established, this would allow us to assess different loci at different time points, i.e. before, during and after activation of Wnt signalling.

In summary, I was able to provide evidence that FoxK is required for expression of a subset of Wg target genes during embryogenesis and wing development. While I conclusively showed that the currently available *foxK* allele, *foxK*^{16} by Casas-Tinto et

al. (2008), is not a *foxK* null allele, my novel *foxK* alleles will provide valuable tools for future experiments. Additionally, my BioID studies suggest different enhanceosome candidates that should be pursued in the future.

6. Material & Methods

6.1. Antibodies

Antibody	Source
Alexa Fluor 488 conjugated Goat α-Rabbit Ig	Life Technologies
Alexa Fluor 488 conjugated Goat α-Rat Ig	Life Technologies
Alexa Fluor 488 conjugated Goat α-Mouse Ig (highly cross-absorbed)	Life Technologies
Alexa Fluor 488 conjugated Goat α-Rabbit Ig (highly cross-absorbed)	Life Technologies
Alexa Fluor 546 conjugated Goat α-Mouse Ig	Life Technologies
Alexa Fluor 546 conjugated Donkey α-Rabbit Ig	Life Technologies
Alexa Fluor 546 conjugated Goat α-Rat Ig	Life Technologies
Alexa Fluor 546 conjugated Goat α-Mouse Ig (highly cross-absorbed)	Life Technologies
Alexa Fluor 647 conjugated Goat α-Rabbit Ig	Life Technologies
α-active β-catenin (α-ABC)	Cell Signaling Technologies
α-actin	Sigma Aldrich
α-Armadillo	Developmental Studies Hybridoma Bank
α-β-catenin	BD Transduction Laboratories
α-BirA	Sino Biological
α-DE-Cadherin	Developmental Studies Hybridoma Bank
α-dpp	Developmental Studies Hybridoma Bank
α-DVL2	Cell Signaling Technologies
α-engrailed (4D9)	Developmental Studies Hybridoma Bank
α-FLAG (mouse)	Sigma Aldrich
α-FoxK	Obtained from immunisation with $FOXK_{216-417}$
α-FOXK1 (ab18196)	Abcam
α-FOXK2 (#12008)	Cell Signaling Technologies
α-β-Galactosidase	Promega
α-GFP (rabbit)	Sigma Aldrich
α-GFP (mouse)	Roche
α-Groucho	Developmental Studies Hybridoma Bank
α-Histone 2	Abcam
HRP-conjugated Goat α-Mouse Ig	Santa Cruz Biotechnology
HRP-conjugated Goat α-Rabbit Ig	Invitrogen
HRP-conjugated Goat α-Rat Ig	Santa Cruz Biotechnology
HRP-conjugated Goat α-Mouse Ig	Santa Cruz Biotechnology
HRP-conjugated Streptavidin (Strep-HRP)	BioLegend
α-Lamin	Manfred Frasch
α-Legless	Obtained from $Lgs_{232-555}$ by M. van Tienen
Biotinylated Goat α-Mouse	Vectorlabs
α-Myc	Santa Cruz Biotechnology
α-hPYGOs (ab109001)	Abcam
α-hPYGO2 (ab99274)	Abcam
α-Pygo (*Drosophila*)	Marc de la Roche, Bienz Lab, MRC LMB

α-Senseless	Prof Hugo J. Bellen
α-TLE3	Santa Cruz Biotechnology
α-vestigial	Developmental Studies Hybridoma Bank
α-Wg (4D4)	Developmental Studies Hybridoma Bank

6.2. Plasmids

Plasmids used in this thesis are listed below. New constructs were generated from parental plasmids using standard methods including QuikChange (Agilent) or Gibson assembly (Gibson et al., 2009). Either KOD DNA Polymerase (Merck Millipore) or Q5 High-Fidelity DNA Polymerase (NEB) were used as appropriate and plasmids verified by Sanger sequencing (Genewiz, UK).

Bacterial DNA was isolated using either QIAprep Spin Miniprep Kit (Qiagen) or PureLink HiPure Plasmid Midiprep Kit (Invitrogen) according to manufacturer's protocols. PCR products were purified with the appropriate kits by Qiagen.

Plasmid	Source
pcDNA5/FRT/TO	Invitrogen (Cat #: V652020)
pOG44	Invitrogen (Cat #: V600520)
pcDNA5/FRT/TO-myc-BirA2	Bienz Lab, based on Kim et al. (2016)
pcDNA5/FRT/TO-FLAG-TLE3-BirA2-NLS	Derived from BirA2 vector
pcDNA5/FRT/TO-FLAG-EGFP-BirA2-NLS	Derived from BirA2 vector
pcDNA5/FRT/TO-FLAG-PYGO-BirA2-NLS	Derived from BirA2 vector
pcDNA5/FRT/TO-FLAG-PYGO$^{\Delta N\text{-}Box}$-BirA2-NLS	Derived from BirA2 vector
pcDNA5/FRT/TO-FLAG-PYGO$^{\Delta PHD}$-BirA2-NLS	Derived from BirA2 vector
V5-TurboID-NES_pCDNA3	Addgene: #107169; Branon et al. (2018)
V5-TurboID-NLS-TLE3_pcDNA3	Derived from Addgene #107169
V5-TurboID-NLS-EGFP_pcDNA3	Derived from Addgene #107169
Super 8x TOPFLASH	Addgene: #12456; Veeman et al. (2003)
CMV-Renilla	Promega (Cat #: E2261)
pcDNA3.1_FLAG-EGFP	Bienz Lab
pSpCas9(BB)-2A-GFP (PX458)	Addgene: #48138
pcDNA3.1-TLE3-HA	Bienz Lab
pcDNA5/FRT/TO-myc-hPYGO2	Bienz Lab
hDVL2-EGFP	Bienz Lab
hDVL2$^{\Delta PDZ}$-EGFP	Bienz Lab
hDVL^{V334E}-EGFP	Bienz Lab
FLAG-FOXK1	Sharrocks Lab
FLAG-FOXK2	Sharrocks Lab

FLAG-FOXM1	Dr Suyan Huang
FLAG-FOXO3a	Sharrocks Lab
pCFD3:U6:3-sgRNA	Addgene: #49410, Simon Bullock, MRC LMB
pHZ-Ubx250	Bienz Lab

6.3. Bacterial transformation & generation of competent cells

For bacterial transformation, chemically competent *E. coli* cells, strain Mach1, were incubated with purified DNA on ice and heat shocked for 45 seconds at 42°C. Bacteria were then incubated in Super Optimal Broth (SOB) medium at 37°C for 45-60 min and plated on lysogeny broth (LB) plates containing the relevant antibiotics.

Competent cells were generated by inoculating 1 L medium LB + 10 mM $MgCl_2$ with 20 mL of an overnight culture of Mach1 cells and incubating at 37°C until $OD_{600} \leq 0.6$ was reached. Cultures were cooled to 4°C, centrifuged (10 min at 2,500 x *g*) and the pellet resuspended in freshly prepared, cold CC buffer (10 mM PIPES pH 6.7, 15 mM $CaCl_2$, 250 mM KCl, 55 mM $MnCl_2$), and the suspension incubated on ice for 10 min. The centrifugation was repeated once before adding 3.5 mL dimethyl sulfoxide (DMSO, Sigma Aldrich) to the cells, incubating on ice for 10 min and flash-freezing aliquots in liquid nitrogen. Aliquots were stored at -80°C.

6.4. Western Blotting

Lysates of mammalian cells or fly tissues were prepared as appropriate for individual experiments and protein concentration determined using Pierce BCA Protein Assay Kit (Thermo Fisher). Briefly, a dilution series of albumin protein was prepared (15.5 – 2000 µg/mL) as a standard alongside several dilutions of lysates to be tested. Pierce BCA reagents were added, and absorption quantified at 562 nm using a microplate reader.

Proteins were denatured in 4x NuPAGE LDS sample buffer (Invitrogen) by heating at 98°C for ~5 min and separated on NuPAGE 4-12% Bis-Tris protein gels (Invitrogen) at 90-120V for 90-120 min unless otherwise stated. Separated protein was transferred to PVDF membrane (Millipore) by semi-dry transfer at constant voltage of 100V for 75 min. Membranes were stained with Ponceau S (0.5% (w/v) Ponceau S, 1% acetic acid) to analyse efficiency of transfer, washed in PBT (PBS, 0.1% Triton X-100) and blocked in blocking buffer (5% milk or 5% bovine serum albumin (BSA) in PBT) for approximately 30 min.

Membranes were incubated in primary antibody in blocking buffer overnight at 4°C and subsequently washed in PBT and incubated with HRP-conjugated secondary antibody for 2-4 hrs at room temperature (RT), followed by additional wash steps in PBT. Western blots were developed in ECL Western Blotting Detection reagent (Amersham) on X-Ray film (Photon Imaging Systems Lt).

6.5. Mammalian cell culture

Mammalian Cell Line	Source
HEK293T	Bienz Lab, MRC LMB
SW480	Bienz Lab, MRC LMB
HeLa	Bienz Lab, MRC LMB
HEK293 Flp-In T-Rex	Marc van Breugel, MRC LMB
DVL TKO (HEK293T$^{\Delta DVL1/2/3}$)	Melissa Gammons, MRC LMB
Cos-7	Bienz Lab, MRC LMB

Unless otherwise stated, mammalian cells were grown in standard Dulbecco's Modified Eagle Medium (DMEM, Thermo Scientific Fisher) with 10% fetal bovine serum (FBS) and supplied with antibiotics (1% Streptomycin, 1% Penicillin). Standard growth conditions were 37°C in a humidified atmosphere with 5% CO_2. Cells were regularly tested for *Mycoplasma* infection.

Induction of Wnt response was achieved by growing cells in Wnt3a-conditioned medium (WCM, derived from L Wnt-3a cells) for 6 hrs or in DMEM containing 20 mM LiCl for 4 hrs. As control media, DMEM containing 20 mM NaCl was used.

For transfections cells were seeded at low confluency and transfected using polyethylenimine (PEI) or Lipofectamine 2000 as recommended by the manufacturer. For IF assays 100 ng plasmid DNA were transfected per 12-well. For luciferase reporter assays under overexpression, 200 ng plasmid DNA was used unless specified.

DNA was isolated from cultured cells after washing cells with PBS, incubation in trypsin and centrifugation for 3 min at 5,000 rpm. Pelleted cells were resuspended in PBS and DNA extracted using Microlysis buffer (Microzone, UK). Genotyping oligonucleotides are listed in the appendix, section 8.2.

6.6. Immunofluorescence of cultured cells

Cells were seeded at low confluency in 24-well plates with coverslips pre-treated with poly-L-lysine (Sigma) to enhance adherence, and grown for 6-24 hrs before fixation in 4% PFA in PBT for 20-30 min. Permeabilisation in 0.2% Triton X-100 in PBS was followed by a blocking step in 5% bovine serum albumin (BSA) in PBT and overnight incubation with primary antibodies in blocking buffer. Cells were subsequently washed in PBT and incubated with appropriate secondary antibodies for 2-4 hrs in the dark at RT. Following additional wash steps in PBT, coverslips were mounted in ProLong Diamond Antifade Mountant with DAPI (Thermo Fisher Scientific). Images were acquired on a Zeiss LSM 710 confocal microscope (Carl Zeiss Inc.).

6.7. TCF reporter assay

Expression of Wnt target genes in different genetic backgrounds was estimated using a luciferase-based reporter (SuperTOP, previously TOPFLASH) assay. For this, HEK293T or SW480 cells were co-transfected with SuperTOP, a plasmid expressing firefly luciferase under the control of multiple TCF-responsive elements (Veeman et al., 2003) and a control plasmid constitutively expressing luciferase (CMV-Renilla), and incubated for 12-24 hrs before inducing with Wnt3a-/LiCl-containing or control medium for 4-6 hrs.

Cells were lysed in UBER buffer (20 mM Tris-HCl (pH 7.4), 10% glycerol, 200 mM NaCl, 0.2% Triton X-100, PhosphoSTOP (Roche), protease inhibitor tablet (EDTA-free, Roche)) and luciferase emission quantified using the Dual-Glo Luciferase Reporter Assay kit (Promega) according to manufacturer's specifications. Values were corrected for background readings of Renilla expression and two technical replicates per condition averaged before statistical evaluation of biological replicates ($n \geq 3$, see figure legend for specifics of individual experiments) by Student's t-test. Results are displayed as normalised to the respective uninduced (control medium, CM), empty vector (ev) control of each experiments, error bars are standard error of mean.

Note that experiments done by Wang et al. and summarised in Chapter 3 use a different control plasmid called FOPFLASH for their experiments. This plasmid is analogous to the TOPFLASH plasmid but contains mutated TCF binding sites and is used as a measure for background luciferase expression.

6.8. CRISPR/Cas9 in mammalian cells

Guide RNAs (sgRNAs) for CRISPR of mammalian cells were designed using the CRISPOR tool from the Zhang lab (available at crispor.tefor.net) and selected to have no or few predicted off-targets with mismatches across the length of the sgRNA to maximise specificity. sgRNAs were cloned into pSpCas9(BB)-2A-GFP (PX458, Addgene) and transfected into HEK293T cells. Oligonucleotides used in CRISPR experiments are listed in the appendix, section 8.3.

Fluorescent cells were detected 48 hrs post transfection by fluorescence-activated cell sorting (FACS) and cells of intermediate GFP fluorescence, indicating successful expression of the Cas9-bearing plasmid, sorted into 96 well plates at 1-3 cells/well. Resulting clones were grown in DMEM for 2-3 weeks before analysis of gene editing by western blot and sequencing.

Edited sequences were determined manually or by using the TIDE analysis tool (Brinkman et al., 2014; https://tide.deskgen.com). Per experiment, multiple lines, preferably generated through editing with different sgRNAs, were chosen for further experiments.

6.9. Proximity labelling by BioID

6.9.1. Construct design and generation of stably transfected cell lines

BioID functions through expression of a fusion protein consisting of the bait protein and a promiscuous biotin ligase that has been engineered to release highly reactive bioAMP (BirA*). Since the first description of this system by Roux et al. (2012) based on the original BirA-R118A enzyme from *E. coli*, which was used for BioID experiments with PYGO2 (described in Chapter 2), several such enzymes have been optimised for use in different organisms and cultured cells. A follow-up study by the

same lab lead to the discovery of BioID2 which is based on the *Aquifex aeolicus* BirA homologue (Kim et al., 2016). More recently, protein engineering in yeast has led to the development of two improved ligases, called TurboID and miniTurbo (Branon et al., 2018). As these novel enzymes require less biotin input as well as shorter labelling times, TurboID was used to generate a TLE3-BioID data set by subjecting cell lines stably expressing the fusion protein to a time course with different durations of biotinylation and Wnt induction.

Since protein interaction studies depend on the normal function of the bait protein, the site of fusion to the BirA* enzyme needs to be carefully chosen. To this end, protein domains and secondary structure were analysed using the online tool Phyre2 (Protein Homology/analogY Recognition Engine (Kelley et al., 2015); http://www.sbg.bio.ic.ac.uk/ ~phyre2/html/page.cgi?id=index) as well as any structural information available on PDB or other data bases, and insertion sites were chosen to be in unstructured regions where possible. Constructs were additionally tagged with a nuclear localisation signal (NLS from SV40 virus, PKKRKV) and either a FLAG-Tag (DYKDDDDK) or a V5-Tag (GKPIPNPLLGLDST).

All BioID experiments were carried out using inducible expression of bait-BirA* fusion proteins to avoid interference with normal protein function and overexpression artefacts. Use of the Flp-In™ 293 T-Rex system (Thermo Fisher Scientific) allows generation of stably transfected, isogenic cell lines under the control of a tetracycline-inducible operator. Cells were transfected with pcDNA5/FRT/TO-"bait"-BirA* as well as the Flp recombinase vector pOG44 and selected with 100-200 µg/ml Hygromycin B (Carl Roth) in DMEM for 2-3 weeks until cell clones expressing the fusion protein were visible. Correct function of BirA* fusions was verified by assessing localisation of the fusion protein as well as ability to biotinylate by evaluating biotin smears after addition of biotin to the medium.

6.9.2. Proximity labelling and pull-down

Labelling and pull-down of biotinylated proteins follows the protocol published by Roux et al. (2013) and differs only in the following points. All cell lines stably expressing the fusion construct were induced with tetracycline (1 µg/ml in DMEM) for 12 hrs before adding 1 mM biotin to prevent experimental bias based on different levels of fusion protein. Biotin labelling times as well as amount of starting material were adjusted based on enzyme and experimental conditions and are stated in the respective result sections. Cells were washed in PBS, trypsinated and pelleted by centrifugation and subsequently flash frozen in liquid nitrogen. Lysis buffer (50 mM Tris-HCl pH 7.4, 500 mM NaCl, 0.2% SDS, 1 tablet EDTA-free Protease Inhibitor (Roche), 1 tablet PhosphoSTOP (Roche)) and Triton X-100 (final concentration 2%) were added to the pellet and cells lysed by sonication. Labelled proteins were bound to streptavidin beads by overnight incubation at 4°C and unbound protein removed by washing three times in 2% SDS. Bound protein was eluted from beads by boiling samples in SDS loading buffer with added biotin (NuPAGE loading dye, 1 mM biotin) at 98°C for 5 min. Samples were run on 8-12% NuPAGE protein gels at 60V until the dye front had run approximately 2.5 cm into the gel. Gels were stained overnight in Imperial stain (Thermo Fisher Scientific) and de-stained in distilled water for 2-3 days before being cut into 1 mm slices for mass spectrometry analysis, which was performed at MRC LMB by Mark Skehel and his team.

6.9.3. Mass spectrometry

In short, gel slices were destained in 50% v/v acetonitrile and 50 mM ammonium bicarbonate prior to reduction with 10 mM dithiothreitol (DTT) and alkylation with 55 mM iodoacetamide. Subsequently, proteins were digested with trypsin (Promega) *in situ* and extracted in a solution of 2% formic acid/2% acetonitrile. Digest analysis

was done by nano-scale capillary LC-MS/MS using an Ultimate U3000 HPLC in conjunction with a C18 Acclaim PepMap100 3 µm, 75 x 250 mm nanoViper (Thermo Fisher Scientific). Peptides were eluted with acetonitrile and analysed with a hybrid dual pressure linear ion trap mass spectrometer (Orbitrap XL, Thermo Fisher Scientific). MS spectra were collected over a m/z range of 300-2000 and searched against the UniProt KB database using the Mascot search engine programme (Perkins et al., 1999); Matrix Science, UK). Mass spectrometry data was analysed by comparing total spectral counts using Scaffold 4 (Keller et al., 2002); Proteome Software Inc.). For specifics of data evaluation please see Chapter 2 for description and discussion of different available methods.

6.10. *Drosophila* standard methods

All *Drosophila* stocks used in this work are listed below. Flies were grown at 18°C or 25°C on Iberian or Cornmeal food kindly provided by the MRC LMB media kitchen. *White*$^{-}$ or *yellow white*$^{-}$ (*yw*) fly strains were used as WT controls in all experiments. Embryos were collected by keeping flies in cages on apple plates supplemented with yeast paste and staging them depending on experimental requirements (see results section). Numbering of stages is according to the definition listed in Campos-Ortega, Jose A., Hartenstein, 1997.

Strain	Source
nos-Cas9	Bloomington: #54591, Bullock Lab, MRC LMB
nos-GAL4::VP16, UAS-Cas9	Bloomington: #54593, Bullock Lab, MRC LMB
yellow white	Bienz Lab
white	Bienz Lab
TM3/TM6	Bienz Lab
CyO/IF; Ki/TM6	Bienz Lab
nos-phiC31, attP2	Bullock Lab
w**; D** *P{FRT(w*^{hs}*)}2A/TM3, Sb*^{1}	Bloomington: #2024
hsFlp;; GFP.nls, FRT2A	Brown Lab, Gurdon Institute, Cambridge
w**; vgFlp, Ki/TM6*	Bienz Lab
w**; vgFlp; GFP.nls, FRT2A*	Bienz Lab

w;;FRT2A, ovo^{D}/DMS,e/TM3,Sb*	St Johnston Lab, Gurdon Institute, Cambridge
w; HsFlp; TM3/Dr*	Bienz Lab
alpha1.2 (expressing *UbxB* on II)	Bienz Lab, see Thüringer and Bienz, 1993
24B-UbxB (expressing *UbxB* from mesodermal driver *24B*)	Bienz Lab
Arm$^{S56F.GMR}$ (F76)	Freeman and Bienz, 2001
PYGO^{S123}	Thompson et al. (2002)
ssdp^{L7}/TM6c-twi::LacZ, Sb	van Meyel et al. (2003)
chip^{e55}	Morcillo et al. (1997)
Df(3L)BSC817/TM6c	Bloomington: #27578
Df(3L)BSC753/TM6c	Bloomington: #26851
Df(3L)ED4470	Bloomington: #8068
w;;FoxK^{16}/TM6b*	Casas Tinto et al. (2008)
w^{1118}; Mi{ET1}FoxK[MB02091]/TM3, Sb^{1}, Ser^{1}	Bloomington: #23964
cn^{1}, ry^{506}	Bienz Lab
TM3, ry/ebony, ry^{506}	Bienz Lab
CyO/black; ry^{506}	Bienz Lab
FM6; ry^{506}	Bienz Lab
yw, hsFlp122; mwh^{1}, jv, hs.CD22y[+]/TM3	Casal-Jimenez Lab, Zoology Dept., Cambridge
FoxK^{2}/TM6	edited in FoxK by sgRNA2, FOXK mutation not lethal, off-target lethality on chromosome III
FoxK^{10}/TM6	edited in FoxK by sgRNA2, FOXK mutation not lethal, off-target lethality on chromosome III
FoxK^{11}/TM6	edited in FoxK by sgRNA6, confirmed FoxK^{KO}
FoxK^{23}/TM6	edited in FoxK by sgRNA5, confirmed FoxK^{KO}
FoxK^{42}/TM6	edited in FoxK by sgRNA6, confirmed FoxK^{KO}

For DNA extraction from adult *Drosophila*, anaesthetised flies were transferred to PCR tubes and ground in 20 µl Squish buffer (10 mM Tris pH 8.0, 1 mM EDTA pH 7.4, 25 mM NaCl) using a pipette tip. Fly tissue was then subjected to a heat cycle programme consisting of repeated alternation between 65°C and 96°C for time intervals of 1-4 min each. 0.5-1.0 µl of the supernatant were directly used in PCR assays. Genotyping oligonucleotides are listed in the appendix, section 8.2.

Protein extraction from *Drosophila* larvae for western blot analysis was carried out by collecting 3rd instar larvae (~30 per strain) and dissecting the heads to remove fatty tissue. Samples were frozen on dry ice, 100 µl UBER buffer (20 mM Tris-HCl (pH 7.4), 10% glycerol, 200 mM NaCl, 0.2% Triton X-100, PhosphoSTOP (Roche)) added and tissue homogenised using a handheld homogeniser and pestle. Additional

homogenisation was achieved by loading the sample onto QIAshredder columns and centrifuging twice at 8,000 x *g* for 1 min each. The samples were then centrifuged at 21,130 x *g* for 10 min to pellet any debris and protein concentration estimated using a standard BCA assay as described above.

6.11. Fly transformation

Purified plasmids for transformation of fly strains were dissolved in injection buffer (0.1 mM Na_2HPO_4 (pH 6.8), 5 mM KCl) and injected into dechorionated stage 2 embryos at a concentration of 200 ng/µl unless stated otherwise. Stable integration of constructs was achieved either by PhiC31-mediated transformation or by random integration using a *rosy*$^+$ marker plasmid to track integration. In the latter case, insertions were mapped using balancer strains carrying visible markers in a homozygous *rosy*$^-$ background and several independent, viable insertion lines used in downstream assays.

6.12. CRISPR/Cas9 genome editing in *Drosophila*

Guide RNAs for CRISPR in *Drosophila* were designed using the target finder design tool available at crisprflydesign.org and ordered as single-stranded oligomers from Sigma-Aldrich. Oligomers were hybridised with their complementary strands in buffer by subjecting them to a thermocycler programme consisting of a denaturation step at 95°C to unfold the forward and reverse oligos followed by a step-wise decrease in temperature of 1°C/15 sec to 25°C for annealing. Oligonucleotides used in CRISPR experiments are listed in the appendix, section 8.3.

Double stranded oligomers were ligated into a *BbsI* restriction site of pCFD3-dU6:3gRNA (Addgene: #49410; kindly provided by Simon Bullock, MRC LMB (Port

et al., 2014)). The resulting sgRNA-containing plasmids were transformed into Mach1 *E. coli* cells and correct clones grown for plasmid isolation as described above.

Injection and fly crosses for CRISPR/Cas9 in *Drosophila* were carried out either via the so-called fast method, which bypasses generation of stable transformants expressing sgRNAs after integration into the genome, or via selection of sgRNA-expressing flies before crossing them to a Cas9 source, which is referred to as the slow method.

For the fast method, embryos expressing UAS-Cas9 in the germ line from a nos-Gal4::VP16 driver (Bloomington stock centre: #54593) were injected directly with sgRNA plasmid and hatching adults crossed individually to appropriate balancer flies (TM3/6 for editing on the 3rd chromosome). From each resulting line approx. 10 males or virgin females were again crossed to balancer flies to establish lines resulting from individually edited germ cells to ensure homogeneity within each line. The resulting lines were either preselected for the expected phenotype (e.g. homozygous lethality) or sequenced randomly.

While this method yields results approximately 3 weeks faster than the slow method, it is also less efficient, which is why I decided to use PhiC31-based stable sgRNA transformation in later stages of this work. To this end, sgRNAs were cloned into a variant of pCFD3-dU6:3sgRNA containing a *white*$^{+}$ marker rather than the original *vermillion*-marked plasmid. SgRNAs were stably integrated into the genome of nos-phiC31; attP2 flies (Bloomington: #25710) and transformants selected based on eye colour and then further crossed to nos-Cas9 flies (Bloomington: #54591). Progeny from this cross was selected based on darker red eye colour due to the combined expression of two *white*$^{+}$ alleles associated with the sgRNA and the Cas9 constructs, respectively, and outcrossed to balancer flies similarly as described above. All CRISPR alleles generated in this thesis are listed in the appendix, section 8.4.

The C-terminal truncation of FoxK to remove the putative PDZ binding element was generated by transient expression of the sgRNA construct which was injected simultaneously with a double-stranded DNA repair template carrying mutations to insert premature STOP codons. The repair template was designed to have asymmetric homology arms with ~90 bp on the side of the mutation and ~30 bp on the opposite side (see section 8.5). The construct was ordered as a dsDNA oligonucleotide from IDT (Integrated DNA Technologies, US) and used at 12.5 µM in injection buffer (see above). The oligo was not HPLC-purified as this can lead to toxicity effects in fly embryos.

Knock-out or truncation lines were confirmed by sequencing and, where available, western blot analysis as well as crosses to deficiency lines to confirm lethality at the appropriate locus as opposed to off-target loci.

6.13. IF of *Drosophila* embryos

Embryos collected on apple plates were transferred to falcons containing a mesh and washed under tap water to clear away yeast and other debris, before dechorionating in 100% bleach for 2-3 min. Following another wash step, embryos were transferred to fixative solution (75% heptane, 4% formaldehyde in PBS) and fixed under shaking for 30 min. The heptane-containing phase was removed and ice-cold methanol added before vigorously shaking the embryos for ~1 min to remove the vitelline membrane.

In order to remove any traces of fixative, embryos were further washed five times in 100% methanol before step-wise rehydration using methanol-PBS mixes with increasing concentrations of PBS (25%, 50%, 75%, 100%). Subsequently, PBT buffer was added for 30 min on a roller to permeabilise embryos before blocking in BBT buffer (PBS, 0.1% Tween-20 or 0.1% Triton X-100, 1% BSA) for 1-2 hrs at RT.

Collections were then incubated in primary antibody diluted in BBT buffer overnight at 4°C on a roller. Unbound antibody was removed by washing three times 10 min in BBT, followed by incubation with secondary antibody for 2-4 hrs. Following two further wash steps in BBT as well as one wash in PBT, embryos were transferred to microscope slides using a cut pipette tip to avoid squishing the embryos. Liquid was removed as much as possible before adding a drop of DAPI-containing mounting medium (Vectashield Hardset Antifade mounting media with DAPI, Vector Labs, USA). Slides were sealed with a cover slip and nail polish before imaging with a Zeiss LSM 510 confocal microscope and Z10 software.

6.14. IF of *Drosophila* wing discs

Per sample, around 20-30 3rd instar ("climbing") larvae were dissected in PBS to remove fatty tissue and the heads transferred to baskets in 24 well plates. Tissue was fixed in 4% formaldehyde in PBT for 30 min at RT. Samples were subsequently washed 5 times in PBT to remove any fixative and blocked in BBT for 1 hr at RT. Larval tissue was then transferred into microcentrifuge tubes in approximately 100 µl BBT containing the respective primary antibodies and stained overnight at 4°C. Primary antibodies were washed off through 3 incubations in BBT for 10 min each, before incubating with appropriate secondary antibodies for 2-4 hrs at RT in the dark. Following one additional wash step in BBT, samples were washed twice in PBT for 10 min each.

Discs were dissected from larval tissue and mounted in DAPI-containing medium with the "pouchy" side to the top to allow visibility of Wg-patterned tissue. Samples were imaged using a Zeiss LSM 510 confocal microscope. Z stacks were acquired with Zen software where appropriate and collapsed into 2D images using the ImageJ analysis tool.

6.15. 3,3'-diaminobenzidine (DAB) staining on *Drosophila* embryos

In order to analyse the embryonic gut phenotype, embryos were mounted in epoxy resin as this offers the advantage of being able to position the sample after fixation, which is impossible in hardset medium as used for fluorescence microscopy.

To this end, strains were used that express LacZ fusions of Wg target genes or carry a *TM6-twi::LacZ* balancer to distinguish homozygous mutant from heterozygous embryos. Embryos were stained with 3,3'-diaminobenzidine (DAB) allowing for use of a normal stereo microscope. This protocol follows the steps of the IF protocol (see 6.14.) up until the addition of primary antibody, for which an anti-LacZ antibody was used in overnight incubation.

Following three wash steps in BBT, embryos were incubated with a biotinylated secondary antibody for 2-4 hrs at RT on a roller. Biotinylated secondary antibody was washed off in 3 wash steps of 10 min each in PBT to remove all traces of azide, during which VECTASTAIN ABC reagent was prepared according to manufacturer's specifications (VECTASTAIN Elite ABC HRP Kit, Vector Labs, USA). Samples were incubated in ABC reagent for 30 min at RT on a roller before being washed in PBT 6 times for 5 min and transferred to staining dishes with a cavity. This step adds avidin/biotinylated peroxidase complexes (ABC) to the secondary antibody and thereby provides the substrate for subsequent DAB staining.

In quick succession, embryos were treated with 250 µl DAB (2 mg/ml in PBS), 12 µl cobalt-nickel mix (1% $CoCl_2$/1% $NiSO_4$) and 5 µl freshly prepared 0.3% hydrogen peroxide. The peroxidase complexed at sites where secondary antibody is bound is required to facilitate the reaction between DAB and hydrogen peroxide, which results in a brown precipitate. As soon as the first embryos showed brown staining the reaction was stopped by adding 1 ml PBT and quickly removing as much solution as possible to avoid overstaining. After a repeated wash step with PBT, embryos

were dehydrated in 100% ethanol before being placed in 100% methylsalicylate, transferred to microscopic slides and enclosed in epoxy resin (Araldite). Kept at -20°C, these preparations remain flexible enough to be manipulated directly under the microscope (Nikon Eclipse TE2000-E).

6.16. Preparation of *Drosophila* cuticles

Denticle belts of embryonic cuticle were analysed by collecting embryos of a *TM6-twi::GFP* balanced strain overnight in cages. Since loss of fluorescence due to metabolic degradation in dead embryos of homozygous mutants was a concern, embryos were directly sorted by GFP fluorescence onto separate apple plates and either left to develop for 48-72 hrs at 25°C to ensure maximum development for germ line clone experiments or used directly for all other experiments.

Embryos were subsequently incubated in bleach to remove the chorion and washed in PBS before being transferred to microscopic slides. Hoyer's medium (Wieschaus and Nüsslein-Vollhard, 1986) mixed with lactic acid (1:1) was used as mounting medium followed by overnight incubation at 65°C to allow the medium to set. Samples were imaged using a Nikon Eclipse TE2000-E microscope and analysed using Axio and ImageJ software.

6.17. Preparation of adult wings

In order to assess mutant clones in adult wings, flies were anaesthetised and dehydrated in 100% ethanol for 24 hrs. Wings were removed and mounted in a 6:5 mixture of lactic acid:ethanol and analysed with a Nikon Eclipse TE2000-E microscope.

6.18. Preparation and imaging of *Drosophila* eyes

Adult eye morphology was captured by photographing detached heads that were glued sideways onto a microscope slide. Images were acquired by mounting a Sony Alpha 6300 camera to a standard dissecting microscope and imaging at low magnification. Pictures were evaluated using ImageJ software by measuring eye area in pixels with the area measuring tool. Data points were found to be Gaussian distributed (Anderson-Darling and Shapiro-Wilk test in GraphPad Prism) and statistically analysed using one-way ANOVA analysis. Values are shown as mean and first and last quartile of at least n = 15 independent measurements per genotype.

6.19. Generation of homozygous mutant clones

Analysis of homozygous lethal mutations such as the *FoxK* alleles was achieved by recombining the mutant allele onto the appropriate FRT strain on chromosome 3L (*w**; *D** *P{FRT(w*^{hs}*)}2A/TM3, Sb*^{1}, insertion at 79D, for *FoxK*). Independently recombined lines were screened for loss of the *Dichaete* marker and confirmed by complementation with original lines.

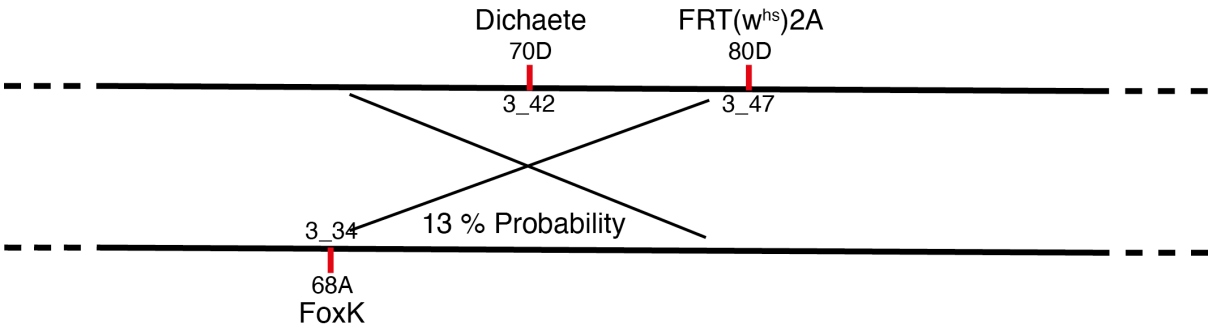

Figure 6.1. Cartoon of chromosome arm 3L with the *FoxK*, *Dichaete* and *FRT2A* loci marked.
According to the recombination map coordinates of *FoxK* and *FRT2A*, the probability of cross-over between both loci should be approx. 13%.

Mutant clones in the wing imaginal disc were generated using flippase constructs driven from a HS (*hsFlp, FRT2A*) or wing-specific (*vgFlp, FRT2A*) promoter. Twin spots were each marked by nuclear expression of GFP.

In order to assess the phenotype of complete null embryos, i.e. embryos lacking maternal contribution of the respective gene, germ line clone-derived embryos were obtained by making use of the ovoD technique (Chou and Perrimon, 1992). Mitotic recombination of females carrying a *hsFlp; FRT2A P{ovoD1}/FRT2A FoxK^{KO}* construct was induced with a single HS of 1.5-2 hrs at 37°C approximately 48-72 hrs post laying. Resulting female virgins were further crossed to *FoxK^{KO}* males balanced with *TM6-twi::GFP* for downstream IF analysis or *TM6-twi::LacZ* for downstream DAB staining.

6.20. Generation of α-FoxK antiserum

As no commercial antibody was available for *Drosophila* FoxK, custom antiserum was prepared by immunisation of rats with FoxK antigen. The following experiments were carried out in collaboration with Marc Fiedler (Bienz Lab, MRC LMB).

Antigenicity programmes such as SVMTriP (Yao et al., 2012) (http://sysbio.unl.edu/SVMTriP/) and the protein analysis tool of MacVector (https://macvector.com/MacVector/proteinanalysis.html) were used to determine the most suitable regions for immunisation, whereby the FKH domain was avoided in order to prevent cross-binding to other FOX proteins.

The antiserum was selected to bind to the unstructured region between the FHA and FKH domains of FoxK (amino acids 216-417) as this should allow discrimination of all FoxK mutant alleles generated in this work, all of which are truncated at or before the FHA domain and are thus not expected to be detected by this antiserum.

The resulting sequence was cloned from a *Drosophila* cDNA library (clone LD11294, Marc Fiedler, unpublished) into a Lip-tagged vector by Marc Fiedler and transformed into a phage-resistant BL21 *E. coli* strain. Transformed cells were grown in LB media to OD_{600} = 0.7 at 24°C and induced with 400 µM Isopropyl β-D-1-thiogalactopyranoside (IPTG) over 4 hrs for protein expression. Bacteria were pelleted at OD_{600} = 1.8 by centrifugation (4°C, 30 min at 4000 rpm) and flash-frozen in liquid nitrogen. Pellets were resuspended in lysis buffer (25 mM Tris-HCl pH 8.0, 200 mM NaCl, 20 mM Imidazole, 1 protease inhibitor tablet (EDTA-free, Roche)) at RT until thawed before adding 500 µl 100x DNase I. Cells were lysed through homogenisation with an Emulsiflex C-3 (Avestin) and cleared through centrifugation for 30 min at 35,000 rpm at 4°C.

The FoxK-Lip fusion protein was bound to a Nickel column by adding the supernatant of the lysed bacteria pellet to Nickel resin and incubating for 45-60 min on a roller at 4°C. Resin material was pelleted by centrifuging at 600 rpm for 3 min and washing in lysis buffer twice. In addition, one wash step with high salt buffer (1 M NaCl final concentration in lysis buffer) was included, followed by an additional wash in lysis buffer. The fusion protein was eluted by adding imidazole buffer (lysis buffer, 500 mM Imidazole).

Protein concentration was measured by dividing absorption at 280 nm with the extinction coefficient (0.432 for Lip-FoxK$^{216-417}$ as calculated using the ProtParam Tool (Gasteiger et al., 2005), available at https://web.expasy.org/protparam/). A fraction of this sample was used for TEV cleavage to cleave off the Lip-Tag by adding 12.5 µg/ml TEV protease and 10 mM DTT overnight at 4°C. As this resulted in precipitation of the cleaved protein construct, the uncleaved fraction was used for all further experiments including for animal immunisation. This bears the possible caveat of developing antibodies against the Lip-Tag; however, due to the low

antigenicity of the Lip tag this is not expected to interfere with the generation of α-FoxK antiserum.

Purified Lip-FoxK$^{216-417}$ was run on a gel filtration column (Sephadex G75, calibrated for small proteins) and fractions of the main peak (A4-A10, Figure 6.2) were applied to an SDS-PAGE (Bis-Tris 4-12%, MES buffer) for 35 min at 200V, then stained overnight in InstantBlue (Sigma Aldrich) and de-stained in distilled water.

The gel showed a largely clean sample with a higher molecular weight band characteristic of multimerisation of the protein (Figure 6.2, red arrow). 50 mM DTT were added to avoid the formation of disulphide bonds leading to these higher molecular weight species, which resolved this issue.

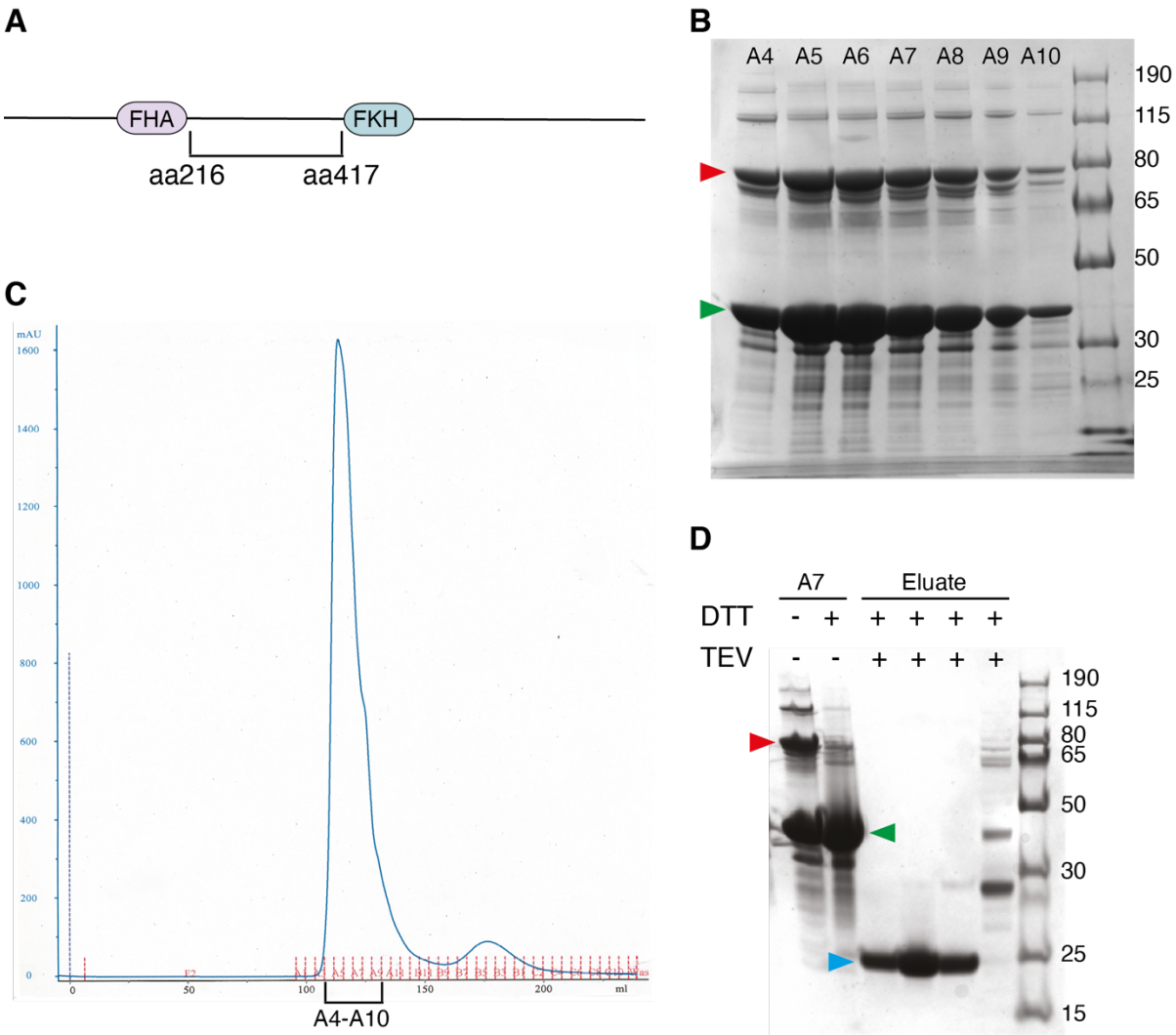

Figure 6.2. Preparation of Lip-FoxK$^{216-417}$ antigen for immunisation of rats for generation of FoxK antiserum.

A) Based on antigenicity analysis via SVMPTriP and the protein analysis tool of MacVector, the region between the FHA and FKH domains was chosen for immunisation, expressed as a Lip-tagged fusion protein in bacteria and purified using a Nickel resin.

B) - D) SDS-PAGE and Gel filtration were used to analyse purity of the sample. The Lip-FoxK fusion protein is expected to run at approx. 40kDa (green arrow in C & D), higher molecular weight bands (red arrow in C & D) indicate dimerisation, which was successfully resolved by addition of 50 mM DTT. TEV cleavage to cut off the Lip tag led to precipitation leaving only the Lip tag in the supernatant (blue arrow in D).

Purified antigen was shipped to Eurogentec in DTT buffer and used for injection of two rats followed by application of their 28-day Speedy Programme. Final bleed antiserum was used without purification for western blot analysis of FoxK mutant flies, whereas use of this FoxK antiserum in IF required further purification.

To this end, 50 µg/well Lip-FoxK$^{216-417}$ antigen was loaded onto a NuPAGE 4-12% Bis-Tris protein gels (Invitrogen) and run at 200V for 35 min. The antigen was transferred onto PVDF membrane by semi-dry transfer (100V, 1:15 h) and the membrane stained with Ponceau S (0.5% (w/v) Ponceau S, 1% acetic acid).

The membrane section containing the antigen was then cut out as small as possible and cut into smaller pieces that were transferred to a 2 ml centrifuge tube and blocked with 5% milk in PBT for 1 hr at RT. The membrane pieces were then washed 3 times in PBT before adding 2 ml antiserum for overnight shaking at 4°C. This was followed by 3 washes in PBT before eluting the antibody from the membrane with 500 µl 100 mM glycine (pH 2.5) for 1 min. The supernatant was then added to 100 µl 1 M Tris-HCl (pH 8.0) to neutralise the solution. Elution was repeated twice and the respective eluates kept separately for testing on western blot. Purified antibody was kept at 4°C in Tris-HCl (pH 8.0).

7. Literature

Affolter, M., Marty, T., Vigano, M.A., and Jazwinska, A. (2001). Nuclear interpretation of Dpp signaling in Drosophila. EMBO J. *20*, 3298–3305.

Agarwal, M., Kumar, P., and Mathew, S.J. (2015). The Groucho/Transducin-like enhancer of split protein family in animal development. IUBMB Life *67*, 472–481.

Ahn, H., Sim, J., Abdul, R., Chung, M.S., Paik, S.S., Oh, Y.H., Park, C.K., and Jang, K. (2015). Increased expression of forkhead box M1 is associated with aggressive phenotype and poor prognosis in estrogen receptor-positive breast cancer. J. Korean Med. Sci. *30*, 390–397.

Alexandre, C., Lecourtois, M., and Vincent, J.P. (1999). Wingless and Hedgehog pattern Drosophila denticle belts by regulating the production of short-range signals. Development *126*, 5689–5698.

Alexandre, C., Baena-Lopez, A., and Vincent, J.P. (2014). Patterning and growth control by membrane-tethered wingless. Nature *505*, 180–185.

Arend, R.C., Londoño-Joshi, A.I., Straughn, J.M., and Buchsbaum, D.J. (2013). The Wnt/β-catenin pathway in ovarian cancer: A review. Gynecol. Oncol. *131*, 772–779.

Aronson, B.D., Fisher, A.L., Blechman, K., Caudy, M., and Gergen, J.P. (1997). Groucho-dependent and -independent repression activities of Runt domain proteins. Mol. Cell. Biol. *17*, 5581–5587.

Axelrod, J.D., Miller, J.R., Shulman, J.M., Moon, R.T., and Perrimon, N. (1998). Differential recruitment of dishevelled provides signaling specificity in the planar cell polarity and Wingless signaling pathways. Genes Dev. *12*, 2610–2622.

Baker, N.E. (1988). Transcription of the segment-polarity gene wingless in the imaginal discs of Drosophila, and the phenotype of a pupal-lethal wg mutation. Development *102*, 489–497.

Barker, N., Hurlstone, a, Musisi, H., Miles, a, Bienz, M., and Clevers, H. (2001). The chromatin remodelling factor Brg-1 interacts with beta-catenin to promote target gene activation. EMBO J. *20*, 4935–4943.

Barolo, S., Stone, T., Bang, A.G., and Posakony, J.W. (2002). Default repression and Notch signaling: Hairless acts as an adaptor to recruit the corepressors Groucho and dCtBP to suppressor of hairless. Genes Dev. *16*, 1964–1976.

Barry, E.R., Morikawa, T., Butler, B.L., Shrestha, K., de la Rosa, R., Yan, K.S., Fuchs, C.S., Magness, S.T., Smits, R., Ogino, S., et al. (2013). Restriction of intestinal stem cell expansion and the regenerative response by YAP. Nature *493*, 106–110.

Bassel-Duby, R., Hernandez, M.D., Yang, Q., Rochelle, J.M., Seldin, M.F., and Williams, R.S. (1994). Myocyte nuclear factor, a novel winged-helix transcription factor under both developmental and neural regulation in striated myocytes. Mol. Cell. Biol. *14*, 4596–4605.

Bejsovec, A. (2006). Flying at the head of the pack : Wnt biology in Drosophila. Oncogene *25*, 7442–7449.

Bejsovec, A., and Arias, A.M. (1991). Roles of wingless in patterning the larval epidermis of Drosophila. Development *113*, 471–485.

Bejsovec, A., and Wieschaus, E. (1993). Segment polarity gene interactions modulate epidermal patterning in Drosophila embryos. Development *119*, 501–517.

Bienz, M. (1994). Homeotic genes and positional signalling in the Drosophila viscera. Trends Genet. *10*, 22–26.

Bienz, M. (2005). ß-Catenin: A Pivot between Cell Adhesion and Wnt Signalling. Curr. Biol. *15*, 64–67.

Bienz, M. (2014). Signalosome assembly by domains undergoing dynamic head-to-tail polymerization. Trends Biochem. Sci. *39*, 487–495.

Bienz, M., and Tremml, G. (1988). Domain of Ultrabithorax expression in Drosophila visceral mesoderm from autoregulation and exclusion. Nature *333*, 576–578.

Bodmer, R. (1993). The gene tinman is required for specification of the heart and visceral muscles in Drosophila. *729*, 719–729.

Bordeleau, M.E., Aucagne, R., Chagraoui, J., Girard, S., Mayotte, N., Bonneil, É., Thibault, P., Pabst, C., Bergeron, A., Barabé, F., et al. (2014). UBAP2L is a novel

BMI1-interacting protein essential for hematopoietic stem cell activity. Blood *124*, 2362–2369.

Bowman, C.J., Ayer, D.E., and Dynlacht, B.D. (2014). Foxk proteins repress the initiation of starvation-induced atrophy and autophagy programs. Nat. Cell Biol. *16*, 1202–1214.

Bramwell, M.E. (1987). Characterization of biotinylated proteins in mammalian cells using 125I-streptavidin. J. Biochem. Biophys. Methods *15*, 125–132.

Branon, T.C., Bosch, J.A., Sanchez, A.D., Udeshi, N.D., Svinkina, T., Carr, S.A., Feldman, J.L., Perrimon, N., and Ting, A.Y. (2018). Efficient proximity labeling in living cells and organisms with TurboID. Nat. Biotechnol. *36*, 880–898.

Brantjes, H., Roose, J., van De Wetering, M., and Clevers, H. (2001). All Tcf HMG box transcription factors interact with Groucho-related co-repressors. Nucleic Acids Res. *29*, 1410–1419.

Brauchle, M., Yao, Z., Arora, R., Thigale, S., Clay, I., Inverardi, B., Fletcher, J., Taslimi, P., Acker, M.G., Gerrits, B., et al. (2013). Protein Complex Interactor Analysis and Differential Activity of KDM3 Subfamily Members Towards H3K9 Methylation. PLoS One *8*, 1–12.

Brent, M.M., Anand, R., and Marmorstein, R. (2008). Structural Basis for DNA Recognition by FoxO1 and Its Regulation by Posttranslational Modification. Structure *16*, 1407–1416.

Brinkman, E.K., Chen, T., Amendola, M., and Van Steensel, B. (2014). Easy quantitative assessment of genome editing by sequence trace decomposition. Nucleic Acids Res. *42*, 1–8.

Buglo, E., Sarmiento, E., Martuscelli, N.B., Sant, D.W., Danzi, M.C., Abrams, A.J., Dallman, J.E., and Züchner, S. (2020). Genetic compensation in a stable slc25a46 mutant zebrafish: A case for using F0 CRISPR mutagenesis to study phenotypes caused by inherited disease. PLoS One *15*, 1–19.

Busser, B.W., Haimovich, J., Huang, D., Ovcharenko, I., and Michelson, A.M. (2015). Enhancer modeling uncovers transcriptional signatures of individual cardiac cell states

in Drosophila. Nucleic Acids Res. *43*, 1726–7139.

Cadigan, K.M., Grossniklaus, U., and Gehring, W.J. (1994). Localized expression of sloppy paired protein maintains the polarity of Drosophila parasegments. Genes Dev. *8*, 899–913.

Campos-Ortega, Jose A., Hartenstein, V. (1997). The Embryonic Development of Drosophila melanogaster.

Casas-Tinto, S., Gomez-Velazquez, M., Granadino, B., and Fernandez-Funez, P. (2008). FoxK mediates TGF-β signalling during midgut differentiation in flies. J. Cell Biol. *183*, 1049–1060.

Cavallo, R. a, Cox, R.T., Moline, M.M., Roose, J., Polevoy, G. a, Clevers, H., Peifer, M., and Bejsovec, a (1998). Drosophila Tcf and Groucho interact to repress Wingless signalling activity. Nature *395*, 604–608.

Chae, W.J., Henegariu, O., Lee, S.K., and Bothwell, A.L.M. (2006). The mutant leucine-zipper domain impairs both dimerization and suppressive function of Foxp3 in T cells. Proc. Natl. Acad. Sci. U. S. A. *103*, 9631–9636.

Chaudhary, V., Hingole, S., Frei, J., Port, F., Strutt, D., and Boutros, M. (2019). Robust Wnt signaling is maintained by a Wg protein gradient and Fz2 receptor activity in the developing Drosophila wing. Development *146*, 1–12.

Cheah, P.Y., Chia, W., and Yang, X. (2000). Jumeaux, a novel Drosophila winged-helix family protein, is required for generating asymmetric sibling neuronal cell fates. Development *127*, 3325–3335.

Chen, C., and Struhl, G. (1999). Wingless transduction by the Frizzled and Frizzled2 proteins of Drosophila. Development *126*, 5441–5452.

Chen, G., and Courey, A.J. (2000). Groucho/TLE family proteins and transcriptional repression. Gene *249*, 1–16.

Chen, G., Fernandez, J., Mische, S., and Courey, A.J. (1999). A functional interaction between the histone deacetylase Rpd3 and the corepressor Groucho in Drosophila development. Genes Dev. *13*, 2218–2230.

Chen, M., Zhu, N., Liu, X., Laurent, B., Tang, Z., Eng, R., Shi, Y., Armstrong, S.A., and Roeder, R.G. (2015a). JMJD1C is required for the survival of acute myeloid leukemia by functioning as a coactivator for key transcription factors. Genes Dev. *29*, 2123–2139.

Chen, X., Ji, Z., Webber, A., and Sharrocks, A.D. (2015b). Genome-wide binding studies reveal DNA binding specificity mechanisms and functional interplay amongst Forkhead transcription factors. Nucleic Acids Res. *44*, 1566–1578.

Cheyette, B.N.R., Waxman, J.S., Miller, J.R., Takemaru, K.I., Sheldahl, L.C., Khlebtsova, N., Fox, E.P., Earnest, T., and Moon, R.T. (2002). Dapper, a Dishevelled-associated antagonist of β-catenin and JNK signaling, is required for notochord formation. Dev. Cell *2*, 449–461.

Chodaparambil, J. V., Pate, K.T., Hepler, M.R.D., Tsai, B.P., Muthurajan, U.M., Luger, K., Waterman, M.L., and Weis, W.I. (2014). Molecular functions of the TLE tetramerization domain in Wnt target gene repression. EMBO J. *33*, 719–731.

Chou, T.B., and Perrimon, N. (1992). Use of a yeast site-specific recombinase to generate embryonic mosaics in Drosophila. Dev. Genet. *13*, 367–375.

Chou, T.B., Noll, E., and Perrimon, N. (1993). Autosomal P[ovoD1] dominant female-sterile insertions in Drosophila and their use in geanerating germ-line chimeras. Development *119*, 1359–1369.

Cirillo, L.A., Lin, F.R., Cuesta, I., Friedman, D., Jarnik, M., and Zaret, K.S. (2002). Opening of compacted chromatin by early developmental transcription factors HNF3 (FoxA) and GATA-4. Mol. Cell *9*, 279–289.

Clark, K.L., Halay, E.D., Lai, E., and Burley, S.K. (1993). Co-crystal structure of the HNF-3/fork head DNA-recognition motif resembles histone H5. Nature *364*, 412–420.

Collins, R.T., and Treisman, J.E. (2000). Osa-containing Brahma chromatin remodeling complexes are required for the repression of Wingless target genes. Genes Dev. *14*, 3140–3152.

Colombani, J., Andersen, D.S., and Léopol, P. (2012). Secreted peptide dilp8 coordinates Drosophila tissue growth with developmental timing. Science (80-.). *336*,

582–585.

Couso, J.P., and Arias, A.M. (1994). Notch is required for wingless signaling in the epidermis of Drosophila. Cell *79*, 259–272.

Cuesta, I., Zaret, K.S., and Santisteban, P. (2007). The Forkhead Factor FoxE1 Binds to the Thyroperoxidase Promoter during Thyroid Cell Differentiation and Modifies Compacted Chromatin Structure. Mol. Cell. Biol. *27*, 7302–7314.

Daniels, D.L., and Weis, W.I. (2005). β-catenin directly displaces Groucho/TLE repressors from Tcf/Lef in Wnt-mediated transcription activation. Nat. Struct. Mol. Biol. *12*, 364–371.

Dasgupta, S., Lonard, D.M., and O'Malley, B.W. (2014). Nuclear Receptor Coactivators: Master Regulators of Human Health and Disease. Annu. Rev. Med. *65*, 279–292.

De, A. (2011). Wnt / Ca 21 signaling pathway : a brief overview The Non-canonical Wnt Signaling Cascade. Acta Biochim. Biophys. Hung. *43*, 745–756.

Dehner, M., Hadjihannas, M., Weiske, J., Huber, O., and Behrens, J. (2008). Wnt signaling inhibits forkhead box O3a-induced transcription and apoptosis through up-regulation of serum- and glucocorticoid-inducible kinase 1. J. Biol. Chem. *283*, 19201–19210.

Doucas, H., Garcea, G., Neal, C.P., Manson, M.M., and Berry, D.P. (2005). Changes in the Wnt signalling pathway in gastrointestinal cancers and their prognostic significance. Eur. J. Cancer *41*, 365–379.

Duman-Scheel, M., Johnston, L.A., and Du, W. (2004). Repression of dMyc expression by Wingless promotes Rbf-induced G 1 arrest in the presumptive Drosophila wing margin. Proc. Natl. Acad. Sci. U. S. A. *101*, 3857–3862.

Durocher, D., Henckel, J., Fersht, A.R., and Jackson, S.P. (1999). The FHA Domain Is a Modular Phosphopeptide Recognition Motif. Mol. Cell *4*, 387–394.

Edmunds, J.W., Mahadevan, L.C., and Clayton, A.L. (2008). Dynamic histone H3 methylation during gene induction: HYPB/Setd2 mediates all H3K36 trimethylation.

EMBO J. *27*, 406–420.

El-Brolosy, M.A., Kontarakis, Z., Rossi, A., Kuenne, C., Günther, S., Fukuda, N., Kikhi, K., Boezio, G.L.M., Takacs, C.M., Lai, S.L., et al. (2019). Genetic compensation triggered by mutant mRNA degradation. Nature *568*, 193–197.

Estella, C., Mckay, D.J., and Mann, R.S. (2008). Molecular integration of Wingless, Decapentaplegic, and autoregulatory inputs into Distalless during Drosophila leg development. Development *14*, 86–96.

Fiedler, M., Sánchez-Barrena, M.J., Nekrasov, M., Mieszczanek, J., Rybin, V., Müller, J., Evans, P., and Bienz, M. (2008). Decoding of Methylated Histone H3 Tail by the Pygo-BCL9 Wnt Signaling Complex. Mol. Cell *30*, 507–518.

Fiedler, M., Mendoza-Topaz, C., Rutherford, T.J., Mieszczanek, J., and Bienz, M. (2011). Dishevelled interacts with the DIX domain polymerization interface of Axin to interfere with its function in down-regulating β-catenin. Proc. Natl. Acad. Sci. U. S. A. *108*, 1937–1942.

Fiedler, M., Graeb, M., Mieszczanek, J., Rutherford, T.J., Johnson, C.M., and Bienz, M. (2015). An ancient Pygo-dependent Wnt enhanceosome integrated by chip/LDB-SSDP. Elife *4*, 1–22.

Fisher, A.L., Ohsako, S., and Caudy, M. (1996). The WRPW motif of the hairy-related basic helix-loop-helix repressor proteins acts as a 4-amino-acid transcription repression and protein-protein interaction domain. Mol. Cell. Biol. *16*, 2670–2677.

Flack, J.E., Mieszczanek, J., Novcic, N., and Bienz, M. (2017). Wnt-Dependent Inactivation of the Groucho/TLE Co-repressor by the HECT E3 Ubiquitin Ligase Hyd/UBR5. Mol. Cell *67*, 181-193.e5.

Freeman, M., and Bienz, M. (2001). EGF receptor / Rolled MAP kinase signalling protects cells against activated Armadillo in the Drosophila eye. EMBO Rep. *2*, 157–162.

Gammons, M., and Bienz, M. (2018). Multiprotein complexes governing Wnt signal transduction. Curr. Opin. Cell Biol. *51*, 42–49.

Gammons, M. V., Rutherford, T.J., Steinhart, Z., Angers, S., and Bienz, M. (2016a). Essential role of the Dishevelled DEP domain in a Wnt-dependent human-cell-based complementation assay. J. Cell Sci. *129*, 3892–3902.

Gammons, M.V., Renko, M., Johnson, C.M., Rutherford, T.J., and Bienz, M. (2016b). Wnt Signalosome Assembly by DEP Domain Swapping of Dishevelled. Mol. Cell *64*, 92–104.

Gan, X.Q., Wang, J.Y., Xi, Y., Wu, Z.L., Li, Y.P., and Li, L. (2008). Nuclear Dvl, c-Jun, ??-catenin, and TCF form a complex leading to stabilization of ??-catenin-TCF interaction. J. Cell Biol. *180*, 1087–1100.

Gao, X.D., Tu, L., Mir, A., Rodriguez, T., Ding, Y., Leszyk, J., Dekker, J., Shaffer, S.A., Zhu, L.J., Wolfe, S.A., et al. (2018). C-BERST: defining subnuclear proteomic landscapes at genomic elements with dCas9–APEX2. Nat. Methods.

Gasteiger, E., Hoogland, C., Gattiker, A., Duvaud, S., Wilkins, M.R., Appel, R.D., and Bairoch, A. (2005). The Proteomics Protocols Handbook. Proteomics Protoc. Handb. 571–608.

Ge, S.X., Jung, D., and Yao, R. (2019). ShinyGO: a graphical gene-set enrichment tool for animals and plants. Bioinformatics *36*, 2628–2629.

Gibson, D.G., Young, L., Chuang, R.-Y., Venter, J.C., Hutchison, C. a, Smith, H.O., Iii, C.A.H., and America, N. (2009). Enzymatic assembly of DNA molecules up to several hundred kilobases. Nat. Methods *6*, 343–345.

Giles, R.H., Van Es, J.H., and Clevers, H. (2003). Caught up in a Wnt storm: Wnt signaling in cancer. Biochim. Biophys. Acta - Rev. Cancer *1653*, 1–24.

Grossniklaus, U., Pearson, R.K., and Gehring, W.J. (1992). The Drosophila sloppy paired locus encodes two proteins involved in segmentation that show homology to mammalian transcription factors. Genes Dev. *6*, 1030–1051.

Häcker, U., Kaufmann, E., Hartmann, C., Jürgens, G., Knöchel, W., and Jäckle, H. (1995). The Drosophila fork head domain protein crocodile is required for the establishment of head structures. EMBO J. *14*, 5306–5317.

Hakimi, M.A., Dong, Y., Lane, W.S., Speicher, D.W., and Shiekhattar, R. (2003). A candidate X-linked mental retardation gene is a component of a new family of histone deacetylase-containing complexes. J. Biol. Chem. *278*, 7234–7239.

Han, B., Qu, Y., Jin, Y., Yu, Y., Deng, N., Wawrowsky, K., Zhang, X., Li, N., Bose, S., Wang, Q., et al. (2015). FOXC1 Activates Smoothened-Independent Hedgehog Signaling in Basal-like Breast Cancer. Cell Rep. *13*, 1046–1058.

Hancock, W.W., and Oezkaynak, E. (2009). Three Distinct Domains Contribute to Nuclear Transport of Murine Foxp3. PLoS One *4*, 1–6.

Hanson, A.J., Wallace, H.A., Freeman, T.J., Beauchamp, R.D., Lee, L.A., and Lee, E. (2012). XIAP Monoubiquitylates Groucho/TLE to Promote Canonical Wnt Signaling. Mol. Cell *45*, 619–628.

Hatta, M., and Cirillo, L.A. (2007). Chromatin opening and stable perturbation of core histone:DNA contacts by FoxO1. J. Biol. Chem. *282*, 35583–35593.

Hecht, a, Vleminckx, K., Stemmler, M.P., van Roy, F., and Kemler, R. (2000). The p300/CBP acetyltransferases function as transcriptional coactivators of beta-catenin in vertebrates. EMBO J. *19*, 1839–1850.

van der Heide, L.P., Wijchers, P.J.E.C., von Oerthel, L., Burbach, J.P.H., Hoekman, M.F.M., and Smidt, M.P. (2015). FoxK2 is required for cellular proliferation and survival. J. Cell. Physiol. *230*, 1013–1023.

Hikasa, H., and Sokol, S.Y. (2011). Phosphorylation of TCF proteins by homeodomain-interacting protein kinase 2. J. Biol. Chem. *286*, 12093–12100.

Hofmann, K., and Bucher, P. (1995). The FHA domain: a putative nuclear signalling domain found in protein kinases and transcription factors. Trends Biochem. Sci. *20*, 347–349.

Holland, D.G., Burleigh, A., Git, A., Goldgraben, M.A., Perez-Mancera, P.A., Chin, S.F., Hurtado, A., Bruna, A., Ali, H.R., Greenwood, W., et al. (2011). ZNF703 is a common Luminal B breast cancer oncogene that differentially regulates luminal and basal progenitors in human mammary epithelium. EMBO Mol. Med. *3*, 167–180.

Holmes, K.A., Hurtado, A., Brown, G.D., Launchbury, R., Ross-innes, C.S., Hadfield, J., Odom, D.T., Carroll, J.S., and Chip, T.L.E. (2012). Transducin-like enhancer protein 1 mediates estrogen receptor binding and transcriptional activity in breast cancer cells. PNAS *109*, 2748–2753.

Hoppler, S., and Bienz, M. (1994). Specification of a Single Cell Type by a Drosophila Homeotic Gene. Cell *76*, 569–702.

Hoppler, S., and Bienz, M. (1995). Two different thresholds of wingless signalling with distinct developmental consequences in the Drosophila midgut. EMBO J. *14*, 5016–5026.

Horton, J.R., Upadhyay, A.K., Qi, H.H., Zhang, X., Shi, Y., and Cheng, X. (2010). Enzymatic and structural insights for substrate specificity of a family of jumonji histone lysine demethylases. Nat. Struct. Mol. Biol. *17*, 38–44.

Ikeda, S., Kishida, S., Yamamoto, H., Murai, H., Koyama, S., and Kikuchi, A. (1998). Axin, a negative regulator of the Wnt signaling pathway, forms a complex with GSK-3β and β-catenin and promotes GSK-3β-dependent phosphorylation of β-catenin. EMBO J. *17*, 1371–1384.

Ingham, P.W., Baker, N.E., and Martinez-Arias, A. (1988). Regulation of segment polarity genes in the Drosophila blastoderm by fushi tarazu and even skipped. Nature *331*, 73–75.

Itoh, K., Brott, B.K., Bae, G.-U., Ratcliffe, M.J., and Sokol, S.Y. (2005). Nuclear localization is required for Dishevelled function in Wnt/beta-catenin signaling. J. Biol. *4*, 12.

Iwafuchi-Doi, M., Donahue, G., Kakumanu, A., Watts, J.A., Mahony, S., Pugh, B.F., Lee, D., Kaestner, K.H., and Zaret, K.S. (2016). The Pioneer Transcription Factor FoxA Maintains an Accessible Nucleosome Configuration at Enhancers for Tissue-Specific Gene Activation. Mol. Cell *62*, 79–91.

Jennings, B.H., Pickles, L.M., Wainwright, S.M., Roe, S.M., Pearl, L.H., and Ish-horowicz, D. (2006). Molecular Recognition of Transcriptional Repressor Motifs by the WD Domain of the Groucho / TLE Corepressor. Mol. Cell *22*, 645–655.

Jürgens, G., and Weigel, D. (1988). Terminal versus segmental development in the Drosophila embryo: the role of the homeotic gene fork head. Roux's Arch. Dev. Biol. *197*, 345–354.

Kadoch, C., and Crabtree, G.R. (2015). Mammalian SWI/SNF chromatin remodeling complexes and cancer: Mechanistic insights gained from human genomics. Sci. Adv. *1*, 1–17.

Kaestner, K.H. (2010). The FoxA factors in organogenesis and differentiation. Curr. Opin. Genet. Dev. *20*, 527–532.

Kaestner, K.H., Knöchel, W., Martínez, D.E., Kno, W., and Martı, D.E. (2000). Unified nomenclature for the winged helix / forkhead transcription factors. Genes Dev. *14*, 142–146.

Keller, A., Nesvizhskii, A.I., Kolker, E., and Aebersold, R. (2002). Empirical statistical model to estimate the accuracy of peptide identifications made by MS/MS and database search. Anal. Chem. *74*, 5383–5392.

Kelley, L.A., Mezulis, S., Yates, C.M., Wass, M.N., and Sternberg, M.J.E. (2015). The Phyre2 web portal for protein modeling, prediction and analysis. Nat. Protoc. *10*, 845–858.

Kim, C.A., Phillips, M.L., Kim, W., Gingery, M., Tran, H.H., Robinson, M.A., Faham, S., and Bowie, J.U. (2001). Polymerization of the SAM domain of TEL in leukemogenesis and transcriptional repression. EMBO J. *20*, 4173–4182.

Kim, D.I., Jensen, S.C., Noble, K.A., KC, B., Roux, K.H., Motamedchaboki, K., and Roux, K.J. (2016). An improved smaller biotin ligase for BioID proximity labeling. Mol. Biol. Cell *27*, 1188–1196.

Kim, J., Sebring, A., Esch, J.J., Kraus, M.E., Vorwerk, K., Magee, J., and Carroll, S.B. (1996). Integration of positional signals and regulation of wing formation and identity by Drosophila vestigial gene. Nature *382*, 133–138.

Kim, S.M., Kim, J.Y., Choe, N.W., Cho, I.H., Kim, J.R., Kim, D.W., Seol, J.E., Lee, S.E., Kook, H., Nam, K. Il, et al. (2010). Regulation of mouse steroidogenesis by WHISTLE and JMJD1C through histone methylation balance. Nucleic Acids Res. *38*,

6389–6403.

King, H.W., and Klose, R.J. (2017). The pioneer factor OCT4 requires the chromatin remodeller BRG1 to support gene regulatory element function in mouse embryonic stem cells. Elife *6*, 1–24.

Knirr, S., and Frasch, M. (2001). Molecular integration of inductive and mesoderm-intrinsic inputs governs even-skipped enhancer activity in a subset of pericardial and dorsal muscle progenitors. Dev. Biol. *238*, 13–26.

Korinek, V., Barker, N., Morin, P.J., van Wichen, D., de Weger, R., Kinzler, K.W., Vogelstein, B., and Clevers, H. (1997). Constitutive transcriptional activation by a beta-catenin-Tcf complex in APC-/- colon carcinoma. Science (80-.). *275*, 1784–1787.

Kosugi, S., Hasebe, M., Tomita, M., and Yanagawa, H. (2009). Systematic identification of cell cycle-dependent yeast nucleocytoplasmic shuttling proteins by prediction of composite motifs. Proc. Natl. Acad. Sci. U. S. A. *106*, 10171–10176.

Kramps, T., Peter, O., Brunner, E., Nellen, D., Froesch, B., Chatterjee, S., Murone, M., Züllig, S., and Basler, K. (2002). Wnt/Wingless signaling requires BCL9/legless-mediated recruitment of pygopus to the nuclear ??-catenin-TCF complex. Cell *109*, 47–60.

Kumar, A., Chalamalasetty, R.B., Kennedy, M.W., Thomas, S., Inala, S.N., Garriock, R.J., and Yamaguchi, T.P. (2016). Zfp703 Is a Wnt/b-Catenin Feedback Suppressor Targeting the b-Catenin/Tcf1 Complex. Mol. Cell. Biol. *36*, 1793–1802.

de la Roche, M., and Bienz, M. (2007). Wingless-Independent Association of Pygopus with dTCF Target Genes. Curr. Biol. *17*, 556–561.

Laissue, P. (2019). The forkhead-box family of transcription factors: key molecular players in colorectal cancer pathogenesis. Mol. Cancer *18*, 1–13.

Lawrence, P., Johnston, P., and Morata, G. (1986). Methods of Marking Cells. In Drosophila: A Practical Approach, pp. 229–242.

Lee, H.H., and Frasch, M. (2000). Wingless effects mesoderm patterning and ectoderm segmentation events via induction of its downstream target sloppy paired.

Development *127*, 5497–5508.

Lee, H.H., and Frasch, M. (2004). Survey of Forkhead Domain Encoding Genes in the Drosophila Genome: Classification and Embryonic Expression Patterns. Dev. Dyn. *229*, 357–366.

Lee, H.H., and Frasch, M. (2005). Nuclear integration of positive Dpp signals, antagonistic Wg inputs and mesodermal competence factors during Drosophila visceral mesoderm induction. Development *132*, 1429–1442.

Lee, H.J., Shi, D.L., and Zheng, J.J. (2015). Conformational change of dishevelled plays a key regulatory role in the wnt signaling pathways. Elife *4*, 1–15.

Lee, J.W., Kim, D.M., Jang, J.W., Park, T.G., Song, S.H., Lee, Y.S., Chi, X.Z., Park, I.Y., Hyun, J.W., Ito, Y., et al. (2019). RUNX3 regulates cell cycle-dependent chromatin dynamics by functioning as a pioneer factor of the restriction-point. Nat. Commun. *10*.

Lehner, B., Semple, J.I., Brown, S.E., Counsell, D., Campbell, R.D., and Sanderson, C.M. (2004). Analysis of a high-throughput yeast two-hybrid system and its use to predict the function of intracellular proteins encoded within the human MHC class III region. Genomics *83*, 153–167.

Lempiäinen, J.K., Niskanen, E.A., Vuoti, K., Lampinen, R.E., Göös, H., Varjosalo, M., and Palvimo, J.J. (2017). Agonist-specific protein interactomes of glucocorticoid and androgen receptor as revealed by proximity mapping. Mol. Cell. Proteomics 1–42.

Levanon, D., Goldstein, R.E., Bernstein, Y., Tang, H., Goldenberg, D., Stifani, S., Paroush, Z., and Groner, Y. (1998). Transcriptional repression by AML1 and LEF-1 is mediated by the TLE/Groucho corepressors. Proc. Natl. Acad. Sci. U. S. A. *95*, 11590–11595.

Li, B., Mackay, D.R., Ma, J., and Dai, X. (2004). Cloning and developmental expression of mouse pygopus 2, a putative Wnt signaling component. Genomics *84*, 398–405.

Li, V.S.W., Ng, S.S., Boersema, P.J., Low, T.Y., Karthaus, W.R., Gerlach, J.P., Mohammed, S., Heck, A.J.R., Maurice, M.M., Mahmoudi, T., et al. (2012). Wnt Signaling through Inhibition of β-Catenin Degradation in an Intact Axin1 Complex. Cell

149, 1245–1256.

Liu, C., Li, Y., Semenov, M., Han, C., Baeg, G., Tan, Y., Zhang, Z., Lin, X., and He, X. (2002). Control of b-Catenin Phosphorylation / Degradation by a Dual-Kinase Mechanism. Cell *108*, 837–847.

Liu, H., Sadygov, R.G., and Yates, J.R. (2004). A Model for Random Sampling and Estimation of Relative Protein Abundance in Shotgun Proteomics proteolytic digestion and liquid chromatography in com-. Anal. Chem. *76*, 4193–4201.

Liu, Y., Ding, W., Ge, H., Ponnusamy, M., Wang, Q., Hao, X., Wu, W., Zhang, Y., Yu, W., Ao, X., et al. (2019). FOXK transcription factors: Regulation and critical role in cancer. Cancer Lett. *458*, 1–12.

Liu, Y.T., Dan, Q.J., Wang, J., Feng, Y., Chen, L., Liang, J., Li, Q., Lin, S.C., Wang, Z.X., and Wu, J.W. (2011). Molecular basis of Wnt activation via the DIX domain protein Ccd1. J. Biol. Chem. *286*, 8597–8608.

Lloyd, R.S., Haidle, C.W., and Robberson, D.L. (1978). Bleomycin-Specific Fragmentation of Double-Stranded DNA. Biochemistry *17*, 1890–1896.

Loh, K.M., van Amerongen, R., and Nusse, R. (2016). Generating Cellular Diversity and Spatial Form: Wnt Signaling and the Evolution of Multicellular Animals. Dev. Cell *38*, 643–655.

López-García, C., Sansregret, L., Domingo, E., McGranahan, N., Hobor, S., Birkbak, N.J., Horswell, S., Grönroos, E., Favero, F., Rowan, A.J., et al. (2017). BCL9L Dysfunction Impairs Caspase-2 Expression Permitting Aneuploidy Tolerance in Colorectal Cancer. Cancer Cell *31*, 79–93.

Ma, F., Bi, L., Yang, G., Zhang, M., Liu, C., Zhao, Y., Wang, Y., Wang, J., Bai, Y., and Zhang, Y. (2014). ZNF703 promotes tumor cell proliferation and invasion and predicts poor prognosis in patients with colorectal cancer. Oncol. Rep. *32*, 1071–1077.

Ma, Z., Zhu, P., Shi, H., Guo, L., Zhang, Q., Chen, Y., Chen, S., Zhang, Z., Peng, J., and Chen, J. (2019). PTC-bearing mRNA elicits a genetic compensation response via Upf3a and COMPASS components. Nature *568*, 259–263.

Mahmoudi, T., Boj, S.F., Hatzis, P., Li, V.S.W., Taouatas, N., Vries, R.G.J., Teunissen, H., Begthel, H., Korving, J., Mohammed, S., et al. (2010). The leukemia-associated Mllt10/Af10-Dot1l are Tcf4/β-catenin coactivators essential for intestinal homeostasis. PLoS Biol. *8*.

Mammucari, C., Milan, G., Romanello, V., Masiero, E., Rudolf, R., Del Piccolo, P., Burden, S.J., Di Lisi, R., Sandri, C., Zhao, J., et al. (2007). FoxO3 Controls Autophagy in Skeletal Muscle In Vivo. Cell Metab. *6*, 458–471.

Mamorstein, L.Y., Ouchi, T., and Aronson, S.T. a a (1998). The BRCA 2 gene product functionally interacts with p53 and RAD51. Pnas *95*, 13869–13874.

Manoukian, A.S., and Krause, H.M. (1992). Concentration-dependent activities of the even-skipped protein in Drosophila embryos. Genes Dev. *6*, 1740–1751.

Maung, S.M.T.W., and Jenny, A. (2011). Planar cell polarity in drosophila. Organogenesis *7*.

Messeguer, X., Escudero, R., Farré, D., Núñez, O., Martínez, J., and Albà, M.M. (2002). PROMO: Detection of known transcription regulatory elements using species-tailored searches. Bioinformatics *18*, 333–334.

Metcalfe, C., Ibrahim, A.E.K., Graeb, M., De La Roche, M., Schwarz-Romond, T., Fiedler, M., Winton, D.J., Corfield, A., and Bienz, M. (2010). Dvl2 promotes intestinal length and neoplasia in the ApcMin mouse model for colorectal cancer. Cancer Res. *70*, 6629–6638.

van Meyel, D.J., Thomas, J.B., and Agulnick, A.D. (2003). Ssdp proteins bind to LIM-interacting co-factors and regulate the activity of LIM-homeodomain protein complexes in vivo. Development *130*, 1915–1925.

Mieszczanek, J., de la Roche, M., and Bienz, M. (2008). A role of Pygopus as an anti-repressor in facilitating Wnt-dependent transcription. Proc. Natl. Acad. Sci. U. S. A. *105*, 19324–19329.

Mieszczanek, J., van Tienen, L.M., Ibrahim, A.E.K., Winton, D.J., and Bienz, M. (2019). Bcl9 and Pygo synergise downstream of Apc to effect intestinal neoplasia in FAP mouse models. Nat. Commun. *10*.

Miller, T.C.R., Rutherford, T.J., Johnson, C.M., Fiedler, M., and Bienz, M. (2010). Allosteric Remodelling of the Histone H3 Binding Pocket in the Pygo2 PHD Finger Triggered by Its Binding to the B9L/BCL9 Co-Factor. J. Mol. Biol. *401*, 969–984.

Miller, T.C.R., Mieszczanek, J., S??nchez-Barrena, M.J., Rutherford, T.J., Fiedler, M., and Bienz, M. (2013). Evolutionary adaptation of the fly Pygo PHD finger toward recognizing histone H3 tail methylated at arginine 2. Structure *21*, 2208–2220.

Miyamoto, K., Fukutomi, T., Akashi-Tanaka, S., Hasegawa, T., Asahara, T., Sugimura, T., and Ushijima, T. (2005). Identification of 20 genes aberrantly methylated in human breast cancers. Int. J. Cancer *116*, 407–414.

Miyata, Y., Shibata, T., Aoshima, M., Tsubata, T., and Nishida, E. (2014). The Molecular Chaperone TRiC / CCT Binds to the Trp-Asp 40 (WD40) Repeat Protein WDR68 and Promotes Its Folding , Protein Kinase DYRK1A Binding , and Nuclear Accumulation *. J. Biol. Chem. *289*, 33320–33332.

Miyoshi, Y., Iwao, K., Nagasawa, Y., Aihara, T., Sasaki, Y., Imaoka, S., Murata, M., Shimano, T., and Nakamura, Y. (1998). Activation of the β-catenin gene in primary hepatocellular carcinomas by somatic alterations involving exon 3. Cancer Res. *58*, 2524–2527.

Molenaar, M., Wetering, M. Van De, Oosterwegel, M., Peterson-maduro, J., Godsave, S., Korinek, V., and Roose, J. (1996). XTcf-3 Transcription Factor Mediates ᴺʟ -Catenin-Induced Axis Formation in Xenopus Embryos. Cell *86*, 391–399.

Morcillo, P., Rosen, C., Baylies, M.K., and Dorsett, D. (1997). Chip, a widely expressed chromosomal protein required for segmentation and activity of a remote wing margin enhancer in Drosophila. Genes Dev. *11*, 2729–2740.

Morin, P.J., Sparks, a B., Korinek, V., Barker, N., Clevers, H., Vogelstein, B., and Kinzler, K.W. (1997). Activation of beta-catenin-Tcf signaling in colon cancer by mutations in beta-catenin or APC. Science *275*, 1787–1790.

Moser, A.R., Pitot, H.C., and Dove, W.F. (1990). A dominant mutation that predisposes to multiple intestinal neoplasia in the mouse. Science (80-.). *247*, 322–324.

Mosimann, C., Hausmann, G., and Basler, K. (2009). β-catenin hits chromatin: regulation of Wnt target gene activation. Nat Rev Mol Cell Biol *10*, 276–286.

Mund, T., and Pelham, H.R.B. (2009). Control of the activity ofWW-HECT domain E3 ubiquitin ligases by NDFIP proteins. EMBO Rep. *10*, 1–7.

Nakamura, M., Choe, S.-K., Runko, A.P., Gardner, P.D., and Sagerström, C.G. (2008). Nlz1/Znf703 acts as a repressor of transcription. BMC Dev. Biol. *8*, 108.

Neer, E.J., Schmidt, C.J., Nambudripad, R., and Smith, T.F. (1994). The ancient regulatory-protein family of WD-repeat proteins. Nature *371*, 297–300.

Neumann, C.J., and Cohen, S.M. (1997). Long-range action of Wingless organizes the dorsal-ventral axis of the Drosophila wing. Development *124*, 871–880.

Nusse, R., Van Ooyen, A., Cox, D., Fung, Y.K.T., and Varmus, H. (1984). Mode of proviral activation of a putative mammary oncogene (int-1) on mouse chromosome 15. Nature *307*, 131–136.

Nüsslein-Volhard, C., and Wieschaus, E. (1980). Mutations affecting segment number and polarity in Drosophila. Nature *287*, 795–801.

Orford, K., Crockett, C., Jensen, J.P., Weissman, A.M., and Byers, S.W. (1997). Serine Phosphorylation-regulated Ubiquitination and Degradation of b-Catenin. J. Biol. Chem. *272*, 24735–24738.

Ormestad, M., Astorga, J., Landgren, H., Wang, T., Johansson, B.R., Miura, N., and Carlsson, P. (2006). Foxf1 and Foxf2 control murine gut development by limiting mesenchymal Wnt signaling and promoting extracellular matrix production. Development *133*, 833–843.

Panda, D., Gold, B., Tartell, M.A., Rausch, K., Casas-Tinto, S., and Cherry, S. (2015). The transcription factor FoxK participates with Nup98 to regulate antiviral gene expression. MBio *6*, 1–10.

Panne, D., Maniatis, T., and Harrison, S.C. (2007). An Atomic Model of the Interferon-?? Enhanceosome. Cell *129*, 1111–1123.

Parker, D.S., Jemison, J., and Cadigan, K.M. (2002). Pygopus, a nuclear PHD-finger

protein required for Wingless signaling in Drosophila. Development *129*, 2565–2576.

Payre, F., Vincent, A., and Carreno, S. (1999). ovo/svb Integrates Wingless and DER pathways to control epidermis differentiation. Nature *400*, 271–275.

Peifer, M., Sweeton, D., Casey, M., and Wieschaus, E. (1994). wingless signal and Zeste-white 3 kinase trigger opposing changes in the intracellular distribution of Armadillo. Development *120*, 369–380.

Perkins, D.N., Pappin, D.J.C., Creasy, D.M., and Cottrell, J.S. (1999). Probability-based protein identification by searching sequence databases using mass spectrometry data. Electrophoresis *20*, 3551–3567.

Perreault, N., Katz, J.P., Sackett, S.D., and Kaestner, K.H. (2001). Foxl1 Controls the Wnt/β-Catenin Pathway by Modulating the Expression of Proteoglycans in the Gut. J. Biol. Chem. *276*, 43328–43333.

Perreault, N., Sackett, S.D., Katz, J.P., Furth, E.E., and Kaestner, K.H. (2005). Foxl1 is a mesenchymal Modifier of Min in carcinogenesis of stomach and colon. Genes Dev. *19*, 311–315.

Pickles, L.M., Roe, S.M., Hemingway, E.J., Stifani, S., and Pearl, L.H. (2002). Crystal structure of the C-terminal WD40 repeat domain of the human Groucho/TLE1 transcriptional corepressor. Structure *10*, 751–761.

Pinto, M., and Lobe, C.G. (1996). Products of the grg (Groucho-related gene) family can dimerize through the amino-terminal Q domain. J. Biol. Chem. *271*, 33026–33031.

Port, F., Chen, H.-M., Lee, T., and Bullock, S.L. (2014). Optimized CRISPR/Cas tools for efficient germline and somatic genome engineering in Drosophila. Proc. Natl. Acad. Sci. U. S. A. *111*, E2967-76.

Port, F., Muschalik, N., and Bullock, S.L. (2015). Systematic evaluation of Drosophila CRISPR tools reveals safe and robust alternatives to autonomous gene drives in basic research. G3 Genes, Genomes, Genet. *5*, 1493–1502.

Pritchard, D.K., and Schubiger, G. (1996). Activation of transcription in Drosophila embryos is a gradual process mediated by the nucleocytoplasmic ratio. Genes Dev.

10, 1131–1142.

Qi, L.S., Larson, M.H., Gilbert, L.A., Doudna, J.A., Weissman, J.S., Arkin, A.P., and Lim, W.A. (2013). Repurposing CRISPR as an RNA-γuided platform for sequence-specific control of gene expression. Cell *152*, 1173–1183.

Ray, M., and Lakhotia, S.C. (2015). The commonly used eye-specific sev-GAL4 and GMR-GAL4 drivers in Drosophila melanogaster are expressed in tissues other than eyes also. J. Genet. *94*, 407–416.

Renko, M., Fiedler, M., Rutherford, T.J., Schaefer, J. V., Plückthun, A., and Bienz, M. (2019). Rotational symmetry of the structured Chip/LDB-SSDP core module of the Wnt enhanceosome. Proc. Natl. Acad. Sci. U. S. A. *116*, 20977–20983.

Reya, T., and Clevers, H. (2005). Wnt signalling in stem cells and cancer. Nature *434*, 843–850.

Rhee, H., Zou, P., Udeshi, N.D., Martell, J.D., and Mootha, V.K. (2013). Proteomic Mapping of Mitochondria in Living Cells via Spatially Restricted Enzymatic Tagging. Science (80-.). *339*, 1328–1331.

Riese, J., Yu, X., Munnerlyn, A., Eresh, S., Hsu, S.C., Grosschedl, R., and Bienz, M. (1997). LEF-1, a nuclear factor coordinating signaling inputs from wingless and decapentaplegic. Cell *88*, 777–787.

Rijsewijk, F., Schuermann, M., Wagenaar, E., Parren, P., Weigel, D., and Nusse, R. (1987). The Drosophila homology of the mouse mammary oncogene int-1 is identical to the segment polarity gene wingless. Cell *50*, 649–657.

Romanelli, M.G., Tato', L., Lorenzi, P., and Morandi, C. (2003). Nuclear localization domains in human thyroid transcription factor 2. Biochim. Biophys. Acta - Mol. Cell Res. *1643*, 55–64.

Roux, K.J., Kim, D.I., Raida, M., and Burke, B. (2012). A promiscuous biotin ligase fusion protein identifies proximal and interacting proteins in mammalian cells. J. Cell Biol. *196*, 801–810.

Roux, K.J., Kim, D.I., and Burke, B. (2013). BioID: A screen for protein-protein

interactions. Curr. Protoc. Protein Sci. *19*, 1–14.

Rubinfeld, B., Robbins, P., El-Gamil, M., Albert, I., Porfiri, E., and Polakis, P. (1997). Stabilization of β-catenin by genetic defects in melanoma cell lines. Science (80-.). *275*, 1790–1792.

Sampietro, J., Dahlberg, C.L., Cho, U.S., Hinds, T.R., Kimelman, D., and Xu, W. (2006). Crystal Structure of a β-Catenin/BCL9/Tcf4 Complex. Mol. Cell *24*, 293–300.

San Filippo, J., Sung, P., and Klein, H. (2008). Mechanism of Eukaryotic Homologous Recombination. Annu. Rev. Biochem. *77*, 229–257.

Sanchez, A., De Vivo, A., Uprety, N., Kim, J., Stevens, S.M., and Kee, Y. (2016). BMI1-UBR5 axis regulates transcriptional repression at damaged chromatin. Proc. Natl. Acad. Sci. U. S. A. *113*, 11243–11248.

Sancho, E., Batlle, E., and Clevers, H. (2004). Signaling Pathways in Intestinal Development and Cancer. Annu. Rev. Cell Dev. Biol. *20*, 695–723.

Schmidtmann, E., Anton, T., Rombaut, P., Herzog, F., and Leonhardt, H. (2016). Determination of local chromatin composition by CasID. Nucleus *7*, 1–9.

Schulz, K.N., Bondra, E.R., Moshe, A., Villalta, J.E., Lieb, J.D., Kaplan, T., McKay, D.J., and Harrison, M.M. (2015). Zelda is differentially required for chromatin accessibility, transcription factor binding, and gene expression in the early Drosophila embryo. Genome Res. *25*, 1715–1726.

Schwarz-Romond, T., Merrifield, C., Nichols, B.J., and Bienz, M. (2005). The Wnt signalling effector Dishevelled forms dynamic protein assemblies rather than stable associations with cytoplasmic vesicles. J. Cell Sci. *118*, 5269–5277.

Schwarz-Romond, T., Metcalfe, C., and Bienz, M. (2007a). Dynamic recruitment of axin by Dishevelled protein assemblies. J. Cell Sci. *120*, 2402–2412.

Schwarz-Romond, T., Fiedler, M., Shibata, N., Butler, P.J.G., Kikuchi, A., Higuchi, Y., and Bienz, M. (2007b). The DIX domain of Dishevelled confers Wnt signaling by dynamic polymerization. Nat. Struct. Mol. Biol. *14*, 484–492.

Sekiya, T., and Zaret, K.S. (2007). Repression by Groucho/TLE/Grg Proteins:

Genomic Site Recruitment Generates Compacted Chromatin In Vitro and Impairs Activator Binding In Vivo. Mol. Cell *28*, 291–303.

Sharma, R.P., and Chopra, V.L. (1976). Effect of the wingless (wg1) mutation on wing and haltere development in Drosophila melanogaster. Dev. Biol. *48*, 461–465.

Shi, X., Wallis, A.M., Gerard, R.D., Voelker, K.A., Grange, R.W., DePinho, R.A., Garry, M.G., and Garry, D.J. (2012). Foxk1 promotes cell proliferation and represses myogenic differentiation by regulating Foxo4 and Mef2. J. Cell Sci. *125*, 5329–5337.

Shimeld, S.M., Degnan, B., and Luke, G.N. (2010). Evolutionary genomics of the Fox genes: Origin of gene families and the ancestry of gene clusters. Genomics *95*, 256–260.

Sierra, J., Yoshida, T., Joazeiro, C. a, and Jones, K. a (2006). The APC tumor suppressor counteracts beta-catenin activation and H 3 K 4 methylation at Wnt target genes. Genes Dev. *20*, 586.

Slorach, E.M., Chou, J., and Werb, Z. (2011). Zeppo1 is a novel metastasis promoter that represses E-cadherin expression and regulates p120-catenin isoform expression and localization. Genes Dev. *25*, 471–484.

Smalley, M.J., Signoret, N., Robertson, D., Tilley, A., Hann, A., Ewan, K., Ding, Y., Paterson, H., and Dale, T.C. (2005). Dishevelled (Dvl-2) activates canonical Wnt signalling in the absence of cytoplasmic puncta. J. Cell Sci. *118*, 5279–5289.

Song, H., Hasson, P., Paroush, Z., and Courey, A.J. (2004). Groucho oligomerization is required for repression in vivo. Mol Cell Biol *24*, 4341–4350.

Sowa, M.E., Bennett, E.J., Gygi, S.P., and Harper, J.W. (2009). Resource Defining the Human Deubiquitinating Enzyme Interaction Landscape. Cell *138*, 389–403.

Staal, F.J.T., van Noort, M., Strous, G.J., and Clevers, H.C. (2002). Wnt signals are transmitted through N-terminally dephosphorylated β-catenin. EMBO Rep. *3*, 63–68.

Städeli, R., and Basler, K. (2005). Dissecting nuclear Wingless signalling: Recruitment of the transcriptional co-activator Pygopus by a chain of adaptor proteins. Mech. Dev. *122*, 1171–1182.

Stambolic, V., Ruel, L., and Woodgett, J.R. (1996). Lithium inhibits glycogen synthase kinase-3 activity and mimics Wingless signalling in intact cells. Curr. Biol. *6*, 1664–1669.

Stamos, J.L., Chu, M.L.H., Enos, M.D., Shah, N., and Weis, W.I. (2014). Structural basis of GSK-3 inhibition by N-terminal phosphorylation and by the Wnt receptor LRP6. Elife *2014*, 1–22.

Steger, D.J., Lefterova, M.I., Ying, L., Stonestrom, A.J., Schupp, M., Zhuo, D., Vakoc, A.L., Kim, J.-E., Chen, J., Lazar, M.A., et al. (2008). DOT1L/KMT4 Recruitment and H3K79 Methylation Are Ubiquitously Coupled with Gene Transcription in Mammalian Cells. Mol. Cell. Biol. *28*, 2825–2839.

Sun, B., Hursh, D.A., Jackson, D., and Beachy, P.A. (1995). Ultrabithorax protein is necessary but not sufficient for full activation of decapentaplegic expression in the visceral mesoderm. EMBO J. *14*, 520–535.

Swarup, S., and Verheyen, E.M. (2012). Wnt / Wingless Signaling in Drosophila. Cold Spring Harb. Perpect Biol 1–16.

Takahashi, K., Tanabe, K., Ohnuki, M., Narita, M., Ichisaka, T., Tomoda, K., and Yamanaka, S. (2007). Induction of Pluripotent Stem Cells from Adult Human Fibroblasts by Defined Factors. Cell *131*, 861–872.

Tauriello, D.V.F., Jordens, I., Kirchner, K., Slootstra, J.W., Kruitwagen, T., Bouwman, B.A.M., Noutsou, M., Rüdiger, S.G.D., Schwamborn, K., Schambony, A., et al. (2012). Wnt/β-catenin signaling requires interaction of the Dishevelled DEP domain and C terminus with a discontinuous motif in Frizzled. Proc. Natl. Acad. Sci. U. S. A. *109*.

Tenbaum, S.P., Ordóñez-Morán, P., Puig, I., Chicote, I., Arqués, O., Landolfi, S., Fernández, Y., Herance, J.R., Gispert, J.D., Mendizabal, L., et al. (2012). β-Catenin confers resistance to PI3K and AKT inhibitors and subverts FOXO3a to promote metastasis in colon cancer. Nat. Med. *18*, 892–901.

Theodorou, V., Stark, R., Menon, S., and Carroll, J.S. (2013). GATA3 acts upstream of FOXA1 in mediating ESR1 binding by shaping enhancer accessibility. Genome Res. *23*, 12–22.

Thompson, B., Townsley, F., Rosin-Arbesfeld, R., Musisi, H., and Bienz, M. (2002). A new nuclear component of the Wnt signalling pathway. Nat. Cell Biol. *4*, 367–373.

Thuringer, F., Cohen, S.M., and Bienz, M. (1993). Dissection of an indirect autoregulatory response of a homeotic Drosophila gene. EMBO J. *12*, 2419–2430.

Thüringer, F., and Bienz, M. (1993). Indirect autoregulation of a homeotic Drosophila gene mediated by extracellular signaling. Proc. Natl. Acad. Sci. U. S. A. *90*, 3899–3903.

van Tienen, L.M., Mieszczanek, J., Fiedler, M., Rutherford, T.J., and Bienz, M. (2017). Constitutive scaffolding of multiple Wnt enhanceosome components by Legless/BCL9. Elife *6*, 1–23.

Tonikian, R., Zhang, Y., Sazinsky, S.L., Currell, B., Yeh, J.H., Reva, B., Held, H.A., Appleton, B.A., Evangelista, M., Wu, Y., et al. (2008). A specificity map for the PDZ domain family. PLoS Biol. *6*, 2043–2059.

Torres, M.A., and Nelson, W.J. (2000). Colocalization and redistribution of dishevelled and actin during Wnt- induced mesenchymal morphogenesis. J. Cell Biol. *149*, 1433–1442.

Townsley, F.M., Cliffe, A., and Bienz, M. (2004). Pygopus and Legless target Armadillo/beta-catenin to the nucleus to enable its transcriptional co-activator function. Nat. Cell Biol. *6*, 626–633.

Tsai, K.L., Huang, C.Y., Chang, C.H., Sun, Y.J., Chuang, W.J., and Hsiao, C.D. (2006). Crystal structure of the human FOXK1a-DNA complex and its implications on the diverse binding specificity of winged helix/forkhead proteins. J. Biol. Chem. *281*, 17400–17409.

Tsuda, M., Kamimura, K., Nakato, H., Archer, M., Staatz, W., Fox, B., Humphrey, M., Olson, S., Futch, T., Kaluza, V., et al. (1999). The cell-surface proteoglycan Dally regulates Wingless signalling in Drosophila. Nature *400*, 276–280.

Valenta, T., Hausmann, G., and Basler, K. (2012). The many faces and functions of b-catenin. EMBO J. *31*, 2714–2736.

Varelas, X., Miller, B.W., Sopko, R., Song, S., Gregorieff, A., Fellouse, F.A., Sakuma, R., Pawson, T., Hunziker, W., McNeill, H., et al. (2010). The Hippo Pathway Regulates Wnt/β-Catenin Signaling. Dev. Cell *18*, 579–591.

Veeman, M.T., Slusarski, D.C., Kaykas, A., Hallagan Louie, S., and Moon, R.T. (2003). Zebrafish Prickle, a Modulator of Noncanonical Wnt/Fz Signaling, Regulates Gastrulation Movements. Curr. Biol. *13*, 680–685.

Vincan, E., and Barker, N. (2008). The upstream components of the Wnt signalling pathway in the dynamic EMT and MET associated with colorectal cancer progression. Clin. Exp. Metastasis *25*, 657–663.

Walker, M.P., Stopford, C.M., Cederlund, M., Fang, F., Jahn, C., Rabinowitz, A.D., Goldfarb, D., Graham, D.M., Yan, F., Deal, A.M., et al. (2015). FOXP1 potentiates Wnt/β-catenin signaling in diffuse large B cell lymphoma. Sci. Signal. *8*, 1–13.

Waltzer, L., and Bienz, M. (1998). Drosophila CBP represses the transcription factor TCF to antagonize Wingless signalling. Nature *395*, 521–525.

Waltzer, L., Vandel, L., and Bienz, M. (2001). Teashirt is required for transcriptional repression mediated by high Wingless levels. EMBO J. *20*, 137–145.

Wang, J., Sinha, T., and Wynshaw-Boris, A. (2012). Wnt signaling in mammalian development: Lessons from mouse genetics. Cold Spring Harb. Perspect. Biol. *4*, 6.

Wang, W., Li, X., Lee, M., Jun, S., Aziz, K.E., Feng, L., Tran, M.K., Li, N., McCrea, P.D., Park, J. Il, et al. (2015). FOXKs promote Wnt/??-catenin signaling by translocating DVL into the nucleus. Dev. Cell *32*, 707–718.

Waterman, M.L., and Jones, K. (1990). Purification of TCF-1 alpha, a T-cell-specific transcription factor that activates the T-cell receptor C alpha gene enhancer in a context-dependent manner. New Biol. *July*, 621–636.

Watson, P.J., Fairall, L., and Schwabe, J.W.R. (2012). Nuclear hormone receptor co-repressors: Structure and function. Mol. Cell. Endocrinol. *348*, 440–449.

Weigel, D., Jürgens, G., Küttner, F., Seifert, E., and Jäckle, H. (1989). The homeotic gene fork head encodes a nuclear protein and is expressed in the terminal regions of

the Drosophila embryo. Cell *57*, 645–658.

Whitworth, A.J., and Russell, S. (2003). Temporally dynamic response to Wingless directs the sequential elaboration of the proximodistal axis of the Drosophila wing. Dev. Biol. *254*, 277–288.

Wieschaus, E., and Nüsslein-Vollhard, C. (1986). Looking at embryos. In Drosophila: A Practical Approach, pp. 199–227.

Winston, J.T., Strack, P., Beer-Romero, P., Chu, C.Y., Elledge, S.J., and Harper, J.W. (1999). The SCF(β-TRCP)-ubiquitin ligase complex associates specifically with phosphorylated destruction motifs in Iκbα and β-catenin and stimulates Iκbα ubiquitination in vitro. Genes Dev. *13*, 270–283.

Wong, L.L., and Adler, P. (1993). Tissue Polarity Genes of Drosophila Regulate the Subcellular Location for Prehair Initiation in Pupal Wing Cells. J. Cell Biol. *123*, 209–221.

Wong, H.C., Bourdelas, A., Krauss, A., Lee, H.J., Shao, Y., Wu, D., Mlodzik, M., Shi, D.L., and Zheng, J. (2003). Direct binding of the PDZ domain of Dishevelled to a conserved internal sequence in the C-terminal region of Frizzled. Mol. Cell *12*, 1251–1260.

Wu, D.C., and Johnston, L.A. (2010). Control of wing size and proportions by Drosophila Myc. Genetics *184*, 199–211.

Wu, D., Sunkel, B., Chen, Z., Liu, X., Ye, Z., Li, Q., Grenade, C., Ke, J., Zhang, C., Chen, H., et al. (2014). Three-tiered role of the pioneer factor GATA2 in promoting androgen-dependent gene expression in prostate cancer. Nucleic Acids Res. *42*, 3607–3622.

Wu, X., Golden, K., and Bodmer, R. (1995). Heart development in Drosophila requires the segment polarity gene wingless. Dev. Biol. *169*, 619–628.

Xia, L., Huang, W., Tian, D., Zhang, L., Qi, X., Chen, Z., Shang, X., Nie, Y., and Wu, K. (2014). Forkhead box Q1 promotes hepatocellular carcinoma metastasis by transactivating ZEB2 and VersicanV1 expression. Hepatology *59*, 958–973.

Yam, A.Y., Xia, Y., Lin, H.-T.J., Burlingame, A., Gerstein, M., and Frydman, J. (2008). Defining the TRiC/CCT interactome links chaperonin function to stabilization of newly made proteins with complex topologies. Nat. Struct. Mol. Biol. *15*, 1255–1262.

Yanagawa, S.I., Van Leeuwen, F., Wodarz, A., Klingensmith, J., and Nusse, R. (1995). The dishevelled protein is modified by wingless signaling in Drosophila. Genes Dev. *9*, 1087–1095.

Yang, Y., and Mlodzik, M. (2015). Wnt-Frizzled/Planar Cell Polarity Signaling: Cellular Orientation by Facing the Wind (Wnt). Annu. Rev. Cell Dev. Biol. *31*, 623–646.

Yao, B., Zhang, L., Liang, S., and Zhang, C. (2012). SVMTriP: A Method to Predict Antigenic Epitopes Using Support Vector Machine to Integrate Tri-Peptide Similarity and Propensity. PLoS One *7*, 5–9.

Ye, T., Xu, J., Du, L., Mo, W., Liang, Y., and Xia, J. (2017). Downregulation of UBAP2L inhibits the epithelial-mesenchymal transition via SNAIL1 regulation in hepatocellular carcinoma cells. Cell. Physiol. Biochem. *41*, 1584–1595.

Yu, X., Hoppler, S., Eresh, S., and Bienz, M. (1996). decapentaplegic, a target gene of the wingless signalling pathway in the Drosophila midgut. Development *122*, 849–858.

Zaffran, S., Küchler, A., Lee, H.H., and Frasch, M. (2001). biniou (FoxF), a central component in a regulatory network controlling visceral mesoderm development and midgut morphogenesis in Drosophila. Genes Dev. *15*, 2900–2915.

Zaret, K.S., and Carroll, J.S. (2011). Pioneer transcription factors : establishing competence for gene expression Parameters affecting transcription factor access to target sites in chromatin Initiating events in chromatin : pioneer factors bind first. Genes Dev. 2227–2241.

Zeng, W., Wharton, K. a, Mack, J. a, Wang, K., Gadbaw, M., Suyama, K., Klein, P.S., and Scott, M.P. (2000). naked cuticle encodes an inducible antagonist of Wnt signalling. Nature *403*, 789–795.

Zeng, X., Tamai, K., Doble, B., Li, S., Huang, H., Habas, R., Okamura, H., Woodgett, J., and He, X. (2005). A dual-kinase mechanism for Wnt co-receptor phosphorylation

and activation. Nature *438*, 873–877.

Zhang, Y., Appleton, B.A., Wiesmann, C., Lau, T., Costa, M., Hannoush, R.N., and Sidhu, S.S. (2009). Inhibition of Wnt signaling by Dishevelled PDZ peptides. Nat. Chem. Biol. *5*, 217–219.

8. Appendix

8.1. Websites

Cancer Today	https://gco.iarc.fr/today/home
Cistrome Project	http://www.cistrome.org
CompPASS	http://besra.hms.harvard.edu/ipmsmsdbs/cgi-bin/tutorial.cgi
CRISPOR	http://crispor.tefor.net
Fly CRISPR	https://www.crisprflydesign.org/
Human Protein Atlas	https://www.proteinatlas.org
NLS Mapper	http://nls-mapper.iab.keio.ac.jp/cgi-bin/NLS_Mapper_form.cgi
ONCOMINE	https://www.oncomine.org/resource/main.html
Phyre2	http://www.sbg.bio.ic.ac.uk/~phyre2/html/page.cgi?id=index
PROMO	http://alggen.lsi.upc.edu
ShinyGO	http://bioinformatics.sdstate.edu/go/
TIDE	https://tide.deskgen.com

8.2. Oligonucleotides for Genotyping

Organism	Gene/Allele	Target	Sequence
Drosophila	FoxK^{11} FoxK^{23} FoxK^{42}	Exon 2_I	Fw: 5′-GCGGCGCTGAATAACTACAA
			Rv: 5′-TTAATGTTCATATTGCTTCGCGA
			Seq: 5′-TAACAACAACAGCGCCGATC
Drosophila	FoxK^{2} FoxK^{10}	Exon 2_II	Fw: 5′-TTGCAGGCCAACAACAACAC
			Rv: 5'-ACGTTGAAGTGAACCAGCGA
			Seq: 5′-TTGCAGGCCAACAACAACAC
Drosophila	FoxK$^{\Delta C\text{-}Term}$	Exon 9	Fw: 5′-AATCAGCACCTGGATCACCG
			Rv: 5′-GTGTGCTTGCATAAGTCGCC
			Seq: 5′-CGTGCGTTCATGTTCCTTAAGTTC

Drosophila	FoxK[16]	Exon1-6	Fw: 5'-ACGTGGTACCCATTTCGTGA
			Rv: 5'-AGCTCTCGCGCGAATTATCT
			Seq: 5′-CTGTCCGGATCAATACGCCA
Human (HEK293T)	FOXK1	Exon 1	Fw: 5′-CCATGCTCAAGTCCACCGAG
			Rv: 5'-CCATTGGCCTGCTTCGGTA
Human (HEK293T)	FOXK2	Exon 1	Fw: 5'-ATACCCCGTTCTTGCCCAAG
			Rv: 5'-GGGAGATGAAGCTCGAGTGG
Human (SW480)	hPYGO2	Exon 3	Fw: 5′-CCGCCTAACACAAGTCCCTT
			Rv: 5′-ATAGGCGCTCTCAGTCATGC
			Seq: 5′-GATCTCACCCACCATGGGAC

8.3. Oligonucleotides used as sgRNAs for CRISPR/Cas9 editing

Organism	Gene	Identifier	Target	Sequence [5′-3′]
Drosophila	FOXK	sgRNA2	Exon 2	AACACCACCGCCTGCAGTAG
Drosophila	FOXK	sgRNA5	Exon 2	TTGAAGCGTAGTTCTCCATA
Drosophila	FOXK	sgRNA6	Exon 2	GTCCAGTGCCTAAGCAAGAA
Drosophila	FOXK	sgRNA2	Exon 9	TACGGTGGCACCGGTTCGCT
Human (HEK293T)	FOXK1	sgRNA1	Exon 1	GCTGCCTCCGGGCGCGATCG
Human (HEK293T)	FOXK1	sgRNA2	Exon 1	CGAGTTCGAGTTCCTCATGC
Human (HEK293T)	FOXK2	sgRNA2	Exon 1	AAGAAGCGCTCGGTGACCAT
Human (SW480)	hPYGO2	sgRNA1	Exon 3	CCAGGCTTGGTGTACCCATG

8.4. FoxK CRISPR alleles generated in this work

Organism	Gene	Identifier	Allele	Sequence [5′-3′]
Drosophila	FoxK	sgRNA2	WT	CACCAATACTGCAGGCGGT
			FoxK[2]	CACCAAT-CTGCAGGCGGT (Δ 1 bp)

			FoxK[10]	CACCA--------GGCGGT (Δ 8 bp)
Drosophila	FoxK	sgRNA5	WT	CTTCCCCGCCATATGGAGGACTACGCTTCAATCA
			FoxK[23]	CTTC----------AA (Δ 25 bp)
Drosophila	FoxK	sgRNA6	WT	GCCTAAGCAAGAATGG
			FoxK[11]	GCCTAAGCA-GAATGG (Δ 1 bp)
			FoxK[42]	GCCTAAG--AGAATGG (Δ 2 bp)

8.5. dsDNA Oligo used as a repair template in CRISPR for FoxK truncation

5′-ACCCATGGGCCTCACTATTTGCCCTTGTTCTGCCGGTGCTTCTGGATCCGCACGCATCAGAGC

ACTTCCGACACGTACTAAGGTCACTTGGCCACGGTGGCATCGGTGGCAGTGGTGACGC

8.6. Measurement of eye size of F76 crossed to FOXK and different Wg mutants – male and female data sets.

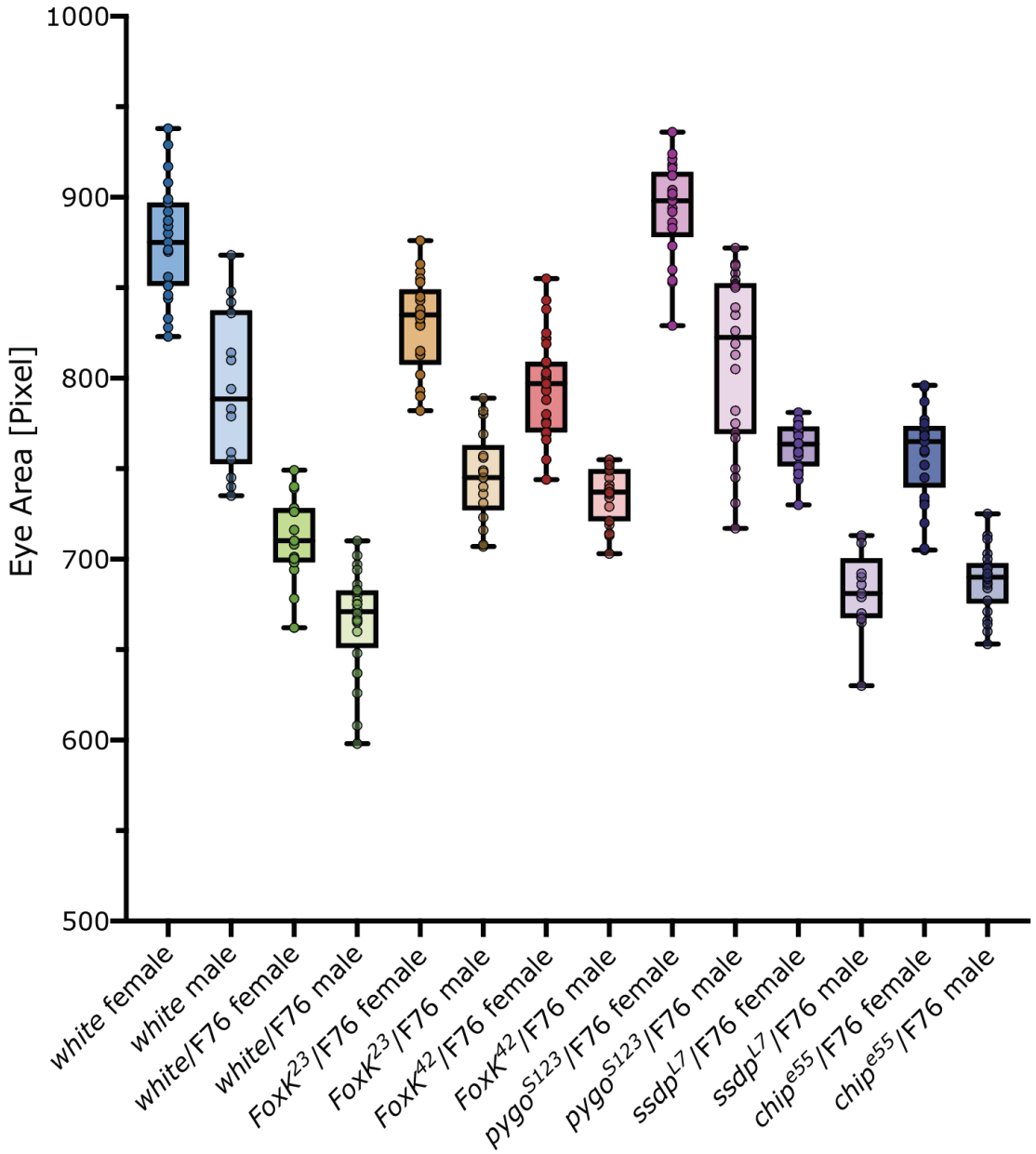

Heterozygosity for *foxK^{KO}* substantially ameliorates the rough-eye phenotype of a constitutively active Armadillo mutant.

Flies heterozygous for constitutively active Armadillo (*Arm^{S56E}* or F76, overexpressed using an eye-specific driver (GMR-Gal4)) as well as *foxK^{KO}* alleles (*foxK^{23}* and *foxK^{42}*) or Wg pathway mutants (*pygo^{S123}*, *ssdp^{L7}* and *chip^{e55}*). Area measurements were done in Pixel using ImageJ as shown (yellow marking). Normal distribution and one-way ANOVA analysis including Turkey's multiple comparison tests were done in GraphPad Prism. Heterozygosity of *pygo^{S123}* in a F76 background leads to full suppression of the rough eye phenotype (white vs. *pygo^{S123}*/F76 not statistically significant). Both *foxK* alleles rescue the rough-eye phenotype significantly. *Ssdp^{L7}*/F76 and *chip^{e55}*/F76 are not significantly different from each other.

Multiple comparison test showed that all other comparisons are statistically significant by one-way ANOVA. $p < 0.0001$.

8.7. Raw Data PYGO2 BioID (Cut-off ≥ 3 TSC)

	Protein ID	Pygo WT	Pygo ΔN-BOX	Pygo ΔPHD
1	ACACA	141	130	110
2	NUMA1	92	97	100
3	FLNA	91	98	79
4	TPR	90	79	61
5	JMJD1C	76	74	59
6	MKI67	68	62	85
7	CHD7	67	67	70
8	FASN	67	59	39
9	FLJ16830	66	65	56
10	PC	63	62	64
11	BCL6/B3	58	69	61
12	SNRNP200	55	60	65
13	BPTF	55	33	31
14	CHD8	52	57	47
15	AHCTF1	52	50	46
16	RANBP2	50	37	21
17	YLPM1	49	63	76
18	BRCA2	49	22	2
19	DHX9	47	56	61
20	XAB2	46	42	44
21	TOP2A	45	37	39
22	TF	44	43	45
23	YEATS2	44	31	9
24	SF3B1	43	50	66
25	SMARCA4	43	42	46
26	FAM208A	43	34	17
27	SMARCA5	42	42	53
28	ARID1A	42	41	42
29	KDM3B	41	50	32
30	CENPF	41	16	4
31	TCERG1	40	46	45
32	ADNP	40	45	52
33	NCOR1	40	45	49
34	BAZ2A	40	45	44
35	HNRNPM	40	44	42
36	PCCA	40	42	38
37	GTF3C1	39	40	41
38	ARID1B	39	32	36
39	SPEN	38	45	67
40	BRIP1	37	35	39
41	SIN3B	37	31	8
42	BAZ1B	37	29	29
43	TTF1	37	25	10
44	NUP153	36	45	27
45	ZBTB33	36	36	33
46	SMEK1	35	40	45
47	ZNF638	35	40	40
48	KIF4A	35	38	42
49	ZFR	35	37	39
50	DDX5	34	36	36
51	PAPOLA	34	34	39
52	DKFZp686E2459	33	45	48
53	SF3B2	33	38	44
54	GNL3	33	31	29
55	ACIN1	31	34	43
56	LENG8	31	32	33
57	POLA1	31	30	33
58	CCT1	31	27	29
59	DDX42	30	39	42
60	SFRS14	30	36	43
61	SF3A1	30	36	25
62	RBM26	30	34	40
63	MCCC1	30	30	31
64	EP400	30	30	9
65	MTA1	30	26	32
66	ARID3B	30	26	25
67	SMCHD1	30	25	19
68	MGA	30	25	16
69	RPRD2	29	35	28
70	ZNF292	29	34	42
71	SCML2	29	31	38
72	ACACB	29	31	21
73	U2SURP	28	31	38
74	PCF11	28	31	29
75	KHSRP	28	30	32
76	WDR36	28	29	35
77	KNOP1	28	25	31
78	TFIP11	27	35	35
79	TCF20	27	34	52
80	MATR3	27	34	37
81	THOC2	27	26	27
82	BLM	27	21	18
83	SART3	26	36	37
84	DIDO1	26	31	38
85	FLJ54552	26	27	33
86	CIC	26	27	31
87	NONO	26	27	29
88	TET1	26	26	11
89	ILF3	25	33	34
90	ADAR	25	30	32
91	ZNF318	25	30	18
92	FLJ58196	25	28	28
93	HCFC1	25	27	15
94	WDR70	25	24	17
95	GSE1	25	21	20
96	SETD2	24	33	32
97	RBM6	24	28	42
98	RBM27	24	28	30
99	HNRNPR	24	27	30
100	THRAP3	24	24	27
101	MRE11A	24	21	22
102	PRPF8	24	20	30
103	GTF3C4	24	19	28
104	FAM208B	24	18	2
105	ZNF609	24	15	9
106	XRN2	23	33	37
107	SART1	23	31	34
108	LYAR	23	31	25
109	HNRNPU	23	30	32
110	EXOSC10	23	30	30
111	SFPQ	23	27	32
112	DHX8	23	26	43
113	CCAR2	23	26	21
114	RAVER1	23	24	25
115	PRPF3	23	22	24
116	TLE3	23	22	19
117	WDR33	23	22	16
118	MDC1	23	21	36
119	BCL9	23	15	0
120	MPHOSPH1	23	14	8
121	ACACA	22	28	19
122	TMPO	22	26	25
123	RPA1	22	23	24
124	SBNO1	22	21	29
125	SUGP1	22	21	26
126	NRF	22	21	7
127	ZNF198	22	15	12
128	EP300	22	12	9
129	CDC5L	21	29	33
130	ZFC3H1	21	29	33
131	SNW1	21	27	27
132	BRD4	21	26	28
133	RBM14	21	26	24
134	ATRX	21	25	31
135	CCAR1	21	24	23
136	HNRNPUL1	21	23	22
137	HSPA1B	21	20	23
138	NCOA3	21	18	17
139	RBBP6	20	31	42
140	hCG_31253	20	28	30
141	TCOF1	20	26	35
142	FLJ94229	20	24	25
143	ZNF281	20	21	26
144	DHX15	20	21	23
145	CHD1	20	20	22
146	TRIM28	20	20	19
147	ESF1	20	17	29
148	DDX10	19	29	27
149	BAZ1A	19	25	26
150	DKFZp667H197	19	24	23
151	NCL	19	23	28
152	CHERP	19	22	26
153	DOT1L	19	21	17
154	COIL	19	20	22
155	hCG_1989366	19	18	25
156	RUVBL1	19	18	17
157	DDX21	19	16	27
158	CHAMP1	18	31	33
159	SON	18	26	29
160	GNL2	18	25	30
161	PARP1	18	23	33
162	PES1	18	23	25
163	IK	18	22	19
164	GTF2I	18	20	21
165	RBM33	18	20	20
166	TRPS1	18	19	24
167	RANBP3	18	18	21
168	KMT2B	18	18	5
169	DHX38	18	17	34
170	NASP	18	14	11
171	RRP1B	18	9	1
172	CASC5	18	8	3
173	DDX46	17	49	56
174	HCTP4	17	31	31
175	TAF1	17	23	23
176	SUPT6H	17	21	30
177	KDM3A	17	21	12
178	FUBP1	17	18	16
179	NCOA2	17	18	5
180	TRIM33	17	17	16
181	SCAF11	17	16	16
182	CDC73	17	15	20
183	MED12	17	8	13
184	CHD6	16	30	45
185	WAPAL	16	22	26
186	DDX17	16	22	20
187	ZNF462	16	21	46
188	MED1	16	20	19
189	MSH6	16	19	32
190	SLU7	16	19	14
191	MYSM1	16	18	22
192	PUF60	16	16	20
193	ORC2L	16	16	20
194	PYGO2	16	15	13
195	CCNT1	16	14	17
196	DNAJB1	16	12	17
197	NAT10	15	34	41
198	POLR2A	15	25	33
199	PPP1R10	15	20	24
200	SPDL1	15	20	18

	Protein ID	Pygo WT	Pygo ΔN-BOX	Pygo ΔPHD		Protein ID	Pygo WT	Pygo ΔN-BOX	Pygo ΔPHD		Protein ID	Pygo WT	Pygo ΔN-BOX	Pygo ΔPHD		Protein ID	Pygo WT	Pygo ΔN-BOX	Pygo ΔPHD
201	PRPF40A	15	19	24	251	HP1BP3	13	13	14	301	SRCAP	11	7	3	351	FNBP4	9	11	13
202	RBM17	15	19	20	252	TTN	13	13	10	302	NBN	11	5	10	352	GPATCH1	9	10	20
203	USP7	15	18	35	253	TOX4	13	12	12	303	PRKDC	11	1	11	353	PPIL4	9	10	14
204	TFAP2A	15	18	19	254	NR2C2	13	11	15	304	RBM15	10	18	29	354	LARP1	9	10	5
205	HNRPA2B1	15	17	23	255	CDK12	12	25	28	305	POLDIP3	10	15	20	355	PCBP1	9	9	14
206	BTBD14B	15	17	20	256	BTAF1	12	19	8	306	TUBB2C	10	14	13	356	HEL-S-114	9	9	12
207	RBMX	15	16	18	257	NCOR2	12	18	23	307	RPS4X	10	14	13	357	RPL10	9	9	12
208	IRS4	15	16	5	258	CDK11B	12	18	22	308	PTBP1	10	12	18	358	CIAPIN1	9	9	11
209	PSPC1	15	15	18	259	MCM4	12	17	4	309	HNRNPA3	10	12	15	359	RPS27A	9	9	7
210	CPSF7	15	15	16	260	ZEB2	12	16	20	310	CXorf56	10	12	14	360	RLF	9	9	7
211	WRNIP1	15	14	0	261	ZBTB9	12	16	12	311	CELF2	10	12	11	361	MLH1	9	9	6
212	HLCS	15	13	6	262	CDKN2AIP	12	16	11	312	TLE1	10	12	4	362	PAF1	9	9	4
213	ZNF280C	15	11	12	263	TRIM24	12	15	18	313	HNRNPH1	10	11	15	363	EPS15L1	9	8	24
214	CHD9	15	9	10	264	CPSF6	12	15	15	314	TCEB3	10	11	14	364	CORO1B	9	8	11
215	COPG2	15	6	0	265	FAM50A	12	14	18	315	AKAP8	10	11	11	365	H2AFY	9	8	9
216	INTS4	14	23	32	266	FIP1L1	12	14	15	316	CECR2	10	11	10	366	ZNF703	9	8	8
217	XRCC6	14	21	23	267	SNRPA	12	14	14	317	FBRS	10	11	7	367	CD2AP	9	8	1
218	SAFB	14	20	27	268	CRK	12	13	17	318	RPL19	10	10	13	368	NKX2-5	9	7	12
219	FLJ94931	14	19	19	269	HNRPD	12	13	16	319	TAF9	10	10	13	369	C11orf49	9	7	6
220	RBM20	14	18	15	270	DPF1	12	12	13	320	PHAX	10	10	12	370	GTF2B	9	6	13
221	ZFHX4	14	18	15	271	GTF2E2	12	11	19	321	REXO4	10	10	12	371	RPS3	9	5	12
222	STRBP	14	18	13	272	NFIA	12	11	18	322	RAD21	10	10	2	372	WRN	9	5	1
223	CXorf57	14	17	31	273	RPL26	12	11	10	323	RCC2	10	9	15	373	SIN3A	9	4	1
224	GATAD2B	14	16	13	274	ZDBF2	12	11	8	324	TP53	10	9	13	374	HSP90AB1	9	2	0
225	CRNKL1	14	16	9	275	NUP98	12	11	5	325	HNRNPDL	10	9	11	375	RBM25	8	20	25
226	HNRPA1	14	15	22	276	MCM3AP	12	10	7	326	HNRNPC	10	9	9	376	RBM5	8	18	17
227	NSD1	14	15	14	277	STK38	12	8	7	327	GTF3C5	10	9	3	377	USP15	8	17	20
228	POGZ	14	15	14	278	ARID2	12	7	1	328	LDB1	10	8	14	378	MASTL	8	16	9
229	CUX1	14	15	11	279	ISL2	12	2	13	329	SUGT1	10	8	12	379	hCG_2005638	8	15	11
230	PLRG1	14	14	18	280	DNMT1	11	21	25	330	VCPIP1	10	8	12	380	RBM41	8	14	11
231	NCOA5	14	14	14	281	NELFE	11	19	19	331	ALX1	10	8	10	381	IRF2BP2	8	14	10
232	DVL2	14	14	12	282	BCLAF1	11	17	24	332	NCOA6	10	8	7	382	INTS9	8	12	13
233	CCNK	14	12	15	283	PPIL2	11	17	18	333	STAT3	10	6	11	383	GTF2F2	8	12	12
234	SALL1	14	11	9	284	WDR3	11	16	24	334	PRIM2	10	5	12	384	NUDC	8	10	13
235	SETX	14	7	14	285	PML	11	16	10	335	GPATCH4	10	5	12	385	NOP56	8	10	12
236	KMT2D	14	4	3	286	CSDE1	11	15	5	336	DDX18	10	4	2	386	HNRPF	8	10	10
237	MYBBP1A	13	19	24	287	WIZ	11	13	21	337	SMARCC1	10	3	0	387	TMPO	8	10	8
238	PHF3	13	19	21	288	KMT2A	11	13	15	338	ZNF536	9	20	21	388	SERBP1	8	10	6
239	WBP11	13	19	21	289	RBM4	11	12	16	339	HTATSF1	9	18	16	389	ZMYND8	8	9	17
240	POLH	13	18	9	290	SAP30BP	11	12	14	340	DGCR8	9	16	11	390	PRPF4	8	9	13
241	ZMYM4	13	18	5	291	TARDBP	11	12	13	341	HSPA8	9	16	8	391	SFRS15	8	9	10
242	XIAP	13	17	22	292	GPKOW	11	11	21	342	SYNCRIP	9	14	14	392	ZMAT2	8	9	10
243	NR2C1	13	17	20	293	GABPA	11	11	14	343	SRRT	9	14	12	393	RPL36AL	8	9	8
244	SF1	13	17	17	294	DACH1	11	11	13	344	ZNF451	9	13	5	394	DVL3	8	9	7
245	SFSWAP	13	16	21	295	CNN3	11	11	13	345	HIVEP1	9	13	4	395	ZNF746	8	9	0
246	FOXK1	13	15	20	296	WAC	11	11	13	346	RBM22	9	12	13	396	ZSCAN21	8	8	12
247	TUBA1B	13	15	14	297	TCF7L2	11	10	12	347	ILKAP	9	12	10	397	FHL1	8	8	11
248	ZC3H14	13	15	13	298	KDM6A	11	10	4	348	CRKL	9	11	17	398	RFC1	8	8	11
249	TOP2B	13	14	27	299	SRFBP1	11	9	10	349	HELLS	9	11	17	399	MMTAG2	8	8	10
250	WWOX	13	13	17	300	SATB2	11	7	11	350	DGCR14	9	11	15	400	CNN2	8	8	7

	Protein ID	Pygo WT	Pygo ΔN-BOX	Pygo ΔPHD		Protein ID	Pygo WT	Pygo ΔN-BOX	Pygo ΔPHD		Protein ID	Pygo WT	Pygo ΔN-BOX	Pygo ΔPHD		Protein ID	Pygo WT	Pygo ΔN-BOX	Pygo ΔPHD
401	RIF1	8	8	6	451	PSME3	7	6	11	501	SSRP1	6	8	3	551	RNGTT	5	11	8
402	NOL11	8	8	5	452	SLC25A5	7	6	10	502	CFDP1	6	7	11	552	EYA1	5	10	11
403	RPS2	8	7	13	453	CCDC174	7	6	10	503	HNRNPAB	6	7	10	553	IRF2BP1	5	10	9
404	HNRPH3	8	7	11	454	GPATCH11	7	6	9	504	HOXB9	6	7	10	554	USP28	5	10	1
405	MFAP1	8	7	11	455	ISY1	7	6	8	505	RFC4	6	7	10	555	ZNF644	5	10	0
406	C5orf21	8	7	9	456	EYA3	7	6	7	506	WIPI2	6	7	8	556	NSRP1	5	9	9
407	ARGLU1	8	7	7	457	RPL8	7	6	6	507	hCG_24487	6	7	8	557	CDC2L5	5	9	4
408	USP14	8	7	4	458	TRMT5	7	6	6	508	PUS7	6	7	8	558	RPS6	5	8	11
409	ERC1	8	7	3	459	EMSY	7	6	1	509	PSIP1	6	7	8	559	TEAD1	5	8	9
410	ELAVL1	8	6	13	460	FRG1	7	5	11	510	MEF2D	6	7	8	560	MAPRE2	5	7	11
411	CTTN	8	6	6	461	RPL5	7	5	10	511	PRCC	6	7	8	561	PRPF31	5	7	11
412	ELF2	8	6	4	462	WRAP73	7	5	6	512	RPS23	6	7	7	562	U2AF2	5	7	10
413	L3MBTL3	8	6	3	463	CWC25	7	5	5	513	RPL27A	6	7	7	563	FEN1	5	7	10
414	EFHD2	8	5	14	464	RAP80	7	5	4	514	RPL32	6	7	7	564	RNF113A	5	7	8
415	LMX1B	8	3	10	465	WDR43	7	5	2	515	RPL28	6	7	7	565	RNMT	5	7	8
416	TOPBP1	8	3	1	466	NOSIP	7	4	11	516	C15orf38-AP3S2	6	7	6	566	EIF3G	5	7	8
417	C9orf78	8	1	7	467	SIX4	7	4	4	517	CSTF2T	6	7	2	567	TBCB	5	7	7
418	ODF2	8	1	0	468	HOXD13	7	3	9	518	NPM1	6	6	11	568	CSTF3	5	7	7
419	ZNF830	7	16	17	469	TP53BP1	7	3	3	519	FBL	6	6	10	569	RBMX2	5	7	6
420	SSB	7	15	13	470	DNAJC8	7	2	12	520	HOXA13	6	6	9	570	ACTB	5	7	6
421	SLC4A1AP	7	14	14	471	ZBTB10	6	15	16	521	FUS	6	6	9	571	PTPN2	5	7	5
422	FLI1	7	12	17	472	GREB1L	6	13	2	522	WBP4	6	6	8	572	ZEB1	5	7	4
423	DROSHA	7	12	9	473	HAT1	6	12	14	523	RBM11	6	6	7	573	SENP6	5	7	2
424	PMS1	7	12	4	474	MORC4	6	12	11	524	PSMD4	6	6	7	574	C14orf43	5	6	19
425	SURF6	7	11	13	475	GPATCH8	6	11	15	525	AFF4	6	6	7	575	ARID5B	5	6	11
426	TAF15	7	11	12	476	HDGFRP2	6	11	15	526	RPL24	6	6	6	576	CDK7	5	6	11
427	DKC1	7	11	11	477	PPME1	6	11	11	527	WDHD1	6	6	4	577	KMT2C	5	6	10
428	LBR	7	10	12	478	NPLOC4	6	10	16	528	RFX1	6	6	2	578	ZNF24	5	6	9
429	SMARCE1	7	10	10	479	SMARCA2	6	10	15	529	TOP1	6	5	12	579	ZRANB2	5	6	7
430	HIST1H1E	7	10	8	480	CTBP2	6	10	10	530	TIPRL	6	5	9	580	RPL34	5	6	6
431	MEPCE	7	10	6	481	ZHX3	6	10	2	531	CWF19L1	6	5	9	581	RPL27	5	6	6
432	PPWD1	7	10	5	482	RAI1	6	9	20	532	C1orf131	6	5	8	582	PCYT1A	5	6	6
433	PSMC5	7	10	2	483	DHX16	6	9	18	533	RPL7	6	5	7	583	RALY	5	6	5
434	FTSJ3	7	9	22	484	WDR18	6	9	9	534	APBB1	6	5	4	584	HDAC1	5	6	5
435	TAGLN2	7	9	12	485	BAZ2B	6	9	9	535	RAD54L2	6	5	3	585	GATAD2A	5	6	4
436	QKI	7	8	14	486	EIF5	6	9	7	536	CWC15	6	4	6	586	RPS11	5	6	4
437	RPS3A	7	8	12	487	PPM1G	6	9	6	537	POLD3	6	4	4	587	MSH3	5	6	1
438	ZC3H18	7	8	10	488	ZKSCAN4	6	8	14	538	PAPOLG	6	4	4	588	GNL3L	5	6	0
439	C19orf47	7	8	9	489	SUPT16H	6	8	14	539	ANLN	6	4	4	589	ZNF687	5	5	11
440	RPL3	7	8	9	490	PDLIM1	6	8	13	540	ARID3A	6	3	2	590	YY1	5	5	8
441	RPS8	7	8	8	491	KIAA1429	6	8	12	541	ATF7IP	6	3	1	591	ONECUT2	5	5	8
442	NUDT5	7	8	8	492	ZNF362	6	8	11	542	LAS1L	6	3	0	592	H1F0	5	5	7
443	RPL13	7	8	7	493	C15orf39	6	8	10	543	E2F6	6	2	12	593	C12orf45	5	5	7
444	RPL23A	7	8	7	494	EEF1A1	6	8	9	544	UBA2	6	2	0	594	IGBP1	5	5	7
445	ESRP2	7	8	3	495	AHSA1	6	8	9	545	ATXN1L	6	1	2	595	SMARCAD1	5	5	7
446	PDCD4	7	7	17	496	TXNDC9	6	8	8	546	UTP14A	5	15	19	596	HIST1H4H	5	5	6
447	AGGF1	7	7	11	497	RPL35	6	8	7	547	DKFZp781C0423	5	11	12	597	SRSF6	5	5	6
448	RPL36	7	7	6	498	KHDRBS1	6	8	7	548	PNN	5	11	12	598	JUN	5	5	6
449	ZNF326	7	7	4	499	RBBP7	6	8	7	549	XRN1	5	11	10	599	CCDC59	5	5	6
450	ZNF217	7	6	12	500	RPL37	6	8	6	550	ENO1	5	11	10	600	PCNP	5	5	5

	Protein ID	Pygo WT	Pygo ΔN-BOX	Pygo ΔPHD		Protein ID	Pygo WT	Pygo ΔN-BOX	Pygo ΔPHD		Protein ID	Pygo WT	Pygo ΔN-BOX	Pygo ΔPHD		Protein ID	Pygo WT	Pygo ΔN-BOX	Pygo ΔPHD
601	RPL18	5	5	5	651	PIAS1	4	7	7	701	NIP30	4	3	10	751	hCG_36935	3	7	2
602	STAG2	5	5	4	652	RPL4	4	7	6	702	XRCC1	4	3	6	752	SAFB2	3	6	12
603	ARFGAP1	5	5	2	653	DDX49	4	7	5	703	GPS2/MLL4	4	3	5	753	CCDC94	3	6	11
604	HNRNPA0	5	4	9	654	SCAF8	4	7	4	704	PSMA4	4	3	5	754	ACOT2	3	6	10
605	C19orf43	5	4	9	655	UBN2	4	7	3	705	ZBTB14	4	3	4	755	RAN	3	6	7
606	PITX2	5	4	6	656	SPT5	4	6	15	706	mcdrh	4	3	3	756	PDCD11	3	6	7
607	DUF	5	4	6	657	CELF1	4	6	8	707	ZNF592	4	3	3	757	RB1	3	6	7
608	RNF8	5	4	6	658	TIAL1	4	6	7	708	EIF4G1	4	3	2	758	MBTD1	3	6	5
609	NIFK	5	4	6	659	RBFOX1	4	6	7	709	CACUL1	4	3	1	759	CIZ1	3	6	3
610	HIST1H2BN	5	4	5	660	STRAP	4	6	6	710	DHX37	4	2	11	760	NELFA	3	6	3
611	YY1AP1	5	4	5	661	SDE2	4	6	5	711	NSA2	4	2	10	761	RAVER2	3	6	1
612	HOXA10	5	4	4	662	CBLL1	4	6	5	712	MBD3	4	2	7	762	DEAF1	3	6	0
613	USF1	5	4	4	663	C17orf85	4	6	4	713	GIPC1	4	2	7	763	MLLT6	3	5	8
614	KDM5C	5	4	3	664	ZNF512B	4	5	13	714	FAM207A	4	2	6	764	FOXC1	3	5	8
615	SNAPC4	5	4	1	665	MAPK9	4	5	9	715	INTS12	4	2	6	765	PCBP2	3	5	7
616	FIGN	5	4	0	666	HDLBP	4	5	9	716	CHORDC1	4	2	6	766	PHF10	3	5	7
617	TNRC15	5	4	0	667	KIF23	4	5	8	717	PAX9	4	2	5	767	PINX1	3	5	6
618	CMTR1	5	3	11	668	NOP58	4	5	8	718	DUS2L	4	2	5	768	TFDP1	3	5	6
619	MNAT1	5	3	6	669	PDS5A	4	5	8	719	SLC25A3	4	2	5	769	EWSR1	3	5	5
620	GTF2E1	5	3	4	670	UFD1L	4	5	8	720	NF1	4	2	4	770	PRR12	3	5	5
621	RPP38	5	3	2	671	UBA3	4	5	8	721	NFRKB	4	2	1	771	ALKBH5	3	5	5
622	FLJ94417	5	2	7	672	STMN1	4	5	7	722	UBR5	4	2	1	772	NACA	3	5	4
623	CENPH	5	2	6	673	SRRM1	4	5	7	723	TSNAX	4	1	10	773	ZNF516	3	5	3
624	OGT	5	2	2	674	PRDX1	4	5	7	724	PRMT7	4	1	6	774	WHSC1L1	3	5	3
625	DNAH6	5	2	1	675	CBX8	4	5	7	725	PPIE	4	1	5	775	ALB	3	5	2
626	NIN	5	2	1	676	hCG_2039588	4	5	6	726	RPS6KA5	4	1	4	776	CDC40	3	5	2
627	SYMPK	5	2	0	677	MSANTD2	4	5	5	727	TIMELESS	4	1	2	777	FLJ55441	3	5	2
628	WDR5	5	1	2	678	KIAA0907	4	5	5	728	FBXO25	4	1	1	778	ZNF146	3	4	11
629	FIGNL1	5	1	1	679	ZNF503	4	5	4	729	SLK	4	1	1	779	DNTTIP2	3	4	10
630	CRSP8	5	1	0	680	DEK	4	5	3	730	DSG1	4	1	0	780	RPL7A	3	4	9
631	ANAPC1	5	1	0	681	PLEKHA1	4	5	2	731	POLR3D	4	1	0	781	PHF6	3	4	9
632	CHMP4B	5	0	3	682	ERCC5	4	5	1	732	DDX27	4	0	4	782	UBE2M	3	4	8
633	STAT1	5	0	0	683	AGFG1	4	4	9	733	PAXBP1	3	21	18	783	TSHZ3	3	4	8
634	LTV1	5	0	0	684	TADA3	4	4	7	734	PRRC2A	3	12	8	784	PDAP1	3	4	7
635	ZC3H4	4	15	18	685	NOLC1	4	4	7	735	ZBTB21	3	11	24	785	RNF2	3	4	7
636	LIG1	4	11	9	686	SET	4	4	6	736	LEMD3	3	10	14	786	RBM42	3	4	7
637	CWC22	4	10	6	687	KIAA1704	4	4	6	737	DDX3X	3	10	9	787	ZNF608	3	4	6
638	BEND3	4	10	3	688	ZCCHC17	4	4	6	738	BMS1	3	9	25	788	RTFDC1	3	4	6
639	CUL4B	4	9	6	689	BCORL1	4	4	5	739	NUDT21	3	9	14	789	DPF2	3	4	6
640	FOXK2	4	9	6	690	LRIF1	4	4	5	740	CTCF	3	9	13	790	PPP1R8	3	4	6
641	HSPH1	4	9	5	691	EHMT1	4	4	5	741	CHD3	3	8	15	791	NUCKS1	3	4	4
642	RAI17	4	8	9	692	RPL11	4	4	4	742	PPHLN1	3	8	10	792	TUBB	3	4	4
643	ZFHX3	4	8	9	693	FUS	4	4	4	743	TFCP2	3	8	8	793	MLLT4	3	4	3
644	SMEK2	4	8	6	694	EIF4H	4	4	4	744	SENP1	3	8	3	794	SALL2	3	4	2
645	RTF1	4	7	14	695	TCF3	4	4	3	745	RREB1	3	8	1	795	CTBP1	3	4	1
646	TAF7	4	7	12	696	RAD18	4	4	2	746	BCL11A	3	7	13	796	FLJ58252	3	4	1
647	PRPF18	4	7	11	697	HPX	4	4	1	747	NVL	3	7	10	797	MKL2	3	4	0
648	NUPL2	4	7	9	698	NCOA1	4	4	1	748	MBNL1	3	7	9	798	SYF2	3	3	10
649	NSFL1C	4	7	7	699	BCL9L	4	4	0	749	ZFP1	3	7	6	799	DIS3	3	3	10
650	PTBP2	4	7	7	700	CHAF1A	4	3	11	750	CLSPN	3	7	4	800	PPP1CC	3	3	9

	Protein ID	Pygo WT	Pygo ΔN-BOX	Pygo ΔPHD			Protein ID	Pygo WT	Pygo ΔN-BOX	Pygo ΔPHD			Protein ID	Pygo WT	Pygo ΔN-BOX	Pygo ΔPHD			Protein ID	Pygo WT	Pygo ΔN-BOX	Pygo ΔPHD
801	CCDC25	3	3	8		851	BRPF3	3	2	3		901	POLD1	2	4	19		951	NR2B1	2	2	7
802	SNRPD2	3	3	7		852	CDX2	3	2	3		902	RHEB	2	4	8		952	YTHDC2	2	2	7
803	RNASEH2B	3	3	7		853	CHAF1B	3	2	3		903	CPSF1	2	4	8		953	MAZ	2	2	6
804	KIAA1143	3	3	6		854	SLIT2	3	2	3		904	THOC3	2	4	7		954	SMNDC1	2	2	6
805	CCDC43	3	3	6		855	RAD51AP1	3	2	3		905	TFAP4	2	4	7		955	NANP	2	2	6
806	NFIB	3	3	5		856	DNAH10	3	2	2		906	ZNF521	2	4	6		956	CASZ1	2	2	5
807	TFAP2C	3	3	5		857	RNPC3	3	2	2		907	GMPS	2	4	6		957	PLEC	2	2	5
808	SNRPA	3	3	5		858	TET2	3	2	1		908	PWP2	2	4	5		958	C2orf49	2	2	5
809	CDCA2	3	3	5		859	FLG2	3	2	1		909	POM121C	2	4	5		959	PQBP1	2	2	5
810	VPS72	3	3	5		860	ZFX	3	2	1		910	UBXN7	2	4	5		960	MCM3	2	2	5
811	BCCIP	3	3	5		861	GNB2L1	3	2	1		911	KDM1A	2	4	5		961	EXOSC9	2	2	4
812	BRD7	3	3	5		862	LEO1	3	2	1		912	FLJ00353	2	4	4		962	NFATC2IP	2	2	4
813	PRRC2B	3	3	4		863	PAXIP1	3	2	1		913	MPP1	2	4	4		963	SSBP3	2	2	3
814	SRSF7	3	3	4		864	ZMYM3	3	2	1		914	DCAF13	2	4	4		964	HIST1H1D	2	2	3
815	CPSF4	3	3	4		865	TRIP12	3	1	11		915	KIN	2	4	1		965	SUB1	2	2	3
816	EMD	3	3	4		866	USP22	3	1	6		916	RARS	2	4	1		966	HIST1H2AC	2	2	3
817	RBM7	3	3	4		867	AGTPBP1	3	1	5		917	TDP1	2	4	1		967	RPS27	2	2	3
818	AASDHPPT	3	3	4		868	DDX56	3	1	5		918	ZCCHC8	2	4	1		968	TLX1	2	2	3
819	BAHCC1	3	3	4		869	RPL6	3	1	4		919	TAF6	2	4	0		969	ZNF207	2	2	3
820	H3F3B	3	3	3		870	LIN54	3	1	3		920	SLFN11	2	3	16		970	FAM192A	2	2	3
821	RPL37A	3	3	3		871	TOE1	3	1	2		921	PFN1	2	3	7		971	RPS14	2	2	3
822	CHMP2B	3	3	3		872	CDC27	3	1	1		922	RRP15	2	3	7		972	ANKRD17	2	2	3
823	PITX1	3	3	3		873	VIM	3	1	1		923	HOXD11	2	3	6		973	MYH9	2	2	3
824	UBFD1	3	3	3		874	ATAD2B	3	1	1		924	NKX2-4	2	3	6		974	POLR3C	2	2	3
825	BRCA1	3	3	3		875	LASP1	3	0	1		925	LYPLA2	2	3	5		975	YTHDF3	2	2	3
826	TDP2	3	3	3		876	MECOM	2	11	15		926	ZNF384	2	3	5		976	RBM48	2	2	3
827	PARG	3	3	2		877	RBM12B	2	10	16		927	TAF9B	2	3	5		977	JUNB	2	2	3
828	DLGAP5	3	3	2		878	ZNF711	2	8	12		928	MYBL2	2	3	5						
829	AHDC1	3	3	2		879	OTUD5	2	7	2		929	ARHGEF17	2	3	4						
830	QRICH1	3	3	2		880	WARS	2	6	9		930	U2AF1	2	3	4						
831	GTPBP4	3	3	1		881	RSBN1L	2	6	8		931	RPL21	2	3	4						
832	UVSSA	3	3	1		882	RECQL5	2	6	2		932	UTP11L	2	3	4						
833	SP2	3	3	0		883	PRDM2	2	5	10		933	ZBTB4	2	3	4						
834	DHPS	3	3	0		884	NOL8	2	5	9		934	SPTBN2	2	3	3						
835	RACGAP1	3	3	0		885	NOP2	2	5	8		935	ACTL6A	2	3	3						
836	MCM6	3	2	10		886	RPS9	2	5	7		936	ZNF346	2	3	3						
837	CDCA8	3	2	10		887	MBIP	2	5	6		937	TRAFIP20	2	3	3						
838	ANKRD11	3	2	9		888	SMARCAL1	2	5	6		938	PDS5B	2	3	3						
839	RAD51C	3	2	8		889	MECP2	2	5	6		939	AP3D1	2	3	2						
840	NIPBL	3	2	7		890	PDCL	2	5	5		940	CTPS1	2	3	2						
841	CACYBP	3	2	7		891	NT5DC1	2	5	5		941	TFAP2E	2	3	1						
842	HOXC9	3	2	6		892	EIF4B	2	5	4		942	GMEB2	2	3	1						
843	GATA4	3	2	6		893	UBE1	2	5	4		943	BYSL	2	3	1						
844	ZNF512	3	2	6		894	UTP3	2	5	3		944	ZFP106	2	3	0						
845	ANP32E	3	2	5		895	POLE	2	5	2		945	ZNF814	2	3	0						
846	FAM32A	3	2	5		896	NOL10	2	5	2		946	ZNF655	2	3	0						
847	MNX1	3	2	5		897	ZMYM1	2	5	1		947	NARG2	2	2	9						
848	DCAF7	3	2	5		898	GCFC2	2	5	1		948	PRDX6	2	2	8						
849	N-PAC	3	2	5		899	CPSF3	2	5	1		949	IPMK	2	2	8						
850	PBK	3	2	4		900	S100A8	2	5	0		950	SPAG7	2	2	7						

8.8. Raw Data TLE3 BioID (Cut-off ≥ 3 TSC)

		TLE3_4/4_LiCl	TLE3_4/4_Ctrl	eGFP_4/4_LiCl	eGFP_4/4_Ctrl	TLE3_4/2_LiCl	TLE3_4/2_Ctrl	eGFP_4/2_LiCl	eGFP_4/2_Ctrl
1	TLE3	227	214	0	2	217	223	0	2
2	HELLS	185	162	13	18	118	140	21	35
3	CCT8	176	237	62	36	362	377	56	121
4	NUP153	129	120	28	14	55	72	27	55
5	NONO	126	95	181	159	60	97	162	130
6	HNRNPM	123	67	19	10	38	62	1	24
7	NUDC	107	89	23	11	68	63	11	15
8	DDX46	101	87	63	59	28	46	37	91
9	FLNA	97	69	5	0	42	26	0	7
10	RPAP3	95	63	3	7	51	24	2	7
11	NCOR1	90	96	1	1	71	76	0	4
12	TLE1	86	81	0	1	99	113	0	2
13	TLE4	85	81	0	0	100	105	0	2
14	SON	84	76	61	56	47	63	86	61
15	SF3B3	66	44	48	37	25	25	34	34
16	TF	59	76	27	38	45	60	36	45
17	CTTN	59	55	8	3	21	22	1	11
18	ANKHD1	58	77	2	1	33	28	0	1
19	CHAMP1	58	53	33	50	22	39	48	54
20	PC	54	50	0	2	47	37	4	16
21	KDM3B	54	39	10	6	19	36	5	17
22	GSE1	53	77	0	0	50	49	1	1
23	SF3B1	50	72	57	53	42	39	54	101
24	RBM14	50	48	43	59	24	36	49	35
25	PARP1	50	34	177	176	19	28	168	114
26	HSPA1A	50	28	11	4	26	24	4	18
27	HNRNPA1	50	21	107	241	14	14	183	70
28	PRRC2A	49	52	2	1	9	11	2	1
29	PRRC2B	49	49	0	1	25	17	1	0
30	DDX42	48	40	59	48	18	26	36	46
31	UBAP2L	46	67	1	0	18	22	2	3
32	RANBP2	46	42	1	3	18	34	0	2
33	CCAR2	46	24	22	10	12	19	14	21
34	DDX5	45	50	123	156	23	31	122	76
35	PRPF3	43	40	47	71	37	38	117	61
36	SPEN	42	45	7	6	24	25	11	6
37	HNRNPK	41	34	121	148	30	34	159	80
38	HELZ	40	36	0	1	30	16	0	2
39	PRPF40A	40	27	21	13	13	17	14	12
40	FOXK1	39	34	6	3	15	22	3	2
41	DHX15	37	35	70	86	17	19	91	45
42	GNL3	36	42	25	23	54	35	27	56
43	SF1	36	36	2	3	19	23	3	7
44	MYO6	36	32	37	36	21	8	32	28
45	TPX2	35	33	71	78	14	29	167	70
46	HCFC1	35	29	3	1	16	18	3	32
47	TCF20	35	27	3	1	15	27	8	2
48	MRE11	35	27	12	20	12	20	16	19
49	DDX17	34	32	67	80	14	17	59	45
50	TAGLN2	33	69	48	105	54	34	89	51

		TLE3_4/4_LiCl	TLE3_4/4_Ctrl	eGFP_4/4_LiCl	eGFP_4/4_Ctrl	TLE3_4/2_LiCl	TLE3_4/2_Ctrl	eGFP_4/2_LiCl	eGFP_4/2_Ctrl
51	CHD4	33	30	32	30	14	26	38	38
52	RBM10	33	27	35	34	13	17	40	30
53	CLINT1	32	29	2	2	7	16	0	1
54	SNRNP200	32	21	87	59	22	25	62	103
55	INTS13	31	45	5	7	28	0	5	19
56	ZNF281	31	30	5	5	21	24	5	4
57	AGFG1	31	28	8	3	19	39	8	17
58	KIF23	30	31	8	6	16	18	4	18
59	HSPA8	30	20	7	3	20	18	2	4
60	UBAP2	29	34	0	0	9	7	0	1
61	SF3B2	29	28	47	60	10	8	35	46
62	SYNRG	28	47	0	0	20	25	0	0
63	U2SURP	28	32	33	46	6	6	26	40
64	ADNP	28	26	29	23	9	7	33	40
65	EEF2	28	20	9	0	18	19	0	10
66	PCBP1	28	19	31	31	11	18	31	29
67	SFPQ	28	18	56	56	14	17	62	27
68	GTF3C4	27	25	11	10	15	19	16	21
69	ARID3B	27	15	0	0	5	19	0	4
70	DHX38	26	28	33	57	23	15	55	36
71	GSPT1	26	27	4	0	18	11	0	8
72	VIM	26	20	33	7	25	14	14	30
73	HSP90AB1	26	17	4	1	21	16	0	5
74	PCBP2	26	17	32	34	11	14	32	22
75	HIST1H1C	26	15	24	47	13	20	40	26
76	CMTR1	25	43	16	15	32	46	20	26
77	TMPO	25	33	61	53	11	18	62	61
78	DDX3X	25	25	24	32	16	18	26	16
79	SART1	25	23	60	77	10	14	89	48
80	CHERP	25	19	18	8	5	7	10	15
81	HIST1H1E	25	12	32	58	14	24	51	29
82	GATAD2B	24	27	20	18	15	19	14	30
83	ZC3H14	24	27	19	23	12	20	33	34
84	RPS27A	24	27	19	18	12	18	24	20
85	RBM12	24	25	0	0	7	12	2	3
86	RPA1	24	20	23	11	11	20	13	29
87	HNRNPA2B1	24	18	31	85	5	7	40	26
88	CORO7	24	12	2	1	12	12	0	7
89	TCERG1	23	30	39	23	10	17	33	27
90	CHD7	23	26	9	7	8	15	7	3
91	KHSRP	22	31	14	1	14	12	1	18
92	TNRC6A	22	26	2	2	9	10	1	1
93	BCORL1	22	25	1	1	13	13	2	1
94	ZNF148	22	22	2	1	17	18	5	3
95	PMS1	22	19	0	0	15	21	1	2
96	CDKN2AIP	22	12	16	6	9	13	9	18
97	KIF4A	21	25	29	32	10	4	28	45
98	SPDL1	21	24	4	2	13	28	2	14
99	SAFB2	21	20	45	25	9	5	35	50
100	PIAS1	21	16	0	0	9	11	0	0

		TLE3_4/4_LiCl	TLE3_4/4_Ctrl	eGFP_4/4_LiCl	eGFP_4/4_Ctrl	TLE3_4/2_LiCl	TLE3_4/2_Ctrl	eGFP_4/2_LiCl	eGFP_4/2_Ctrl
101	CNN2	21	14	18	20	9	3	17	8
102	FASN	21	8	1	2	21	11	1	0
103	NCOR2	20	26	2	1	21	21	0	0
104	YTHDF2	20	26	2	3	10	14	3	2
105	YTHDF3	20	26	1	4	9	13	3	2
106	SAFB	20	24	48	33	11	6	43	56
107	PIK3C2A	20	22	1	1	19	14	1	0
108	ZNF384	20	19	12	12	16	18	20	17
109	ZBTB10	20	19	9	10	4	10	10	9
110	TARDBP	20	17	31	23	6	14	31	19
111	SLU7	20	16	11	30	10	19	22	22
112	NKX2-5	20	15	1	6	4	9	4	0
113	EDC3	20	14	13	6	16	32	12	23
114	TUBA1B	19	22	13	8	13	26	7	22
115	C15orf39	19	21	0	0	7	10	0	0
116	EXOSC10	19	20	39	44	14	15	38	36
117	ILKAP	19	20	39	37	12	17	51	28
118	ZBTB33	19	20	4	1	7	17	1	3
119	RBM22	19	19	24	27	11	13	26	18
120	CNN3	19	18	11	37	6	4	22	13
121	HSP90AA1	19	11	3	1	16	11	0	5
122	UPF1	18	29	7	5	10	9	3	13
123	ZNF703	18	26	1	0	14	15	1	10
124	XRN1	18	24	0	1	17	13	0	1
125	ANKRD17	18	22	2	0	15	10	0	2
126	SART3	18	21	62	51	12	0	33	48
127	CXorf56	18	19	12	40	8	8	27	14
128	CCAR1	18	19	5	1	7	5	3	6
129	XAB2	18	16	0	0	16	17	0	6
130	HOXC9	18	9	0	8	3	5	4	0
131	PABPC1	17	25	5	8	10	9	4	4
132	POLR3F	17	22	12	14	12	11	17	16
133	TMPO	17	21	99	107	7	10	109	75
134	HNRNPUL1	17	20	13	11	13	11	4	22
135	NUMA1	17	20	136	143	11	18	148	92
136	GPATCH1	17	20	7	5	7	5	5	11
137	IK	17	19	28	36	5	16	44	34
138	SMARCA5	17	18	41	28	3	2	23	32
139	EP300	17	14	0	0	11	7	2	0
140	STAU1	17	13	13	10	6	8	13	7
141	TUBB4B	17	10	5	0	10	24	2	12
142	FAM50A	17	10	37	56	8	15	53	28
143	CHD8	17	10	12	4	6	10	7	5
144	PSPC1	17	10	26	22	5	16	21	18
145	CPSF7	17	9	4	0	4	8	1	5
146	RPS23	16	43	11	13	32	16	21	11
147	CCNT1	16	29	2	6	6	9	7	9
148	RPL36A	16	27	10	13	24	16	15	8
149	SNW1	16	25	24	33	11	17	37	31
150	WDR70	16	25	12	14	8	10	22	24

		TLE3_4/4_LiCl	TLE3_4/4_Ctrl	eGFP_4/4_LiCl	eGFP_4/4_Ctrl	TLE3_4/2_LiCl	TLE3_4/2_Ctrl	eGFP_4/2_LiCl	eGFP_4/2_Ctrl
151	DHX9	16	21	60	72	10	7	49	49
152	GSPT2	16	17	2	0	12	9	0	6
153	NCOA2	16	17	0	0	9	10	0	1
154	HOXC11	16	16	0	4	9	10	5	1
155	HLCS	16	16	0	0	9	6	1	4
156	FAM192A	16	16	7	15	3	0	15	11
157	NUP50	16	15	16	8	5	12	9	24
158	HOXA10	16	15	3	7	5	8	7	0
159	PAK2	16	14	13	2	7	10	6	26
160	HOXB9	16	13	4	10	10	8	9	1
161	CENPH	16	13	0	0	6	4	0	2
162	NOSIP	16	11	13	29	6	6	31	15
163	E1B15	16	9	8	2	6	0	7	10
164	RACK1	16	8	5	3	7	0	2	2
165	HOXA9	16	7	0	5	4	5	4	1
166	RBM17	15	24	26	25	7	17	31	29
167	RBM25	15	19	25	19	2	3	25	18
168	RPL19	15	19	6	54	0	7	11	3
169	CDC5L	15	18	37	64	7	9	51	27
170	ZFR	15	18	12	11	3	7	12	16
171	PPP4R3A	15	17	13	6	13	17	6	21
172	YAP1	15	17	0	1	5	7	0	0
173	POLA2	15	16	11	11	17	23	5	17
174	HNRNPU	15	15	51	44	11	8	70	74
175	EIF4B	15	15	18	18	10	10	7	9
176	POLR2A	15	15	13	4	8	17	3	3
177	PRPF8	15	14	22	12	18	27	8	15
178	SUGT1	15	14	5	0	11	4	2	8
179	TUBB	15	14	6	0	10	25	3	15
180	ZNF292	15	14	2	0	7	9	6	1
181	MB21D2	15	14	1	0	5	7	2	6
182	CDK11B	15	13	25	46	2	8	33	15
183	KMT2D	15	12	1	0	1	5	2	3
184	TFAP2A	15	11	2	0	5	6	1	3
185	IRS4	15	8	1	0	2	1	1	0
186	SYMPK	15	6	2	2	10	12	1	2
187	ADAR	15	5	22	2	3	8	3	13
188	ACTB	15	4	7	10	3	0	4	3
189	TTN	14	21	29	22	15	12	24	15
190	TNRC6B	14	19	0	1	6	7	0	0
191	RHEB	14	18	11	16	11	10	17	14
192	HNRNPF	14	16	28	17	8	16	29	23
193	FLNC	14	13	0	1	10	3	1	2
194	FUBP1	14	13	3	0	9	10	0	10
195	POLA1	14	12	26	9	6	12	26	23
196	SMARCA4	14	11	5	0	9	13	1	4
197	CPSF6	14	11	4	1	6	11	5	18
198	TTC4	14	9	6	1	6	5	0	6
199	GTPBP4	14	9	19	28	4	9	23	14
200	TDP2	14	9	11	17	3	5	22	9

		TLE3_4/4_LiCl	TLE3_4/4_Ctrl	eGFP_4/4_LiCl	eGFP_4/4_Ctrl	TLE3_4/2_LiCl	TLE3_4/2_Ctrl	eGFP_4/2_LiCl	eGFP_4/2_Ctrl
201	RPL36AL	13	23	9	9	15	13	13	6
202	CEP85	13	22	2	2	7	9	2	0
203	SUGP2	13	18	3	3	6	9	1	7
204	BRD4	13	16	4	0	5	10	2	5
205	LYPLA2	13	15	8	27	12	10	24	10
206	ZC3H11A	13	15	67	29	10	19	35	56
207	FUBP3	13	15	4	0	6	11	0	7
208	DPYSL3	13	12	1	0	9	5	0	1
209	MASTL	13	12	0	0	6	7	0	2
210	TCF7L2	13	12	0	0	2	8	0	1
211	HOXB6	13	11	0	8	4	5	4	0
212	GPKOW	13	11	21	21	3	7	20	21
213	EZR	13	9	2	0	9	8	0	10
214	RPL8	13	9	5	12	1	2	15	4
215	RUVBL2	13	8	3	2	5	0	1	12
216	RPL13	13	6	5	33	3	2	15	9
217	USP7	12	19	34	41	4	5	32	32
218	WDR36	12	16	20	28	5	15	36	31
219	PCNP	12	14	9	63	11	13	42	16
220	HOXD11	12	14	0	4	4	9	6	1
221	FHL1	12	11	30	75	7	7	31	19
222	GTSE1	12	11	2	0	5	1	2	7
223	ACACA	12	10	2	1	15	15	1	0
224	TRIM33	12	10	2	1	8	8	1	3
225	RBM39	12	10	9	20	5	6	15	20
226	HP1BP3	12	10	33	59	3	13	83	34
227	TAF9	12	10	5	7	3	2	5	13
228	EEF1A1	12	9	15	14	5	10	9	17
229	WIPI2	12	8	2	3	3	4	1	3
230	RPRD2	12	7	1	0	3	4	0	1
231	TOP2A	12	6	76	58	7	16	80	54
232	HNRNPA3	12	6	20	42	1	4	23	17
233	DOCK7	12	3	2	1	3	3	0	2
234	SNRPD2	11	21	14	20	19	12	30	25
235	IRF2BP2	11	18	0	0	11	9	0	0
236	FOXK2	11	17	2	2	7	7	0	2
237	DVL2	11	17	0	0	4	6	1	0
238	OCRL	11	16	2	1	11	8	1	1
239	PPP1R10	11	16	17	0	5	7	6	16
240	ZNF629	11	16	8	6	0	5	15	3
241	VBP1	11	13	3	1	16	10	4	3
242	SBNO1	11	13	3	14	13	19	17	5
243	NELFE	11	13	13	29	7	9	22	14
244	MSH6	11	13	39	7	2	11	14	14
245	PABPC4	11	12	6	7	7	5	3	2
246	HES1	11	12	0	0	7	4	1	1
247	KHDC4	11	11	1	0	9	0	1	2
248	ZMIZ1	11	11	0	0	8	8	1	1
249	PRCC	11	11	4	5	3	7	7	5
250	ZMAT2	11	10	2	38	9	8	17	18

		TLE3_4/4_LiCl	TLE3_4/4_Ctrl	eGFP_4/4_LiCl	eGFP_4/4_Ctrl	TLE3_4/2_LiCl	TLE3_4/2_Ctrl	eGFP_4/2_LiCl	eGFP_4/2_Ctrl
251	CORO1C	11	10	5	0	7	4	0	8
252	MMTAG2	11	9	14	24	7	5	22	12
253	SATB2	11	9	0	0	5	6	0	0
254	HDLBP	11	9	3	3	5	2	1	2
255	CIAPIN1	11	8	6	6	3	2	7	8
256	SATB1	11	6	0	0	3	8	0	0
257	SF3A1	11	5	7	0	3	9	0	14
258	FKBP4	11	4	0	0	3	1	0	0
259	EIF4G1	11	4	4	0	1	2	0	1
260	KMT2C	11	3	0	0	1	4	3	0
261	ASCC3	11	2	5	0	7	2	0	1
262	BCOR	10	27	5	1	29	23	2	2
263	YTHDF1	10	17	1	0	7	10	0	2
264	ZFP91	10	14	7	16	9	12	19	13
265	RTF1	10	14	22	21	6	11	14	21
266	ARID1B	10	14	2	0	3	7	0	0
267	DVL3	10	13	0	0	7	6	1	1
268	PHF3	10	13	4	0	0	6	2	3
269	HTATSF1	10	12	29	16	4	5	21	25
270	TAF15	10	12	29	13	4	2	29	13
271	RPS6	10	11	8	14	9	8	8	15
272	CDCA2	10	11	4	11	9	6	22	14
273	KBTBD6	10	11	3	3	7	6	8	11
274	PKN1	10	11	2	0	5	0	2	1
275	ZMIZ2	10	10	0	1	7	8	1	1
276	EFHD2	10	10	11	15	5	5	7	7
277	TRPS1	10	10	0	0	4	2	0	1
278	ESS2	10	10	2	3	2	0	0	0
279	RAVER2	10	9	0	0	8	10	0	2
280	TCP1	10	9	1	0	8	8	0	1
281	MNX1	10	9	0	5	4	9	6	1
282	CDC73	10	9	22	19	4	8	15	27
283	FIP1L1	10	9	6	11	4	7	13	15
284	NCL	10	9	57	50	4	4	35	36
285	RBM27	10	9	17	15	2	6	15	10
286	NIPBL	10	9	2	1	2	1	0	4
287	SNRPB	10	8	4	15	5	8	7	10
288	PDCD5	10	7	8	8	4	5	12	9
289	EYA3	10	7	0	0	4	5	0	0
290	SDE2	10	7	7	7	4	3	5	7
291	DPF1	10	7	1	0	1	5	3	2
292	C1orf198	10	7	1	1	1	0	1	3
293	CTBP1	10	6	7	0	2	5	0	3
294	RPL3	10	5	11	13	6	8	19	8
295	CHD3	10	5	11	9	6	8	8	11
296	JUN	10	5	2	0	5	5	1	1
297	NR3C1	10	5	0	1	5	4	1	2
298	NFIB	10	5	4	2	4	5	5	6
299	CEP350	10	4	0	1	6	2	2	1
300	TLK2	10	3	0	2	3	4	0	4

		TLE3_4/4_LiCl	TLE3_4/4_Ctrl	eGFP_4/4_LiCl	eGFP_4/4_Ctrl	TLE3_4/2_LiCl	TLE3_4/2_Ctrl	eGFP_4/2_LiCl	eGFP_4/2_Ctrl
301	CCT6A	9	21	0	0	17	17	0	1
302	MORC4	9	16	0	0	6	15	0	0
303	RPL35	9	14	6	10	14	10	17	7
304	ATN1	9	14	1	0	4	5	0	0
305	SEC16A	9	13	0	0	3	4	0	0
306	INCENP	9	12	25	36	5	5	40	33
307	STAT3	9	12	0	0	4	8	0	2
308	RPL27A	9	12	7	8	3	8	12	3
309	FUS	9	12	18	14	3	4	20	11
310	FBRS	9	12	0	0	3	4	0	0
311	STMN1	9	11	13	9	8	8	13	11
312	TCF12	9	10	0	0	11	5	0	3
313	CHD6	9	10	9	4	5	7	7	4
314	LEF1	9	10	0	0	3	6	0	1
315	NKX3-1	9	10	0	4	2	4	4	0
316	NUFIP2	9	10	0	0	2	1	0	0
317	NAB1	9	9	2	0	4	10	2	3
318	ZNF362	9	9	3	5	3	7	6	8
319	TES	9	9	21	12	3	1	6	12
320	POM121C	9	9	1	2	1	3	0	0
321	PSMC5	9	8	2	0	4	7	0	4
322	PDLIM1	9	8	5	5	4	1	5	5
323	PKM	9	8	10	1	2	4	3	3
324	GTF2I	9	8	7	2	1	5	0	6
325	KDM1A	9	8	1	0	1	2	0	1
326	GPATCH4	9	7	17	21	5	6	27	32
327	TAF9B	9	7	6	7	3	1	5	11
328	SUGP1	9	7	3	2	1	7	4	13
329	CCDC87	9	6	14	23	12	14	13	9
330	TFAP2C	9	6	1	0	5	4	1	2
331	SRSF1	9	6	2	1	5	0	6	13
332	TRIM25	9	6	3	0	4	4	1	4
333	C19orf54	9	5	4	1	4	5	1	6
334	MCM3AP	9	5	1	0	1	4	1	1
335	ZNF318	9	5	5	1	0	6	0	1
336	RAN	9	4	2	29	2	3	7	6
337	MBD3	9	4	3	2	2	1	1	5
338	PUS7	9	4	2	2	1	0	2	14
339	ABCF1	9	3	4	1	2	2	1	1
340	SRP54	9	2	0	0	8	1	0	1
341	ELMSAN1	8	25	0	1	5	8	0	0
342	PFDN2	8	22	1	0	23	8	0	0
343	TXN	8	17	10	35	12	8	23	9
344	MGA	8	16	3	1	13	27	11	3
345	IRF2BP1	8	13	0	0	7	6	0	0
346	PPP4R3B	8	11	3	3	4	7	2	6
347	PSME3	8	11	2	1	4	4	0	2
348	WBP11	8	11	10	18	2	2	14	10
349	SLK	8	10	9	2	6	8	2	8
350	PAPOLA	8	10	7	4	6	6	2	12

		TLE3_4/4_LiCl	TLE3_4/4_Ctrl	eGFP_4/4_LiCl	eGFP_4/4_Ctrl	TLE3_4/2_LiCl	TLE3_4/2_Ctrl	eGFP_4/2_LiCl	eGFP_4/2_Ctrl
351	ETF1	8	9	9	11	4	5	9	7
352	NXF1	8	9	15	17	3	4	16	9
353	PPME1	8	9	25	19	2	8	27	11
354	TRIM28	8	8	3	1	10	9	2	26
355	GNL3L	8	8	8	8	9	5	1	13
356	KBTBD7	8	8	3	0	5	3	3	9
357	POGZ	8	8	15	11	3	5	9	11
358	DPYSL2	8	7	1	0	7	5	0	3
359	MYH9	8	7	0	1	5	3	3	1
360	LDB1	8	7	1	1	4	7	0	1
361	MPP1	8	7	11	10	4	5	14	13
362	SMAP2	8	7	1	0	3	6	0	1
363	ANXA2	8	7	5	9	3	0	9	6
364	THRAP3	8	7	66	68	0	2	47	69
365	JMJD1C	8	6	1	1	13	11	3	2
366	CACYBP	8	6	1	5	8	4	1	4
367	IGBP1	8	6	2	6	7	8	5	5
368	PRDX1	8	6	9	15	7	7	16	11
369	KIF22	8	6	20	21	5	6	28	25
370	RNMT	8	6	20	21	4	9	28	18
371	L3MBTL3	8	6	3	0	2	5	2	5
372	RBM4	8	6	3	3	2	3	4	1
373	MSX2	8	6	0	4	2	3	4	0
374	SNCA	8	5	8	9	5	10	9	11
375	LBR	8	5	47	35	4	0	62	44
376	DACH1	8	5	0	6	3	6	3	1
377	ACIN1	8	5	29	36	3	2	40	26
378	RBBP4	8	5	9	3	2	4	2	8
379	TARS	8	5	1	0	2	2	1	2
380	LARP4B	8	5	0	0	2	1	0	0
381	TAF7	8	4	5	1	4	3	2	2
382	CDC37	8	3	4	1	4	2	2	5
383	TFIP11	8	3	3	0	3	5	0	8
384	PBX2	8	3	0	1	2	8	0	0
385	PINX1	8	3	6	9	2	1	20	9
386	JPT2	8	3	7	11	2	0	12	9
387	RPS11	8	3	4	4	1	6	1	3
388	RPL36	8	3	9	7	0	2	2	0
389	CUX1	8	2	1	0	4	8	1	0
390	RPS3	8	2	1	1	3	1	0	4
391	PUF60	8	1	6	0	1	6	1	6
392	SSRP1	7	12	7	4	4	6	5	14
393	STRBP	7	12	25	17	2	6	14	27
394	PAPOLG	7	11	10	5	6	7	5	13
395	CD2AP	7	10	0	0	9	3	0	5
396	YTHDC2	7	10	2	2	2	0	0	1
397	BUD13	7	9	3	5	5	7	10	6
398	PKN2	7	9	11	1	2	0	5	3
399	NECAP2	7	9	6	15	1	4	6	6
400	RERE	7	9	0	0	1	1	1	0

		TLE3_4/4_LiCl	TLE3_4/4_Ctrl	eGFP_4/4_LiCl	eGFP_4/4_Ctrl	TLE3_4/2_LiCl	TLE3_4/2_Ctrl	eGFP_4/2_LiCl	eGFP_4/2_Ctrl
401	PDLIM5	7	8	1	1	6	5	1	4
402	ACOT1	7	8	6	3	5	7	6	6
403	HSPH1	7	8	1	0	4	4	1	1
404	HNRNPH3	7	8	7	11	4	0	9	5
405	BRIP1	7	8	1	0	1	1	1	1
406	USP48	7	8	12	0	0	0	5	5
407	RPS8	7	7	6	12	7	5	3	13
408	GATA6	7	7	0	0	4	7	0	0
409	ZYX	7	7	0	1	4	1	0	0
410	PRRC2C	7	7	0	1	3	3	0	2
411	SYNE2	7	7	4	3	2	6	4	2
412	U2AF2	7	7	8	9	1	6	17	15
413	TRIP6	7	7	0	0	1	4	1	0
414	SFSWAP	7	7	9	7	0	2	9	8
415	MAGED2	7	6	8	2	9	7	1	7
416	HOXA13	7	6	1	1	5	7	1	2
417	ARNT	7	6	0	0	5	7	0	0
418	EPS15L1	7	6	2	1	5	5	0	2
419	DNAJC7	7	6	2	0	5	1	0	0
420	MEF2D	7	6	1	0	4	8	0	4
421	RXRA	7	6	1	2	4	4	5	3
422	NSRP1	7	6	9	8	2	4	22	12
423	HNRNPA0	7	6	10	29	1	2	12	10
424	PRDX6	7	6	5	20	1	1	8	6
425	SKP1	7	5	6	2	8	4	3	3
426	FERMT2	7	5	1	1	6	3	0	1
427	DNAH5	7	5	1	3	5	6	3	3
428	PTBP1	7	5	17	19	4	2	21	10
429	NUDT21	7	5	3	14	4	2	8	8
430	HNRNPH1	7	5	13	4	3	9	13	9
431	GPALPP1	7	5	9	13	2	4	8	12
432	PDX1	7	5	0	4	2	3	4	0
433	ANLN	7	5	13	3	2	2	6	18
434	CHORDC1	7	5	3	0	2	2	1	3
435	PITX1	7	4	2	3	3	5	3	0
436	RUVBL1	7	4	0	0	3	3	0	5
437	RPS6KA1	7	4	0	0	2	1	0	1
438	PCCA	7	3	0	0	5	5	0	0
439	EIF4G2	7	3	0	0	3	2	0	0
440	XRCC6	7	3	4	4	2	8	3	16
441	WASL	7	3	5	0	2	4	1	5
442	RAD51C	7	3	2	1	2	4	1	1
443	ARGLU1	7	3	5	10	2	3	6	7
444	KIN	7	3	16	25	2	1	24	15
445	SNAP29	7	3	0	0	2	1	0	1
446	NKRF	7	2	12	8	4	3	1	14
447	TTK	7	2	0	0	3	1	0	0
448	CCT5	6	15	0	0	7	11	0	0
449	RAVER1	6	12	1	0	3	2	0	0
450	MSH3	6	11	13	10	2	3	11	12

		TLE3_4/4_LiCl	TLE3_4/4_Ctrl	eGFP_4/4_LiCl	eGFP_4/4_Ctrl	TLE3_4/2_LiCl	TLE3_4/2_Ctrl	eGFP_4/2_LiCl	eGFP_4/2_Ctrl
451	GTF2F2	6	9	15	37	5	2	12	13
452	MYBL2	6	9	2	0	2	5	0	0
453	SMG7	6	8	1	0	6	1	0	0
454	RPL24	6	8	9	11	5	11	13	7
455	CDK1	6	8	9	7	5	4	3	9
456	RFC4	6	8	8	7	5	2	8	8
457	FBRSL1	6	8	0	0	4	4	1	0
458	LIG3	6	8	17	30	1	2	20	25
459	PUM2	6	7	1	0	3	3	0	0
460	TMOD3	6	7	2	0	1	3	0	1
461	MCM7	6	7	0	0	1	3	0	0
462	NCBP3	6	7	13	14	0	2	9	13
463	MCCC1	6	6	1	1	8	8	0	0
464	WDHD1	6	6	9	13	4	3	23	24
465	PHF21A	6	6	0	0	3	4	0	0
466	ZRANB2	6	6	14	29	3	3	27	16
467	BRD2	6	6	15	13	1	3	14	4
468	CFDP1	6	6	7	2	1	3	14	10
469	KPNA3	6	5	14	9	5	2	13	8
470	RPS2	6	5	1	4	5	2	1	3
471	ZNF217	6	5	2	2	2	4	1	1
472	PSMA4	6	5	2	3	2	2	2	4
473	SERBP1	6	5	9	9	2	1	11	7
474	RPL26	6	5	5	3	1	5	4	1
475	ALB	6	4	11	1	22	18	9	16
476	TOP1	6	4	4	13	7	2	8	11
477	QSER1	6	4	0	0	6	5	0	1
478	CDK12	6	4	8	3	4	6	5	4
479	RRM2	6	4	3	1	4	6	2	5
480	AHSA1	6	4	7	6	3	3	9	11
481	DNAJC9	6	4	11	14	3	1	12	8
482	HOXD13	6	4	0	0	2	4	1	2
483	QKI	6	4	0	0	2	3	0	0
484	RPL7A	6	4	9	3	2	2	3	3
485	KNOP1	6	4	14	17	1	2	28	23
486	LDHA	6	4	0	0	1	1	0	4
487	BAZ1B	6	4	68	57	0	3	68	26
488	VPS13D	6	3	1	2	5	2	2	2
489	HNRNPD	6	3	12	11	3	1	12	3
490	GPS2	6	3	1	1	2	2	1	0
491	STIP1	6	3	0	0	2	2	1	0
492	LARP1	6	3	1	0	1	1	1	1
493	ISL2	6	3	0	0	0	3	0	0
494	DCAF7	6	3	0	0	0	1	0	0
495	RPL18A	6	2	2	2	7	6	2	5
496	GLO1	6	2	1	3	5	3	2	7
497	MAP1B	6	2	0	2	5	1	1	3
498	UBE2T	6	2	5	22	4	2	6	4
499	EIF4H	6	2	0	13	2	2	4	5
500	CCNB1	6	2	3	2	2	1	4	5

		TLE3_4/4_LiCl	TLE3_4/4_Ctrl	eGFP_4/4_LiCl	eGFP_4/4_Ctrl	TLE3_4/2_LiCl	TLE3_4/2_Ctrl	eGFP_4/2_LiCl	eGFP_4/2_Ctrl
501	RPL15	6	2	2	1	2	0	1	4
502	SMARCD3	6	2	0	1	1	2	1	1
503	RPL4	6	2	11	11	0	2	17	6
504	TIAL1	6	2	1	0	0	2	0	0
505	AIP	6	2	1	0	0	1	0	1
506	SLC25A5	6	1	0	2	5	4	0	3
507	SYAP1	6	1	0	1	2	2	0	0
508	SMCHD1	6	1	20	9	1	2	12	8
509	MATR3	6	1	11	4	0	0	3	1
510	IRAK4	6	1	3	0	0	0	0	3
511	RAE1	6	1	0	0	0	0	0	0
512	MAP4	6	0	0	0	3	2	2	0
513	SKA3	6	0	0	0	0	1	0	0
514	ATXN2L	5	19	0	0	4	1	1	0
515	CCT2	5	13	0	0	3	6	0	0
516	RAI1	5	13	4	3	2	8	9	1
517	LENG8	5	12	1	0	4	7	0	2
518	PAXIP1	5	12	0	2	3	1	1	0
519	MAZ	5	11	8	9	1	4	6	8
520	NUDT5	5	10	9	8	8	4	7	14
521	DHX16	5	10	41	50	2	1	30	21
522	PFDN5	5	9	0	1	8	7	0	0
523	PUM1	5	9	1	2	4	1	0	0
524	WDR18	5	9	7	3	3	5	6	2
525	RPL29	5	8	4	14	9	10	17	10
526	CDK13	5	8	7	3	5	7	6	4
527	ZNF503	5	8	0	0	5	2	1	4
528	GPATCH8	5	8	1	2	4	4	1	2
529	ANXA1	5	8	10	22	2	2	12	6
530	SLC4A1AP	5	8	16	6	1	7	9	13
531	AP3D1	5	7	11	18	6	1	19	28
532	PPIL2	5	7	7	17	3	11	19	11
533	HMCES	5	7	5	6	3	9	6	9
534	HAT1	5	7	7	1	3	5	3	10
535	TFAP4	5	7	0	0	1	5	0	1
536	NFIC	5	7	4	2	1	3	4	3
537	CC2D1A	5	7	5	1	1	0	0	0
538	NKX2-4	5	7	0	0	0	4	0	0
539	CNOT4	5	7	0	0	0	3	0	0
540	AKAP8	5	6	1	0	4	5	1	0
541	MECOM	5	6	0	0	4	0	0	0
542	AKAP9	5	6	5	6	3	3	4	4
543	NFIA	5	6	5	1	3	2	5	4
544	LRRC42	5	6	1	0	2	6	2	5
545	PRPF4	5	6	17	18	2	5	21	20
546	UBE2M	5	6	8	6	2	4	10	9
547	GATAD2A	5	6	12	17	1	3	17	9
548	GTF2B	5	6	10	14	1	1	4	6
549	TWF2	5	6	10	8	1	1	5	4
550	RPL32	5	6	8	9	0	4	12	7

		TLE3_4/4_LiCl	TLE3_4/4_Ctrl	eGFP_4/4_LiCl	eGFP_4/4_Ctrl	TLE3_4/2_LiCl	TLE3_4/2_Ctrl	eGFP_4/2_LiCl	eGFP_4/2_Ctrl
551	BCLAF1	5	6	30	25	0	1	30	46
552	MBNL1	5	5	3	3	5	4	1	2
553	UNG	5	5	4	10	4	3	9	5
554	VCAN	5	5	4	2	3	3	1	3
555	RACGAP1	5	5	12	10	2	2	10	10
556	TWF1	5	5	5	4	2	0	6	0
557	RDX	5	5	2	0	2	0	0	4
558	GATA4	5	5	1	1	1	4	3	1
559	LMCD1	5	5	19	12	1	2	13	12
560	ELAVL1	5	5	7	8	1	2	8	5
561	NSUN2	5	5	4	1	1	1	0	0
562	XIAP	5	5	6	7	0	6	14	7
563	CTBP2	5	5	1	0	0	5	0	0
564	UBLCP1	5	5	8	2	0	2	2	3
565	TBCB	5	4	11	8	6	0	11	8
566	EYA4	5	4	0	0	4	5	0	0
567	SUB1	5	4	5	8	4	4	10	5
568	VARS	5	4	4	3	4	0	1	2
569	RPL10	5	4	6	4	3	4	2	2
570	APBB1	5	4	0	0	3	4	0	1
571	VCL	5	4	1	2	3	1	3	1
572	SULT1A1	5	4	1	0	3	0	1	2
573	MBTD1	5	4	5	2	2	3	8	4
574	EBF3	5	4	0	0	1	7	0	0
575	PPWD1	5	4	8	11	1	2	7	7
576	MIS18A	5	4	0	7	1	1	8	6
577	BRCC3	5	4	0	0	1	0	1	1
578	ZNF609	5	3	1	1	4	7	1	1
579	PHAX	5	3	7	1	4	3	10	9
580	HNRNPDL	5	3	7	11	4	1	8	3
581	EMD	5	3	10	15	4	0	11	13
582	MTA1	5	3	0	3	3	5	1	9
583	UTP14A	5	3	26	56	2	5	41	24
584	YLPM1	5	3	3	4	2	3	2	4
585	DCLRE1A	5	3	0	0	2	0	1	1
586	PBK	5	3	3	2	1	1	4	4
587	NUDCD3	5	3	0	0	1	0	0	0
588	DEPDC7	5	3	0	0	0	4	0	0
589	NCAPG	5	3	1	1	0	2	0	0
590	ATXN10	5	3	0	0	0	1	0	1
591	TOP2B	5	2	35	31	5	5	34	27
592	PRPF40B	5	2	1	0	2	0	1	0
593	CSTF2T	5	2	0	0	1	3	0	2
594	ABCF2	5	2	0	0	1	2	0	1
595	ZC3H7A	5	2	1	1	1	1	0	1
596	RPL5	5	2	15	24	0	2	19	13
597	CLIC1	5	2	3	2	0	0	2	4
598	PDAP1	5	2	1	14	0	0	7	4
599	DNAH17	5	1	7	2	2	6	2	4
600	POP4	5	1	0	3	2	2	4	8

		TLE3_4/4_LiCl	TLE3_4/4_Ctrl	eGFP_4/4_LiCl	eGFP_4/4_Ctrl	TLE3_4/2_LiCl	TLE3_4/2_Ctrl	eGFP_4/2_LiCl	eGFP_4/2_Ctrl
601	SPAG9	5	1	0	0	2	2	0	0
602	SCAF4	5	1	0	1	1	1	0	0
603	RANBP1	5	1	0	1	1	0	1	2
604	PRPF31	5	1	16	15	0	2	18	14
605	RBMX2	5	1	6	7	0	2	6	3
606	NECAP1	5	1	0	3	0	2	1	2
607	STRAP	5	1	4	1	0	0	0	4
608	ZCCHC17	5	1	0	1	0	0	0	1
609	RPL23	5	0	5	4	3	3	4	4
610	HIST1H4A	5	0	8	12	2	4	11	13
611	RPS15A	5	0	3	1	1	5	4	4
612	OGT	5	0	0	0	0	1	0	0
613	RPS4X	5	0	0	6	0	0	8	4
614	MBD2	5	0	0	2	0	0	1	2
615	RPL37	4	27	4	17	41	19	21	3
616	FAU	4	9	5	5	5	5	11	6
617	WRNIP1	4	9	3	0	3	6	1	5
618	VEZF1	4	9	5	3	1	6	8	4
619	TAB1	4	8	2	0	1	6	0	6
620	SKI	4	7	0	0	5	6	0	0
621	ZEB2	4	7	0	0	5	4	0	0
622	BPLF1	4	7	1	1	2	0	2	0
623	UBN1	4	7	0	3	2	0	1	0
624	RECQL	4	7	14	13	1	8	15	31
625	HDAC2	4	7	8	2	1	2	9	10
626	ZNF207	4	7	4	1	1	1	6	3
627	PRDM16	4	6	1	0	4	3	1	0
628	NOB1	4	6	0	0	4	3	1	0
629	IRF2BPL	4	6	0	0	4	2	0	0
630	RNF113A	4	6	12	12	3	6	10	7
631	PTBP2	4	6	10	9	3	3	7	6
632	NPM1	4	6	17	18	1	2	9	12
633	MAGED1	4	5	0	0	5	2	0	1
634	ARID1A	4	5	1	2	4	4	0	3
635	LIN54	4	5	0	1	3	6	0	1
636	TRIM24	4	5	0	0	3	2	1	5
637	LIMD1	4	5	0	0	2	4	0	0
638	SKP2	4	5	3	3	2	3	4	2
639	H1F0	4	5	1	11	2	2	5	4
640	FRG1	4	5	10	14	2	0	14	10
641	LPP	4	5	0	0	1	2	0	0
642	CWF19L1	4	5	12	10	0	4	15	18
643	AUNIP	4	5	0	0	0	3	0	0
644	SYNE1	4	4	5	2	6	5	3	3
645	RRP1B	4	4	22	56	6	2	57	35
646	PRPF18	4	4	6	8	4	5	12	2
647	SMARCA2	4	4	6	1	4	5	2	1
648	GRK2	4	4	2	1	4	2	0	1
649	MTA2	4	4	1	3	3	5	0	11
650	GMEB2	4	4	0	0	3	5	0	0

		TLE3_4/4_LiCl	TLE3_4/4_Ctrl	eGFP_4/4_LiCl	eGFP_4/4_Ctrl	TLE3_4/2_LiCl	TLE3_4/2_Ctrl	eGFP_4/2_LiCl	eGFP_4/2_Ctrl
651	FTSJ3	4	4	23	24	3	2	41	16
652	SYNCRIP	4	4	19	24	3	2	37	33
653	FOXC1	4	4	0	0	2	5	0	0
654	VPS37A	4	4	0	0	2	2	0	0
655	SEPTIN9	4	4	1	0	2	0	0	5
656	GON4L	4	4	1	0	1	7	0	1
657	CDCA5	4	4	4	7	1	1	7	5
658	RBM5	4	4	7	5	0	5	1	4
659	SRFBP1	4	4	11	23	0	2	13	14
660	DDX27	4	3	6	13	7	6	7	14
661	CHMP2B	4	3	3	4	4	0	5	3
662	STAU2	4	3	5	1	3	2	2	2
663	C3	4	3	0	1	3	2	2	1
664	SRSF8	4	3	2	1	3	0	1	5
665	RPL23A	4	3	7	4	2	4	5	8
666	CNOT8	4	3	0	0	2	1	0	2
667	HDGF	4	3	14	9	2	0	8	13
668	RPL18	4	3	6	3	1	5	10	4
669	PDCD4	4	3	13	6	1	3	10	11
670	XRCC5	4	3	1	1	1	3	0	3
671	DLX5	4	3	1	0	1	3	0	1
672	SF3A3	4	3	2	0	1	2	1	2
673	ZIC2	4	3	0	0	1	2	1	0
674	SARNP	4	3	10	8	1	1	13	5
675	MNAT1	4	3	2	2	1	1	0	2
676	MVB12A	4	3	1	2	1	1	1	1
677	GLOD4	4	3	5	3	1	0	1	6
678	XRN2	4	3	1	0	0	4	0	2
679	DIDO1	4	3	6	1	0	2	4	5
680	CDK7	4	3	5	11	0	0	10	6
681	ZNF830	4	3	3	1	0	0	1	1
682	MCM4	4	2	1	0	5	9	0	2
683	BMS1	4	2	29	43	3	4	42	22
684	EXOSC8	4	2	1	5	2	2	3	0
685	RCC2	4	2	23	16	2	0	26	19
686	RPS27	4	2	3	0	1	4	3	2
687	GPATCH11	4	2	4	7	1	2	5	6
688	PSMC3	4	2	1	1	1	2	0	4
689	PPID	4	2	2	1	1	1	0	1
690	HSPA4L	4	2	2	0	1	1	0	0
691	SCAF8	4	2	0	0	1	1	0	0
692	H2AFY	4	2	2	2	1	0	3	2
693	IREB2	4	2	1	1	1	0	2	0
694	TCOF1	4	2	70	79	0	2	99	82
695	TIPRL	4	2	5	3	0	2	5	5
696	LASP1	4	2	1	2	0	1	1	1
697	PPP1CC	4	2	5	14	0	0	12	4
698	MNT	4	2	0	0	0	0	1	1
699	PATL1	4	1	0	0	3	1	0	0
700	UBE2V2	4	1	5	5	2	1	5	3

		TLE3_4/4_LiCl	TLE3_4/4_Ctrl	eGFP_4/4_LiCl	eGFP_4/4_Ctrl	TLE3_4/2_LiCl	TLE3_4/2_Ctrl	eGFP_4/2_LiCl	eGFP_4/2_Ctrl
701	QRICH1	4	1	1	0	2	1	2	0
702	RTF2	4	1	6	9	1	1	9	5
703	CCDC88A	4	1	2	1	1	0	0	1
704	PRPF6	4	1	3	4	0	4	0	0
705	DIS3	4	1	18	9	0	3	5	2
706	SPTBN5	4	1	1	2	0	1	1	3
707	TSNAX	4	1	0	0	0	0	0	1
708	DNAH10	4	0	3	3	3	4	10	12
709	APC2	4	0	0	1	1	0	0	2
710	CPSF4	4	0	1	3	0	0	2	3
711	NAV1	4	0	0	1	0	0	2	3
712	EIF5	4	0	0	0	0	0	0	3
713	PRR12	3	15	1	1	7	5	1	1
714	ZNF687	3	10	5	8	7	6	6	9
715	ATXN1L	3	10	0	0	4	6	0	0
716	DHX8	3	9	15	25	5	4	21	13
717	DOT1L	3	8	1	0	3	6	1	1
718	CHMP4B	3	7	8	7	1	1	2	6
719	RBM41	3	6	6	9	3	5	15	19
720	SPAG7	3	6	0	17	3	5	8	6
721	MACF1	3	5	7	4	5	6	6	3
722	CUL4B	3	5	0	0	3	4	0	3
723	SPATA2	3	5	1	0	3	3	0	2
724	ENO1	3	5	4	1	3	2	1	2
725	ILF3	3	5	39	22	2	4	18	30
726	DAB2	3	5	0	0	2	1	0	0
727	CWC27	3	5	7	7	1	4	8	8
728	AASDHPPT	3	5	6	11	1	0	7	3
729	CCDC43	3	5	4	4	1	0	3	3
730	PQBP1	3	5	0	4	1	0	0	2
731	RPS9	3	5	1	2	0	2	1	0
732	CNOT2	3	5	1	0	0	0	0	0
733	NUDCD2	3	4	1	1	6	1	2	1
734	PGD	3	4	0	3	3	2	0	0
735	CHD1	3	4	32	25	3	1	29	11
736	SWAP70	3	4	6	0	3	1	0	4
737	RBBP6	3	4	3	2	2	2	9	5
738	ARFGAP1	3	4	1	0	2	1	0	1
739	RPL34	3	4	4	3	1	4	4	4
740	G3BP1	3	4	4	1	1	1	0	2
741	MAPRE1	3	4	3	0	1	1	1	6
742	PTGES3	3	4	0	0	1	1	1	1
743	DKC1	3	4	21	15	0	7	23	19
744	ZNF24	3	4	7	7	0	5	7	4
745	DMRTA2	3	4	0	1	0	2	0	1
746	NR2C1	3	4	1	0	0	1	0	3
747	PGAM5	3	4	3	1	0	0	3	1
748	CASZ1	3	4	1	0	0	0	1	0
749	LANA1	3	3	2	10	11	0	1	1
750	TBX3	3	3	1	1	7	2	1	0

		TLE3_4/4_LiCl	TLE3_4/4_Ctrl	eGFP_4/4_LiCl	eGFP_4/4_Ctrl	TLE3_4/2_LiCl	TLE3_4/2_Ctrl	eGFP_4/2_LiCl	eGFP_4/2_Ctrl
751	CCT4	3	3	0	0	4	2	2	0
752	ARCN1	3	3	11	6	3	3	9	9
753	AHNAK2	3	3	1	2	3	3	6	6
754	SRSF7	3	3	1	1	3	0	2	5
755	CAPZB	3	3	4	2	2	1	0	4
756	SP2	3	3	3	3	1	4	4	6
757	INTS12	3	3	7	2	1	3	2	3
758	PARK7	3	3	2	1	1	2	3	4
759	IST1	3	3	1	0	1	2	1	2
760	ZNF512B	3	3	4	3	1	1	10	3
761	PEG10	3	3	3	2	1	1	2	3
762	WDFY1	3	3	3	2	1	1	2	2
763	ING3	3	3	0	0	1	0	0	0
764	BRCA2	3	3	1	0	0	5	1	4
765	XRCC1	3	3	4	6	0	3	2	5
766	TLX1	3	3	0	1	0	2	0	0
767	DHX36	3	3	10	2	0	1	1	1
768	CASP3	3	3	4	1	0	1	3	4
769	HAUS4	3	3	0	2	0	0	2	0
770	WAC	3	3	0	1	0	0	0	0
771	HIST1H2BC	3	2	8	15	6	2	16	9
772	TOX4	3	2	0	0	5	2	0	1
773	TTC9C	3	2	1	0	4	2	1	0
774	SNF8	3	2	0	0	2	4	0	0
775	RPL17	3	2	4	7	2	3	2	0
776	TP73	3	2	1	1	2	3	1	0
777	HNRNPAB	3	2	8	8	2	1	6	2
778	RPS26	3	2	4	3	2	1	3	3
779	PPM1G	3	2	2	0	2	1	1	2
780	YY1	3	2	8	9	2	0	14	6
781	EIF3J	3	2	0	0	2	0	0	1
782	DNAH1	3	2	2	2	1	5	3	4
783	BLM	3	2	16	12	1	4	23	11
784	MED15	3	2	0	1	1	4	0	0
785	SMAP1	3	2	0	0	1	3	0	1
786	PES1	3	2	20	11	1	2	12	12
787	RBM26	3	2	5	5	1	2	5	7
788	BCCIP	3	2	2	2	1	2	5	4
789	DYNC1H1	3	2	3	0	1	1	4	2
790	MCM10	3	2	3	0	1	1	3	0
791	FXR1	3	2	1	1	1	1	0	0
792	STUB1	3	2	0	0	1	0	1	1
793	PPIL4	3	2	14	18	0	3	14	13
794	EIF3D	3	2	8	6	0	1	13	6
795	PHF23	3	2	3	0	0	1	3	3
796	ZCCHC3	3	2	2	0	0	1	2	1
797	SH3GL1	3	2	2	0	0	1	1	2
798	WAPL	3	2	2	0	0	0	2	1
799	ZNF598	3	2	1	2	0	0	0	2
800	SPART	3	2	0	0	0	0	0	1

		TLE3_4/4_LiCl	TLE3_4/4_Ctrl	eGFP_4/4_LiCl	eGFP_4/4_Ctrl	TLE3_4/2_LiCl	TLE3_4/2_Ctrl	eGFP_4/2_LiCl	eGFP_4/2_Ctrl
801	RPL6	3	1	2	4	6	6	8	16
802	DNAH9	3	1	3	1	2	2	2	5
803	KMT2A	3	1	1	3	2	2	5	1
804	UBE2V1	3	1	4	7	2	1	5	4
805	API5	3	1	14	7	2	0	7	9
806	PPP2R2A	3	1	0	0	2	0	1	0
807	DLX1	3	1	1	1	1	4	0	1
808	RPL21	3	1	4	1	1	2	0	1
809	RAI14	3	1	0	5	1	2	0	0
810	BCL11A	3	1	0	1	1	2	0	0
811	SETX	3	1	7	1	1	1	9	2
812	NSA2	3	1	3	2	1	1	2	2
813	MOB3A	3	1	0	3	1	1	0	2
814	MYO5A	3	1	3	3	1	0	0	1
815	TFCP2	3	1	3	1	1	0	4	0
816	ALKBH2	3	1	2	6	1	0	6	1
817	C9orf78	3	1	1	1	1	0	1	1
818	CKB	3	1	0	0	1	0	0	1
819	POU2F1	3	1	0	0	1	0	0	0
820	CWF19L2	3	1	4	6	0	4	3	2
821	DDX21	3	1	19	30	0	2	36	20
822	CDK5RAP2	3	1	3	4	0	2	4	2
823	PDS5A	3	1	2	0	0	2	0	4
824	U2AF1	3	1	1	3	0	2	2	1
825	POLDIP3	3	1	27	34	0	1	31	14
826	CALD1	3	1	4	0	0	1	1	1
827	DDB2	3	1	3	0	0	1	0	3
828	G6PD	3	1	0	1	0	1	0	2
829	SUPT16H	3	1	24	27	0	0	21	21
830	CHMP5	3	1	3	3	0	0	5	2
831	TTF2	3	1	1	1	0	0	1	1
832	IFIT5	3	1	1	1	0	0	0	1
833	SIX4	3	1	1	0	0	0	0	0
834	TBCC	3	1	0	1	0	0	0	1
835	PLEKHA2	3	1	0	0	0	0	1	0
836	ASRGL1	3	1	0	0	0	0	0	1
837	SRP68	3	0	0	0	2	3	0	0
838	DDX39B	3	0	16	3	2	1	9	9
839	DDX39A	3	0	11	4	2	1	7	9
840	LYSMD2	3	0	1	3	2	0	1	2
841	SETD5	3	0	0	0	1	2	0	1
842	LZIC	3	0	6	3	1	1	6	3
843	NOP14	3	0	2	4	1	1	1	2
844	COL7A1	3	0	1	1	1	0	1	3
845	RUNX1	3	0	0	0	1	0	0	0
846	SNX3	3	0	6	6	0	2	7	3
847	PPP1CA	3	0	5	11	0	2	11	5
848	CELF1	3	0	3	0	0	1	3	6
849	DHFR	3	0	1	2	0	1	1	0
850	DSN1	3	0	0	0	0	1	1	1

		TLE3_4/4_LiCl	TLE3_4/4_Ctrl	eGFP_4/4_LiCl	eGFP_4/4_Ctrl	TLE3_4/2_LiCl	TLE3_4/2_Ctrl	eGFP_4/2_LiCl	eGFP_4/2_Ctrl
851	NOP2	3	0	28	34	0	0	32	21
852	MRPS5	3	0	1	0	0	0	0	0
853	RTCB	3	0	0	0	0	0	0	0
854	SUZ12	3	0	0	0	0	0	0	0
855	MEPCE	2	9	7	2	3	1	8	16
856	NCOA3	2	6	0	0	5	8	0	0
857	LRIF1	2	6	2	4	4	3	3	5
858	SHROOM3	2	6	6	2	2	8	5	0
859	TCF3	2	6	0	0	2	6	0	0
860	BRCA1	2	6	1	0	2	4	1	0
861	CHD1L	2	6	12	6	2	3	6	4
862	PDCL3	2	6	2	1	2	0	2	3
863	BAZ2A	2	6	17	3	1	1	21	4
864	EIF4G3	2	6	1	4	0	3	0	0
865	RBM6	2	6	10	18	0	0	9	3
866	SRSF3	2	5	1	1	7	6	7	8
867	CHD2	2	5	21	16	3	2	19	8
868	NUP98	2	5	0	0	3	1	1	1
869	MAGOHB	2	5	10	9	2	2	10	7
870	RPS3A	2	5	4	9	2	2	7	6
871	PDLIM7	2	5	3	0	2	0	3	0
872	DNAJA1	2	5	1	0	1	0	0	2
873	ZSCAN25	2	5	1	1	0	2	5	2
874	RIOK1	2	4	3	6	4	4	2	2
875	SP9	2	4	0	1	3	4	0	1
876	PRC1	2	4	9	4	3	3	10	10
877	RPL11	2	4	4	3	2	3	2	3
878	PIH1D1	2	4	0	1	2	0	1	0
879	KIF20B	2	4	11	0	0	3	10	4
880	PICALM	2	4	1	0	0	3	0	0
881	BEND3	2	4	1	1	0	2	0	0
882	MYO1E	2	4	2	0	0	0	0	0
883	SURF6	2	3	9	15	5	4	18	7
884	TDRP	2	3	2	7	3	4	4	4
885	AGFG2	2	3	1	0	3	2	0	1
886	CREB1	2	3	3	2	3	1	1	1
887	AMZ2	2	3	1	3	3	0	0	1
888	HNRNPR	2	3	21	38	2	2	38	28
889	PTAR1	2	3	1	0	2	2	0	2
890	SFI1	2	3	1	0	2	2	0	2
891	NACA	2	3	4	7	2	0	5	5
892	CSK	2	3	2	0	2	0	0	2
893	BBX	2	3	0	1	1	5	5	1
894	SSBP3	2	3	0	0	1	4	0	0
895	HNRNPL	2	3	16	20	1	2	20	15
896	RPS14	2	3	3	4	1	2	6	3
897	NUPL2	2	3	3	3	1	2	2	3
898	SNX9	2	3	0	0	1	0	0	0
899	NACC1	2	3	0	0	0	3	0	0
900	SCML2	2	3	12	13	0	2	12	14

		TLE3_4/4_LiCl	TLE3_4/4_Ctrl	eGFP_4/4_LiCl	eGFP_4/4_Ctrl	TLE3_4/2_LiCl	TLE3_4/2_Ctrl	eGFP_4/2_LiCl	eGFP_4/2_Ctrl
901	CBLL1	2	3	2	0	0	2	3	2
902	MDC1	2	3	30	14	0	1	16	19
903	DNAJC17	2	3	5	11	0	1	8	3
904	MED1	2	3	1	0	0	1	5	0
905	ATXN2	2	3	1	0	0	1	0	0
906	GTF3C1	2	3	9	2	0	0	5	1
907	HDAC3	2	3	2	0	0	0	1	1
908	SEC24A	2	3	1	1	0	0	0	0
909	CDC25C	2	3	0	1	0	0	0	1
910	USP15	2	3	0	0	0	0	1	0
911	PALLD	2	3	0	0	0	0	0	0
912	SOX13	2	3	0	0	0	0	0	0
913	EXOSC9	2	2	20	17	3	3	19	22
914	HMCN1	2	2	4	0	2	4	2	4
915	RPL27	2	2	2	1	2	3	3	1